

EXPLORING A SUSTAINABLE SYNTHESIS OF ARTEMISININ

Nasiru Sharif, M.Sc.

Thesis submitted to The University of Nottingham for the

Doctor of Philosophy

Supervisors: Prof. Michael W. George & Prof. Sir Martyn Poliakoff

January / 2022

In the Name of Allah, the Most Beneficient, the most Merciful.

Dedicated

To

my late father Alh. Sharif Sulaiman

ABSTRACT

Malaria causes many deaths per year, according to report released by WHO in November 2020, there were 229 million cases of malaria in 2019, with estimated number of deaths which stood at 409, 000. With the children under the age of 5 years being the most vulnerable, accounting for 67 % (274 000) of all malaria death worldwide. The World Health Organization has recommended Artemisinin-based combination therapies (ACTs) for the treatment of uncomplicated malaria caused by the parasite P. *falciparum*.

Artemisinin is a sesquiterpene lactone compound known for its antimalarial properties. Artemisinin has been isolated for centuries from *Artemisia annua* plant, accounting for 0.6 – 1.0 % of the dried mass of the plant material. After the development of its synthetic route and subsequent commercialisation by Sanofi in 2013,[1] efforts have been made to improve its yield, thereby reducing the cost of the final antimalarial drug.[2, 3] This work shows how the use of a simple photo-reactor, the PhotoVap, can improve the yield of Artemisinin.[4, 5]

In Chapter 2 the semi-synthesis of Artemisinin from DHAA, through semi-continuous method in the PhotoVap reactor has been reported, employing two-step and one-pot strategies. Various conditions were optimised with the view to finding the best possible route to the improved industrial production of Artemisinin **1**. Highest yield of 75 % Artemisinin **1** was obtained through one-pot approach using $[Ru(bpy)_3]Cl_2$ and TFA as photosensitiser and acid catalyst respectively, at -10 °C.

Chapter 3 involved the mechanistic consideration for the various steps involved in the synthesis of Artemisinin **1**. With the aim of identifying most of the side products responsible for the reduction in the overall yield, selectivity, and productivity of Artemisinin **1**. These side products include the aldehyde **32**, δ– and γ–lactones (**33** and

37), deoxyartemisinin **35**, polymers and unidentified oligomers. The synthesis, and isolation of δ-lactone **33** and its crystal information has been described. Its reactivity has been studied to explore the possibility of opening its ring back to enol intermediate, which can undergo thermal oxidation to Artemisinin **1**.

Various esters and carbonates of DHAA **3** have been synthesized, which include methyl ester **8**, ethyl ester **90**, isopropyl ester **91**, hexafluoro isopropyl ester **92**, methyl carbonate **93**, and ethyl carbonate **43**. The esters and carbonates have been used for the synthesis of Artemisinin **1** through one-pot and two-step process, with the aim finding the possible method of blocking the formation of some of the lactone side-products, for improving the yield and productivity of Artemisinin **1**.

ACKNOWLEDGEMENTS

I would like to thank my supervisors Prof. Mike George and Prof. Sir, Martyn Poliakoff for supervising my PhD studies and their support and encouragements throughout my stay in Nottingham. This could not be achieved without the scholarship grant from the management of Federal University Gusau, Zamfara, Nigeria, through Tertiary Education Trust Fund (TetFund) Nigeria, and PhD admission by the University of Nottingham, UK.

I must express my appreciations to the members of Artemisinin project team; Dr Darren Lee, for technical support throughout the research, Dr Hamza Boufroura for technical support, guidance, advise and criticism, which help me greatly during the thesis writing, and Dr Marcus V. Hernando, and James Herron for their support. I will also thank Dr Charlotte Clark, from whose work led to the design of PhotoVap reactor, and for the training on its use and other supports during my research. I also like to thank all the technicians from the University of Nottingham's workshop; Shaz Aslam for NMR support and training, Dr Stephen Argent for XRD measurements, and Sue.

I wish to thank Bryan Tambosco for the silica-supported catalyst, Dr Ashley Love, and Xue Wu for their support during my first-year project. I want to thank other members of George group working in the fort, B13, B 19 and B21 and my friends in Nigeria Yusuf, Akilu, Usman and many others, and those in Nottingham, Muhammad, Mubarak, Basiru, Mahmud, Umar, Kamal, and many others.

I must thank my parents Alh. Sharif Sulaiman and Amina Garba for their prayers, support, and encouragements, especially my father who could not witness the end of my PhD. I must thank my wife Fatima Abdullahi for all her enduring support during this prolonged period, and her great effort in taking care of our kids Hafsat, Ibrahim, and newborn Abdullah, and my brothers and sisters for support and prayers.

DECLARATION

I declare that the work presented in this Thesis is a record of my own work for the period of April 2017 to September 2021. Where any work has been carried out in collaboration, the relevant researcher has been acknowledged. This Thesis has not been accepted in partial or complete fulfilment of any other degree or personal qualification.

Nasiru Sharif 25th January, 2022

ABBREVIATION LIST

$^1\Delta g$	Singlet oxygen in the excited state
^{1}H-NMR	Proton nuclear magnetic resonance
$^1O_2$	Singlet oxygen in the $^1\Delta g$ excited state
$^3O_2$	Triplet oxygen
$^1\Sigma_g$	highest energy singlet state
2-MeTHF	2-methyltetrahydrofuran
4-MeTHF	4-methyltetrahydrofuran
9-BBN	9-Borabicyclo[3.3.1]nonane
A	Electron acceptor
AA	Artemisininic Acid
ACTs	Artemisinin combination therapies
API	Active Pharmaceutical Ingredients
BP	Biphenyl
bpy	2,2'-Bipyridine
COSY	COrrelation SpectroscopY
Conv.	Conversion
D	Electron donor
DCA	9,10-dicyanoanthracene
DCE	Dichloroethane
DCM	Dichloromethane
DHAA	Dihydroartemisinic Acid
DHAAl	Dihydroartemisinic aldehyde
DHAMC	Methyl carbonate of Dihydroartemisinic
DHAEC	Ethyl carbonate of Dihydroartemisinic
DHAME	Methyl ester of Dihydroartemisinic
DHAEE	Ethyl ester of Dihydroartemisinic
DHAIP	Isopropyl ester of Dihydroartemisinic

DHAHFIP	Hexafluoroisopropyl ester of Dihydroartemisinic
DMAP	Dimethylaminopyridine
DMC	Dimethyl carbonate
DMSO	Dimethyl sulfoxide
DPD	Diphenyl-1,4-dioxetene
dtbbpy	4,4'-Di-*tert*-butyl-2,2'-dipyridyl
E1	Unimolecular elimination
EBiB	Ethyl-2-bromoisobutyrate
EGDB	Ethylene glycol dibenezene
EtOH	EtOH
Equiv.	Equivalent
FEP	Fluorinated ethylene propylene
HFIP	1,1,1,3,3,3-Hexafluoro-2-propanol
HMBC	Heteronuclear Multiple Bond Correlation
HOMO	Highest occupied molecular orbital
HPLC	High performance liquid chromatography
HSQC	Heteronuclear Single Quantum Coherence
IC	Internal conversion
ISC	Intersystem Crossing
L	Ligand
LEDs	Light emitting diodes
LMCT	Ligand to Metal charge transfer
LUMO	Lowest unoccupied molecular orbital
MB	Methylene Blue
MeCN	Acetonitrile
MLCT	Metal to Ligand Charge Transfer
MoA	Mechanism of Action
Nf	Nafion®
NS	Not Soluble
NM	Not Miscible

n-PrOH	Propan-1-ol
OEP	Octaethylporphyrin
ORTEP	Oak Ridge Thermal Ellipsoid Plot
PC	Photo-catalyst
PDT	PhotoDynamic Therapy
P.E.	Petroleum Ether
PET	Photo-induced electron transfer
PFR	Plug Flow Reactor
ppy	2-Phenylpyridine
PS	Photosensitiser
PTFE	Polytetrafluoroethylene
RB	Rose Bengal
RM	Redox mediator
RSC	Royal Society of Chemistry
RT	Room Temperature
SCE	Standard Calomel Electrode
SM	Starting Material
S_N^2	Bimolecular nucleophilic substitution
STY	Space Time Yield
TBAF	Tetrabutylammonium fluoride
TCA	Trichloroacetic acid
TCCA	Trichloroisocyanuric acid
TFA	Trifluoroacetic acid
Temp.	Temperature
TfO	Triflate
THF	Tetrahydrofuran
THPP	Tetrahydroxyphenylporphyrin
TMS	Trimethylsilyl
TMSTFA	Trimethylsilyltrifluoroacetic acid
TPP	Tetraphenylporphyrin

TsOH	*p*-Toluenesulfonic acid
UPLC	Ultra performance liquid chromatography
VOC	Volatile Organic Compounds
WHO	World Health Organisation

TABLE OF CONTENTS

ABSTRACT **3**
ACKNOWLEDGEMENTS **5**
DECLARATION **6**
ABBREVIATION LIST **7**
TABLE OF CONTENTS **11**
CHAPTER 1: INTRODUCTION **14**
PHOTO-OXIDATION OF ORGANIC COMPOUNDS 17
1.1.1. Properties of singlet oxygen: lifetime and quenching of singlet oxygen *22*
1.1.2. Methods for the generation of singlet oxygen *24*
1.1.2.1 Chemically generated singlet oxygen 24
1.1.2.2 Photo-generated singlet oxygen 26
1.1.1.2.1 Organic Photocatalyst 27
- Porphyrins and derivatives 27
- Other Organic Photosensitisers 29

1.1.1.2.2 Transition Metal Catalysis 32
1.1.1.2.3 Immobilised photo-oxidation catalyst systems 36
REACTORS FOR PHOTOCHEMICAL PROCESSES 40
1.2.1. Batch reactors for photochemical processes *40*
1.2.2. Semi-continuous reactors for photochemical processes *43*
1.2.3. Continuous flow reactors for photochemical processes *45*
- Microfluidic reactors 47
- Taylor-Couette flow reactors 50

2.3.1. Examples of reactions performed by singlet oxygen *53*
ARTEMISININ AND ITS ANTIMALARIAL DERIVATIVES 58
Malaria and its treatments *58*
1.3.2. Mode of action of Artemisinin *60*
1.3.3. Sources of Artemisinin *62*
1.3.4. The extraction and isolation of Artemisinin *63*
SYNTHESIS OF ARTEMISININ 64
1.4.1. Total synthesis of Artemisinin *65*
1.4.1.2 Citronellal based strategies 66
1.4.1.2 Cyclohexane and its derivatives based strategies 67
Total synthesis of DHAA toward the semi-synthesis of Artemisinin *71*
1.4.3. Semi-synthesis of Artemisinin *76*
THE AIMS OF THE THESIS 84
CHAPTER 2: OPTIMIZING THE SYNTHESIS OF ARTEMISININ IN THE PHOTOVAP REACTOR **86**
INTRODUCTION AND BACKGROUND 86
SCREENING OF THE SOLUBILITY OF DHAA IN ORGANIC SOLVENTS UNDER DIFFERENT CONDITIONS 89
SEMI-SYNTHESIS OF ARTEMISININ IN PHOTOVAP REACTOR 91
2.3.1. Two Steps Synthesis of Artemisinin from DHAA in PhotoVap reactor. *91*
2.3.1.1 The 1st step: photo-oxidation of DHAA in the PhotoVap Reactor 92
2.3.1.1.1 Effects of Temperature and nature of Photosensitiser on DHAA Photo-oxidation 93
2.3.1.1.2 Effects of the nature of solvents on the DHAA photo-oxidation PhotoVap reactor 97
2.3.1.2 Study of the second step: Acid catalysed Hock cleavage followed by the "thermal oxidation". 100
2.3.1.3 Two steps synthesis of Artemisinin using heterogenous catalyst system 103
2.4.1. One-pot synthesis of Artemisinin in PhotoVap reactor *107*
2.4.1.1 The effect of varying the photosensitiser on the yield and productivity of Artemisinin 108
2.4.1.2 Effect of the Acid Catalyst and Solvent on the yield of Artemisinin 111
2.5.1. Solubility studies of DHAA, different Aqueous solvent mixtures *117*

2.5.1.1 Solubility study of DHAA at room temperature and different concentrations in Alcohol/Water mixtures....120
2.6.1. Synthesis of Artemisinin in an alcohol/water mixture in the PhotoVap reactor....124
2.6.1.1 Two-step approach in an alcohol/water mixture in PhotoVap reactor. 125
2.6.1.2 One-pot synthesis Artemisinin in alcohol/water mixtures 128
STUDYING THE EFFECT OF BIPHENYL ON DHAA PHOTO-OXIDATION....130
2.3.1. Exploring Photo-oxidation of DHAA, using DCA-biphenyl.....130
2.7.2. Photo-oxidation of DHAA using $[Ru(bpy)_3]Cl_2$ -biphenyl system....133
2.7.3. One-pot synthesis of Artemisinin using $[Ru(bpy)_3]Cl_2$-biphenyl system in DCE.....134
2.7.4. Competing electronic and energy transfer processes during photo-oxidation process 136
CHAPTER SUMMARY....144
CHAPTER 3: LACTONES DERIVED FROM THE SYNTHESIS OF ARTEMISININ AND THEIR ROLES IN ITS PRODUCTIVITY....146
INTRODUCTION AND MECHANISTIC STUDIES....146
MECHANISM AND SELECTIVITY IN THE SEMI-SYNTHESIS OF ARTEMISININ....147
3.2.1. Mechanism and selectivity of DHAA photo-oxidation process....147
3.5.2.2 Mechanism of the acid catalysed Hock-cleavage process 149
3.5.2.2 Mechanism of the Thermal Oxidation and final Cyclisation Cascade 156
3.2.2. Reactions of lactones....158
LACTONES AS BY-PRODUCTS OF THE ARTEMISININ SYNTHESIS....163
3.3.1. Synthesis of δ-lactone in the PhotoVap reactor....164
SYNTHESIS OF ARTEMISININ FROM Δ-LACTONE....169
3.4.1. Acid catalysed hydrolysis of 6-membered lactone in $MeOH/H_2O$ solution....169
3.4.2. The Acid catalysed hydrolysis of the δ-lactone in THF/H_2O solution....173
SYNTHESIS OF DHAA DERIVATIVES AND THEIR APPLICATION IN THE SYNTHESIS OF ARTEMISININ....178
3.5.1. Solubility study of DHAA derivatives at room temperature and different concentrations in alcohol/water mixtures....179
3.5.2. DHAA derivatives as precursors to Artemisinin....180
3.5.2.1. The Semi-synthesis of Artemisinin from the DHAA derivatives: 2 step process 181
3.5.2.1.1. 1st step: Photo-oxidation 181
3.5.2.1.2. 2nd step: Hock cleavage / Thermal oxidation 182
3.5.2.2. One-pot Synthesis of Artemisinin 1 using DHAA Derivatives. 188
SUMMARY OF THE CHAPTER....194
CHAPTER 4: CONCLUSIONS AND FURTHER WORK....196
CONCLUSIONS....197
FURTHER WORK....201
CHAPTER 5: EXPERIMENTAL....203
GENERAL ANALYTICAL METHODS....203
5.1.1. nmr spectroscopic analysis....203
5.1.1.1 Quantitative proton-NMR Measurements....203
5.1.1.2 Calculations of the productivity of Artemisinin 204
5.1.2. mass spectroscopy and x-ray diffraction analysis....205
5.1.3. uv-visible and infra-red absorption spectroscopy....205
PHOTOVAP REACTOR SETUP....206
5.2.1 Light source for PhotoVap reactor....206
5.2.2 PhotoVap reactor standard operation procedure....207
5.2.3 General procedure for the semi-continuous photo-chemical process in PhotoVap reactor 207
SYNTHESIS OF ARTEMISININ IN PHOTOVAP REACTOR 208
5.3.1 Photo-oxidation of DHAA in PhotoVap Reactor....209

5.3.2 Acid catalysed Hock-cleavage and thermal oxidation *209*
5.3.3 General procedure for the one-pot synthesis of Artemisinin in photovap reactor *210*
5.3.4 Optimising the synthesis of Artemisinin in PhotoVap reactor *211*
SYNTHESIS OF [RU(BPY)$_3$](TFA)$_2$ 211
5.4.1 Synthesis of Artemisinin using [Ru(bpy)$_3$](TFA)$_2$ *212*
THE IMMOBILISATION OF [RU(BPY)$_3$]CL$_2$ CATALYST ON SILICA 212
5.5.1 Synthesis of Artemisinin using silica supported catalyst *213*
SOLUBILITY STUDIES OF DHAA IN AQUEOUS SOLUTION 213
5.6.1 Solubility studies of 50 and 500 mM DHAA in alcohol/water solution at room temperature *213*
5.6.2 Screening of the solubility of DHAA and photosensitiser mixtures at different temperatures *214*
STUDYING THE EFFECT OF BIPHENYL ON DHAA PHOTO-OXIDATION 214
5.7.1 Studying the effect of biphenyl on DHAA photo-oxidation using DCA as photosensitiser *214*
5.7.2 Studying the effect of biphenyl on DHAA photo-oxidation using [Ru(bpy)$_3$]Cl$_2$ as Photosensitiser *215*
SYNTHESIS OF δ– LACTONE 215
5.8.1 Isolation and crystallisation of δ-lactone *216*
5.8.2 Scale-up of the Synthesis of δ-lactone in large Vortex Reactor *218*
5.8.3 Reactions of δ-lactone *218*
5.8.3.1 Acid catalysed hydrolysis of δ-lactone in MeOH/H_2O Solution 218
5.8.3.2 Acid Catalysed hydrolysis of δ-lactone in THF/H_2O solution 219
SYNTHESIS OF DHAA DERIVATIVES 219
5.9.1 General procedure for the synthesis of the DHAA ester derivatives *219*
5.9.2 General procedure for the synthesis of DHAA carbonates derivatives: *222*
5.9.3 Synthesis of Artemisinin using DHAA derivatives *224*
5.9.3.1 Photo-oxidation 224
5.9.3.2 Acid catalysed Hock-cleavage and thermal oxidation 224
5.9.3.3 One-pot Method 224
REFERENCES **226**
APPENDIX **233**

CHAPTER 1: INTRODUCTION

Photochemistry deals with the chemical transformations that are caused by the absorption of light, through the process of photolysis. Photolysis is usually initiated by direct absorption of ultraviolet light or visible light but can also be driven following infrared irradiation. Photochemical reactions are of great importance for the support of life on this planet, for example the chemical changes involving atmospheric gases are initiated by solar radiation and modified by the suspended particles. The study of upper atmospheric photochemical reactions has significantly contributed to the knowledge of depletion of the ozone layer, acid rain, and global warming.

The foundation for the understanding of photochemistry is based on two fundamental principles of photochemical transformations, as postulated by two laws of photochemistry: **The first law of photochemistry**, the Grotthuss-Draper law,[6] states that light must be absorbed by a compound for a photochemical reaction to take place. **The second law of photochemistry**, the Stark-Einstein law,[7] states that for each photon of light absorbed by a chemical system, only one molecule is activated for subsequent reaction. This is called "photo equivalence law". Therefore, a photon of light of energy ($h\nu$) is absorbed by the molecule at ground state, resulting in its excitation to a higher energy state, at which it can involve in a chemical reaction leading to the formation of products.

Photochemical processes are traditionally known to involve interaction of a substance with sun light, and many photochemical reactions were known due to accidental or intentional exposure of substances to light[8], although the underlying principles were poorly understood.[9] However, the pioneer work of Ciamician and co-workers gave rise to a drastic change in the understanding of photochemical reactions and its consider a milestone in modern photochemistry.[9]

During his famous lecture at the International Congress of Applied Chemistry in New York in 1912, Giacomo Ciamician, presented his spectacular vision on "The Photochemistry of the Future":

> *"On the arid lands there will spring up industrial colonies without smoke and without smokestacks; forests of glass tubes will extend over the plains, and glass buildings will rise everywhere; inside of these will take place the photochemical processes that hitherto have been the guarded secret of the plants, but that will have been mastered by human industry which will know how to make them bear even more abundant fruit than nature, for nature is not in a hurry and mankind is."*

During that time, photochemical experiments mostly took place on the rooftops of chemical Institutes, as illustrated by the famous photochemical reaction's setup by Ciamician (Figure 1), where the reaction mixtures were exposed to direct sunlight over long periods of time, often several months.

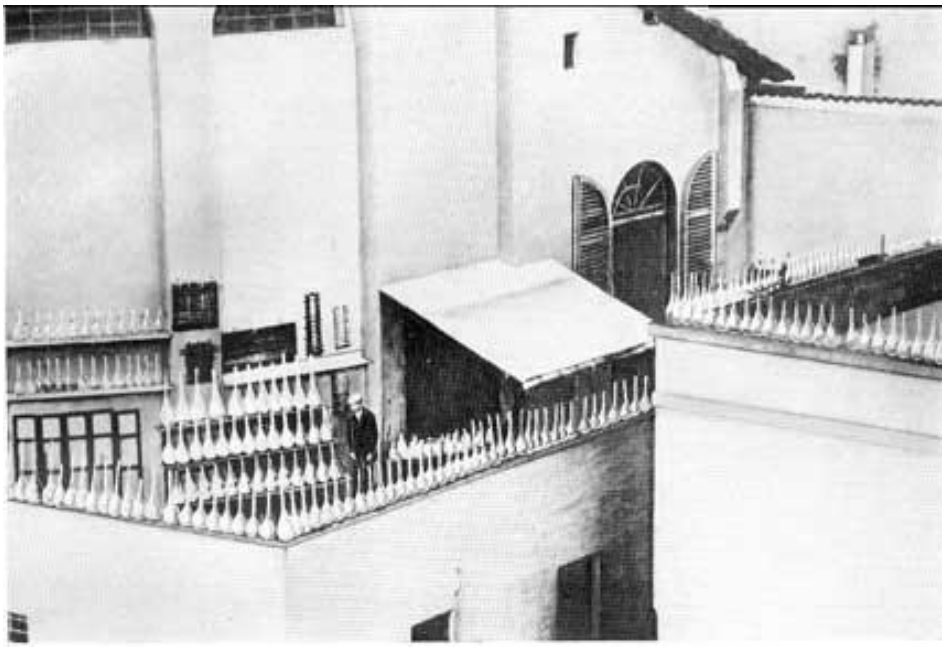
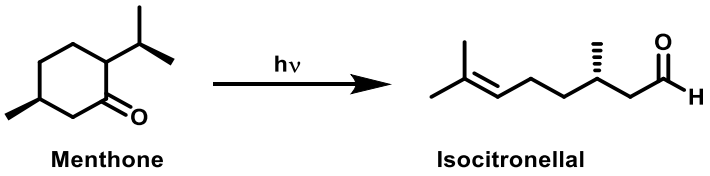


Figure 1: Professor Giacomo Ciamician and Dr Paolo Silber on their roof laboratory at the University of Bologna, Italy, in 1912.[10]

In their contributions, Ciamician *et al.* explored the behaviour of several carbonyl derivatives in their reactions with light and reported the processes of photoreductions, intramolecular cycloaddition, and α- and β-cleavage. For example, they reported the α-cleavage of menthone to isocitronellal (Scheme 1).



Scheme 1: photoinduced a-cleavage of menthone the reaction reported by Ciamician[11]

These studies later revealed fundamental principles such as the concepts of excited singlet and triplet as well as n, π* and π, π* states. With the development of powerful artificial light-sources,[12] photochemistry finally moved into the laboratories and since then it has become more accessible research field.

Over the last decades, the call for environmentally friendly technologies has led to an increasing interest in photochemical processes. Among the known sustainable approaches, solar photochemistry can serve as a valuable application since sunlight is used as energy and as light source.[13] This concept leads back to the beginnings of organic photochemistry in the late 19th century and consequently "back to the roofs".

From the second law of photochemistry: the efficiency with which a given photochemical process occurs is given by its Quantum Yield (Φ). Since many photochemical reactions are complex, and may compete with unproductive energy loss, the quantum yield is usually specified for a particular event. Thus, quantum yield can be defined as "the number of moles of a stated reactant disappearing, or the number of moles of a stated

product produced, per Einstein of monochromatic light absorbed.", where an Einstein is one mole of photons (Equation **1**).

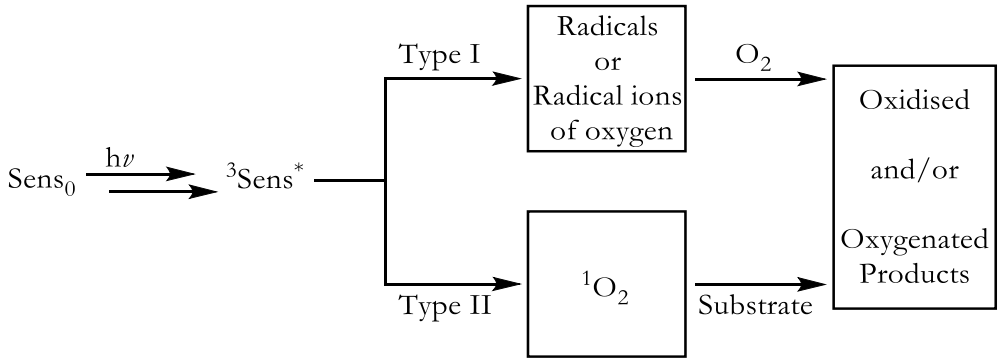
$$\textbf{Quantum Yield } (\boldsymbol{\Phi}) = \frac{\textit{number of molecules of products formed}}{\textit{number of photons absorbed by substance}} \quad (\mathbf{1})$$

The values obtained from Quantum Yield (Φ) usually ranged between 0 and 1 for reactions that do not involve chain reactions,[14] the photochemical reactions span over different organic reactions types, i.e., since the beginning of photochemistry a myriad of examples has been reported including: photohalogenation, photosulfonation, photopolymerisation and photo-oxidation processes.

PHOTO-OXIDATION OF ORGANIC COMPOUNDS

Photo-oxidation is the absorption of light radiation of a given wavelength by a chemical substance which result in its excitation, leading to either loss of one or more electrons from the substance or the transfer of the excitation energy to another substance. Photo-oxidation process is divided into two types: type I and II (Scheme 2).

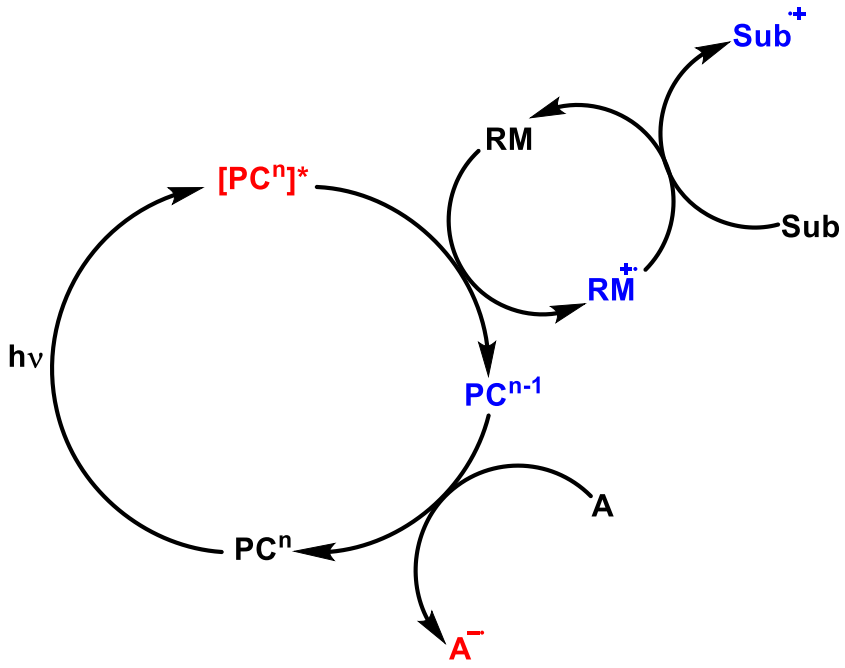
Type I photo-oxidation involves a reaction between an organic substrate in its excited state such as alcohols, with triplet oxygen ($^3O_2$) in form of a superoxide radical, which can be produced through donation of electron from photosensitiser to $^3O_2$, by charge transfer or hydrogen atom abstraction from organic substrate by the photosensitiser in its excited state.[15-17]



Scheme 2: Schematic representation of type I and II photo-oxidation reactions. Adapted M. S. Baptite et al. [15]

Type I photosensitisers are commonly: diaryl ketones, acetophenone, aromatic aldehydes, and their heterocyclic analogues. The majority of substrates can only undergo Type I photo-oxidation with ketones or quinones having (n, π*) excited states but not with quinoid dyes (very weak n - π*) as their (π, π*) states cannot abstract H atoms.[17] The relative half-cell potential of the photocatalyst and substrate, is used to determine the possibility of redox activation step. Most of the synthetically useful photoredox reactions involve exothermic electron transfer, but there are some photoredox reactions that are too slow or endothermic in nature. Therefore, to overcome these limitations, a strategy that has been previously reported is the use of a compound that can undergo an electron transfer process with both, the catalyst, and the substrate in separate events, known as the co-catalyst or redox mediator.[18]

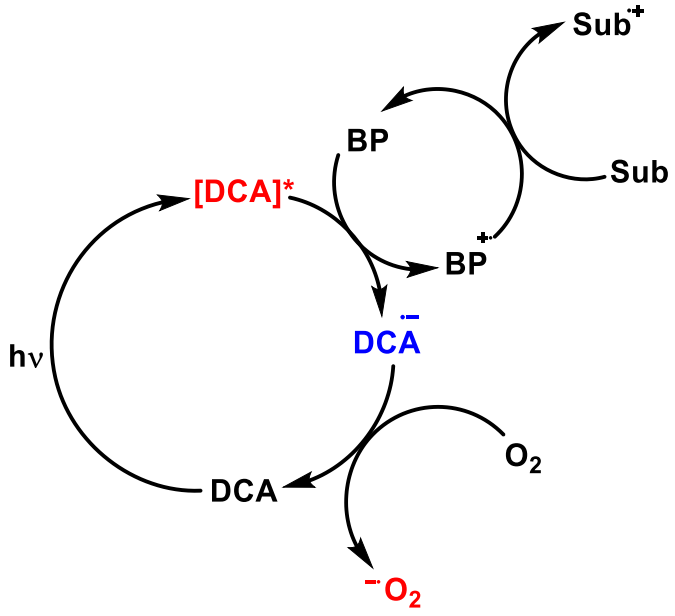
There are different mechanistic scenarios in which the use of redox mediator may increase the rate of redox process, among which are the transformations involving direct exothermic oxidation of the substrate by the photocatalyst, in which the inefficient rates of electron transfer result in a slow overall reaction.



Scheme 3: Dual-catalytic cycle for an oxidative transformation, where RM = redox mediator, PC = photocatalyst, and A = electron acceptor

In this case, the appropriate choice of a redox mediator involves the one that could react rapidly with both photo-excited catalyst (PC*) and the substrate. The use of which could mitigate the unfavourable kinetics of the direct electron-transfer process (Scheme 3).[18]

An example that clearly illustrates the potential of this method is the use of DCA/BP as the photocatalyst/redox mediator pair, which has been reported to improve the rate of photo-oxidation process compared to the unmediated ones.[19, 20] According to Foote[21] the success of this method lies on the fact that the photoinduced electron transfer process can proceed spontaneously if the electrode potential against SCE in acetonitrile is less than 2 V. At higher potentials the process require the use of biphenyl (BP) as cocatalyst because biphenyl can easily be oxidised than the substrate, and the radical cation ($BP^{+\cdot}$) produced is more stable than the excited catalyst (Scheme 4).[22]



Scheme 4: the dual-catalysis cycle for the pair DCA/BP electron transfer mechanism for the co-catalysis involving biphenyl in photo-oxidation processes.

The type II photo-oxidation process involves energy transfer from the excited photosensitiser to the ground state triple molecular oxygen leading to the production of singlet oxygen ($^1O_2$) and further reaction with reactive species. Here, the photo-excited sensitiser in presence of molecular oxygen, produces $^1O_2$ through the bimolecular energy transfer from the excited sensitiser to the ground state triplet molecular oxygen ($^3O_2$), a process that occurs during the collision between pairs of molecules.

The Jablonski diagram (Figure 2) describes the various transitions that can be undergone by the sensitiser. The absorption of a photon ($h\nu$) of light radiation by the photosensitiser causes transition from the ground state (S_0) to a singlet excited state (S_2), which relaxes to the lowest vibrational level of lowest excited state of the sensitiser S_1 through internal conversion (IC).

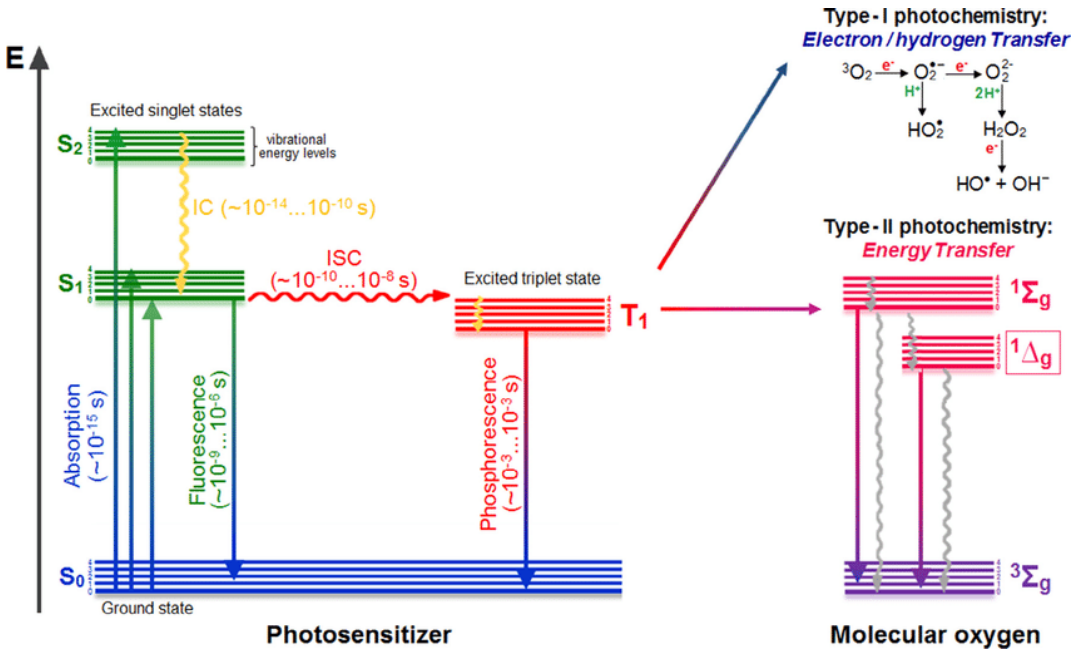


Figure 2: Jablonski diagram illustrating the generation of excited states of photosensitiser and triplet state photosensitized production of Singlet Oxygen. S; indicates discrete singlet states of the photosensitiser and T; indicates triplet states. IC and ISC denote internal conversion and intersystem crossing, respectively. Picture reproduced from J. Dabrowski et al. [23]

Intersystem crossing (ISC) of the S_1 of sensitiser generates the triplet state (T_1) with longer lifetime (μs) than that of the S_1 state (ns), allowing it to interact with molecular oxygen ($^3O_2$) through energy transfer which results in its excitation to its higher energy singlet state ($^1\Sigma_g$) a spin allowed transition. The $^1\Sigma_g$ has very short life span (ns) therefore relaxes rapidly to the lowest singlet state $^1\Delta_g$ with relatively longer life span (μs). [17, 23, 24]

Therefore, photo-oxidation processes involve the reaction of relatively stable $^1\Delta_g$, with the organic substrate, the lifetime of which is reportedly dependent on the reaction condition such as solvents, and temperature as described in the following sections.

1.1.1. PROPERTIES OF SINGLET OXYGEN: LIFETIME AND QUENCHING OF SINGLET OXYGEN

The lifetime of singlet oxygen depends on the extent of its interaction with other molecules in the surrounding, which range from > 1 hour in gas phase to microseconds (μs) in highly polar solvents. In the later, solvent molecules outnumber other substances present to a large extent and therefore, contribute actively to $^1O_2$ quenching or deactivation. Deactivation of $^1O_2$ can occur through either a radiative decay pathway accompanied by emission of light at a wavelength of 1270 nm or by a non-radiative decay that occurs by the transfer of electronic excitation energy into vibrational modes of the solvents. The extension of the quenching depends largely on the number of C-H and O-H bonds with high vibrational energy and hydrogen bonding ability and plays an important role in $^1O_2$ deactivation. Use of deuterated solvent is one of the techniques reportedly employed to increase the lifetime of $^1O_2$ through prevention of hydrogen bonding. [16, 25]

Because solvents molecules outnumber those of any other substance in solution. Solvents with high vibrational frequencies provide the most efficient relaxation. Thus, the lifetime is shortest in water (due to the -OH vibration near 3600 cm^{-1}), while solvents with -CH bond (-3000 cm^{-1}) are the next most efficient. Replacement of either -OH or -CH by deuterium decreases the quenching rate constant of the solvent. Lifetimes of 30-100 μs in organic solvents are typical, and the lifetime can reach several hundred microseconds in deuterated organic solvents, reaching lifetimes of >1 ms in solvents with neither hydrogens nor deuterium (Table 1).

Table 1: lifetime of singlet oxygen in various solvents.[26]

ENTRY	SOLVENT	LIFETIME (μS)
1	H_2O	3.1
2	D_2O	68
3	CH_3OH	9.5
4	Hexane	23.4
5	CH_2Cl_2	99
6	$CHCl_3$	229
7	$CDCl_3$	740
8	C_6H_6	30
9	C_6D_6	681
10	CH_3CN	77.1
11	CD_3CN	554
12	Toluene	27
13	Toluene-d_8	320

Finally, $^1O_2$ deactivation can occur by energy transfer to a suitable acceptor (Figure 3) based on the energy and momentum conservation rule. This process can take place for organic compounds with excitation energy less than that of $^1O_2$ - $^3O_2$ relaxation energy (< 22 kcal mol^{-1}), which is found in some organic molecules like β-carotene (E_T = 20 kcal mol^{-1}).[14]

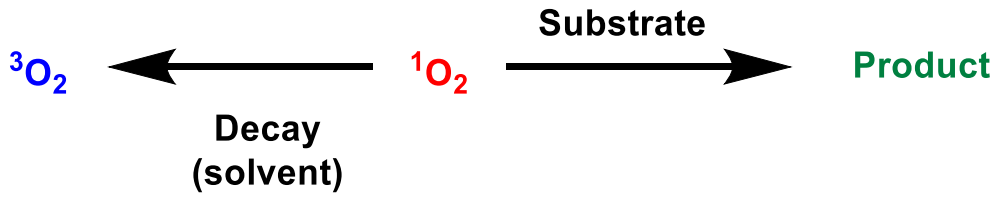


Figure 3: illustrating the competition between reaction and decay of singlet oxygen

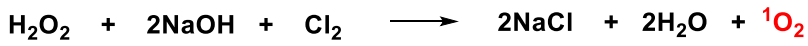
In the same way, molecules in as excited triplet state, like photosensitisers, are also reported to quench singlet oxygen by energy transfer, through the reverse process of its formation, especially at high concentrations.[25] Additionally, it has been reported that $^1O_2$ can also undergo self-quenching in potassium phosphate buffer of pH = 7.4 in acetone, saturated with oxygen (100 to 1400 μmol L^{-1}) in the presence of TPP. This singlet oxygen depopulation is believed to be predominantly caused by excited singlet state.[27]

The temperature is also a key factor in the quenching of triple oxygen, for instance the lifetime of singlet oxygen in D_2O decrease more than 10% when the temperature was raised to 37 ºC.[28]

1.1.2. METHODS FOR THE GENERATION OF SINGLET OXYGEN

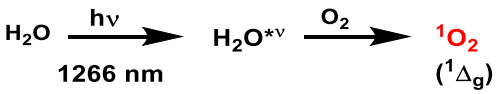
1.1.2.1 CHEMICALLY GENERATED SINGLET OXYGEN

Chemical sources of singlet oxygen are quite diverse, among the countless examples, a widely used and well-known method for the generation of $^1O_2$ is the reaction of NaOCl with H_2O_2 which gives rise to oxygen in nearly quantitative yield.[29] Other sources of singlet oxygen include the disproportionation of hydrogen peroxide (H_2O_2), this process involves reaction of hydrogen peroxide with hypochlorite generated *in situ*, by bubbling chlorine gas through alkaline hydrogen peroxide, the process can proceed with efficiency of up to 80 % (Scheme 5).[30]



Scheme 5: chemical generation of singlet oxygen through disproportionation of H_2O_2

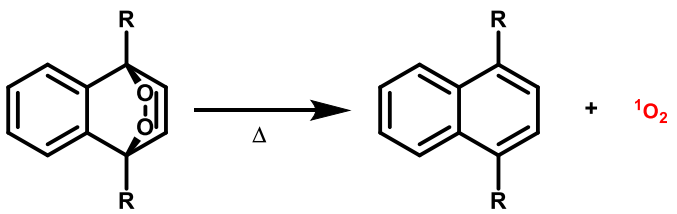
Singlet oxygen was reported to form through energy transfer from vibrationally excited water molecules, this was observed under high pressure of oxygen (15 MPa or less) on exposure to IR radiation at wavelength of 1266 nm and takes place according to the following Scheme 6.



Scheme 6: generation of singlet oxygen using vibrationally excited water.[31]

This was confirmed from the observed decomposition of tryptophan in H_2O but not in D_2O, which is because the efficiency of vibrational energy transfer from vibrationally excited H_2O to oxygen is greater than from vibrationally excited D_2O, because of the process of hydrogen bonding in the latter, that is why the singlet oxygen possess longer lifetime in D_2O than H_2O.[31]

One of the cleanest chemical methods of producing singlet $^1O_2$, that doesn't involve production of reactive oxidants is the decomposition of endoperoxides (particularly substituted naphthalene). These compounds undergo the reverse Diels-Alder reaction (Scheme 7) to give singlet $^1O_2$ and the aromatic compound in very high yields [14]



Scheme 7: Reverse Diels-Alder reaction for the generation of singlet oxygen

A drawback of chemical sources for preparative reactions is that many substrates do not trap singlet $^1O_2$ efficiently, therefore a large excess must be used to obtain appreciable substrate conversions, most especially for the naphthalene endoperoxides On the other hand, while many of the other sources use strong oxidizing agents, which can produce severe side reactions, chemical generation of singlet oxygen appears to be very useful for mechanistic purposes or where light is detrimental for the process.

1.1.2.2 PHOTO-GENERATED SINGLET OXYGEN

A photo-oxidation catalyst also known as photosensitiser can absorb radiant energy and transfer it electronically to molecular oxygen in its ground triplet state ($^3O_2$) which is then transformed into an excited singlet ($^1O_2$).[16, 32, 33] The choice of a photo-oxidation catalyst with high quantum efficiency to ensure efficient light harvesting is one of the crucial steps in scaling up the photo-chemical reactions, as it ensures the minimisation of energy usage and therefore efficient $^1O_2$ generation.

The triplet state of photosensitiser should have an energy of at least 94.2 $kJmol^{-1}$ (excitation energy of $^3O_2$ to $^1O_2$).[34] Therefore, an ideal photosensitiser should have the following properties:

i) high absorption coefficient in the spectral region of the light source,

ii) A triplet state of appropriate energy, enough for efficient transfer to the ground state oxygen.

iii) high quantum yield and long lifetime of the triplet state, and good stability after irradiation.

Generally, these compounds are highly coloured, consisting of many organic dyes, aromatic hydrocarbons, porphyrins and their derivatives, and transition metals complexes.[33, 34]

1.1.1.2.1 ORGANIC PHOTOCATALYST

- Porphyrins and derivatives

Porphyrin and its derivatives are naturally occurring intensely coloured macrocyclic compound with an unusual aromatic structure.[35] These compounds have received much attention for decades due to their extensive use as photosensitisers in photochemical conversions, catalysis, molecular semiconductors, solar energy storage,[33, 36, 37] and their presence in natural systems as part of haemoglobin,[38] and chlorophyll.[39]

The use of porphyrins in singlet oxygen generation has been known since 1930 when Kautsky first reported its generation by energy transfer from photo excited organic molecules to molecular oxygen,[35] since then a lot of work has been published and extensively reviewed.[14, 15, 18, 32, 35, 38, 40-42] Porphyrins have found application in the treatment against some types of cancer using photodynamic therapy (PDT). This novel approach is based on the localized $^1O_2$ generation in the presence of light.[33, 43] Their photophysical and, photochemical properties, influence their high $^1O_2$ quantum yields, especially the long live triplet state.[33, 44] The porphyrin structure consists of four pyrrole units attached through four methine bridges (=CH-), resulting into an extended π–conjugated system responsible for absorption of light in wide range of wavelengths in the visible and UV regions of the spectrum, with different intensities. [37, 38] Porphyrin and its well-known derivatives such as meso-tetraphenyl porphyrin (TPP), octaethylporphyrin (OEP) and *N-methyl pyridyl* substituted compounds l (Figure 4), can serve as the basis for the synthesis of many water-soluble porphyrins and metalloporphyrin through sulfonation, carboxylation, or alkylation. [33, 37]

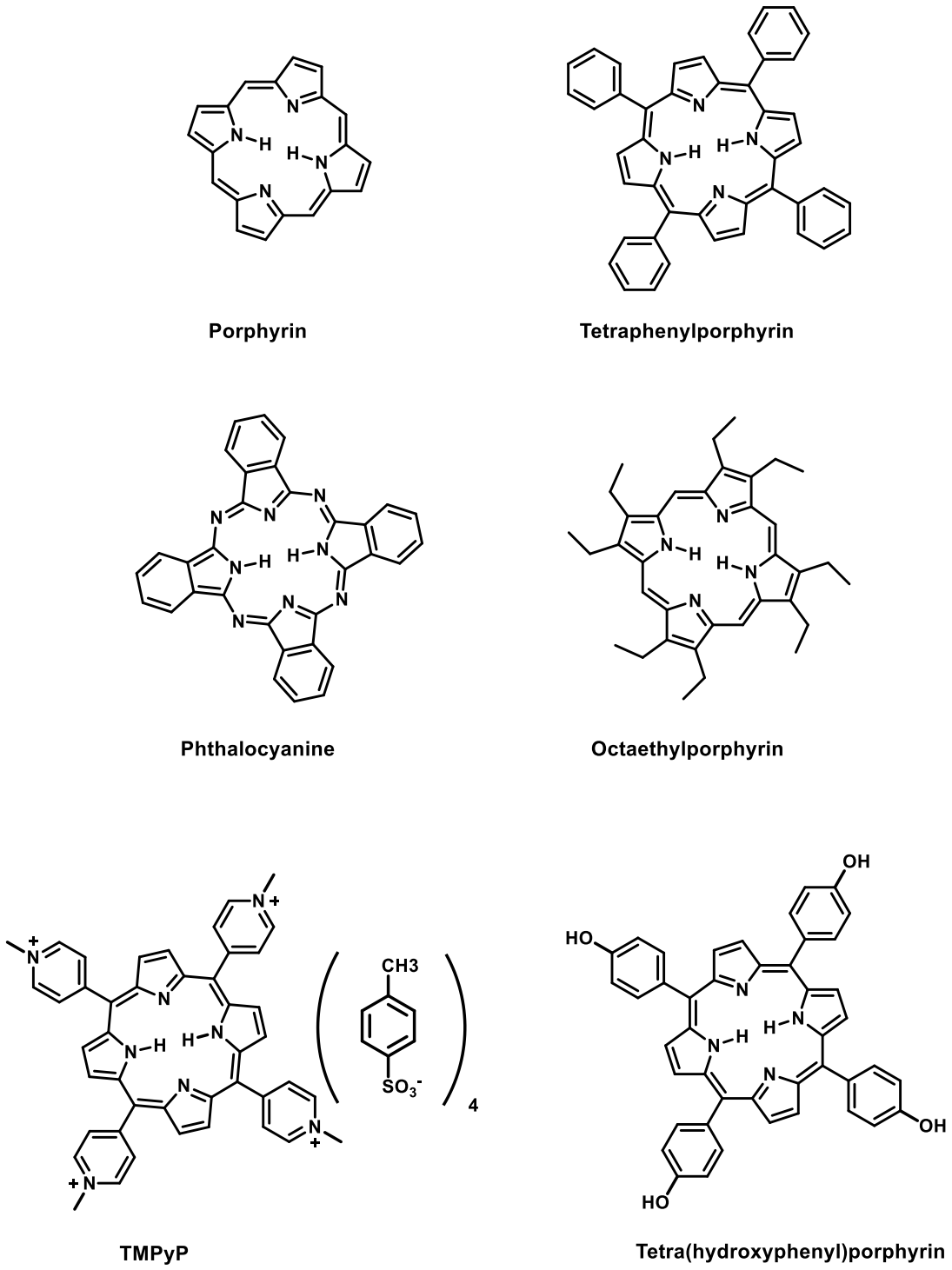


Figure 4: Commonly encountered porphyrins for application in photo-oxidation processes

TPP is a hydrophobic photosensitiser, with strong absorption maximum at 420 nm [44] and singlet oxygen quantum yield of 0.88 in chloroform and toluene.[45] It is the porphyrin of choice because its photophysical properties can be tuned by incorporating different substituents with electrons donating and withdrawing ability or metal atoms in the

porphyrin core thereby leading to water soluble metalloporphyrin with improved photophysical and photochemical properties. For example, water soluble GaTPP is characterised by appreciable photochemical stability and experiments have shown that this compound has high quantum yield of singlet oxygen generation measured to be in the range of 0.85 to 0.98 in most of the solvents.[46] Additionally in the presence of acids such as trifluoro acetic acid (TFA), it is protonated to H_4TPP causing the shift in its absorption maximum from 420 to 435 nm,[3] and possible improvement in its singlet oxygen quantum yield.[47]

However, under high concentration, TPP can undergo self-quenching resulting into a low yield of the product.[48] Moreover, Burgard *et al.* demonstrated that photo bleaching of TPP can cause the loss of its conjugation, thereby destroying its photophysical properties.[3] An important family of porphyrin derivatives are the phthalocyanines that constitute a class of intensely coloured macrocycles which differs from porphyrins by having nitrogen atoms linking the individual pyrrole units and extended conjugation created by the benzene ring attached to the edge of each pyrrole unit (Figure 4) influence light absorption at longer wavelength. Metallo phthalocyanines containing diamagnetic metal ions such as Cu^{2+} and Zn^{2+} are characterised by long lifetimes of triplet excited state and a relatively high quantum yield of 0.92 and 0.56 respectively, which are important characteristics of a good photosensitiser for singlet oxygen generation.[33, 49]

- Other Organic Photosensitisers

The ability of coloured substances to absorb visible light led to the investigation of the correlation between chemical structure of an organic substance and its colour, the process that resulted in the development of synthetic dyes having the system of conjugated double bonds. In 1876, Witt developed a theory concerning coloured organic compounds, which

states that a compound is coloured due to the presence of a chromophore group, a chemical system of conjugated double bonds, like those found in the organic dyes.[42]

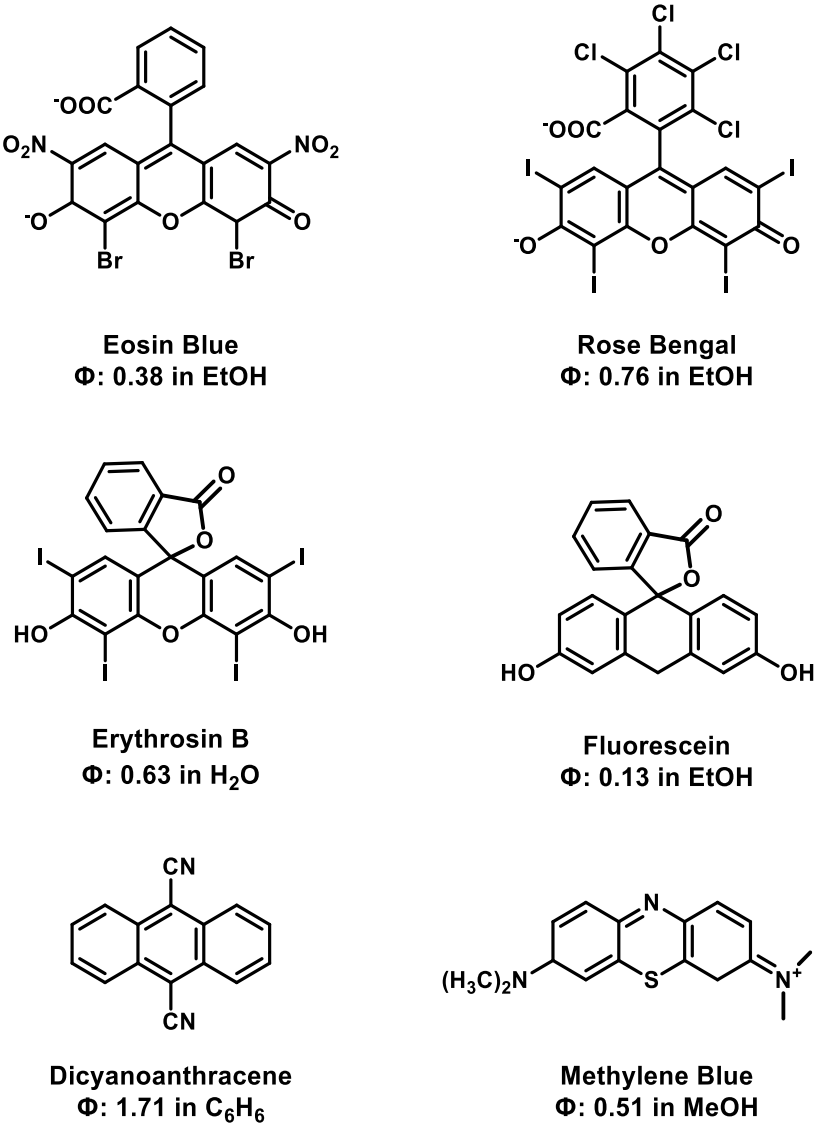


Figure 5: Some commonly used organic photosensitisers.[33]

Organic dyes such as rose bengal and methylene blue (Figure 5) are well known for their use as photosensitiser for singlet oxygen generation due to their triplet state that present appropriable energies. These dyes have strong absorption between 480-550 nm and 550-700nm, with a significant quantum yield (Φ) of 0.76 and 0.52, respectively.

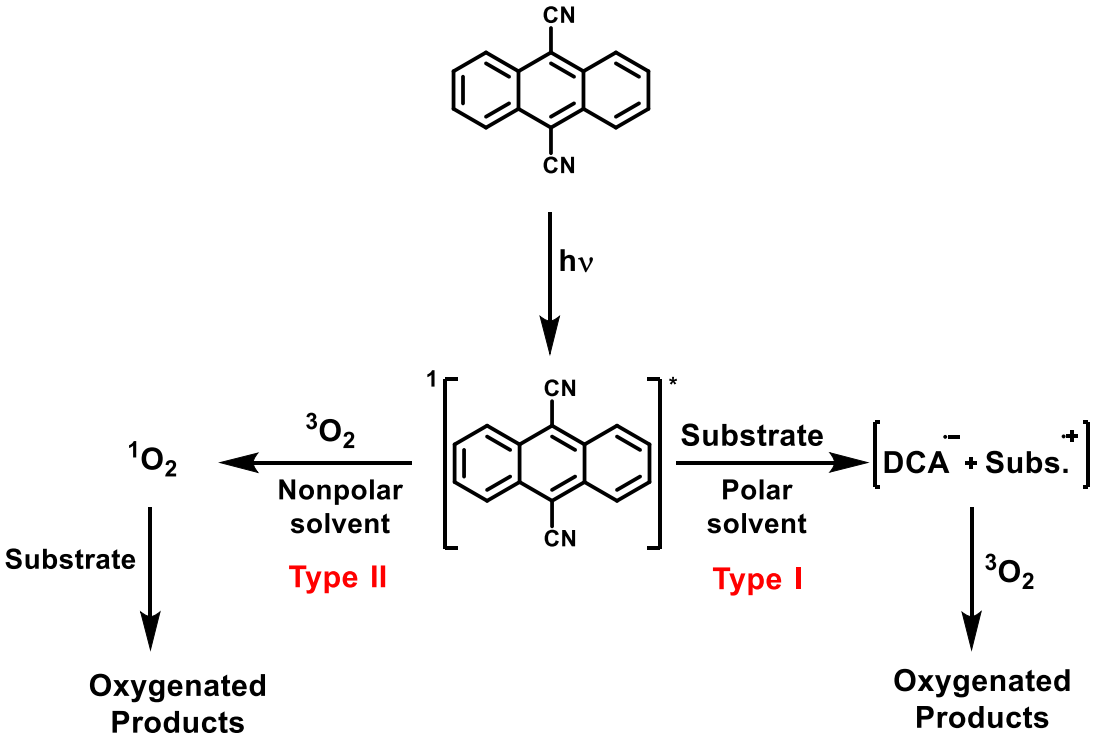
In xanthene dyes such as rose bengal and eosin blue there is a change in both quantum yield and absorption maximum with the increase in the atomic mass and number of halogens. The presence of heavier halogens increases the yield of intersystem crossing to the triplet state of the dye, thereby improving the efficiency of photosensitiser (Figure 5).[33] Other important aromatic frameworks such as naphthalenes, anthracenes, and biphenyls have also been studied due to their potential as photosensitisers in PDT, owing to their peculiar ability in the generation, storage and slow release of singlet oxygen to cancer cells.[41]

Cyano derivatives of anthracenes are well established photosensitizers, with wide applications for photo-induced oxidation, and electron transfer (PET) reactions.[21, 50] One of these important compounds is 9,10-dicyanoanthracene (DCA),[51] the properties of which have been extensively studied due to its broad applications, particularly due to its absorption of light at wavelengths longer than 400 nm.[21]

Its reactions can proceed either through energy transfer, particularly efficient with ground state oxygen, leading to formation of singlet oxygen ($^1O_2$) with quantum yields ranging from 1.46 to 2.06 in acetonitrile and 1.71 in benzene at an infinite oxygen concentration.[50] Or alternatively, through PET depending on the reactants, giving rise to redox reactions, during which in the presence of molecular oxygen ($^3O_2$), the superoxide radical anion is easily produced.[50, 52] Because of these properties, DCA and similar photosensitisers allow photo-oxidation of a large number of molecules under mild conditions in solution.[53]

The contribution of each of these mechanisms depends on the solvent polarity and nature of substrate. Regarding the solvent, the effect of solvent polarity on the DCA-sensitized reactions can serve as guide to the possible mechanism of a given transformation. Electron-transfer photo-oxygenation can occur predominantly in polar solvents, such as acetonitrile and methanol.[21, 54] This is due to the formation of an intermediate ion pair

which is too poorly solvated to diffuse apart in a non-polar solvent.[52] In contrast, singlet oxygen reactions show only a very limited response to changes in solvent polarity, which results for most of the DCA promoted photo-oxidation in non-polar solvents to occur via energy transfer mechanisms (Scheme 8).[52]



Scheme 8: Mechanism for the DCA catalysed Type I and II, photo-oxidation processes.[52]

1.1.1.2.2 Transition Metal Catalysis

Metal complexes of d–block elements absorb light due to electronic transition between d-orbitals of the metal or charge transfer within the complex. Charge transfer transitions can occur either by transfer of electron from the d-orbitals of the metal to the ligands or vice versa. The transition involving bonding ligands molecular orbitals and antibonding metals molecular orbitals are classified as the Ligand to Metal charge transfer (LMCT) transition, and they occur mostly when ligands can easily oxidise, and the metal can easily reduce. Metal to Ligand charge

transfer (MLCT) is found in complexes where the ligands have low-lying empty orbitals, the transition occurs between the non-bonding metal centred molecular orbitals and antibonding ligands centred molecular orbitals. MLCT are found in a situation where a metal is easily oxidised, and the ligand easily reduced. Several transition metal complexes (Figure 6) have been used in the photo-oxidation process due to their relatively high triplet energies and the long lifetimes of their triplet states.

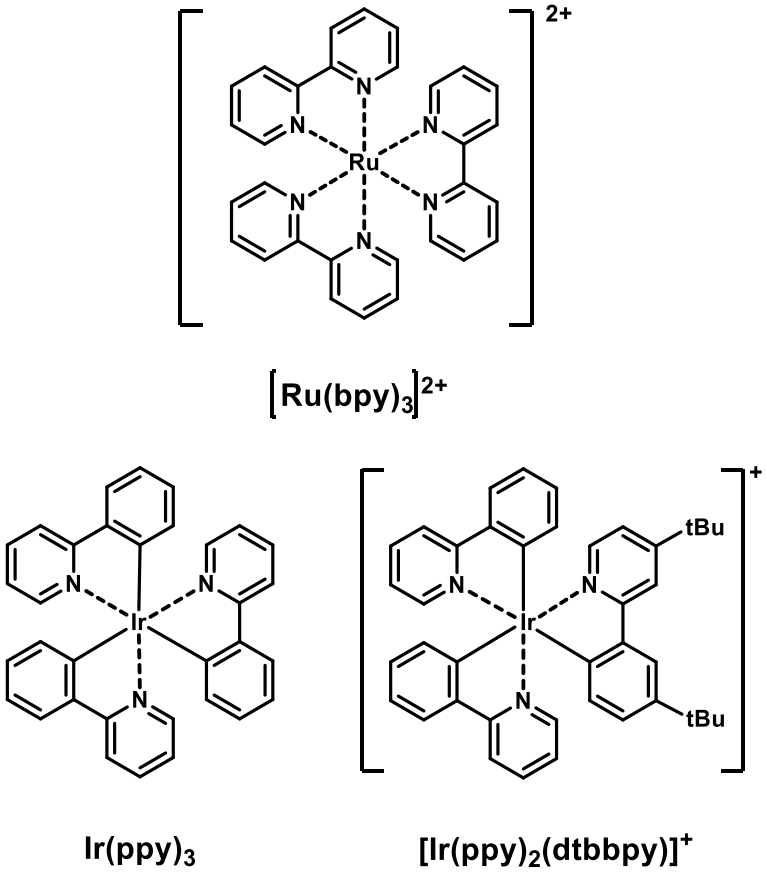


Figure 6: Structure of some common transition metals complexes.[55]

A common example of an MLCT is seen in ruthenium(II) trisbipyridyl complex $[Ru(bpy)_3]^{2+}$ (Figure 6) which upon photoexcitation, a d-electron is transferred from the ruthenium into the antibonding π*-orbitals of bipyridyl ligand where it becomes delocalised over extensive aromatic conjugation of the ligand. [55, 56]

The ruthenium and iridium based catalysts, in particular the tris-chelated complexes of Ru(II) with bidentate ligands 2,2'-bipyridyl or 1,10-phenanthroline, have been widely studied and utilized because of their outstanding photophysical and chemical properties. In ruthenium(II) trisbipyridyl complex $[Ru(bpy)_3]^{2+}$, Ru(II) has a d^6 system and the bipyridine ligands possess σ donor orbitals which are localized on the nitrogen atoms of the ligand, while the π donor and π* acceptor orbitals are delocalized on the aromatic rings. Because of this important structural arrangement these compounds can undergo both electron transfer and energy transfer transitions processes through absorption of light at room temperature. The energy transfer transition method involves single-electron transfer from a metal d orbital to the π* ligand orbitals, giving rise to MLCT excited states.[57] The entire photocatalytic process involving transition metal catalyst follows three steps: (1) the initial light absorption; (2) MLCT excited states and (3) quenching process.[58]

$$\underset{(d\pi)^6}{[Ru^{II}(bpy)_3]^{2+}} \xrightarrow{\text{light } (h\nu)} \underset{(d\pi)^5\,(\pi^*)^1}{[(bpy)_2Ru^{III}(bpy^{\bullet -})]^{2+*}}$$

Scheme 9: the photoinduced electron transfer process involving $[Ru(bpy)_3]^{2+}$ complex.[58]

Upon exposure to light, an electron of the Ru^{2+} is transferred from a d^{π} orbital of the metal to a low-lying π* orbital of the bipyridyl ligand (Scheme 9). The lowest ^{3}MLCT excited state of $[Ru^{II}(bpy)_3]^{2+}$ has a long half-life to interact with other molecules in solution even at low concentration and can serve either as energy donor, or electron acceptor. According to Meyer,[58] for an effective photocatalyst, the MLCT excited state should have several desirable features: (1) the excited state must be reached with efficiency after light absorption; (2) a long half-life that can last long enough to undergo chemical reaction; (3) good stability so that a catalytic cycle can form. Because of the MLCT excited

state of the complex depends on the energy of the π* orbital, its photophysical and electrochemical properties can be tuned by changing the electronic properties of the ligand of complexes.[57]

$$[Ru(bpy)_3]^{2+*} + Q \longrightarrow [Ru(bpy)_3]^{2+} + Q^* \text{ Energy transfer}$$

$$[Ru(bpy)_3]^{2+*} + Q \longrightarrow [Ru(bpy)_3]^{3+} + Q^- \text{ Oxidative quenching}$$

$$[Ru(bpy)_3]^{2+*} + Q \longrightarrow [Ru(bpy)_3]^{+} + Q^+ \text{ Reductive quenching}$$

Scheme 10: Quenching processes of $[Ru(bpy)_3]^{2+*}$, through either energy transfer of electron transfer processes.[57]

Lastly, the quenching processes can be used to sensitize other molecules that are not able to absorb light, or which can absorb light of higher energy (shorter wavelength), by either inducing chemical changes or energy state changes, thereby facilitating the process to occur with minimum energy consumption. The quenching processes are of great importance chemical processes, the two most important quenching processes are energy transfer and electron transfer (Scheme 10) where the latter includes the oxidation or the reduction of the excited state, namely oxidative quenching, or reductive quenching. In 1959 Paris and Brandt reported the first observation of fluorescence from $[Ru(bpy)_3]^{2+}$ since then, the complex has received much attention in research industry, with many of its photophysical and photochemical properties found to be attractive for application in both solar energy conversion and complex chemical synthesis.[59] These properties include; absorbance in the visible range (380 and 455 nm), good quantum yield, its chemical stability, long-lived excited-state originating from MLCT, and the favourable redox potentials in the excited state that can be fine-tuned by the adjacent ligands.[59-61] The quenching of the luminescence by oxygen results in generation of singlet oxygen ($^1O_2$).

In most of these reactions, the complex upon absorption of light is excited to $[Ru(bpy)_3]^{2+*}$ followed by reduction to Ru^+ in the presence of sacrificial electron donors

such as tertiary amines, the photo-catalyst serves as electron donor for different kinds of substrates.[61, 62] It was also reported to undergo both reductive or oxidative quenching depending on whether a reductant or an oxidant is present during photocatalytic reaction.[59, 63]

1.1.1.2.3 IMMOBILISED PHOTO-OXIDATION CATALYST SYSTEMS

Another approach designed to enhance the usefulness and recyclability of photosensitiser is through immobilisation. The process is considered because it removes the need for the separation of highly coloured dye sensitisers which often result in the loss of desired products. The process involved keeping both catalyst and substrate in different phases, which allows easier product isolation, purification, and the possibility of recycling the catalyst. This method has been demonstrated in the synthesis of various target compounds such as agrochemicals, pharmaceuticals and so on.[64] An illustrative example is the immobilised catalyst system of the $[Ru(bpy)_3]^{2+}$ on the Nafion-Silica system.[65]

Nafion® is an anionic perfluorinated polymer with sulfonate groups, it is an efficient ion exchange resin. exchanging its ions with catalyst through an electrostatic interaction which result in attraction of the catalyst molecules on its surface.

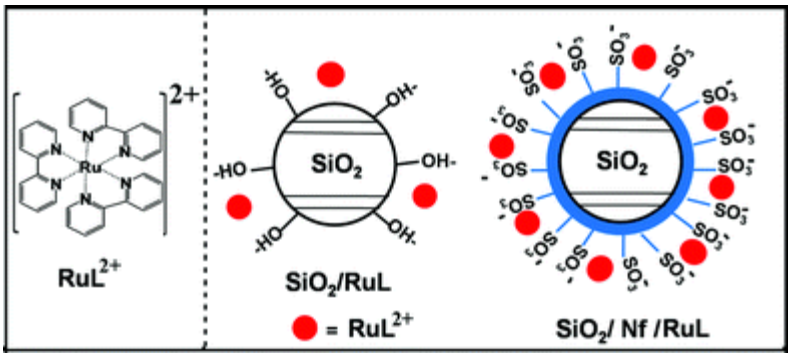
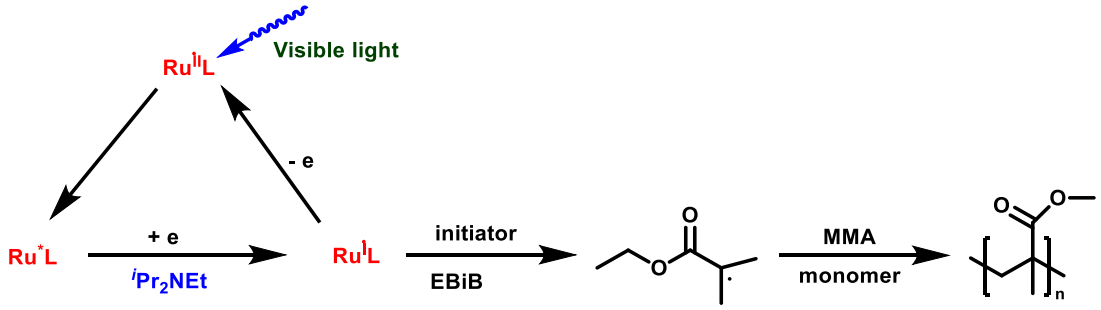


Figure 7: Illustration of immobilized ruthenium complex ($[Ru(bpy)_3]^{2+}$) on bare silica and Nafion® polymer coated silica support. [65]

Zhang and co-workers reported the immobilisation of $[Ru(bpy)_3]^{2+}$ on Silica and Nafion® supported Silica (Figure 7) and their use in the polymerisation of methacrylate using ethyl-α-bromoisobutyrate as an initiator and a household fluorescent lamp as the light source (Scheme 11). The proposed mechanism involves initial excitation of $Ru^{II}L$ confined on the Nafion surface to Ru*L through visible light absorption, upon reductive quenching by amine ($^{i}Pr_2NEt$) the excited catalyst is converted to powerful single electron reductant $Ru^{I}L$. Followed by removal of bromide from the initiator (EBiB) by the reductant, to generate a carbon centred radical species, finally the reductant ($Ru^{I}L$) is then oxidised to regenerate $Ru^{II}L$.[65]



Scheme 11: the reported proposed mechanism of free radical polymerisation of methyl methacrylate (MMA) through visible light photocatalysis using Nafion® coated immobilised ruthenium catalyst.[65]

The process requires simple immobilisation technique, the catalyst can be recycled for up to five times without significant leaching, especially for the Nafion supported catalyst and requires mild energy.[65]

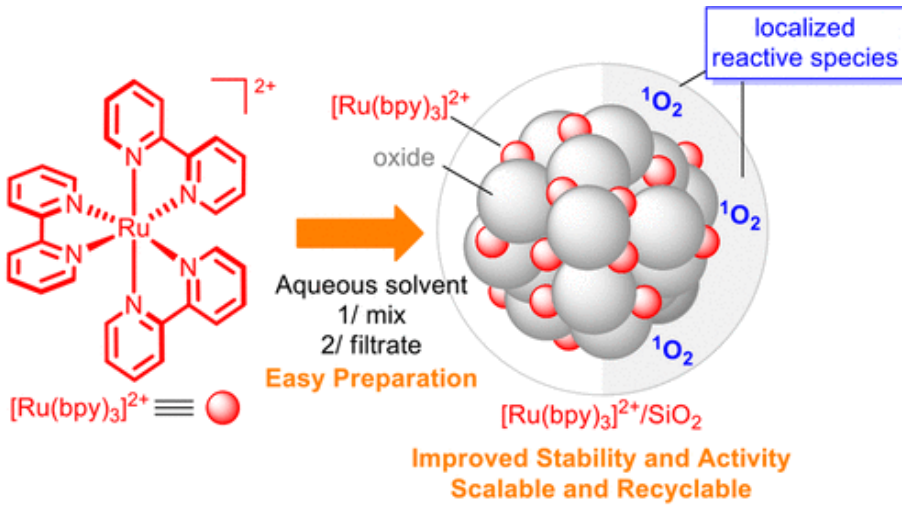
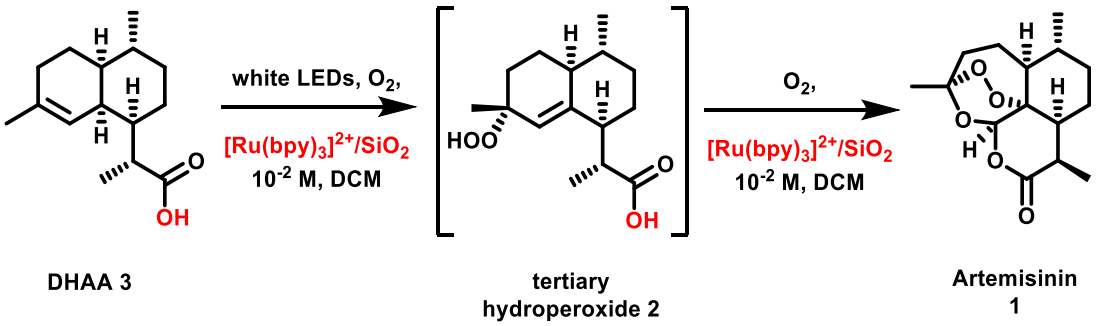


Figure 8: Illustration of immobilised ruthenium complex catalyst on silica gel.[66]

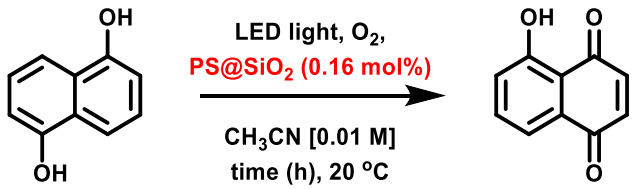
Immobilisation on the silica can be achieved through weak electrostatic interaction between the silanol group on the silica and the catalyst.[65] A straightforward catalyst immobilisation technique was reported by Tambosco *et al.* in which $[Ru(bpy)_3]Cl_2$ was supported on silica (Figure 8), the system demonstrated to serve a dual purpose in the synthesis of Artemisinin **1**, by facilitating both the photo-oxidation and the subsequent acid catalysed Hock–cleavage required to form the potent antimalarial compound (Scheme 12).[66]



Scheme 12*: one-pot synthesis of Artemisinin* ***1*** *using silica immobilised-*$[Ru(bpy)_3]^{2+}$ *catalysts system.*[66]

The same group has recently reported the use of immobilised $[Ru(bpy)_3]Cl_2$ and sulphonate salt of tetra(*N*-methylpyridinium-4-yl)porphyrin ion in a continuous flow set,

by trapping the silica supported catalyst system in a homemade cartridge using polytetrafluoroethylene (PTFE) tube, the system was applied to the synthesis of juglone from 1,5-dihydroxynapthalene (Scheme 13).[67]



Scheme 13: conversion of 1,5-DHN to juglone using silica immobilised [Ru(bpy)3]$^{2+}$ and TMPyP in a continuous flow reactor.[67]

Amara *et al.* recently demonstrated the use a simple immobilisation process involving the adsorption of TPP on the surface of Amberlyst–15 (Figure 9), enabling again a dual catalytic system with both photocatalytic and Brönsted acidic activity, the technique was employed to synthesise Artemisinin (**1**) using super critical carbon dioxide ($scCO_2$) as the reaction solvent in a high pressure continuous photochemical set-up with yields of up to 50 %.[2] The process has the advantage of removing the need to separate the photo-oxidation and acid mediated Hock – cleavage steps, which as reported earlier can lead to the formation of by-products. The TPP/Amberlyst – 15 system can easily be separated from the products and recycled with limited leaching.[2]

With the increasing interest in photochemistry, due to its experimentally simpler and more sustainable than the temperature-driven reactions, there is need to develop reactions that are potentially suitable for industrial uses.

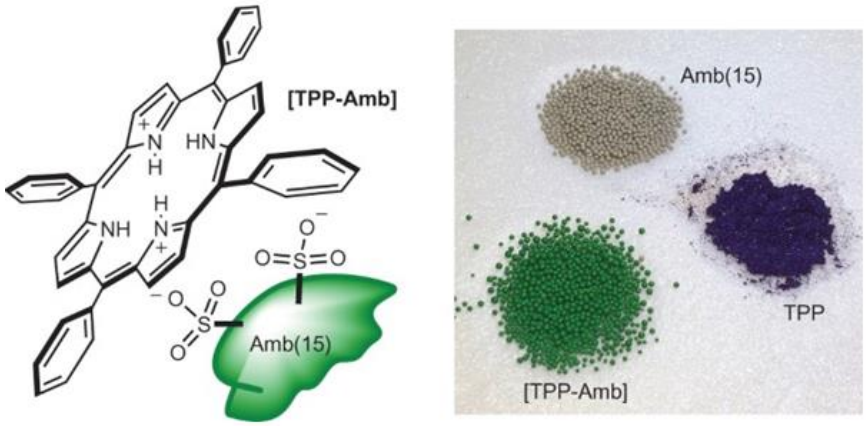


Figure 9: Amberlyst-15-supported TPP used for the synthesis of Artemisinin 1, in liquid CO_2, adapted from Amara et al.[2]

REACTORS FOR PHOTOCHEMICAL PROCESSES

Studies of photochemical reactions are of increasing interest, with the aim of improving the sustainability in production of chemicals through the adoption of greener methodologies. According to Alberto and co-workers every chemical reactor design must address the following requirement among other things that depend on its application; mode of operation (i.e. batch, continuous flow, or semi batch, and single or multiphase), geometry, flow rate, optimisation of temperature, pressure and catalyst loading, mixing, construction materials sustainability, control, safety, routine maintenance and control of other environmental factors.[68] However, for photochemical applications, other factors such as radiation source specification, spectral distribution and arrangement, and construction materials must be given special emphasis.[68] Based on the above requirements photo-oxidation reactors are broadly classified into three different categories depending on whether they are operated in batch, semi-continuously or continuously.

1.2.1. BATCH REACTORS FOR PHOTOCHEMICAL PROCESSES

The Batch reactors for photochemistry made through traditional designs include fixed reaction vessel and light source, with no continuous input of reactant or removal of

products during the reaction process. Some well-known batch reactors for photochemistry include immersion well and chamber reactors, for both of which the total reaction volume is often in millilitres in most laboratory settings.

The immersion well reactors are among the most efficient for photochemical reactions since the lamps are effectively surrounded by the solution to be irradiated. The lamps are contained in double-walled immersion wells with inner tube made of quartz, allowing water cooling and/or filtering of excitation radiation. Various flask designs enable reactions to be conducted under anaerobic conditions at low or constant temperature.[69]

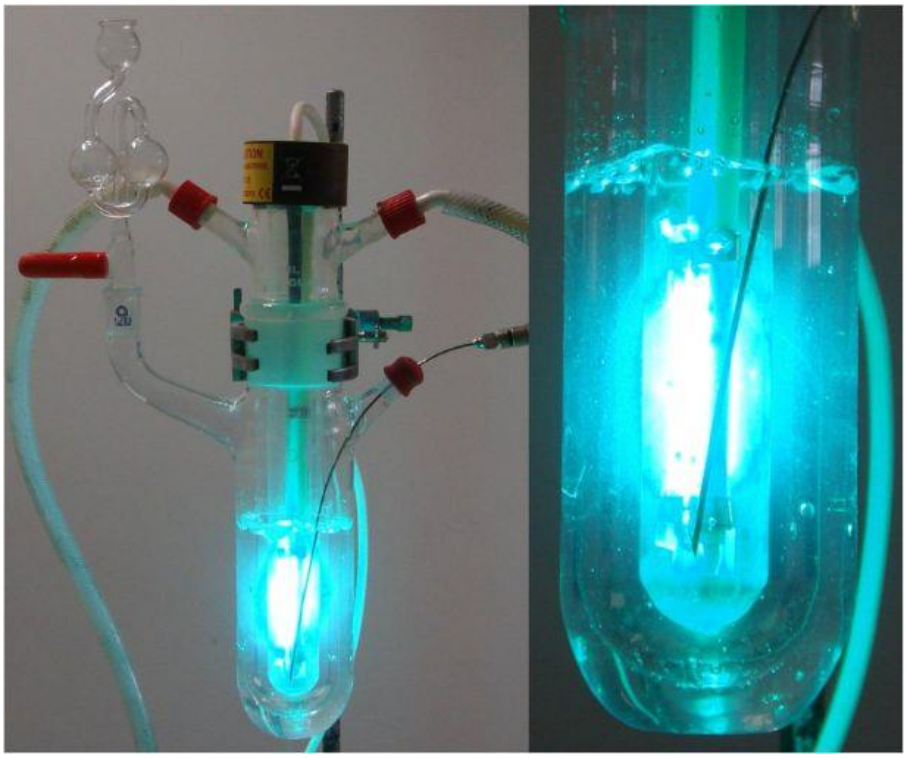


Figure 10: Immersion well reactor with 125 W medium pressure Hg lamp.[70]

The inlet and outlet tubes that provide air or water cooling are designed to accommodate a single low, medium, or high-pressure mercury lamp, and in some recent design light emitting diodes (LEDs), as the light source. A polytetrafluoroethylene (PTFE) tube

extends to the bottom of the annular space to allow coolant liquid to flow upwards from the bottom of the well. The space between the walls allows filtering of certain wavelengths with coolant liquids such as cobalt, nickel, copper sulphate, sodium nitrate solutions (Figure 10).

Batch photochemical reactors are ideal for early-stage research due to lower cost, ease of operation, reaction monitoring and ease of optimization. It was recently demonstrated that, the problem of over irradiation which often occur in a batch photochemical setup can be avoided through careful matching of the power of the lamp with a concentration of substrate. For example for batch reactor using a 400 W lamps and 400 mL volume, immersion wells are well suited for reactions up to 10 - 15 g scales, and in some cases, even larger.[71] In 2013, a photo-oxidation process involving generation of singlet oxygen was successfully scaled-up using batch reactor by Sanofi, this reactor was used for the synthesis of important anti malaria drug Artemisinin, with the capacity of producing 60 tons of Artemisinin per annum, with average size of 370 kg of isolated Artemisinin per batch (Figure 11).[1]

Despite countless efforts being made on the developments and optimisation of photochemical batch reactors, the major drawback in their applications for photochemistry include limitations for the light penetration, which according to Beer-Lambert law depend on the concentration and path-length, although reducing the concentration can improve light absorbance and hence the reaction rate, batch photochemical reactions are mostly suited for laboratory scale reaction and often difficult for scale-up in an industrial applications.[72]



Figure 11*: Batch reactor designed by Sanofi for the industrial production of Artemisinin* ***1****, copied.*[1]

Other limitations include mass transfer of gaseous reactants such as oxygen due to poor mixing, the danger of explosion at high pressures, inefficient control of temperature and difficulty in automation due to frequently encountered problems such as over-irradiation, formation of polymer deposit (reactor fouling), and degradation under strong UV irradiation.[73, 74] To address the limitations encountered in using batch reactors, many continuous or semi-continuous reactor designs have been developed.**SEMI-CONTINUOUS REACTORS FOR PHOTOCHEMICAL PROCESSES**

Semicontinuous reactors, also called semi-batch reactors, are used for small scale operations, such as testing new procedures in process development engineering. For example, they are used to manufacture expensive products, for processes that are difficult to be converted to continuous operation, and those that require a tight control of operating parameters and the minimization of unwanted side reactions by means of reactant concentration manipulation. They are also used when multiphase reactions are

being carried out, such as the continuous bubbling of a gaseous reactant in a liquid medium.[75]

Semi-continuous processes involved two basic types of operations; the first type of semi-continuous process involves slow addition of a reactant into a reactor containing another reactant which has been loaded prior to the beginning of the reaction run. Several tactics of addition of the reactants can be applied, as well as different set-ups. The reactant can be added continuously at a constant rate as the reaction proceeds or fed in a varying rate sequence as a function of time. This approach is used mainly when unwanted side reactions are to be avoided, or when the reactions involved are highly exothermic[75]

In the second type, both reactants are charged simultaneously and one of the products is continuously withdrawn to shift equilibrium toward the products formation. In this case higher conversions are often achieved with improved productivity.

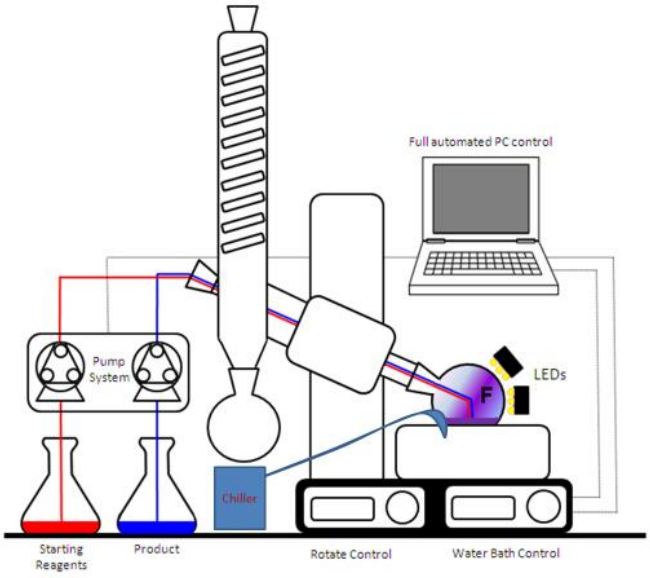


Figure 12: Schematic diagram showing the general setup LEDs PhotoVap.

One of the reported photochemical reactor designs that operates in a semi-continuous mode is the PhotoVap reactor; a modified rotary evaporator that can operate in both batch and semi continuous modes using a variety of different size flasks. Thin Polytetrafluoroethylene (PTFE) tubes thread through the neck of the rotating flasks to

convey reactants in both gaseous and solution phase into and out of the reactor with the aid of peristaltic pumps as shown in the Figure 12.[5, 76]

In the PhotoVap, the semi-continuous mode is based on running series of sequential batches, automatically controlled by a micro controller linked to a computer using an Arduino Uno which controls the filling and emptying of reactants at pre-set flow rates and time interval and switching on and off the reactor. The Controller is also set to control the rotation of the flask at 175 rpm. This rotation speed has been reported to generate a thin film of *ca.* 260 μm,[76] that allows maximum penetration of light in the solution from the high-power LEDs. This reactor has advantages of efficient gas-liquid mass transport, easy temperature control using cooling bath and potential of scale-up by simply changing the size of the flask. This reactor has shown excellent results when converting 1,4,4a,8a-tetrahydro-1,4-methanonaphthalene-5,8-dione to Cookson's dione with a productivity of up to 210.6 g h^{-1}. [5, 76]

1.2.3. CONTINUOUS FLOW REACTORS FOR PHOTOCHEMICAL PROCESSES

The principle of continuous flow reactor operation involves uninterrupted flow of reacting materials into the reactor and stream of the products out of the reactor, with the aid of narrow tubes. In photochemical applications these tubes are made up of transparent polymer materials such as FEP or PTFE. In these reactors the reagents are combined at the inlet set at reaction conditions, like in widely reported plug flow reactors (PFR) which operate under plug flow approximation. The continuous flow systems for photochemical reactions used generally the same approached as those reported for batch and semi-continuous reactors. With the overall aims toward meeting the growing need for large scale production of important compounds such as API (active pharmaceutical ingredient), through greener and sustainable approach using light. Continuous flow

processes often demonstrated to occur with enhanced penetration of light, better mixing (especially for heterogeneous systems), improved heat and mass transfer, as well as shorter residence (and reaction) times. Limited residence time is important particularly for photochemical processes, in which short residence time minimises the possibilities of over irradiation, which results in decomposition of products or reactants and consequently lower the overall yield of desired products.[77, 78]

To address these problems various reactors design evolved for decades with the following characteristic features: the thin film generation in narrow annular gap, between two transparent cylinders for efficient light penetration.[71] Rotation of flask of different sizes containing certain volumes of solutions at different speed to effectively generate thin film for photochemistry.[5, 76] Generation of Taylor vortices using rotating cylinders at very high speed enable excellent gas – liquid interaction, with effective light penetration in an annular gap between rotating (inner) and static outer cylinders.[79] Also, the use of very narrow and transparent micro[80-82] and macro tubing provides enabling environment with efficient light penetration for photochemistry and ease of scale-up.[83, 84] This was demonstrated by Seeberger *et al.* in the design of a continuous flow reactor, which was used to perform low temperature photo-oxidation to access Artemisinin **1**, using dihydroartemisinic acid **3** as the precursor.

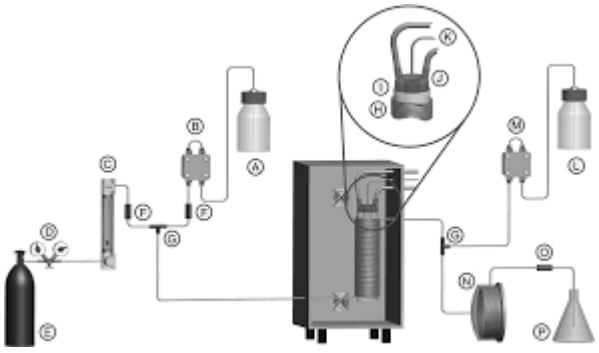


*Figure 13: Design of Seeberger and his co-workers continuous-flow setup for the synthesis of Artemisinin **1**, reproduced.*[83]

Figure 13 is the schematic diagram of Seeberger and his co-workers continuous flow reactor, the reactor can potentially provide higher productivity of **1** more efficiently than Sanofi's batch reactor, because of its smaller size with projected capacity of 1-tonne of Artemisinin **1** per annum.[85] The major challenges of continuous flow photo-oxidation process is large-scale generation of singlet oxygen, at elevated pressure of oxygen gas.

- Microfluidic reactors

Microfluidic reactors usually consist of a solid support with a network of channels, the scale of which are typically in the range of 100s of micrometres in width and depth. The overall size can reach up to several centimetres in length, with the width and depth depending on the configuration. These reactors have become increasingly popular in research, and analytical applications, particularly in photochemical transformations, where they are equipped with miniaturised light-sources. With this development, several commercially available microreactors have been commonly adopted for photochemical applications, which include among others, the serpentine channel, glass microchip,[86] triple channel,[80] micro-capillary film[81] and falling film reactors.[87-89]

The serpentine microreactor is designed with long path length ranging from several centimetres to meters, thereby increasing the residence time of the reactants. For example, the dwell glass manufactured by mikroglas has total path length of 1.15 m (20 turns) on a 118 mm x 73 mm aperture (Figure 14a).[69, 73, 90]

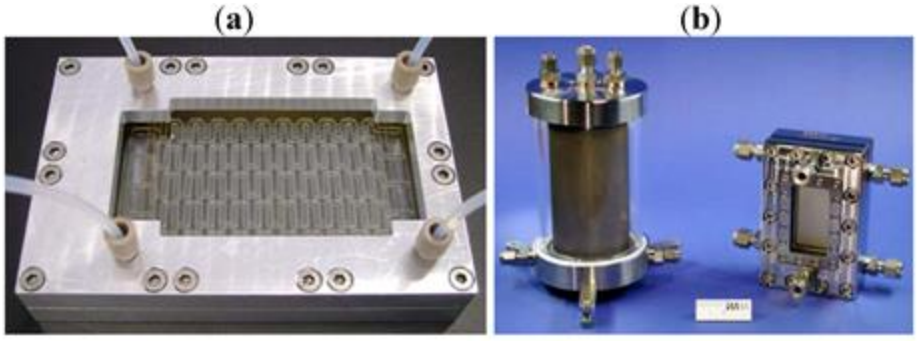
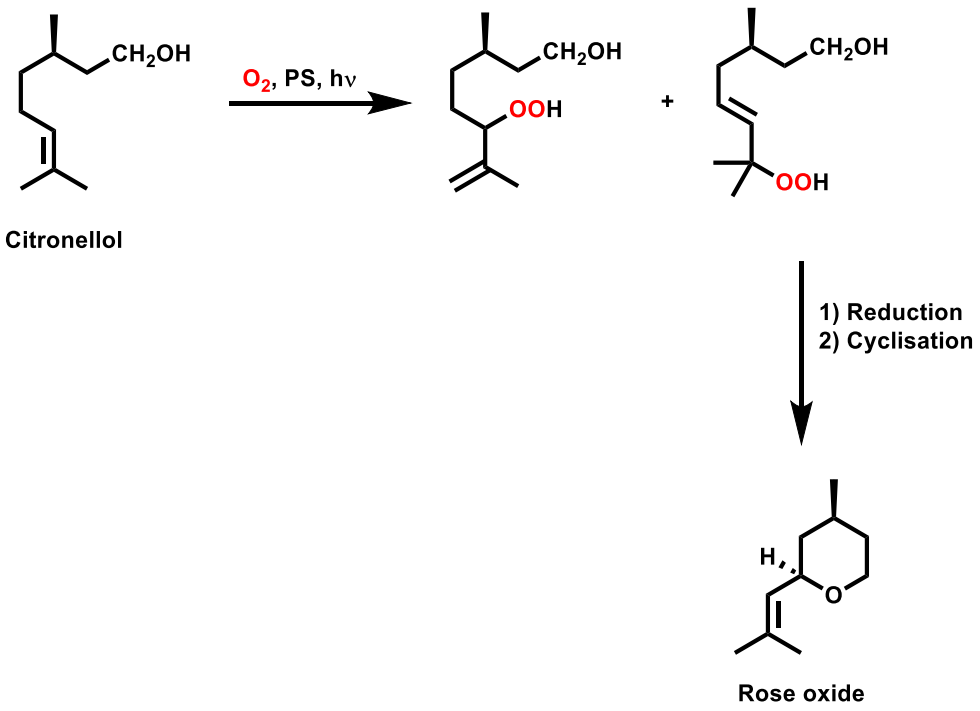


Figure 14*: the pictures of (a) serpentine and (b) falling film micro reactors, reproduced from.*[90]

A falling film microreactor is beneficial for gas-liquid photochemical reaction in which thin films are generated by gravity force in parallel micro-structured channels. In reactions such as oxidation and hydrogenation the high specific interfacial area of up to 20 000 m^2/m^3 results in sufficient saturation of the film with reactant gas (Figure 14b), these reactors consist of a temperature controlled heat exchanger and a pumping system that controls the flow rate of the reactants and products. These flow operations can prevent or drastically reduce the side reaction or decomposition caused by over-irradiation.[69, 90]

The application of these reactors as photo-oxidation devices has been widely exploited, employing different strategies with the aims of improving the productivity of commercially important compounds in a sustainable and economical ways.[91] Susann and co-workers compared the productivity of batch Schlenk-reactor and microfluid reactor with volumes of 40 mL and 0.27 mL respectively, in the photosensitised oxidation of citronellol to commercially important fragrance Rose Oxide (Scheme 14). From the space time yield (STY) analysis of each reactor it appears that after 20 minutes of reaction the STY is about one order of magnitude higher in a microreactor than in a batch Schlenk-reactor.[69]



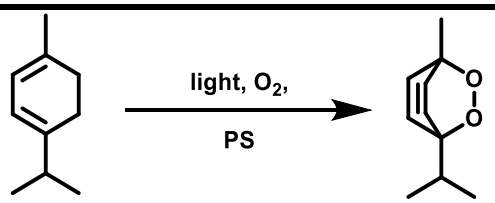
Scheme 14: synthesis of Rose Oxide from photo-oxidation of citronellol in serpentine microreactor [69]

Another widely exploited model photo-oxidation process in microfluidic reactors is the synthesis of Ascaridole from α-terpinene employing different sensitisers, as shown in the *Table 2*, which shows improved product yield using different design of microfluidic reactors compared to the more traditional batch reactors.

These applications of singlet oxygen mediated photo-oxidation in microfluidic reactors have been extensively reviewed, with the aim of exploiting advantages such as productivity, use of minimum amount of oxygen gas thus reducing risk of explosion, and improved throughput over traditional batch reactors. Although photo-microfluidic reactors are considered to have better light penetration, one of the major challenges in their design is the mass transfer of oxygen gas, which is achieved through premixing oxygen with the solution before the mixture is passed to the irradiation chamber. However, in other designs oxygen is introduced by diffusion through a permeable

membrane of the tube containing the solution at specific flow rate, with the rate of formation of products depending strongly on partial pressure of oxygen gas.[80-82]

Table 2: Some reported results for the synthesis of Ascaridole from a-terpinene in different micro-reactors



α-terpinene ascaridole

Entry	Yield (%)	Catalyst	Reactor	Time	STY	ref.
1	85	Rose Bengal	Glass microchip	4 hours	-	Wootton *et al.* 2002[86]
2	53	Fullerene (60)	Microflow	50 sec.	54 sec.	Carofiglio *et al.* 2008[92]
3	91	Methylene Blue	Triple channel Microreactor	1 min	99 times >batch	Park *et al.* 2011[80]
4	90	Rose Bengal	Microcapillary Film	14 min	20 times >batch	Elvira *et al.* 2013[81]
5	92	Rose Bengal	Microflow	-	6 mL/min	Ziegenbalg *et al.* 2014[82]

In these reactors scale-up can be achieved by increasing the length and volume of the tubing which results in an increase in the residence time and time of irradiation, or by increasing the flow rate. Another straightforward scale-up method is through numbering-up approach in which several capillary micro-reactors are connected in parallel and incorporating individual lamps, achieving stable gas-liquid flow distribution over several photoreactors and often with improved product yield.[73, 74, 90]

- Taylor-Couette flow reactors

The operation of a Taylor vortex reactor is based on laminar flow between two concentric cylindrical surfaces where one or both surfaces are rotating about the other. Initial slow rotation generates Couette flow, and increasing the rotation speed result into an unstable flow during which the angular velocity exceeds a critical value and a steady axisymmetric

secondary flow in form of regularly spaced toroidal vortices are generated, the process known as Taylor – Couette flow (Figure 15).[79]

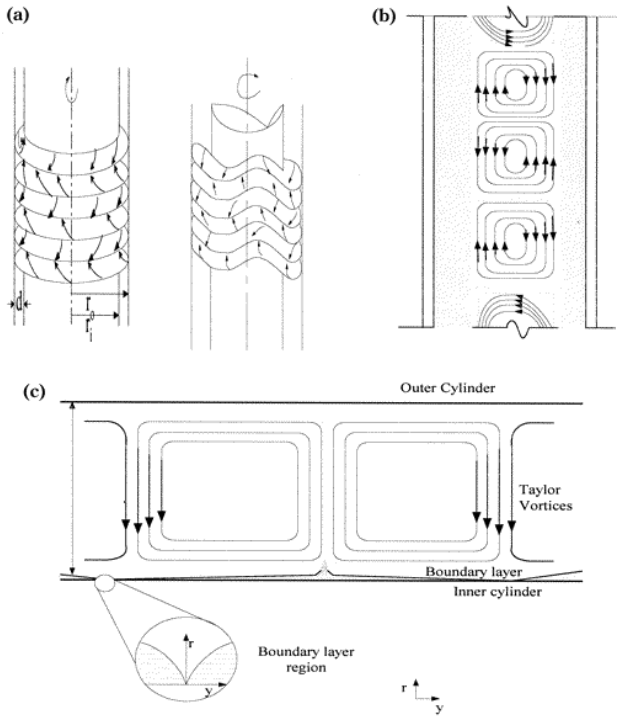


Figure 15: (a) Vortices without and with circumferential waves, (b) schematic presentation of streamlines in vortical cells, and (c) radial mass transfer in Taylor–Couette flow. [93]

This fluid dynamic flow property gave rise to the Taylor-Couette reactor, referred to as vortex flow reactor, developed over 30 years,[93-95] consisting of two concentric cylinders with the most reported configurations the outer one is fixed while the inner one is rotating.[95] This technology was applied to heterogeneous photocatalytic water purification through recirculation of fluid continually between the annular gap of rotating inner cylinder surface and the stationary outer one in which the catalyst is immobilised on the surface of the inner rotating cylinder, thereby allowing efficient mass transport of the pollutant to the catalyst bed, through development of wavy vortex flow in the laminar-flow arrangement and ensuring good transfer of a fluid between neighbouring vortices in a cyclic fashion.[93] An efficient vortex reactor for continuous photochemistry was developed recently in our group, combining the key features of the previous vortex

reactors which includes, the use of a transparent outer tube, gas liquid interaction and drawing air into the reactor from the surrounding and coupled with the use of modern high powered LED as light source giving rise to an efficient photo-oxidation reactor.[5, 79, 93, 94]

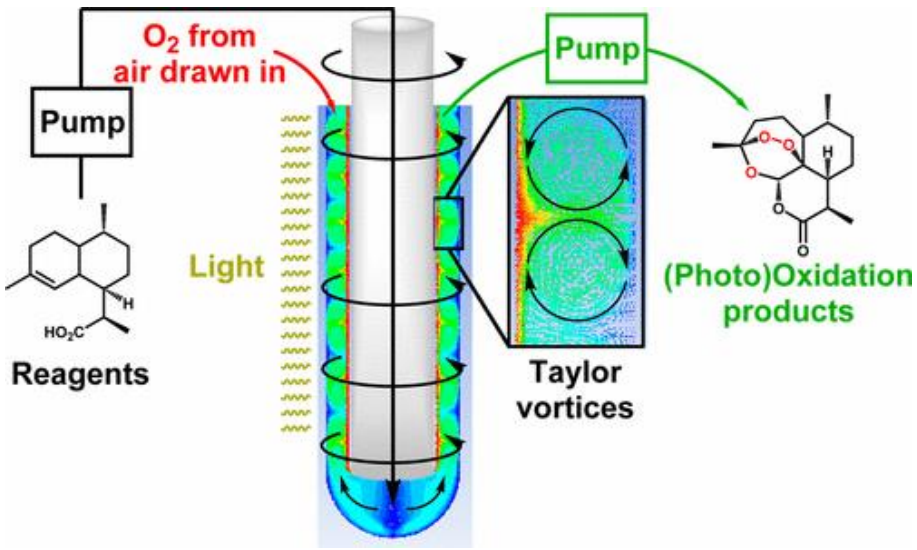


Figure 16: Diagram of Vortex reactor showing the direction of fluid flow, and its application in the synthesis of Artemisinin using air drawn from the laboratory. [79]

The reactor consists of a stationary outer tube and rotating inner tube, fluid is continuously introduced from a central tube within the rotating tube and exits the reactor from top edge of the annular gap. Air is sucked into the reactor from the free surface at the top of the annular gap when the inner tube is rotating due a negative pressure that is generated near the inner rotating surface by the centrifugal force in the rotating fluid region ensuring good fluid-gas mixing (Figure 16).

A speed-controlled motor drives the inner tube through a belt at the top of the test section, the rotating speed of the inner tube can be controlled continuously from 0 to 4000 rpm, this rotation speed is also directly related to the amount of oxygen drown from the surrounding. The inner shaft was also designed to be rotationally stable at the operating speeds and it only operates at about 10 % of the critical rotational speed.[79] The

reactor was successively applied for the synthesis of important antimalarial drug; artemisinin through photochemical generation of singlet oxygen using air drawn from the laboratory.[79]

For the industrially interesting photo-oxidation processes, the kilogram scale vortex reactor has been developed, and it has shown to be promising in the continuous photo-oxidation of Citronellol with the achieved scale-up of over 300X with a visible light in the presence of oxygen, and 10X with a UV-induced [2+2] cycloaddition of Cookson's dione to produce diketone with productivity of 7.45 kg/day (Figure 17).[96]

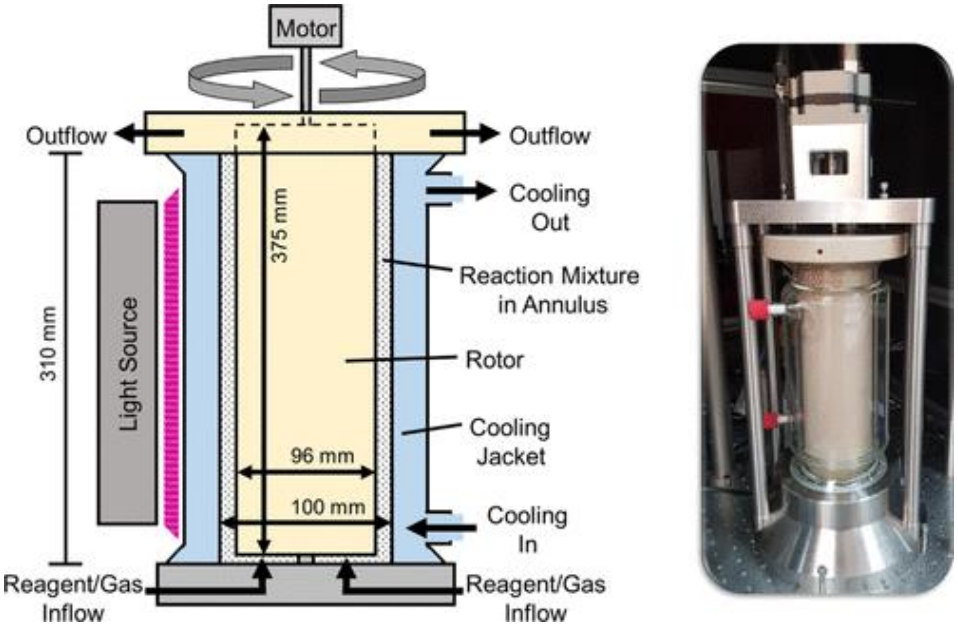
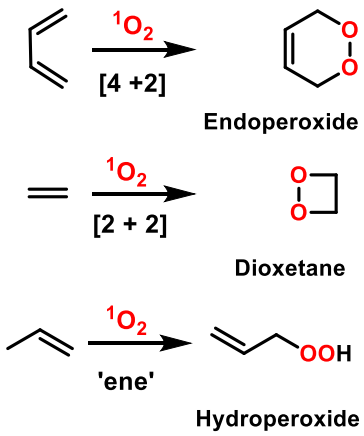


Figure 17: cross section of large vortex reactor showing key dimensions of the glassware and rotor.[96]

2.3.1. EXAMPLES OF REACTIONS PERFORMED BY SINGLET OXYGEN

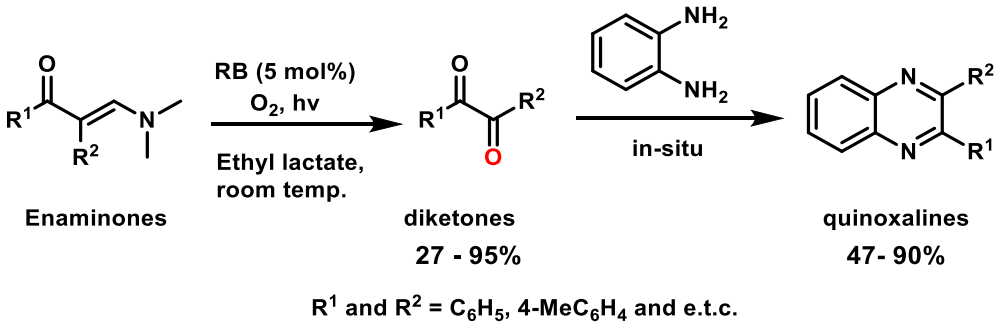
For decades various reviews has been published regarding the generation, and the synthetic and non-synthetic uses of $^1O_2$.[25, 34, 30] The reactions of $^1O_2$ following type II photo-oxidation mechanism includes; cycloadditions [4+2] and [2+2] of $^1O_2$, and ene reaction (Schenk reaction)(Scheme 15).[97] In ene-reactions $^1O_2$ reacts with allylic hydrogen

atoms to form allylic hydroperoxides, for asymmetrically substituted olefins, hydrogen abstraction by $^1O_2$ takes place preferentially at the most substituted carbon of the double bond (*cis* effect).[98]



Scheme 15*: Example of type II photo-oxidation reactions*

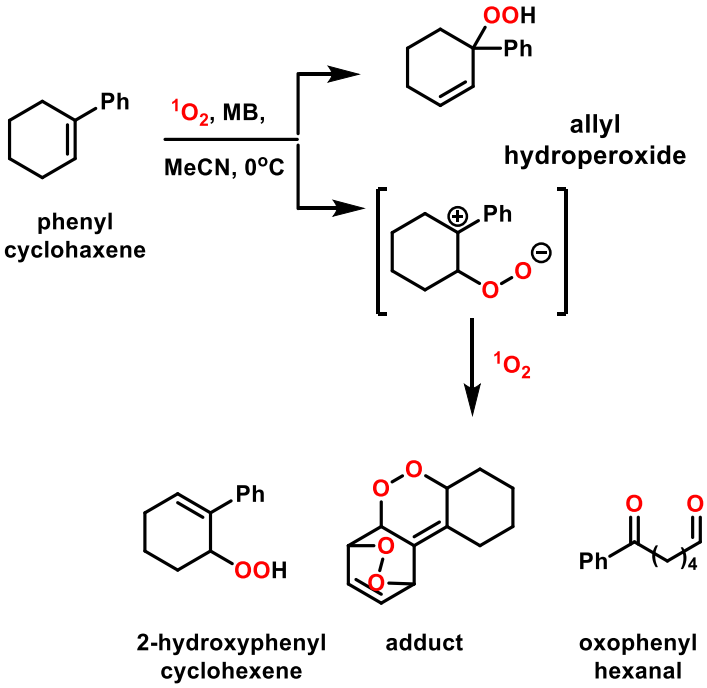
Cao and co-workers reported the $^1O_2$ mediated double bond cleavage of enaminones under ambient conditions using dilute solution of rose bengal (RB) (1.5 x 10^{-5} M) as photosensitiser under visible light to produce 1,2-diketones, which serve as *in-situ* precursors for the synthesis of quinoxalines through one-pot process (Scheme 16).[99, 100]



Scheme 16: Synthesis of 1,2-diketones via singlet oxygen mediated C=C bond cleavage of enaminones.

However, RB aggregates at high concentration (> 5.0 x 10^{-5} M) which impair its photochemical response and undergoes degradation in solution caused by the presence of singlet oxygen ($^1O_2$), which limits its application in photo-oxidation processes.[33, 101, 102]

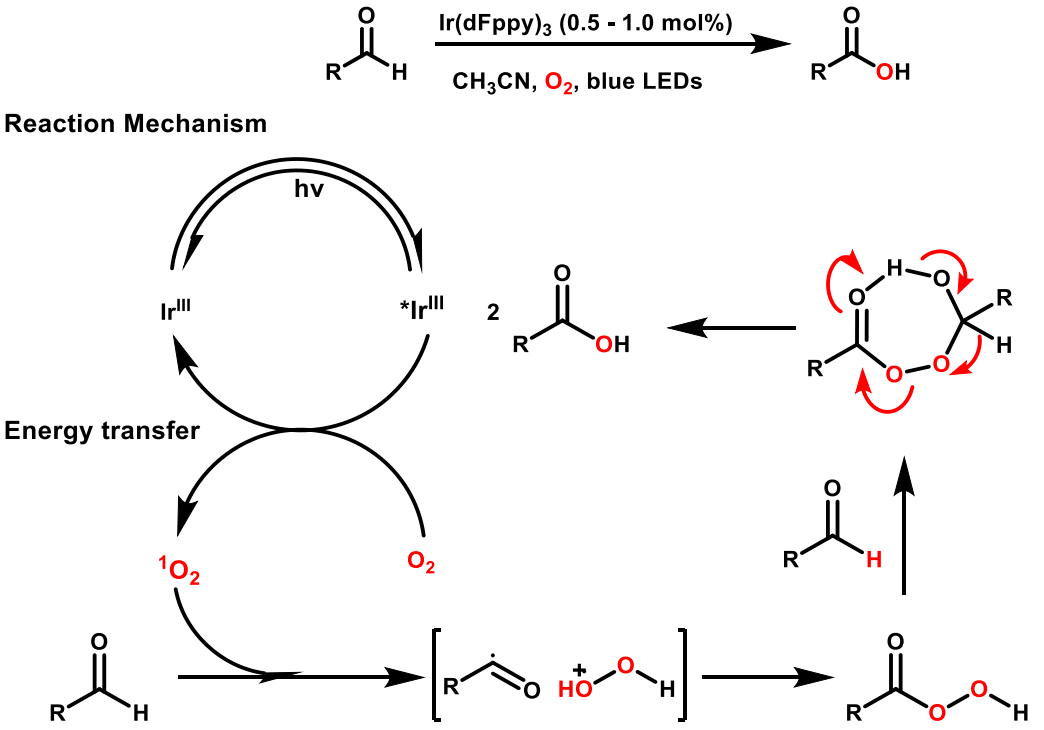
Methylene blue (MB) was recently reported to sensitise the photo-oxygenation of 1-aryl-1-cyclohexenes with $^1O_2$ generated through ene-reaction under continuous flow conditions, the resulting allyl hydroperoxide intermediate enable various functionalisation to alcohols, carbonyls, epoxides, triols etc.[103]



Scheme 17: Isolated products of the photo-oxygenation of phenylcyclohexene.[103]

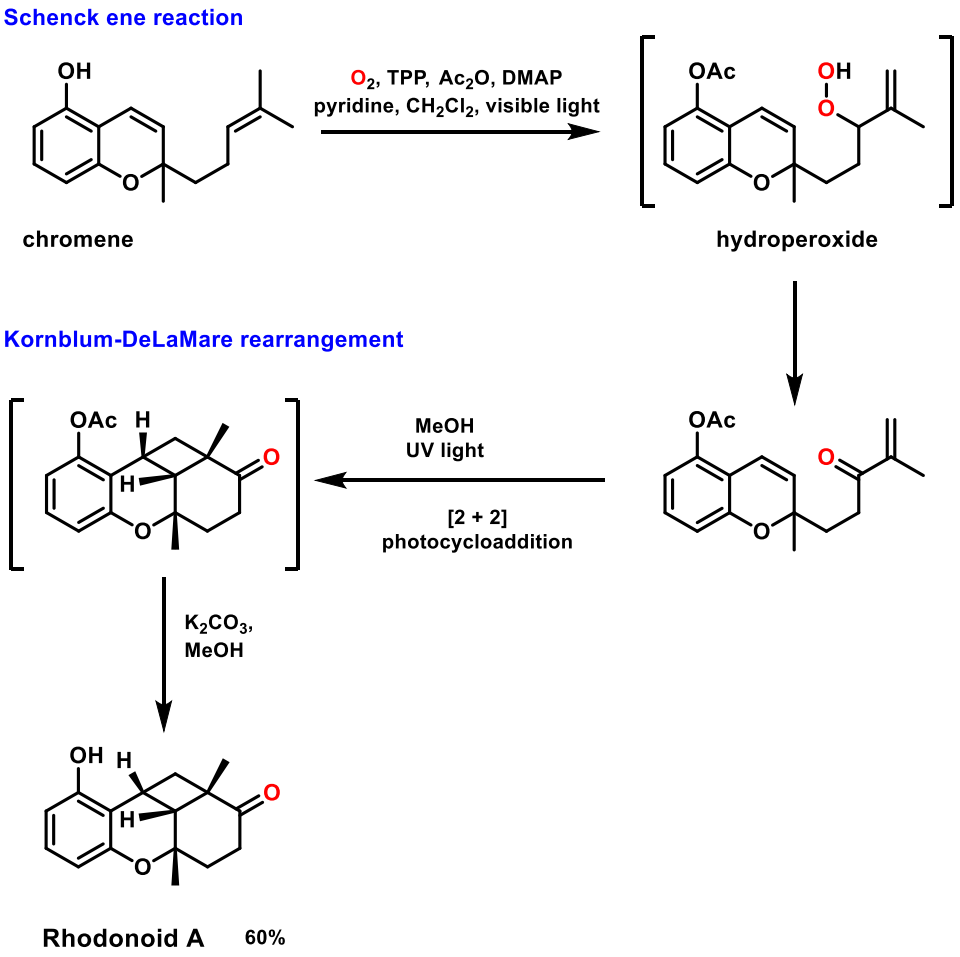
50 sec. irradiation in a flow reactor using red LEDs, under 30 bar O_2, at 0 °C, a solution 0.1 M of the phenyl cyclohexene in MeCN and 1 mol% methylene blue (MB), resulted in the formation of two major product 2-hydroperoxyphenylcyclohexene and the cycloadduct. Other three minor products 6-oxo-6-phenylhexanal, the other $^1O_2$-ene regioisomer were also isolated, while reductive workup with triphenylphosphine, resulted in the formation of 1,2-diol, and dihydroxy derivative (anti/syn = 4/1) (Scheme 17).[103]

A visible-light photo-oxidation of aldehydes to carboxylic acids using an Iridium (II) complex as photocatalyst ($Ir(dFppy)_3$) was reported. In this study the alkyl and aryl aldehydes were irradiated with blue LEDs, using oxygen as an oxidant result in an efficient conversion of up to 90 – 99% (Scheme 18).



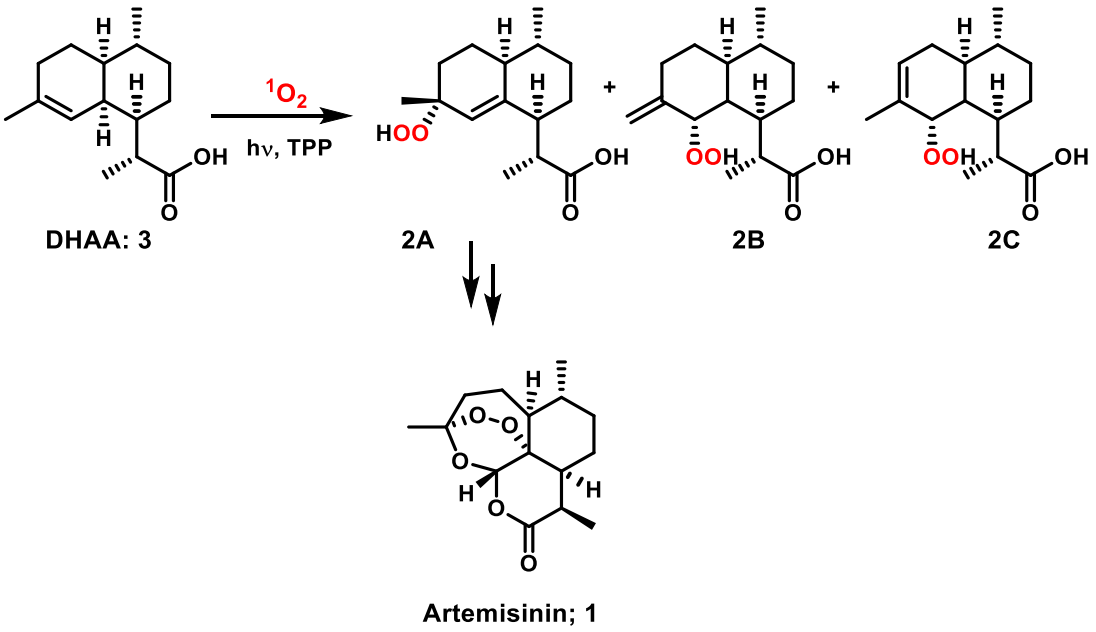
Scheme 18: Conversion of aldehydes into carboxylic acids through photosensitised energy transfer process.[55]

The reaction mechanism involves initial activation of ground-state oxygen ($^3O_2$) to excited $^1O_2$ through energy transfer from the excited triplet photocatalyst. The $^1O_2$ reacts with the aldehyde to afford hydroperoxide intermediate through schenk-ene reaction, which finally undergoes rearrangement to carboxylic acid. Another example was recently reported to catalyse the singlet oxygen ene-reaction and the [2 + 2] cycloaddition (Scheme 19), in the biomimetic synthesis of Rhodonoids A, B, E and F, a novel concise route that minimised redox reactions and the use of protecting groups. Starting from the reported likely biosynthetic precursor of the Rhodonoids C and D, one-pot synthesis was proposed, but due to different light sources and reaction condition requirements for each photo-oxidation step, an efficient two steps process was developed. During the process prenyl side chain of chromene was oxidised using visible light and TPP as sensitiser in the presence of an excess of pyridine, Ac_2O and catalytic amount of 4-dimethylaminopyridine (DMAP) to give the hydroperoxide.



Scheme 19: Biomimetic total synthesis of Rhodonoid A.[104]

Another important application of TPP as photosensitiser was reported extensively in the semi-synthesis of Artemisinin **1**. The semi-synthesis of **1** begins with low temperature photo-oxidation of DHAA **3** in the presence of TPP at low concentration to produce hydroperoxides (**2A - C**) through Schenk-ene reaction, with **2A** as the major product while, **2B** and **2C** are produced as minor and trace respectively (Scheme 20).[2, 3, 105, 106] The different steps for the synthesis of Artemisinin **1** were performed in different photochemical reactors, in batch, semi-continuous and continuous flow using different photosensitisers and acid catalysts, under different conditions of solvents and temperatures.



*Scheme 20: the semi-synthesis of Artemisinin **1**, using DHAA **3**.*[1]

This Thesis focuses on the production of Artemisinin. Therefore, the following sections described the sources of this important anti-malarial drug Artemisinin **1**, its extraction from plant and various methods for its synthesis, that have been reported in decades, through both total and semi-synthetic approaches, with initial brief description of Malaria, and its treatments using various drugs that have been used for its treatments.

ARTEMISININ AND ITS ANTIMALARIAL DERIVATIVES

1.3.1. MALARIA AND ITS TREATMENTS

Malaria is caused by *Plasmodium* parasites, from the female *Anopheles* mosquitoes, which is the malaria vector. Among the parasite species that cause malaria in humans, *P. falciparum* and *P. vivax* – pose the greatest threat. The disease is spread to humans through bites from infected mosquitoes, making infection very difficult to prevent. The attempts to create a vaccine have still proved unsuccessful, making the treatment as the only option for curing the disease.

In 2018, *P. falciparum* accounted for 99.7 % of estimated malaria cases in Africa, 50 % of cases in the South-East Asia region, 71 % of cases in the Eastern Mediterranean and 65 % in the Western Pacific, while *P. vivax* is the predominant parasite on the American continent, representing 75 % of malaria cases. This makes malaria caused by P. *falciparum*, more life-threatening.

Malaria causes many deaths per year. According to a report released by WHO in November 2020, there were 229 million cases of malaria in 2019, with an estimated number of deaths of 409, 000. Children under the age of 5 years are the most vulnerable, accounting for 67 % (274 000) of all malaria death worldwide. The high volume of cases means that production of these treatments is needed at industrial scale. Additionally, these cases are concentrated in less economically developed parts of the world, making it important that treatments for the disease are available at low cost.

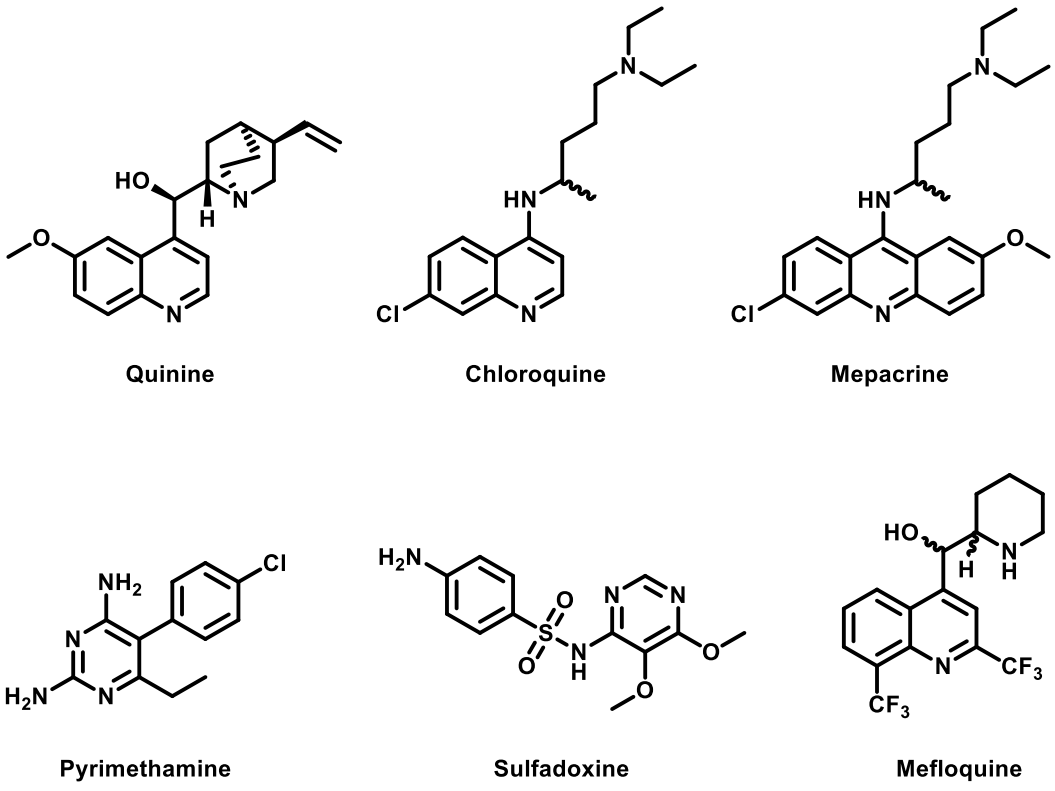


Figure 18: some anti-malarial drugs active ingredients.[107]

The first effective antimalarial drug was quinine, isolated from the bark of cinchona plant. Since then, malaria has been treated with quinoline based drugs such as chloroquine, quinine, mefluoquine and mepacrine, and with antifolates such as Fansidar (sufadoxine /pyrimethamine) (Figure 18)

Unfortunately, many P. *falciparum* strains have now become resistant to these most of these drugs.[107, 108] During the 1940s, chloroquine was used to treat all forms of malaria with few side effects. Resistance to chloroquine was first reported in the 1950s and over the years many strains of malaria have developed resistance. And now many resistant strains of the malaria parasite are now used in potency evaluation assays as a way of showing efficacy. Despite the resistance by many strains, chloroquine is still on the WHO's model list of essential medicines for the treatment of *P. vivax* in regions where resistance has not been developed.[107, 109, 110]

1.3.2. MODE OF ACTION OF ARTEMISININ

Because of its ability to rapidly eradicate the malaria parasite at the so-called 'blood stage', Artemisinin **1** was recommended an anti-malarial agent.[111] The direct use of Artemisinin **1** as an active ingredient in the antimalarial drugs is limited because of its hydrophobic nature, which results in its derivatisation into water soluble active substance such as Artesunate. This group of compounds combined with other known antimalarial compounds are termed Artemisinin Combination Therapies (ACTs). ACTs consist of the treatment with artemisinin derivatives, such as artesunate, Artemether, Arteether, and so on, combined with longer acting antimalarial drugs, like Quinine, Doxycycline, Mefluoquine and Benflumetol in different proportions (Figure 19),[112] thereby producing highly efficient combination against Malaria.

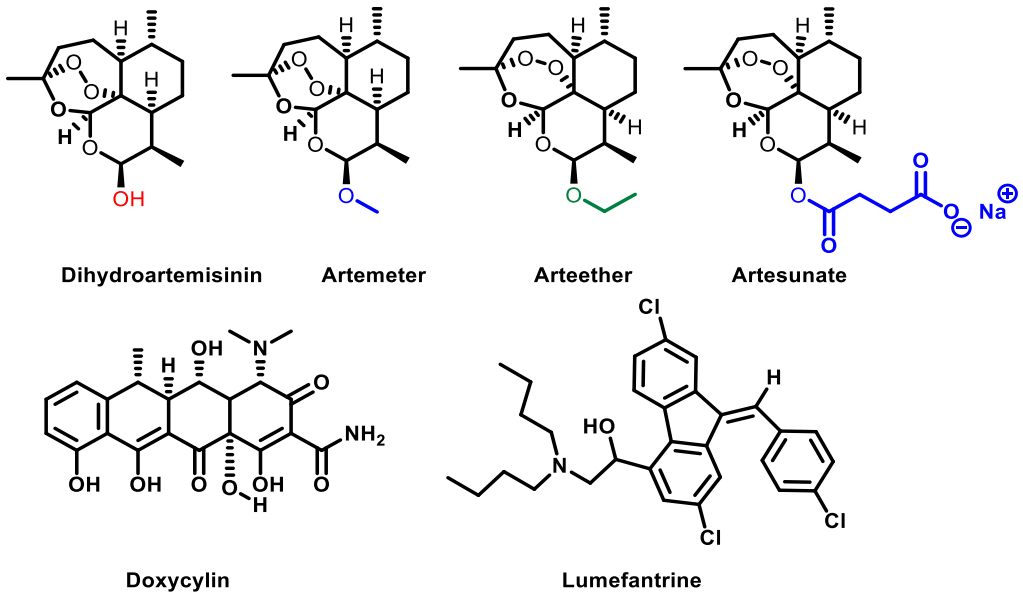


*Figure 19: Artemisinin **1** and its derivatives and other compounds with proved applications for the treatment of Malaria and other diseases such as Cancer.*

Other important derivatives of Artemisinin **1** are 6 and 11- aza-artemisinin in which carbon (6 position) and oxygen (11 position) respectively are replaced by amine or its derivatives. These compounds are reported to possess both antimalarial and anticancer properties (Figure 20).[113-115]

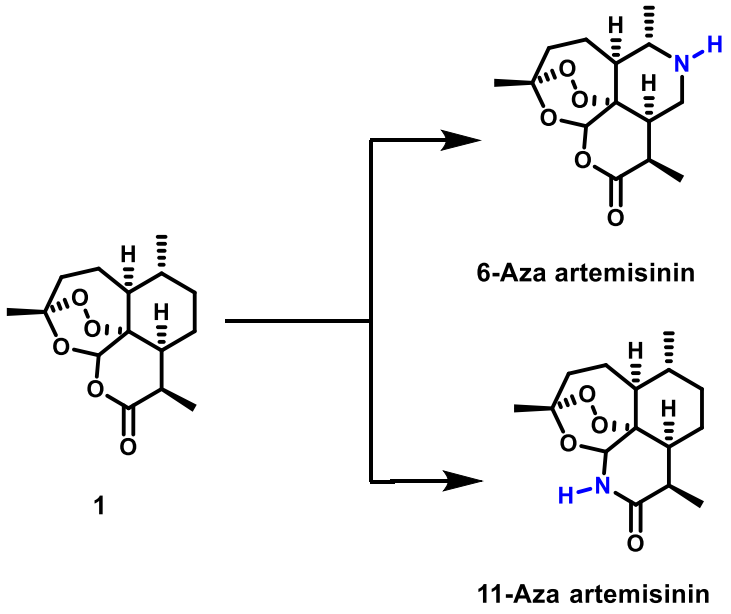
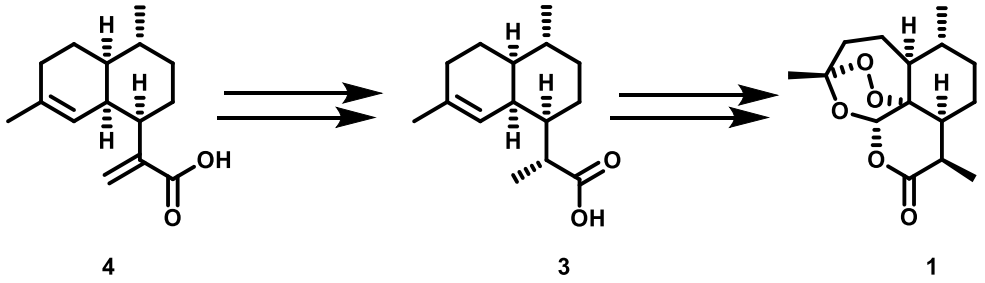


*Figure 20: the derivatives of Artemisinin **1** in which carbon (6 position) and oxygen (11 position) respectively are replaced by amine.*

The mechanism of action through which Artemisinin **1** acts has been widely debated, suggesting that the primary activator binds to an iron source, arising either in form of Fe^{2+}, haem or both [116]. The most accepted theory is that the molecule is activated by haem to generate free radicals, which in turn damage proteins required for parasite survival.[117]

1.3.3. SOURCES OF ARTEMISININ

Artemisinin **1** is a naturally occurring antimalarial compound of the sesquiterpene compound containing 1,2,4-trioxane motif in its structure.[118] It is one of natural products was isolated from the plant *Artemisia Annua*, a species of wormwood known as Qinghao to the Chinese, who have used the plant to treat malaria for at least 1700 years. Artemisinin **1** was first isolated in 1971 by Tu YouYou from *A. annua*, a herb that has been used in Chinese traditional medicine for at least 1700 years.[111] Due to the great positive impact of Artemisinin **1** in combating malaria, Dr Tu shared 2015 Nobel Prize in Physiology or Medicine for "*her discoveries concerning a novel therapy against malaria*".[111] Artemisinin **1** has been shown to be efficacious against all multi-drug resistant forms of P. *falciparum*.



*Scheme 21: illustration of the conversion of Artemisinic acid **4** into Artemisinin **1***

Artemisinin **1** was also reported to be effective against other infectious diseases such as Cancer, HIV, bilharzia, hepatitis B. and so on.[118, 119] The plant-derived Artemisinin **1** accounts for only 0.6 – 1.0 % of its dry weight; other compounds can be obtained from

the plant, such as Artemisinic acid (AA) **4** and Dihydroartemisinic acid (DHAA) **3** in large quantities (Scheme 21). The amount of the product that can be extracted varies depending on the geographical origin of the plant.[120]

The most common derivatives of Artemisinin **1** are Artemether, Artesunate and Arteether. These semi-synthetic derivatives are prodrugs which are transformed to the pharmacologically active metabolite, Dihydroartemisinin in vivo.[107]

1.3.4. THE EXTRACTION AND ISOLATION OF ARTEMISININ

Artemisinin **1** is obtained from leaves, flowers, and buds of the A. *annua,* in the range of 0.01 to 1.4 % of the dry weight. Despite very low isolated yield, the supply of Artemisinin **1** from the plant is always limited by problems, which include poor harvest, insects, flooding, drought, and their seasonal nature among others.

The traditional way of extracting Artemisinin **1** involves a time-consuming solvent extraction processes, which includes steeping or stirring the leaves in the solvent for several days. Ethers, n-hexane, and ethanol are the most common solvents used for with ethers being the more commonly used, but other solvents such as acetone are also used. The process usually takes place at elevated temperature and refluxing (at 40 °C or higher) of plant material for over 10–48 h to increase the extraction yield of Artemisinin **1**.[121]

In fact, as the amount of **1** present in A. *annua* is extremely low, continuous efforts have been devoted to find more effective and environmentally friendly extraction methods, e.g. Soxhlet, ultra-sound and microwave-assisted extraction, supercritical fluid extraction (often supercritical CO_2 extraction), and pressurised hot water extractions, to increase extraction yield of this compound.[121-123] Other techniques such as ultrasound assisted extraction method, using series of non-toxic monoether based solvents have also been reported.[124] These modern extraction techniques which include super critical fluid and

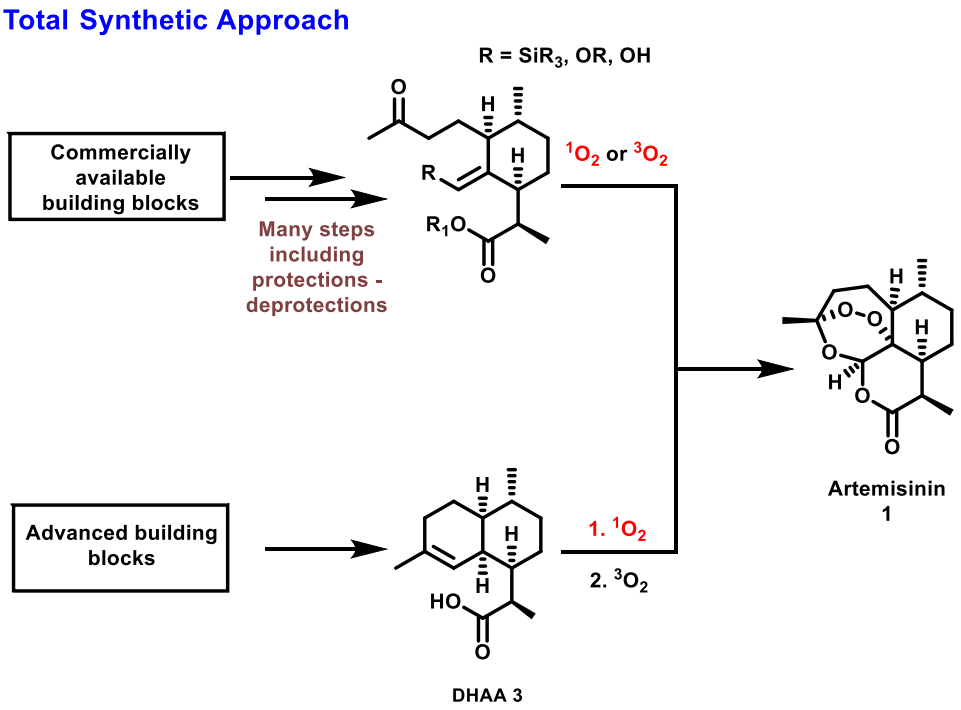
ultrasound-assisted extraction are methods of choice, due to their advantage to improve the productivity of Artemisinin **1**, compared to traditional Soxhlet extraction. Extraction can be coupled with the use of inline analytical tools for quantitative and qualitative determination of Artemisinin **1** such as LC-based techniques, including HPLC and UPLC.[121]

As it became clear that increasing cultivation of *A. Annua* could not keep up with the increasing demand for **1**, attempts to increase production by conventional breeding of the plant were made, through production of improved variety of A. *annua*, by genetic modification of the existing variety. this resulted in an improvement of Artemisinin **1** content to 1.38 % for the genetically modified hybrid strain,[25, 125] compared to 1.07 % dry weight from the highest yielding wild strain. Since then, detailed genetic mapping of the traits effecting yields of **1** have been performed, allowing breeding programs to produce crops exceeding 1.6 % of **1**.[126]

SYNTHESIS OF ARTEMISININ

The dependence on the plant-based Artemisinin **1** has made the ACTs drugs very expensive over the decades due to seasonal nature of the plant cultivars and an increasing demand for the drugs, which clearly illustrates the need of a synthetic approach.

This resulted in fluctuations in its supply,[127] making the drugs more expensive especially to the people from sub-Saharan Africa where the majority cannot afford it. This increasing demand for Artemisinin **1** has given rise to many substandard antimalarial drugs on the market, increasing the mortality rate especially amongst pregnant women and children who are more vulnerable to malarial attack.



*Scheme 22: the summary of the synthetic route to Artemisinin **1**, the total synthesis for most of the reported cases involve construction of an intermediate with all the stereochemistry found in Artemisinin **1**, followed by oxidation to artemisinin, and the semi-synthetic route starts from DHAA **3**.*

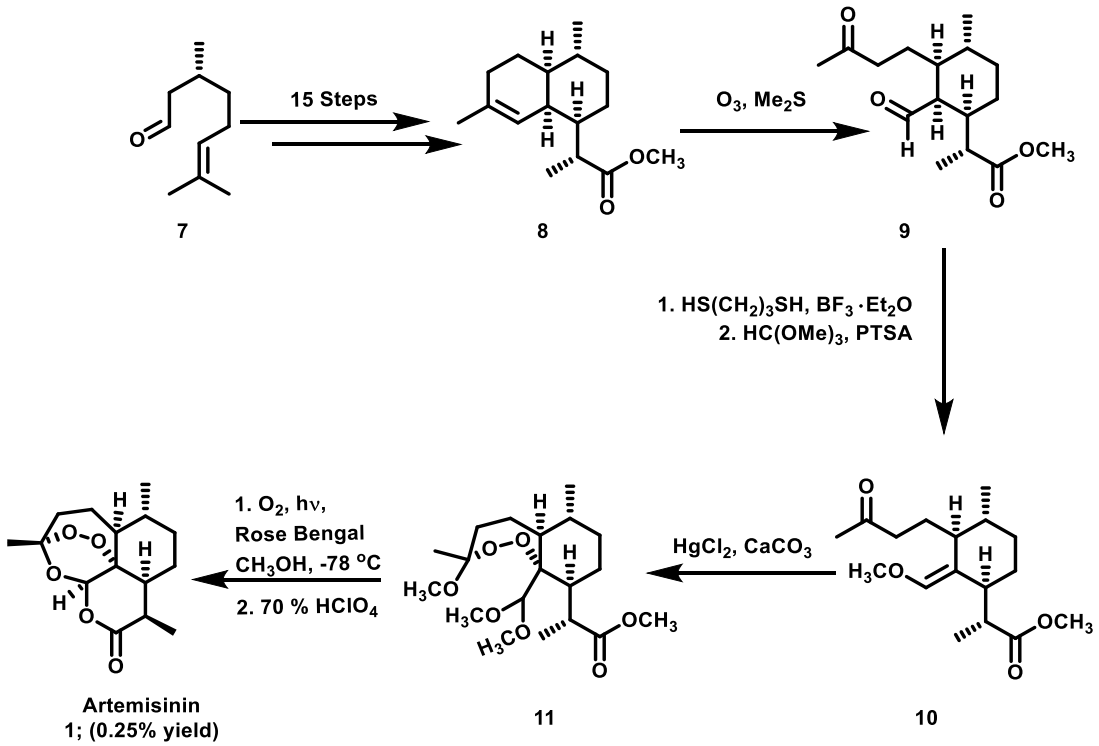
These limitations in the supply and increased demand results in the development of various approaches, aiming to achieving a more sustainable supply of ACTs. Some of the strategies employed over the years include the total synthesis of Artemisinin **1**, involving the initial synthesis of an intermediate possessing all the stereochemistry needed for its final oxidation to Artemisinin **1**,[128-131] and semi-synthetic approaches using DHAA **3** and its derivatives as precursors (Scheme 22).[2, 48, 83, 132-136]

1.4.1. TOTAL SYNTHESIS OF ARTEMISININ

Research papers and review articles have been published covering total synthesis of Artemisinin **1** through different approaches,[108, 125, 137, 138] involving initial construction of the key enol intermediate **10** through various methods (Scheme 23) involving the use of readily available starting materials such as citronellol and cyclohexane or its derivatives, to construct the carbon backbone with stereochemistry relative to the intermediate.

1.4.1.2 CITRONELLAL BASED STRATEGIES

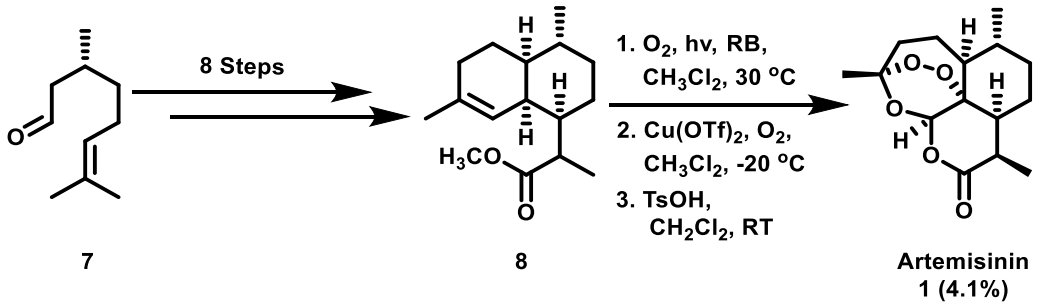
The total synthesis of Artemisinin **1** starting from available *R*-(+)-citronellal **7** was reported by Zhou and co-workers in 1986,[139] the process involved 19 steps. It involved the initial synthesis of DHAA methyl ester **8** in 15 steps to give 72 % overall yield, this was followed by ozonolysis affording the ketoaldehyde **9.** The protection of the aldehyde's ketone was followed by transformation of the resulting acetal into enol-methyl ester **10**, and deprotection to give enol-ester **11** with 33 % yield in 5 steps. Finally, reaction with photochemically generated singlet oxygen using Rose Bengal at – 78 °C resulted in the formation of another intermediate which cyclised in the presence of 70 % $HClO_4$ at room temperature to provide Artemisinin **1** (Scheme 23).



*Scheme 23: the reported total synthesis of Artemisinin **1**, through initial 11 steps synthesis of DHAA methyl ester **8** and ozonolysis to aldehyde **9**, which is finally transformed into **1** by Zhou et al.*[139]

A more concise and efficient total synthesis of Artemisinin **1** involving citronellal was achieved by Yadav and co-workers starting from (*R*)-citronellal **7** to methyl ester of

DHAA **3** in 8 steps with an overall yield of 13 % and no protecting group involved, making this the shortest total synthesis of Artemisinin **1** ever achieved.

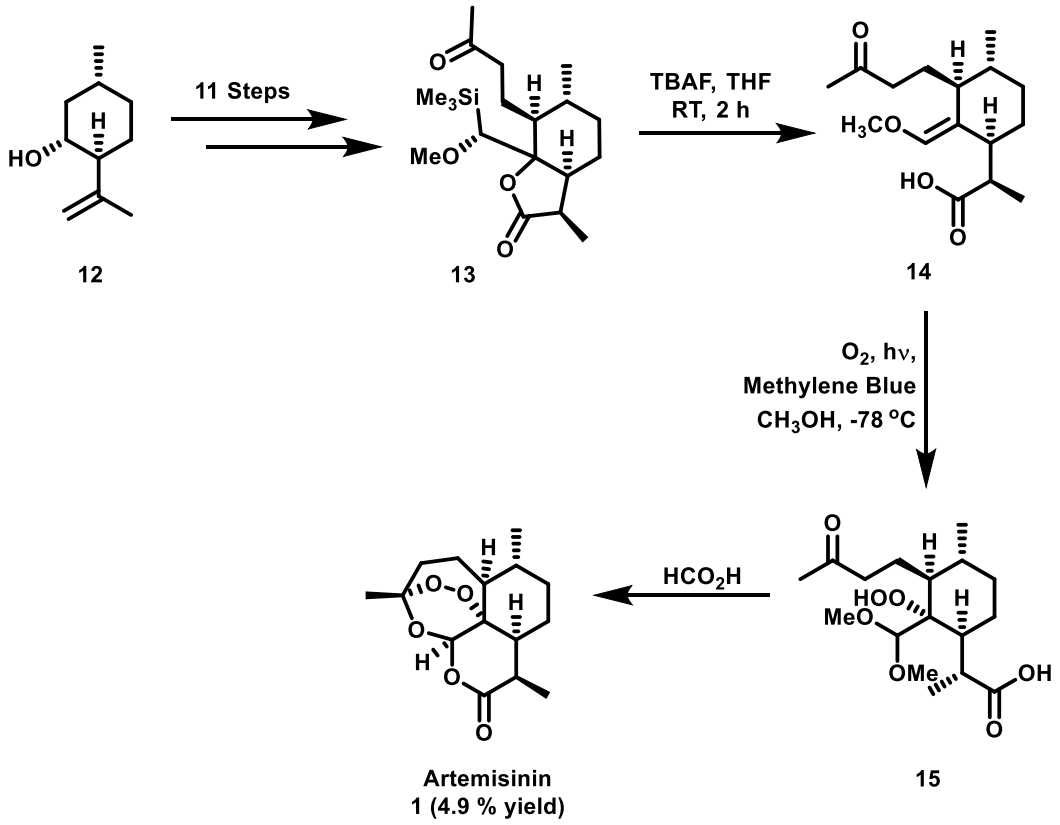


*Scheme 24: the concise total synthesis of Artemisinin **1**, reported by Yadav et al. through initial 7 steps synthesis of DHAA **3**, followed by esterification to **8**, and oxidation to **1**.*

The ester was then subjected to low temperature photo-oxidation using Rose Bengal as photo-catalyst in acetonitrile, employing the method reported by Haynes[140] to produce Artemisinin **1** using Lewis acid catalyst $Cu(OTf)_2$ in DCM at 25 °C (Scheme 24).[128]

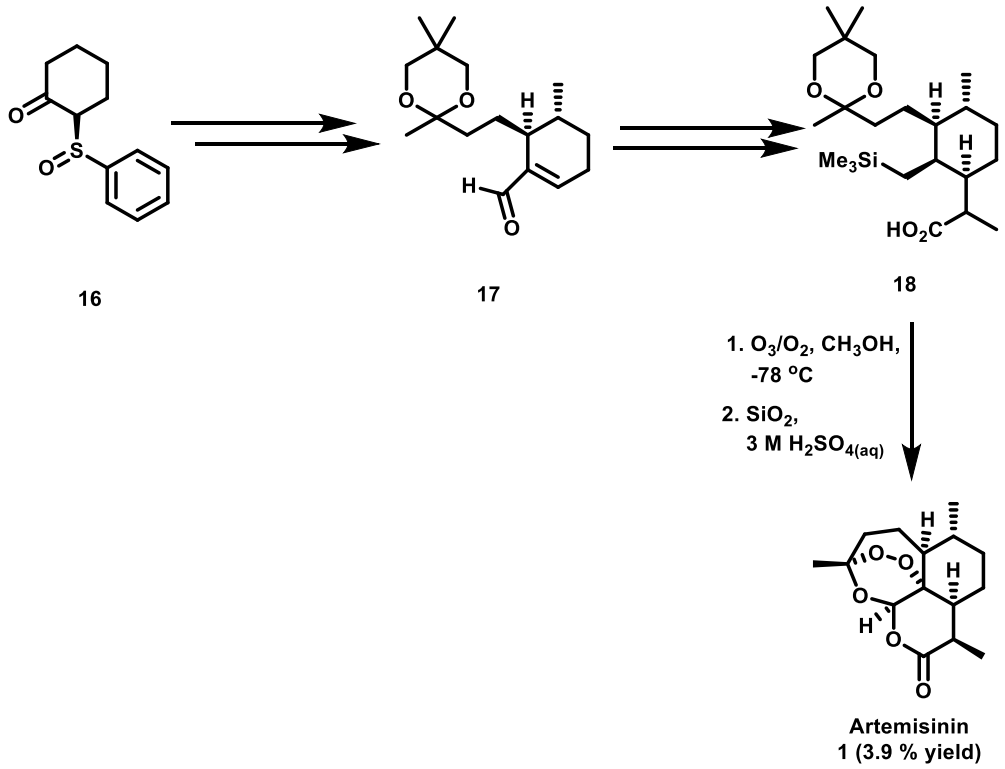
1.4.1.2 Cyclohexane and its derivatives based strategies

Cyclohexane and its derivatives have also been used as starting materials for the total synthesis of Artemisinin **1**, some of these compounds are direct products of ene-cyclisation of (+)-citronellal **7**, for example (-)-isopulegol **12** was used for the total synthesis of Artemisinin **1** by Schmid and Hafheinz.[141]. The (-)-isopulegol **12** was initially converted into lactone **13** in 11 steps, was desilylated to simultaneously generate enol ether and carboxylic acid function in **14**, which subsequently was submitted to a reaction with photochemically generated singlet oxygen ($^1O_2$) (Scheme 25). The isolated crude product was treated with formic acid at 0 °C for 24 hours to afford Artemisinin **1** with a 4.9% yield.



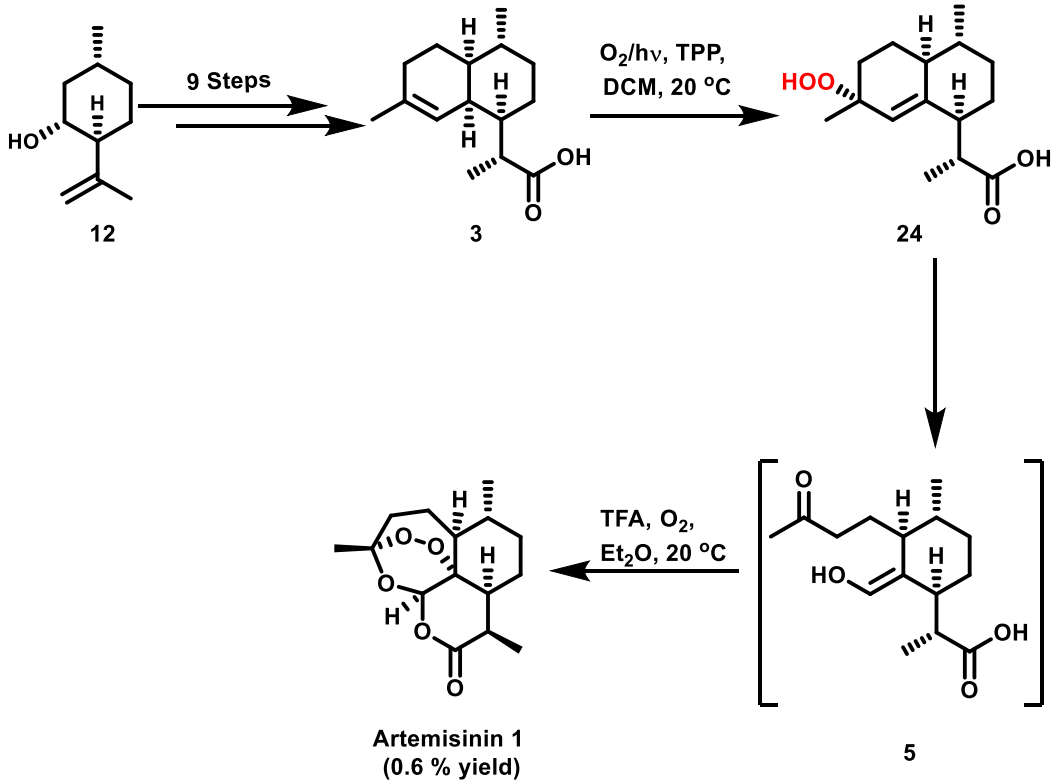
*Scheme 25: Total synthesis of Artemisinin **1**, from (-)-isopulegol **12** reported by Schmid and Hefheinz.*[141]

Avery *et al.* reported the total synthesis of Artemisinin **1** using (*R)*-5-methyl-2-(phenylsulfinyl)cyclohexanone **16** as precursor in 10 steps,[130] The approach include diastereoselective trimethylsilyl anion addition to the α,β-unsaturated aldehyde **17** and a tandem Claisen ester-enolate rearrangement/dianion alkylation to afford the diastereomerically pure erythro acid **18**. Finally, acid **18** was converted in a one-pot procedure involving sequential treatment with ozone followed by wet acidic silica gel to give rise to a complex process of dioxetane formation, ketal deprotection, and multiple cyclisation to the natural product Artemisinin **1** (Scheme 26)**.**



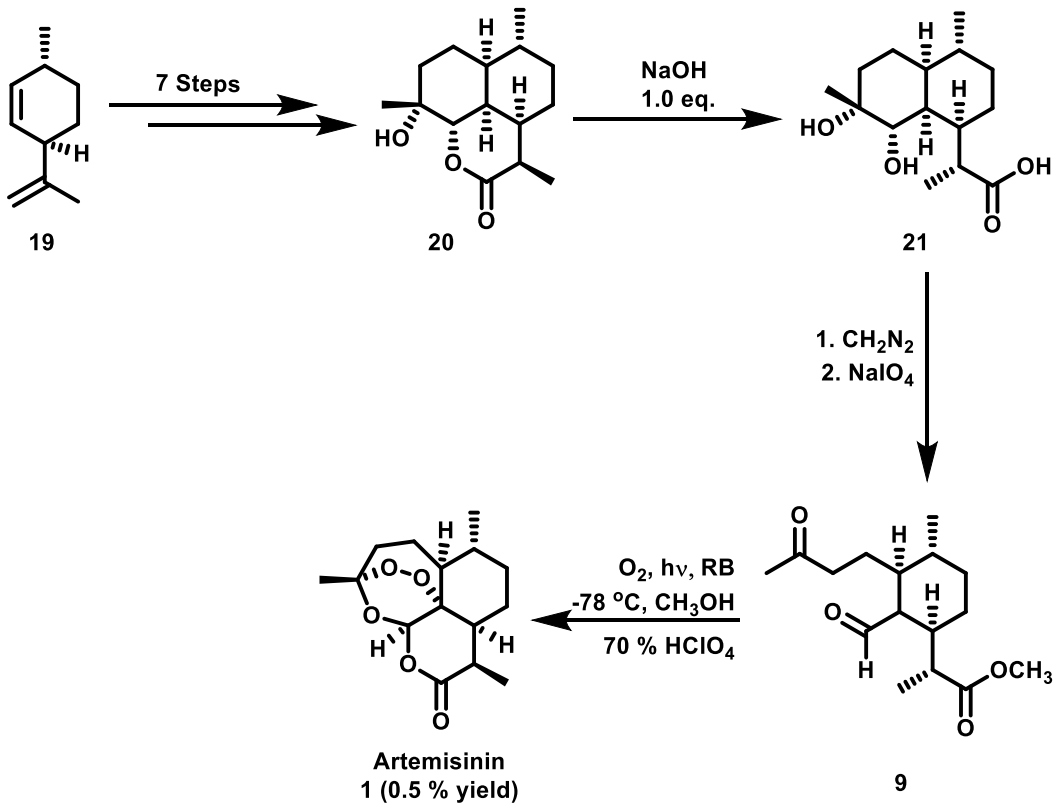
Scheme 26*: the total synthesis of Artemisinin* ***1****, (R)-5-methyl-2-(phenylsulfinyl)cyclohexanone* ***16*** *as the initial precursor reported by Avery et al.*[130]

Constantino *et al.* designed a very concise synthesis of Artemisinin **1** in 11 steps,[142] starting from (-)-isopulegol **12** to obtain DHAA **3** in 9 steps. The use of TPP and TFA as photo and acid catalysts respectively, resulted in the overall product yield of 4.1 % Artemisinin **1**. Unlike previous method by Schmid *et al.* here (-)-Isopulegol **12** was converted to DHAA **3.** Next, conversion to Artemisinin **1** employing the method reported by Acton and Ruth by a sequence of photo-oxidation using air as oxidant and acid catalysed thermal oxidation at 20 °C, (Scheme 27).[142]



*Scheme 27: Total synthesis of Artemisinin **1**, using (-)-isopulegol **12** as starting material by Constantino et al.*[142]

Another cyclohexane derivative used is (+)-isolimonene **19** derived from very cheap and highly abundant monoterpene (+)-3-carene was reported by Ravindranathan *et al.,*[129] a highly stereoselective process was used to produce aldehyde **9** with the stereochemistry required for the conversion to Artemisinin **1** in 8 steps (Scheme 28) compared to the 15 steps approach reported earlier in this chapter by Zhou *et al.* without any further protection. Next, the intermediate aldehyde reacts with photochemically generated singlet oxygen to afford Artemisinin 1 in a total of 10 steps.



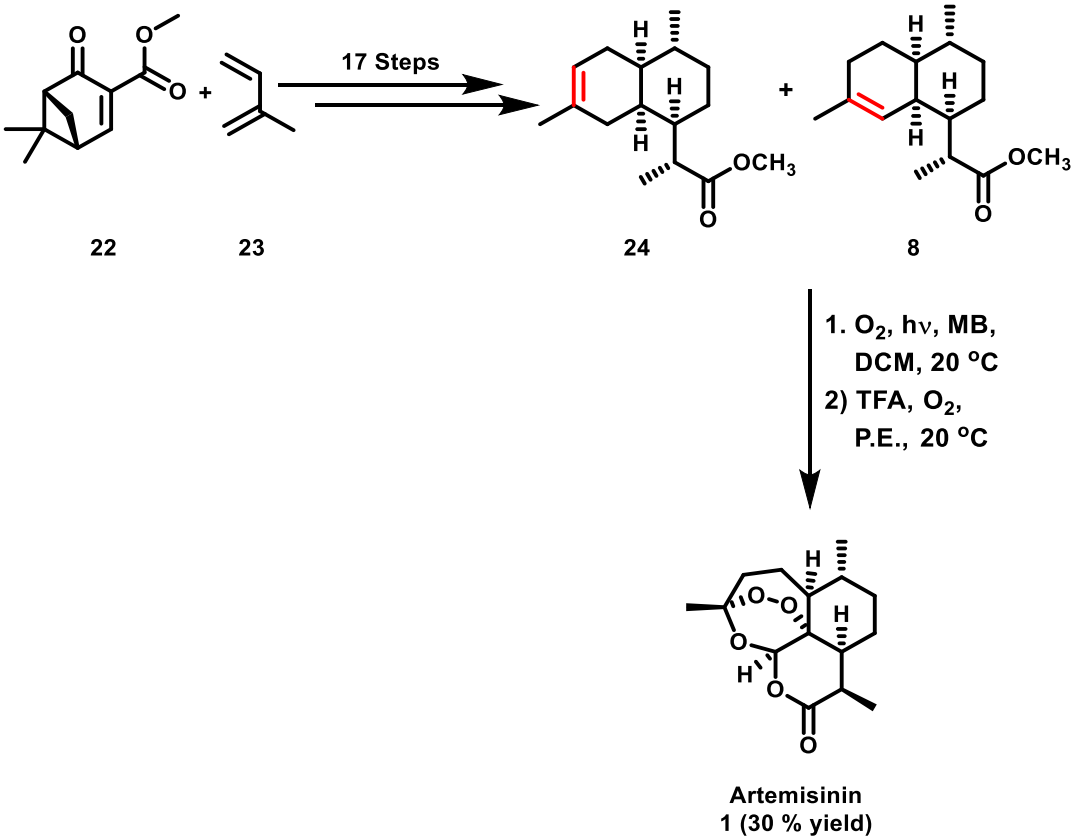
Scheme 28*: Total synthesis of Artemisinin* ***1****, from isolimonene* ***19*** *reported by Ravindranathan et al.*[129]

It is important to note that the intermediates which were synthesised by Zhou and Ravindranathan groups (Schemes **23** and **28**) have differences in terms of reactivity toward the photochemically generated singlet oxygen, with the vinyl ester group being more reactive toward the addition reaction than the aldehyde. However, both intermediates react under the same conditions to produce Artemisinin **1**.

1.4.2. TOTAL SYNTHESIS OF DHAA TOWARD THE SEMI-SYNTHESIS OF ARTEMISININ

Crude mixture of two isomers of DHAA methyl esters (**24** and **8**) were earlier produced by Jang *et al.* in 17 steps, for the total synthesis of Artemisinin **1** (Scheme 29). Initial photo-oxidation of the crude mixture of the esters was performed in dichloromethane (DCM) using Methylene Blue (MB) as the photosensitiser at 20 °C, this was followed by treatment of the crude mixture with TFA in petroleum ether (P.E.) using oxygen as

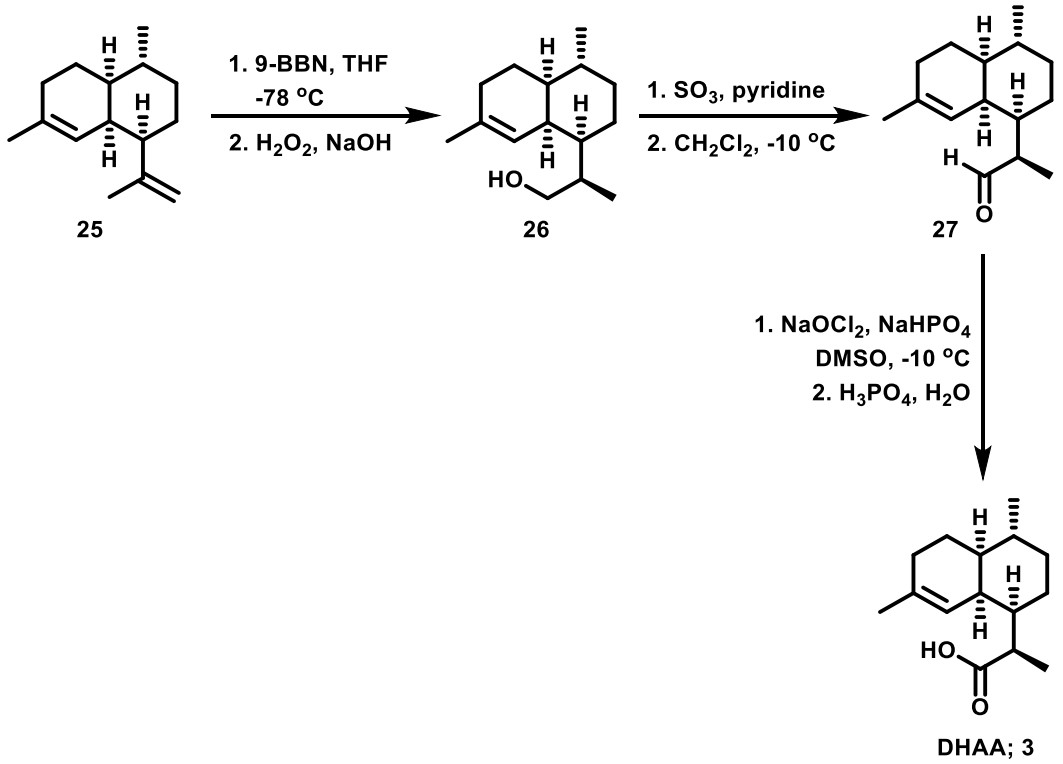
oxidant, to give 30 % of Artemisinin **1**. The crude product does not any of the esters (**24** and **8**), indicating the possible conversion of both isomer to Artemisinin **1**.[143]



*Scheme 29: synthesis of Artemisinin **1** from the crude mixture of two isomers of DHAA Methyl ester **24** and **8**.*[143]

With the current drive toward cost-effective routes to **1** through green and sustainable approach, exploiting much cheaper and available precursor like amorpha-4,11-diene **25** could provide a way forward of addressing this problem. The compound can be found as a by-product of the fermentation process using engineered yeast, and it can also be obtained in a very high quantity of up to 2-fold higher than artemisinic acid **4** from A. *annua* plant. Because it contains all the required stereochemistry found in **3**, various researchers have attempted to convert amorpha-4,11-diene **25** into DHAA **3** using different approaches.[67, 144, 145]

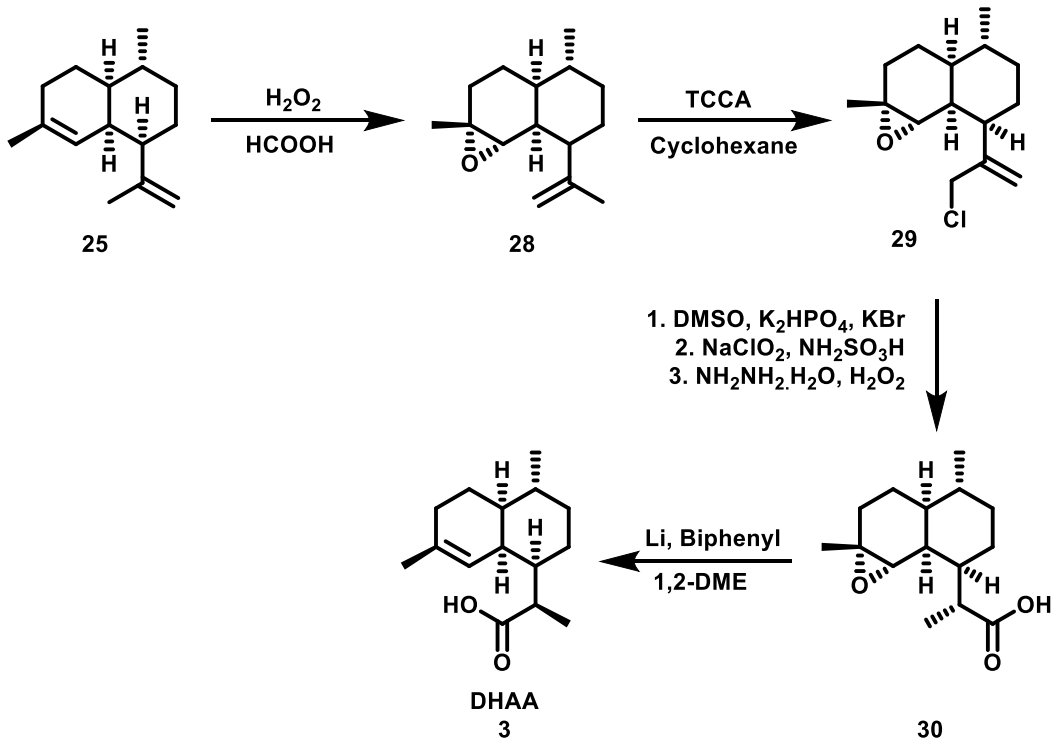
The initial selective hydroboration of the external double bond at 11-position by treatment with borane 9-borabicyclo[3.3.1]nonane (9-BBN) and subsequent hydrogen peroxide addition to provide alcohol **26** with 79.3% yield and 85% diastereoselectivity towards the *R*-epimer. A two steps oxidation processes initially converts the alcohol into an aldehyde with a yield of 76.4 %. Next treatment of the aldehyde **27** with the strong oxidant $NaClO_2$ in DMSO results in the formation of 79.9 % of Artemisinin **1** with an overall yield of 48.4 %. The use of DSMO is necessary since it reacts with the NaOCl generated *in-situ* precluding in this way its potential reaction on the double bond at 4-position (Scheme 30).[144]



*Scheme 30: the conversion of Amorpha-4,11-diene **25** to Dihydroartemisinic acid **3**.*

The major problem with this method is that the hydroboration agent (9-BBN) used is very expensive making the whole process unattractive for industrial production of Artemisinin **1**.[144]

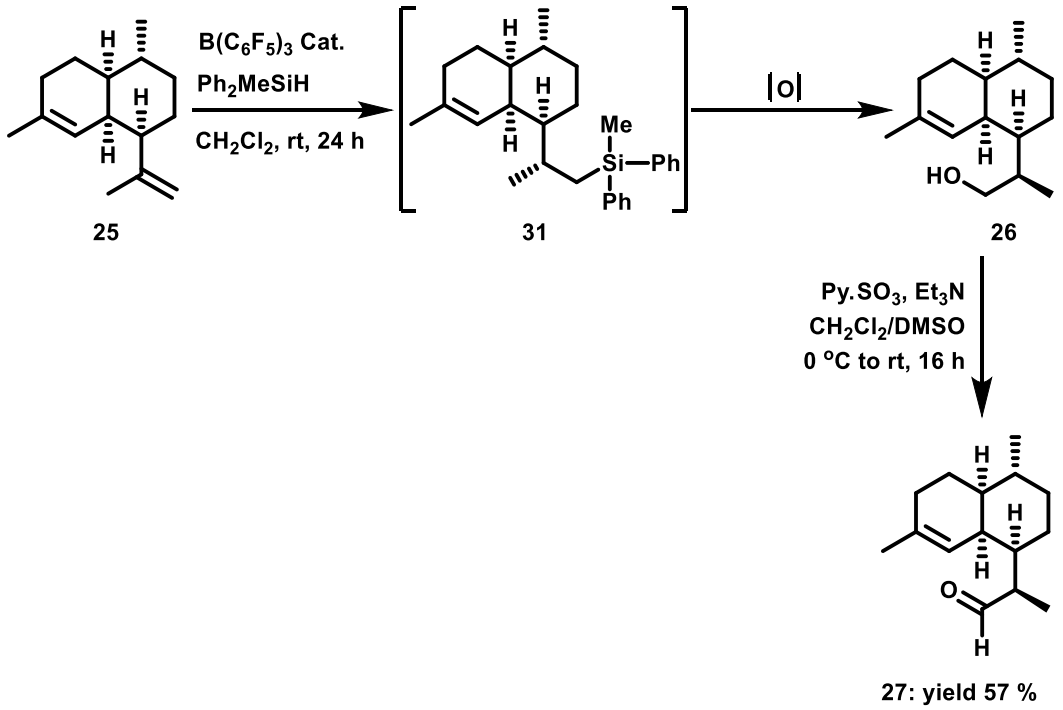
Another method was reported for conversion of amorphadiene **25** to DHAA **3** through selective functionalisation of the isopropenyl group. This was performed through initial protection of the more reactive endocyclic double bond by highly regioselective epoxidation using H_2O_2 in the presence of HCOOH as catalyst (Scheme 31), chlorination of the epoxide, followed by a sequence of oxidations and final deprotection affording DHAA **3**.[31]



*Scheme 31: the conversion of amorpha-4,11-diene **25** to DHAA **3**, by initial protection of endocyclic double at 4-position to epoxide **28**, sequential oxidation of the epoxide, followed by deprotection afford DHAA **3**.*[145]

Recently Amara and co-workers reported the conversion of amorpha-4,11-diene **25** through a chemo and diastereoselective hydrosilylation to dihydroartemisinic aldehyde (DHAAl) **27**. The process was performed through a one-pot hydrosilation catalysed by $B(C_6F_5)_3$ and the subsequent oxidation to produced alcohol **26** of the silyl intermediate **31**. The silyl intermediate **31** was transformed into **27** with good overall yield of 57.8 % and a selectivity of 95:5 for (11*R*)-DHAA **27** (Scheme 32). The most promising feature

of this reaction is that the internal double bond does not undergo hydro-silylation, thereby removing the need for the protection and deprotection steps.



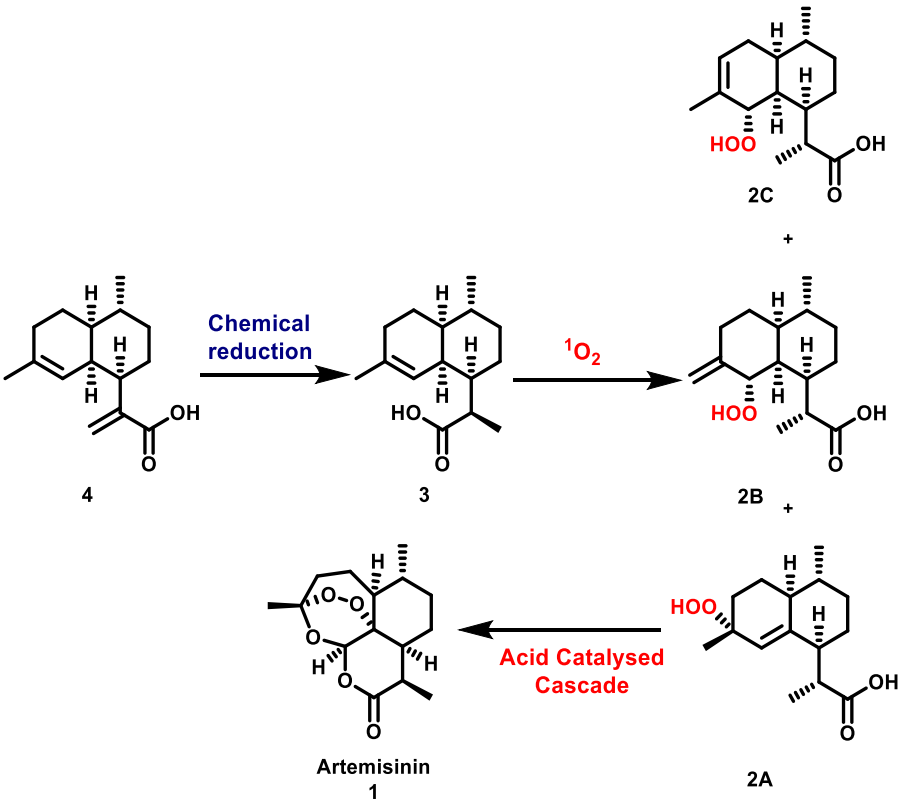
*Scheme 32: The conversion of amorpha-4,11-diene **25** to dihydroartemisinic aldehyde **27**.*[146]

The synthetic strategies reported by Liu *et al.,*[143] Constantino *et al.*,[142] and Yadav *et al.*,[128] produced **3** or its ester as an intermediate for the synthesis of **1**. These synthetic routes involved many reaction steps with different protections and deprotections, as well as various solvents switches. The processes that contribute largely to the decrease in the overall productivity of **1**, with the generation of large amount of waste, making the process unattractive for the industrial production.

Both Artemisinic acid **4** and DHAA **3** are found in A. *annua* plant at the higher abundance than much desired Artemisinin **1**. This coupled with the reported biosynthetic route for the large scale production of **4** by Amyris,[127] and successful genetic modification of baker's yeast strain by Paddon and co-workers resulted in the massive yield of **3**,[147] which forms the bases for the semi-synthetic approach to Artemisinin **1**.

1.4.3. SEMI-SYNTHESIS OF ARTEMISININ

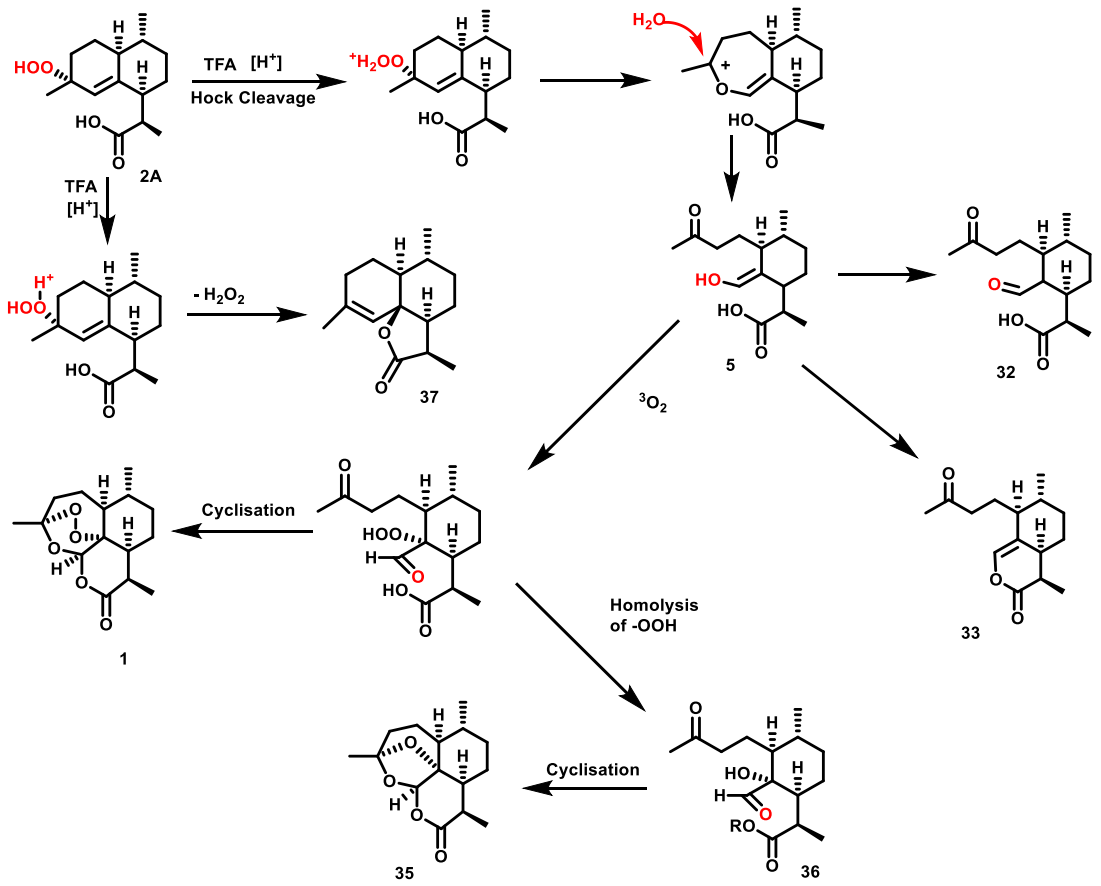
Following the development of a biosynthetic pathway for the generation of **4**, Artemisinin **1** has been synthesised through a semi-synthetic approach. This process involved initial photo-oxidation of DHAA **3** or its derivatives using singlet oxygen ($^1O_2$) generated either photochemically with the aid of photosensitiser or chemically through disproportionation of hydrogen peroxide and followed by the acid catalysed thermal oxidation of the hydroperoxide intermediate **2A** and thermal oxidation cascade to Artemisinin **1** as shown in Scheme 33.



Scheme 33*: Semi-Synthesis of Artemisinin **1** from DHAA **3**, following the highly diastereoselective reduction of Artemisinic acid **4** to DHAA **3** using engineered yeast.*[147]

The photo-oxidation involves the reaction of either photo-chemically or chemically generated singlet oxygen ($^1O_2$) with starting material **3**, its esters and carbonate derivatives. The mechanism of the process involved a highly stereoselective Schenck reaction, which results in the oxygenation of the alkene bond in **3** to generate three allylic hydroperoxides

(**2A-C**). Among the hydroperoxides produced, the tertiary hydroperoxide **2A** was reported to be the major product, while secondary hydroperoxides **2B** and **2C** are produced as minor and trace respectively.[48]



*Scheme 34: Proposed mechanism of the conversion of DHAA **3** and its ester and carbonate derivatives peroxides into Artemisinin, via Hock cleavage, thermal oxidation, and cyclisation. Adapted from.* [79]

The selectivity in the photo-oxidation process was described to be due to the chiral nature of DHAA **3** and large group effect, causing the blockage of one face of the alkene, and thereby directing the attack by the $^1O_2$ to occur at only one side. Other factors such as the nature and the stability of the peroxide intermediates formed, side selectivity and end selectivity favour the formation of the desired tertiary hydroperoxide **2A**.[25]

The next step for the synthesis of Artemisinin **1** is the acid catalysed Hock cleavage of the tertiary hydroperoxide **2A** followed by thermal oxidation process to give Artemisinin

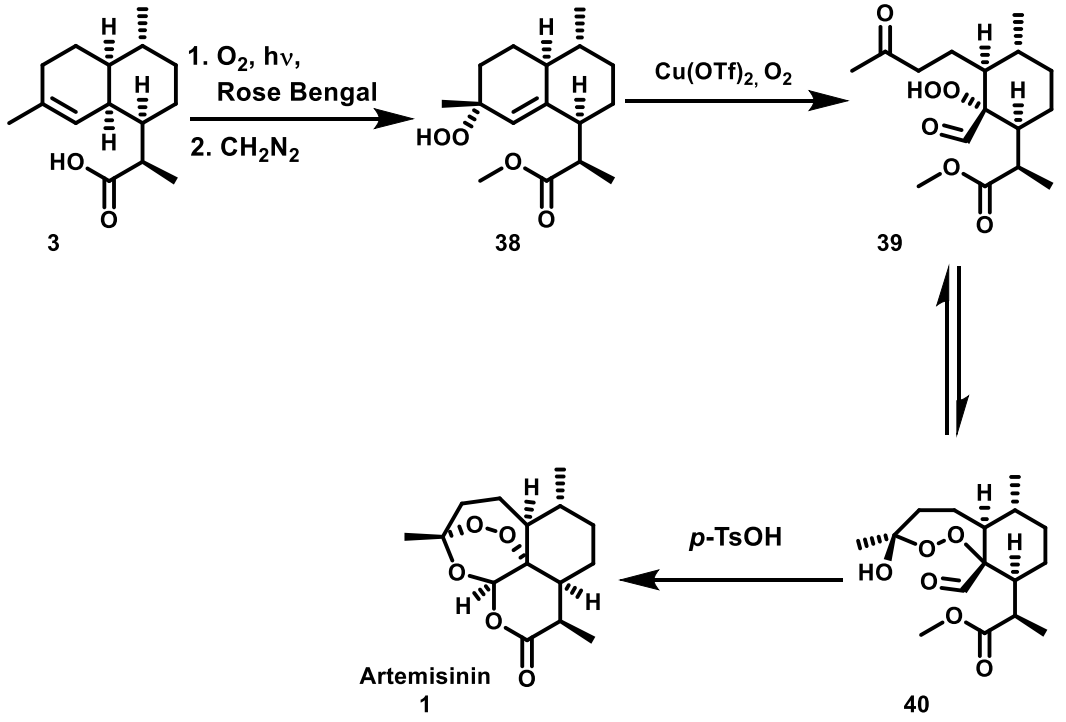
1. This is a very important step as the nature and yield of the final product depends on the careful selection of acid catalyst, solvent, and temperature of this step.[2, 3, 48] Scheme 34 gave the detailed mechanistic consideration of this step which involves acid catalysed Hock-cleavage through initial protonation of either the terminal or internal oxygen of the peroxide. It was reported that when the proximal oxygen is protonated the resulting intermediate can lose hydrogen peroxide leading to the formation of 5-membered lactone by-product **37**.

In non-polar solvents such as toluene, on distal protonation, the **2A** undergoes Hock cleavage to form the corresponding enol **5** which reacts with molecular oxygen to form another hydroperoxide intermediate, which finally cyclises to form Artemisinin **1**. In a polar solvent such as ethyl acetate, the enol formed was reported to undergo tautomerism into another keto intermediate which cyclises to form the δ–lactone **33**,[48, 79, 83] and this lactone by-product was also reported to form due to insufficient supply of triplet oxygen after acid catalysed Hock cleavage,[3] or in the presence of perchloric acid solution in 50 % THF/H_2O after 7 hour of stirring.[148]

After the initial work of Acton and Roth on the semi-synthesis of **1** starting from DHAA **3**, various research groups reported different routes to Artemisinin **1** employing **3**,[2, 48, 79, 83, 84] or its methyl ester **8**,[128, 143, 149] and carbonates,[1, 3] derivatives as precursors of Artemisinin **1**, with the methyl ester being the most frequently used DHAA derivative for this process.

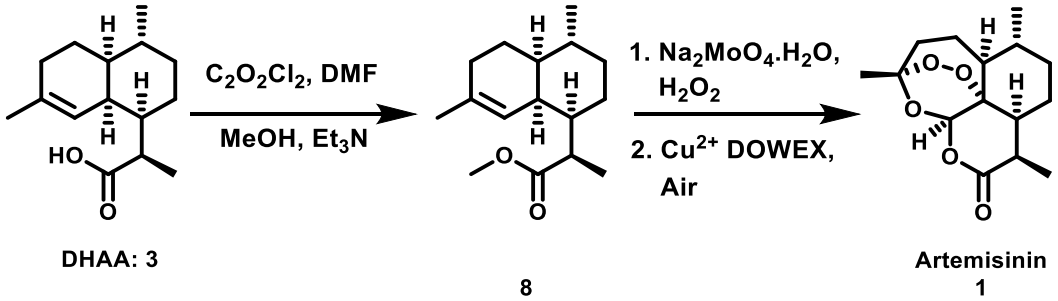
The derivatisation of DHAA **3** to its methyl ester by Haynes and Vonwiller for the synthesis of **1**, was performed through initial photo-oxidation of **3** and subsequent treatment with diazomethane (CH_2N_2) to produce the corresponding hydroperoxide of DHAA methyl ester **38**. In the presence of $Cu(OTf)_2$ (0.1 equiv.) the ester **38** gave a mixture of hydroperoxide **39** and peroxy hemiacetal **40**. Finally the treatment of the crude

mixture with *p*-TsOH results in the cyclisation of the intermediate to **1** with the overall yield of 28 % (Scheme 35).[149]



*Scheme 35: the synthesis of Artemisinin **1** from DHAA methyl ester **8** using $Cu(OTf)_2$ as acid catalyst, final treatment with p-TsOH results in the cyclisation of hemiacetal intermediate to Artemisinin **1**.*[149]

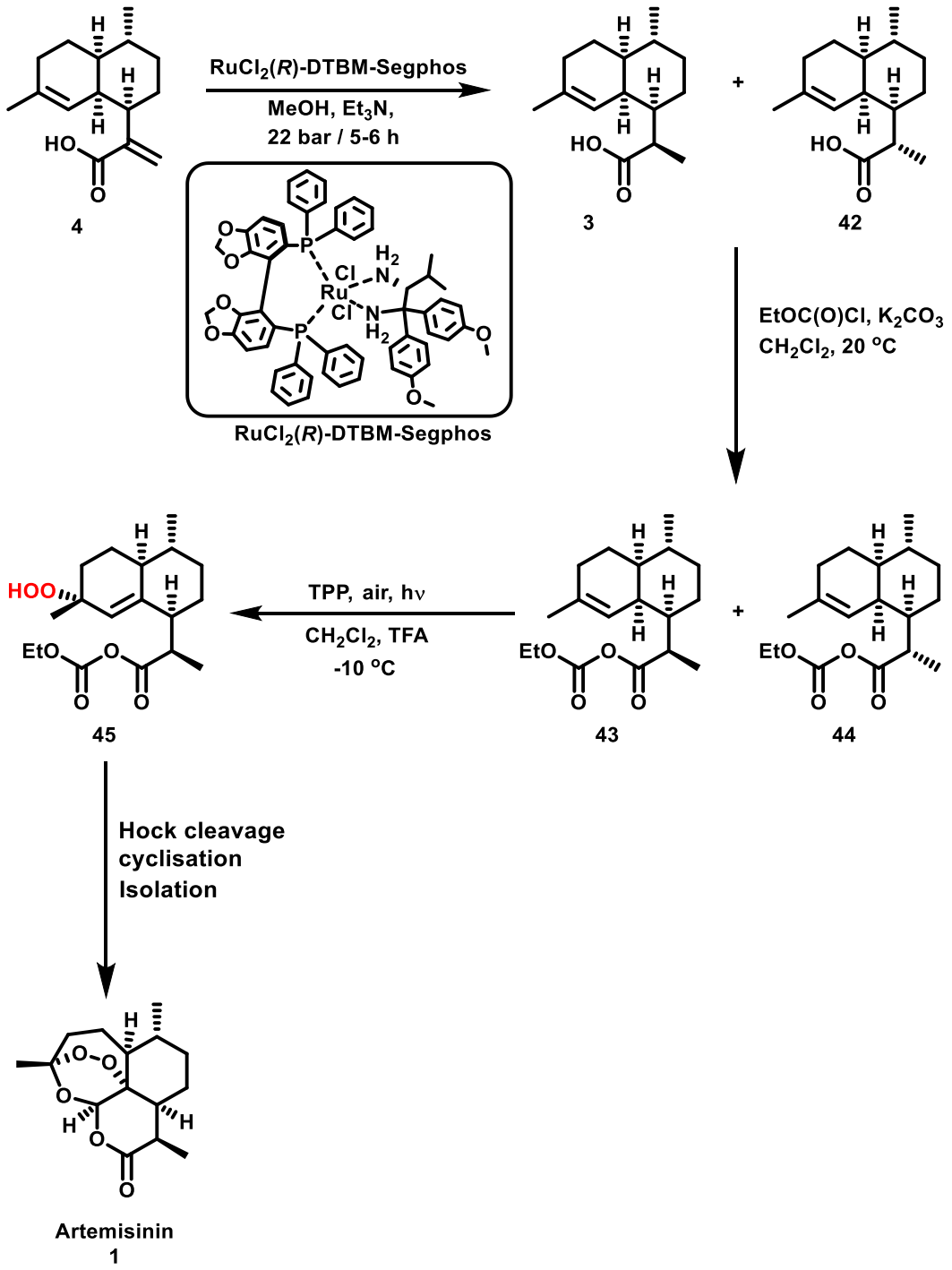
However, when the DHAA **3** was used directly without derivatisation under the same conditions, only 29 % of **1** was isolated, which might indicate that additional esterification does not result in the improvement of final yield of the product.



*Scheme 36: synthesis of Artemisinin from DHAA methyl ester **8** through the chemical generation of singlet oxygen from H_2O_2 using Molybdenum catalyst.*[150]

Paddon and co-workers,[127] also report the synthesis of Artemisinin **1** by initial esterification of DHAA **3** to its methyl ester **8** through readily accomplished large scale esterification process (Scheme 36). The esterification was performed with the aim of blocking the formation of γ-lactone **37**, a side product that occurs when the free carboxylic acid of **3** is subjected to strong acidic condition. This was followed by the use singlet oxygen ($^1O_2$) generated by a novel method through disproportion of H_2O_2 using molybdate catalyst for the oxidation,[151] with this technique clean tertiary hydroperoxide **2A** was produced with no evidence of any of the isomers or rearrangement products. The authors do not report the yield of the photo-oxidation product, but after the final acid catalysed Hock cleavage and cyclisation 40 - 45 % overall yield of Artemisinin **1** was realised. This was a notable improvement over the reported photosensitised singlet oxygen ($^1O_2$) routes.[83, 133, 149] The derivatisation step does not seem to improve the yield of Artemisinin **1**, because the same strategy was later employed by Yikang Wu to realise similar yield of **1** using TFA as an acid catalyst.[152]

In 2013, Sanofi started the industrial production of Artemisinin **1**,[1] after improving the selectivity of the hydrogenation of AA **4** to DHAA **3** from 90:10 reported by Amyris, to 95:5, through the development of less expensive Ruthenium catalyst ($RuCl_2$[(R)-DTBM-Segphos](DMF)) at lower S/C level 8,000 and 22 bar of H_2 to achieve full hydrogenation within few hours.[127] Mixture of DHAA enantiomers obtained from the hydrogenation process were converted to mixed anhydride with the used of ethyl chloroformate (EtOC(O)Cl and K_2CO_3 mixture in DCM at room temperature (Scheme 37). The activated ester obtained was used to synthesise **1**, adopting a one-pot approach to produce 55 % isolated yield of **1**.[1]



Scheme 37*: Synthesis of Artemisinin* ***1*** *using DHAA ethyl carbonate* ***43****, employed by Sanofi for industrial production.*[1]

The use of DHAA ethyl carbonate **43** and DHAA **3** as starting materials for the industrial synthesis of **1**, was optimised by Burgard *et al.* employing the method used by Sanofi to synthesise ethyl carbonate of **43**, using the same conditions for both substrates, higher

yield of 59 % of **1** were obtained from **43**, compared to the 50 % yield of Artemisinin **1**, obtained from **3** through One-pot approach.[3]

The use of fully integrated continuous flow reactor for the semi-synthesis of Artemisinin **1** was reported by Seeberger group using **3** as a precursor, and employing low temperature photo-oxidation technique, on overall yield of 39 % was recorded at -20 °C.[83] This was followed by optimisation of other reaction conditions including the nature and concentrations of photo-oxidation and acid catalysts, as well the temperature, which resulted in the improvement of the overall Artemisinin **1** yield to 59 %.[48]

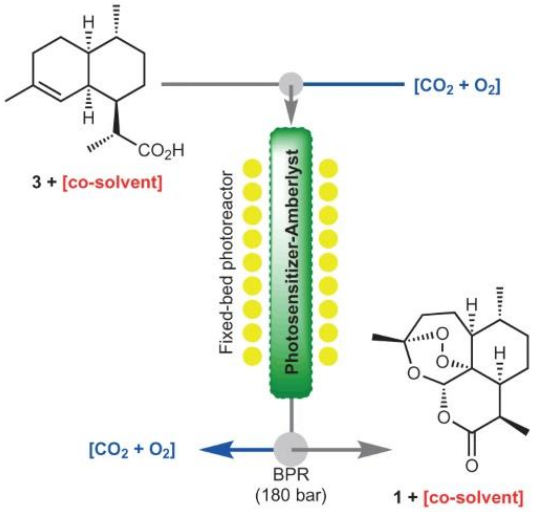


*Figure 21: schematic diagram of the CO_2/TPP supported Amberlyst continuous-flow reactor for the synthesis of Artemisinin **1**, modified from George and coworkers.*[2]

In the quest of finding more efficient route to Artemisinin **1** in 2015 George and his co-workers reported the use of liquid CO_2, a supported photosensitiser and ethanol/water mixture in its production.[2] The work demonstrated the used of acidic heterogeneous catalyst consisting of tetraphenyl porphyrin (TPP) supported on Amberlyst, which allows the system to facilitate both photo-oxidation and Hock-cleavage processes simultaneously. This avoids a second step with prolonged heating and another oxygen atmosphere in contrast to the synthesis developed by Seeberger,[83] and the use of

alcohol/water mixture at ambient temperature, reduced the energy consumption associated with cooling. Each of the methods has advantage of allowing an easier crystallization of Artemisinin **1** with little contamination from highly coloured photosensitisers. Although the process proved to be promising, the use of high pressure for generation of supercritical CO_2 and low isolated yield of Artemisinin **1** in the water experiments are the major limitations of the method.

Synthesis of Artemisinin 1 was also reported by this group through the work of Lee and Co-workers using the Vortex reactor.[79] The technique involve use of air drawn from the laboratory to facilitate the photo-oxidation process, unlike the traditional set-up which requires pressurised oxygen source. Through this method Artemisinin **1** was synthesised, employing one-pot procedure which involve addition of acid to the reaction mixture to produce 50 % of Artemisinin **1** at the outlet. The reactor has very good mixing properties that are beneficial for biphasic and triphasic mixture. Relatively low yield of Artemisinin **1** obtained in Vortex reactor bring the need for further optimisation of the process, to harness potentials for the synthesis of Artemisinin **1** at industrial scale.

The use of immobilised catalyst was also reported by Tambosco *et al.* for the synthesis of Artemisinin. Their strategy used of $[Ru(bpy)_3]Cl_2$ immobilised on the surface of Silica gel. The catalyst system also served a dual purpose, as the immobilised $[Ru(bpy)_3]Cl_2$ served as photocatalyst, while the weakly acidic silanol group on the silica gel facilitated the subsequent acid catalysed Hock-cleavage process.[66] Very low yield of Artemisinin **1** was obtained from this system, which can be attributed to the weak acidity of the silanol group on the silica.

To address these challenges, in this work we report the use of a simple and flexible photo-reactor (PhotoVap) in the semi-synthesis of Artemisinin **1** through semi-continuous approach, following a sequential two steps or one-pot strategies starting from DHAA **3**.

THE AIMS OF THE THESIS

The thesis involves development of methodology for the semi synthesis of an important anti-malarial compound, Artemisinin, with reference to the reported routes, and with the goal of enhancing the current route of its industrial production, through sustainable approach. The overall aim is to identify the best possible starting material and the most productive conditions for converting the starting material to Artemisinin **1**; to identify various side-products responsible for the decrease in the overall yield of Artemisinin, and to explore their reactivities and possible method of preventing their formation. We have four objectives:

(i) To optimise the semi-synthesis of Artemisinin **1** in both a sequential two-step and one-pot approach using the PhotoVap reactor. Moreover, the use of a previously reported silica immobilised photo-catalyst will be studied in the one-pot approach.

(ii) To determine the solubilities of the starting materials, and the photosensitisers, at different temperatures and concentrations in different solvent that will allow us to optimise of the onward semi-synthesis of Artemisinin, in aqueous solvents using the PhotoVap reactor.

(iii) To explore and exploit the use of a photosensitiser-biphenyl system through a redox mediation process to produce peroxides and to measure the effects that this will have on the formation of Artemisinin **1**.

(iv) To study the yield of various side products of thermal oxidation step of Artemisinin **1** synthesis and identify the best condition for their formation in higher yield. Explore the possible method of isolation and study their reactivity under various conditions to identify possible ways of preventing

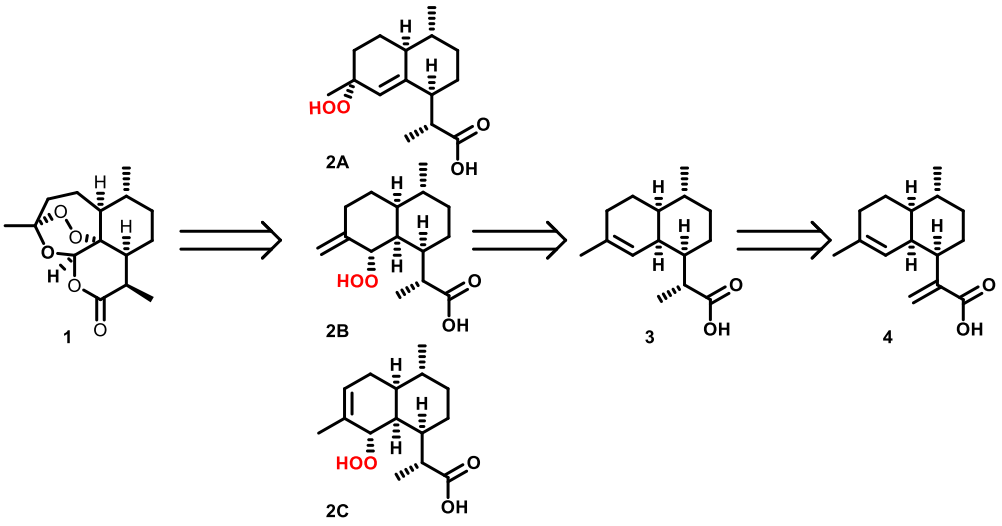
their formation or their conversion to other important intermediates that can be converted to Artemisinin **1**.

CHAPTER 2: OPTIMIZING THE SYNTHESIS OF ARTEMISININ IN THE PHOTOVAP REACTOR

This Chapter involves the development of a methodology for the semi-synthesis of Artemisinin **1**, an important anti-malarial compound using a modified rotary evaporator developed at Nottingham namely: the PhotoVap Reactor. The overall aim of this work was to optimise the conversion of DHAA **3** to Artemisinin **1** for the highest yields and productivities using an accessible reactor. In this Chapter, the background to the semi-synthesis of Artemisinin **1** will be first summarised and then the different objectives of this research will be discussed.

INTRODUCTION AND BACKGROUND

Dihydroartemisinic acid or (DHAA) **3**, is a key intermediate in the semi-synthesis of Artemisinin **1**. DHAA **3** is obtained from artemisinic acid (AA) **4** by the selective reduction of the acyclic alkene. AA **4** is obtained with high yields through a very sophisticated, process that uses genetically engineered yeast.[1] Together these steps form the start of semi synthesis of artemisinin **1** and are outlined in Scheme 38.



Scheme 38*: Retrosynthetic analysis for the semi-synthesis of artemisinin* ***1****.*

The second part of the semi-synthesis of **1** involves the chemical reactions of DHAA **3**. DHAA **3** is converted into a mixture of peroxides through an ene reaction with reactive oxygen species. This has been accomplished in several ways, but the major routes involve either catalytically,[145, 150, 153] or photochemically,[3, 48, 79] generated singlet oxygen ($^1O_2$). Following the ene reaction, the addition of an acid in presence of molecular oxygen, promotes the conversion of peroxide **2A** to Artemisinin **1** *via* a Hock-cleavage and thermal oxidation. This route was first discovered by Keasling[127] and since then considerable effort has been undertaken to develop and optimise the method further, and more specifically to this work, through the development of photochemical reactors that could either be operated in batch,[1, 3, 66] or in continuous flow.[2, 48, 79, 96] These studies have been driven, in part, by the hope to pave the way for an efficient scaling up of the process leading to Artemisinin **1** through semi-synthetic route to provide a cost effective alternative for this key drug for malaria. The reactors used for the synthesis of **1** have described in Chapter 1.

This Chapter involves development of methodology for the semi synthesis of important anti-malarial compound (Artemisinin). With reference to the reported routes, with the goal of enhancing the current route of its industrial production, through a sustainable approach. The overall aim is to identify the best possible starting material and the most productive conditions for converting the starting material to artemisinin. We have three objectives:

(i) To determine the range of parameters such as the solubilities of the starting materials and photosensitisers, at different temperatures and concentrations in different solvents.

(ii) To optimise the semi-synthesis of Artemisinin **1** in both a sequential two-step and one-pot approach using the PhotoVap reactor.

(iii) To optimise the semi-synthesis of Artemisinin **1** employing one-pot approach using a previously reported silica immobilised photo-catalyst the PhotoVap reactor.

(iv) To explore a redox mediation process on the production of peroxides (**2A**-**C**) and the effect this will have on the formation of Artemisinin **1**.

SCREENING OF THE SOLUBILITY OF DHAA IN ORGANIC SOLVENTS UNDER DIFFERENT CONDITIONS

The solubility of the solute in a particular solvent is dependent on temperature, acidity, and presence of other reaction mixtures. These make it imperative to determine the solubility of the reactants under intended conditions, especially for low-temperature continuous flow processes where undissolved or crystallised solids can potentially block the tubing used in the reactor causing pressure build-up and other safety issues.

The photo-oxidation of DHAA **3** was reported[48, 83, 133] to proceed with an improved yield and productivity at -20 °C,[48] therefore it is important to ensure that all the reaction mixtures are efficiently kept in solution under that condition, the solubilities of the mixtures of **3** and photosensitisers at concentrations of 0.05 M and 0.5 mol% respectively, has been determined under different temperatures.

*Table 3: Solubility of the complete reaction mixture screening at different temperatures in different solvent using a solution of DHAA **3** at 0.05 M.*

Entry	SM	PS	Solvent	Temperature (°C)					
				RT	0.6	-10	-18.7	-30	-40
1	DHAA	$[Ru(bpy)_3]Cl_2$	DCM						Cloudy
2			DCM + 2% EtOH						
3		TPP	DCM						
4			Toluene					Cloudy	Cloudy
5		DCA*	DCM					Cloudy	Cloudy
6			Toluene			Cloudy	Cloudy	Cloudy	Cloudy

In all cases, the organic solvent was added to the mixture of the solutes and mixed with the aid of a vortex mixer, the orange Colour = cloudy and the Green Colour = complete dissolution of the mixture, the same concentration of 0.5 mol% of each photosensitiser is used. * For DCA higher concentration of 50 mM has been tested in DCM and toluene.

In dichloromethane (DCM) there is increased solubility at room temperature down to -30 or - 40 °C, for mixtures containing TPP, and $[Ru(bpy)_3]Cl_2$ respectively (Table 3, Entries 1 and 3). In the latter case the decrease in solubility is attributed to the ionic nature of $[Ru(bpy)_3]Cl_2$, however the solubility of ionic photosensitizer $[Ru(bpy)_3]Cl_2$ can be improved by the addition of 2 % [v/v] ethanol to the mixture, thereby increasing the

solubility at - 40 °C (Table 3, Entry 2). In the presence of TPP, the mixture is fully dissolved at -40 °C in DCM. Changing the solvent to toluene reduced the solubility and the solution became cloudy at -30 °C (Table 3, Entry 3 and 4). The decrease in the solubility of the reaction mixture in toluene could be due to the polarity of DHAA **3**, causing the solubility in organic solvent to decrease at low temperature. The organic photosensitiser remained in solution at these temperatures.

Unlike for other photosensitisers, for DCA a higher concentration of 5 mol% has been used for the solubility test because a higher loading of DCA is required for the photo-oxidation process to be efficient. In DCM, the mixture remained fully dissolved at *ca* -20 °C (Table 3, Entry 5), but changing the solvent to non-polar toluene there is further reduction in solubility, because cloudy solution has been obtained at -10 °C. Thus, indicating the limitation of using high concentration of DCA at low temperature. This could also largely be due to its increased polarity coupled with the polarity of DHAA **3**. 5 mol% of DCA was employed by Seeberger and co-workers, for the continuous synthesis of Artemisinin **1** in flow reactor using 0.5 M DHAA **3** at slightly lower temperature of -20 °C. Here the improvement in its solubility may be to the presence of TFA before the photo-oxidation process.[48]

The results presented in this section show that better solubility of the reaction mixtures containing $[Ru(bpy)_3]Cl_2$ and TPP has been obtained in DCM, with the mixture remaining in solution at -30 °C. For the mixture containing DCA, the decrease in solubility is because higher concentration 5 mol% has been used for the screening. The results obtained have been used as a guide for the synthesis of Artemisinin **1**, as described in the following sections.

SEMI-SYNTHESIS OF ARTEMISININ IN PHOTOVAP REACTOR

The PhotoVap reactor has been described in detail in the previous Chapter, in this Chapter its application the semi-synthesis of Artemisinin **1** will be discussed. The optimisation of the reaction was carried in two ways; i) a single step process, where acid is added before the photo-oxidation; ii) a two-step process, where the acid is added after the photo-oxidation. Figure 22 consist of the structures and chemical shifts of DHAA **3**, photo-oxidation products of Artemisinin **1** and δ-lactone **33**.

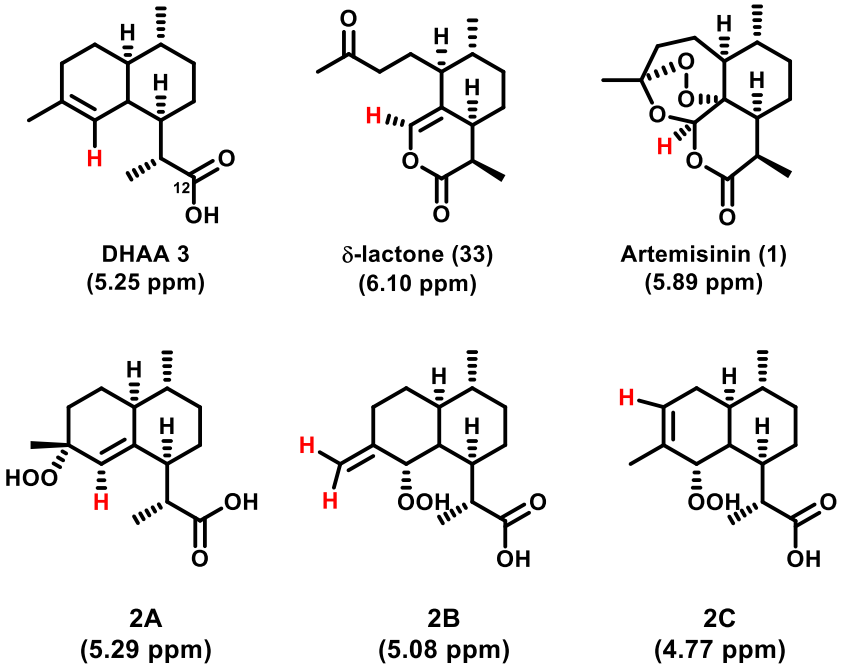
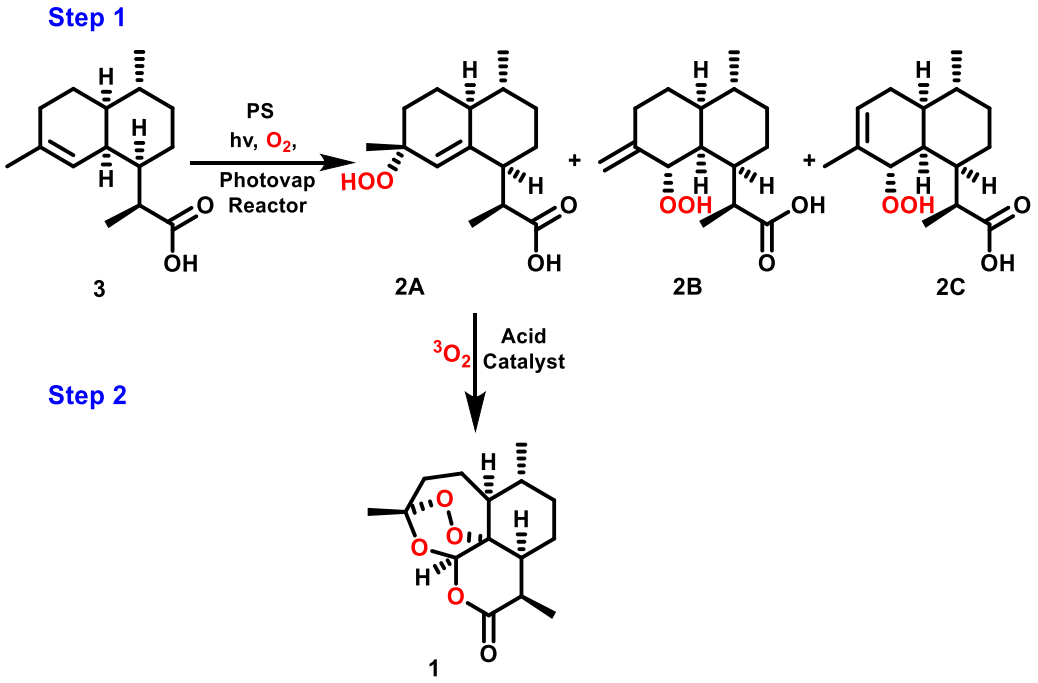


*Figure 22: the structures of Artemisinin **1**, DHAA **3**, hydroperoxide **2A-C**, δ-lactone **33**, and the ^{1}H-NMR chemical shifts of the alkene hydrogen atoms (shown in red)*

2.3.1. TWO STEPS SYNTHESIS OF ARTEMISININ FROM DHAA IN PHOTOVAP REACTOR.

A sequential two-step approach has the advantage of allowing for study of each step individually and the possibility of isolation and characterisation of the most stable and

persistent reaction intermediates. This is important because it provides information about the mechanism of the formation of Artemisinin **1** and side products produced at each step of the process.



*Scheme 39: The conversion of DHAA **3** into Artemisinin **1**, involving initial conversion of DHAA **3** into a mixture of hydroperoxides **2A-C**, followed by acid catalysed thermal oxidation yielding **1**.*

As discussed in Chapter 1, the initial photo-oxidation result in the formation of hydroperoxide intermediates (**2A** – **C**) among which only tertiary hydroperoxide **2A** lead to Artemisinin **1** (Scheme 39), while the remaining secondary hydroperoxides are degraded by the acid.

2.3.1.1 The 1st step: photo-oxidation of DHAA in the PhotoVap Reactor

The photo-oxidation of DHAA **3** has been performed in the PhotoVap reactor at ambient and low temperatures. For the latter the reactor was cooled using a chiller immersed into the cooling liquid (ethylene glycol/water mixture) in a reactor's bath, the chiller is set at the desired reaction temperature. The optimisation of photo-oxidation

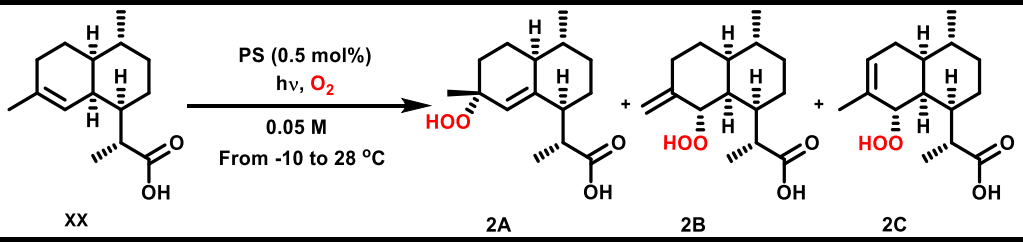
step has involved screening various temperatures, photosensitisers, and solvents, as described in the following sections.

2.3.1.1.1 Effects of Temperature and nature of Photosensitiser on DHAA Photo-oxidation

Temperature screening was performed using different sets of condition solvents and photosensitisers. The solubility of the photosensitiser varies with the solvent and temperature as described in the previous section. TPP, $[Ru(bpy)_3]Cl_2$, and DCA, were chosen for the photo-oxidation of **3** as these have been well described in the literature.[1-3, 48, 79] The use of these photosensitisers can possibly be explored due to their strong absorbance in the visible region, relative to the emission wavelength of the 300W LEDs having absorbance maxima at 456 and 595 nm, used in PhotoVap reactor. The choice of photosensitiser with high quantum efficiency can ensure efficient light harvesting for the photochemical processes, especially for applications involving $^1O_2$ generation, for the photo-oxidation of DHAA **3**. Table 4 describes the results obtained from the photo-oxidation of DHAA **3** in PhotoVap reactor using different photosensitisers under various conditions.

The photo-oxidation process was performed, at +28 and -10 ^oC using TPP as photosensitiser in toluene. This resulted in change in yield of **2A** from 90 to 84 % respectively. The higher temperature of 28 ^oC, favours the formation of 90 % of desired hydroperoxide intermediate **2A** (Table 4, Entry 1).

*Table 4: showing the percentage yields of hydroperoxides obtained after photo-oxidation of DHAA **3** under different conditions.*



Entry	PS (mol %)	Solvent	Temp. (°C)	Time (min)	Conv (%)	2A Yield (%)	2B Yield (%)	2C Yield (%)	Selectv. of 2A
1	TPP (0.5)	Toluene	28	7.5	100	90	7	2	90
2			-10	2.5	92	84	6	2	91
3		DCM	-10	7.5	100	64	8	4	64
4			-20	7.5	100	80	7	7	80
5	$[Ru(bpy)_3]Cl_2$ (0.5)	DCM/EtOH (98/02)	-05	7.5	97	62	6	2	64
6			-10		97	66	07	01	68
7			-20		92	61	04	03	66
8	$[Ru(bpy)_3](TFA)_2$ (0.5)	DCM	-10	7.5	90	52	09	02	57
9	DCA (5.0)	DCM	0	15	35	21	03	02	60
10				45	100	60	05	10	60
11		DCE	10	15	57	39	04	04	68
12				30	96	62	06	05	64
13		Toluene	10	15	37	22	03	02	59
14				30	51	21	03	03	41

Unless specified otherwise, the reaction was conducted in semi-continuous mode using 5 mL of solution in a 1 L round-bottom flask rotating at 175 rpm with O_2 bubbling through the solution at 60 sccm (sccm = standard cubic centimetres per minute). The yields and conversions were obtained from the corresponding integrals of proton-NMR chemical shifts of the DHAA **3** and the products, using 10 % biphenyl as internal standard, and the selectivity of **2A** was calculated from: conversion (%)/yield of **2A** (%).

Full conversion was achieved at -10 °C in DCM after 7.5 minutes irradiation, however, poor yield and selectivity of 64 % was obtained (Table 4, Entry 3). Decreasing the temperature to -20 °C under the same condition improved the yield to 80 % after full conversion (Table 4, Entry 4).

Although a higher yield of **2A** was realised at high temperature in toluene, better selectivity of 91 % was realised at lower temperature of -10 °C and increased productivity, because

92 % conversion has been achieved after 2.5 minutes irradiation in PhotoVap reactor (Table 4, Entry 2). Lower temperatures have been reported to favour the photo-oxidation process, owing to the better solubility of gasses at low temperature and increased stability of the excited photosensitiser,[48] and increased stability of the peroxides. For the photo-oxidation of DHAA **3**, lower temperatures was reported to result in the increased yield and selectivity of the tertiary hydroperoxide.[1, 48, 154] This is confirmed when $[Ru(bpy)_3]Cl_2$ was used as photosensitiser at temperatures ranging from -5 to -20 °C in DCM/EtOH (98:2) mixture (Table 4, Entry 5 – 7). The yield and selectivity of **2A** are 62 and 64 % respectively, were obtained after 97 % conversion of DHAA **3** at -5 °C (Table 4, Entry 5). Decreasing the temperature to -10 °C results in slight improvement of the yield and the selectivity to 66 and 68 % respectively (Table 4, Entry 6). However, further reduction in the temperature to – 20 °C does not improve the yield, and only 92 % conversion was achieved, with a yield of 61 % of **2A** (Table 4, Entry 7). The decrease in the yield at -20 °C could be due to poor solubility of $[Ru(bpy)_3]Cl_2$ in DCM at low temperature even after addition of 2 % [v/v] of EtOH.

The solubility of $[Ru(bpy)_3]Cl_2$ in DCM was improved by replacing the chloride anions with organic trifluoroacetate anion (TFA^-) through an anion metathesis (Equation 1).

$$[Ru(bpy)_3]Cl_{2(aq)} + 2AgTFA_{(aq)} \longrightarrow [Ru(bpy)_3](TFA)_{2(aq)} + 2AgCl_{2(s)}$$

Equation 1: Anion metathesis reaction for the conversion of $[Ru(bpy)_3]Cl_2$ to $[Ru(bpy)_3](TFA)_2$

The limited solubility of $[Ru(bpy)_3]Cl_2$ in DCM coupled with the potential of generating undesired strong acid (HCl) during acid catalysed thermal oxidation step, encouraged the synthesis of $[Ru(bpy)_3](TFA)_2$, to study its use as the photosensitiser in the photo-oxidation process. The absorption spectrum of the $[Ru(bpy)_3](TFA)_2$ is like that of $[Ru(bpy)_3]Cl_2$, with no obvious changes in the peak intensity, as shown in Figure 23. The

photo-oxidation of DHAA **3** with $[Ru(bpy)_3](TFA)_2$ in DCM under the same condition as $[Ru(bpy)_3]Cl_2$ did not improve the yield of **2A**, with 54 % **2A** obtained (Table 4, Entry 7) compared to 66 % of **2A** with $[Ru(bpy)_3]Cl_2$ (Table 4, Entry 5).

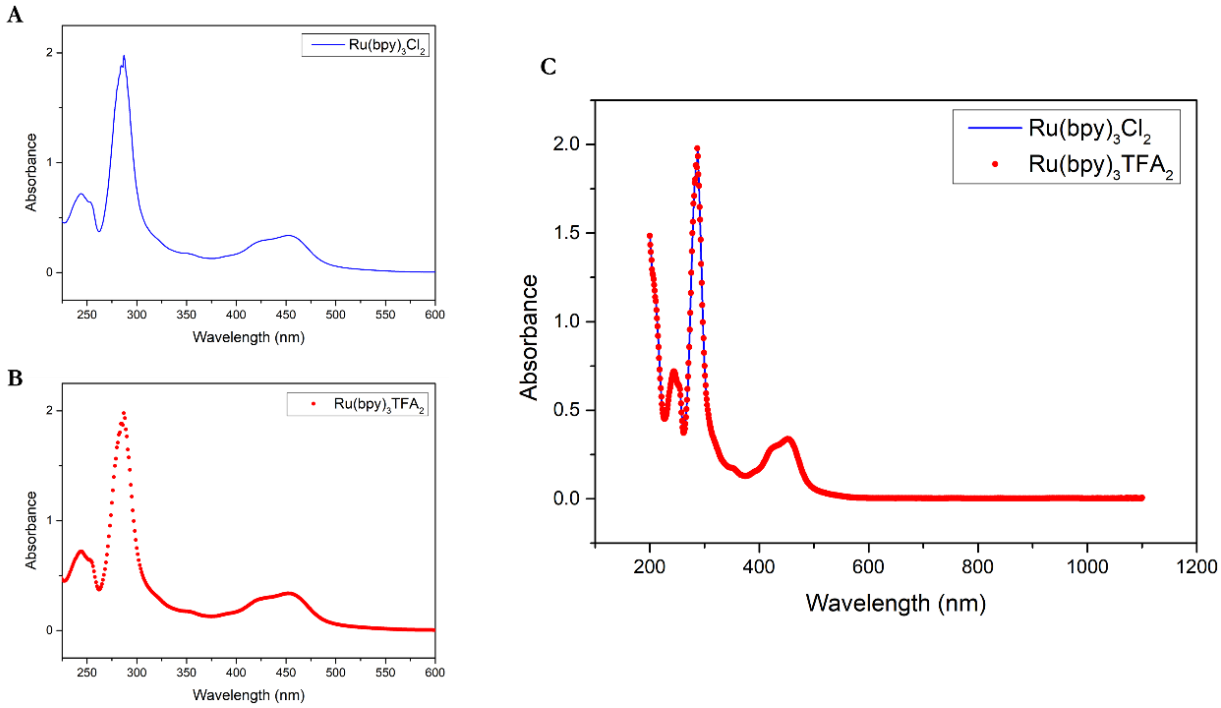


Figure 23: Comparison of the UV-Visible absorption spectrum obtained using 1 cm path length cuvette, 0.01 mM of $[Ru(bpy)_3]Cl_2$ (A) to that of $[Ru(bpy)_3](TFA)_2$ (B) in DCM, showing that the anion exchange has negligible effect on the absorption spectra. C shows the overlap of the spectra.

Like TPP and $[Ru(bpy)_3]Cl_2$, the properties of DCA have been extensively studied particularly its absorption of light at wavelength longer than 400 nm, with strong fluorescence in both polar and non-polar solvents,[50, 51] although it possesses a low absorption coefficient compared to highly coloured TPP and $[Ru(bpy)_3]Cl_2$.[50, 54] Because of its low absorption coefficient, a high concentration of it, is required to achieve a reasonable conversion of starting material. For the photo-oxidation of DHAA **3** in DCM using PhotoVap reactor, 5.0 mol% of DCA is used at low temperature (0 °C) to achieve 35 % conversion in 15 min with 21 % yield of tertiary hydroperoxide **2A** and 60 % selectivity (Table 4, Entry 9), prolonged irradiation for 45 minutes results in full

conversion and 60 % yield of **2A** with no change in the selectivity after prolonged irradiation. Due to high volatility of DCM at temperatures > 25 °C, the process was performed in dichloroethane (DCE) to prevent evaporation.

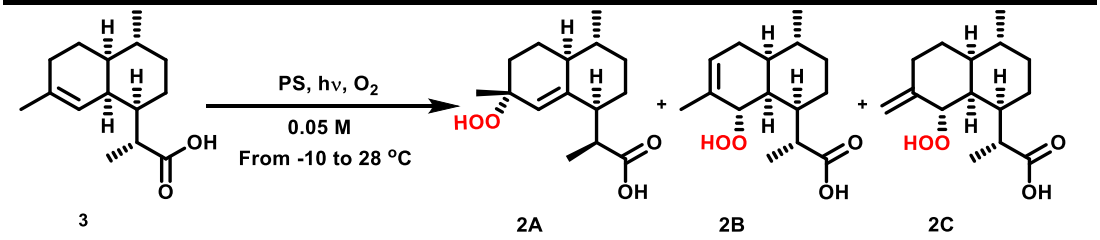
Increasing the temperature of the reaction to 10 °C, in DCE resulted in an improvement of the yield and selectivity to 39 and 68 % respectively after 15 min irradiation (Table 4, Entry 11). After 30 min irradiation, 96 % conversion was achieved with 62 % yield of **2A** (Table 4, Entry 12). In toluene, with DCA, there is decrease in the yield and selectivity of **2A** over time of irradiation (Table 4, Entries 13 and 14). This is an indication of the effect of nature of solvent on the photo-oxidation using DCA as photosensitiser which will be discussed in the following section.

2.3.1.1.2 Effects of the nature of solvents on the DHAA photo-oxidation PhotoVap reactor.

In solution, solvent molecules outnumber other substances present to a large extent and therefore, contribute actively to singlet oxygen quenching or deactivation.[28, 155] The non-radiative decay depends largely on the number of C-H and O-H bonds of the solvent, the non-radiative quenching increased with increase in the number of O-H bonds due to their high vibrational energy and the hydrogen bonding ability.[16, 54, 156]

Toluene, ethyl acetate, and DCM were used for the photo-oxidation processes, the $^1O_2$ lifetime in these solvents are 29, 45, and 99 μs at 25 °C respectively, using different photosensitisers. Chlorinated solvents have a higher lifetime of singlet oxygen as there is a decreased quenching rate.[155] Table 5 shows the results for the photo-oxidation of DHAA **3** in different solvents and solvents mixture, at different conditions of temperatures and photosensitiser.

*Table 5: show changes in the yields and selectivity, of photo-oxidation products of DHAA **3** in different solvents and temperatures.*



Entry	Solvent	PS (mol%)	Temp. (ºC)	Time (min)	Conv. (%)	Yield of 2A (%)	Yield of 2B (%)	Yield of 2C (%)	Selectv. of 2A
1	Toluene	TPP (0.5)	-10	2.5	92	84	06	02	91
2	Ethyl acetate			7.5	100	79	06	00	79
3	DCM			7.5	100	64	08	04	64
4	DCM/EtOH (98/02)	$[Ru(bpy)_3]Cl_2$ (0.5)		7.5	97	66	07	01	68
5	Toluene	TPP (0.5)	28	7.5	100	74	06	04	74
6	Ethyl acetate			7.5	100	90	07	02	90
7	Toluene	DCA (5.0)	10	15	37	22	03	02	59
8	DCE			15	57	39	04	04	68

Unless specified otherwise, the reaction was conducted in semi-continuous mode using 5 mL of solution in a 1 L round-bottom flask rotating at 175 rpm with O_2 bubbling through the solution at 60 sccm (sccm = standard cubic centimetres per minute). The yields and conversions were obtained from the corresponding integrals of proton-NMR chemical shifts of the DHAA **3** and the products, using 10 % biphenyl as internal standard, and the selectivity of **2A** was calculated from: conversion (%)/yield of **2A** (%).

The yield of **2A** in non-polar toluene is 84 % at -10 ºC, using TPP as photosensitiser, with 92 % conversion of DHAA **3** achieved after 2.5 minutes irradiation (Table 5, Entry 1). When the solvent is changed to polar aprotic ethyl acetate, the yield of **2A** decreased to 79 % after full conversion of **3** under the same condition (Table 5, Entry 2), surprisingly the yield further reduced when the solvent is changed to chlorinated solvent DCM, as only 64 % of **2A** (Table 5, Entry 3) was obtained after full conversion of DHAA **3** under the same conditions as in toluene and ethyl acetate. This is unexpected because the results are not consistent with the lifetime $^1O_2$ 29, 45, and 99 μs, in toluene, ethyl acetate, and DCM respectively, at 25 ºC. These results indicate that although the lifetime of singlet

oxygen in each solvent play an important role in the photo-oxidation process, the yield of the photo-oxidation products does not solely depend on its lifetime in each solvent.

The addition of 2 % ethanol to DCM (to increase the solubility of $[Ru(bpy)_3]Cl_2$) resulted in an increase in the yield and selectivity of **2A** to 66 and 68 % respectively, at 97 % conversion after 7.5 min irradiation (Table 5, Entry 4) the addition of ethanol appears to slow the rate of reaction. In toluene the yield and selectivity decreased when increasing the temperature (Table 5, Entries 1 and 5), which could be due to the decrease of solubility of molecular oxygen gas at higher temperature. However, in ethyl acetate the increase of temperature affected positively the yield and selectivity of tertiary hydroperoxide **2A** (Table 5, Entries 2 and 6). Moreover, it is worth noting that increasing the temperature from -10 °C to 28 °C resulted in a better selectivity towards the tertiary hydroperoxide **2A** in ethyl acetate while temperature increase was detrimental to the selectivity of the desired hydroperoxide **2A** in toluene, when TPP was used as the photosensitiser.

The effect of solvent on the photo-oxidation of DHAA **3** was also studied in toluene and DCE using DCA as the photosensitiser at 10 °C. Unlike other photosensitisers the reaction proceeds at slower rate, due to the decrease in absorption coefficients of DCA as discussed in the previous section. After 15 min irradiation at 10 °C only 37 % conversion of DHAA **3** was achieved with a yield of 22 % of **2A** in toluene (Table 5, Entry 7), while in DCE the conversion increased to 57 % with the yield of 39 % of **2A** (Table 5, Entry 8).

From the results discussed the best condition for the photo-oxidation of DHAA **3** in PhotoVap reactor was found to be with a polar aprotic solvent ethyl acetate at room temperature to produce 90 % of **2A** after 7.5 minutes irradiation using TPP as photosensitiser (Table 5, Entry 6). A similar selectivity was obtained in toluene using TPP at -10 °C. The used of ethyl acetate is considered as the best option due to its lowest

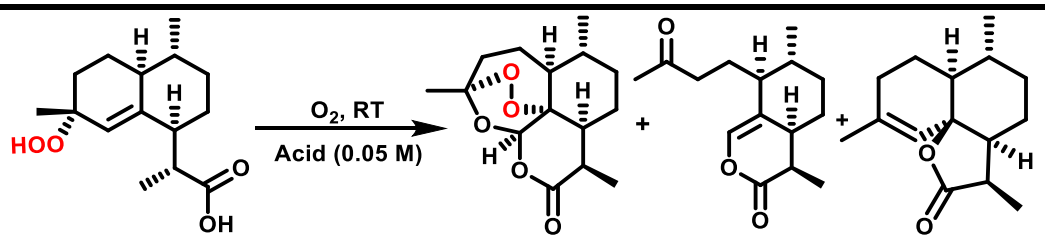
toxicity and reduced cost of Artemisinin **1** production, as the process does not involve cooling.

2.3.1.2 STUDY OF THE SECOND STEP: ACID CATALYSED HOCK CLEAVAGE FOLLOWED BY THE "THERMAL OXIDATION".

The synthesised tertiary hydroperoxide **2A**, obtained from photo-oxidation of DHAA **3**, reacts with acid the process known as Hock-cleavage, this is then followed by a thermal oxidation process with molecular oxygen to produce **1**. Due to the complexity of this stage, it is believed that the yield and the productivity of the desired product depend on the careful control of reaction conditions, as well as the solvents and acid catalyst.[106, 157] Brown *et al.* described the role of carboxylic acid group at 12-position on spontaneous autoxidation of the tertiary hydroperoxide,[157] with a detailed description of various possible reaction pathways undergone by this photo-oxidation product. The formation of various side products, including polymers formed from the condensation of some unstable intermediates. Which illustrates the complex nature of this step and the difficulty in obtaining high yields of **1**.

shows the results obtained for the Hock cleavage/thermal oxidation experiments, which were achieved by bubbling of oxygen gas to the crude photo-oxidation products in solution, after the addition of 0.5 equiv. of TFA. The experiments were monitored until consumption of peroxide **2A**, resulting in the formation of 14 % of **1** after 1 h in toluene with a productivity of 0.19 g/day (, Entry 1). In DCM, a yield of 31 % was obtained which did not greatly increase after 24 h, as only 45 % of **1** was realised. The δ-lactone **33** appeared to degrade over time from 15 to 4 %. (, Entry 2 and 3).

*Table 6: Acid catalysed thermal oxidation of DHAA **3** in different solvents.*



Entry	Solvent	Time (h)	Acid (equiv.)	Yield of 1 (%)	Yield of δ-lactone 33 (%)	Yield of γ-lactone 37 (%)	Prod. of 1 (g/day)
1	Toluene	1	TFA (0.5)	14	07	04	0.19
2	DCM	3	TFA (0.5)	31	15	03	0.21
3		24	TFA (0.5)	45	04	02	0.03
5	Ethyl acetate	1	TFA (0.5)	17	30	03	0.20
6		24	TFA (0.5)	46	00	02	0.03
7		24	TFA (1.0)	39	02	02	0.02
8	Toluene	1	TMSTFA (0.5)	69	02	02	0.64

Unless specified otherwise, the reaction was conducted in semi-continuous mode using 5 mL of solution in a 1 L round-bottom flask rotating at 175 rpm with O_2 bubbling through the solution at 60 sccm (sccm = standard cubic centimetres per minute). The yields and conversions were obtained from the corresponding integrals of proton-NMR chemical shifts of the DHAA **3** and the products, using 10 % biphenyl as internal standard. The productivity was calculated from [Conc. (DHAA)*(vol.(mL)/1000/total time(min.))*1440*Molecular weight of Art.*Yield (%)], total time = time of photo-oxidation + time of thermal oxidation.

In ethyl acetate the ^{1}H-NMR spectrum taken immediately after addition of 0.5 equiv. of TFA to the oxygen saturated mixture of peroxide **2A** - **C**, shows complete consumption of **2A** and 17 % of Artemisinin **1** and a significant yield of δ-lactone **33** (30 %) (, Entry 5). Prolonged bubbling of oxygen for 24 hours at room temperature produced 46 % of **1** (, Entry 6) with loss of all the δ-lactone, presumably *via* degradation. Although, the photo-oxidation gave highest yield and selectivity of **1**, the second step performed poorly. Increasing the amount of TFA to 1.0 equiv. did not improve the outcome (, Entry 7). Using TMSTFA resulted in the production of 69 % of **1** with the projected productivity of 0.64 g/day (, Entry 8).

The duration of acid catalysed reaction step shows that prolonged bubbling of oxygen or exposure to acid is accompanied by a decrease in yield of **1**. It is possible that oligomerisation involving some reactive intermediates occurs before the final cyclisation to Artemisinin **1**,[2] or the Artemisinin **1** itself is unstable. Another observation here is that upon addition of acid there is formation of δ-lactone **33**, but upon prolonged bubbling of oxygen, the δ-lactone **33** disappears with a non-linear increase in the yield of **1**. This suggest that not all δ-lactone **33** is converted to Artemisinin **1** and could be attributed to one or more of the many possible side reactions leading to the formation of unwanted products.

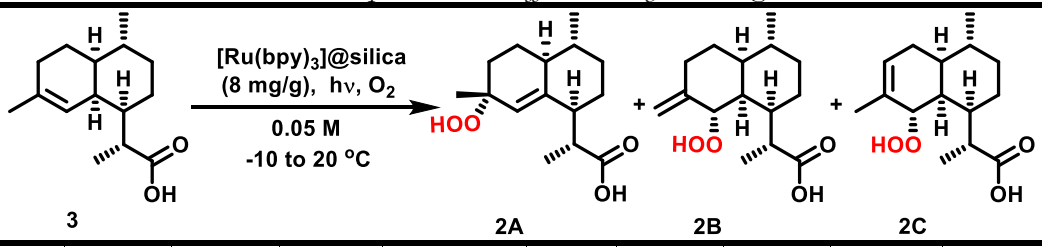
For the acid catalysed Hock-cleavage and the thermal oxidation cascade to Artemisinin **1** described, a good yield is achieved with TMSTFA. The use of TMSTFA, when further optimised, has the potential of replacing the traditionally used TFA in the industrial production of Artemisinin **1**. Also upon further optimisation, this method could serve as an alternative route for the industrial production of **1**, to replace the current method involving initial derivatisation of **3** to its carbonate, the process that further increase the cost of Artemisinin production.[1]

An acid catalysed thermal oxidation, through simple immobilisation of TPP on Amberlyst containing sulfonic acid moieties acting as the acid catalyst was reported.[2] The system functions well in the one-pot synthesis of **1**, with little leaching after the initial reaction cycle, thereby removing the need of separating the highly coloured photosensitiser which often leads to the decrease in the amount of isolated products.

2.3.1.3 TWO STEPS SYNTHESIS OF ARTEMISININ USING HETEROGENOUS CATALYST SYSTEM

Another approach to the synthesis of Artemisinin **1** is through heterogeneous catalysis involving photo-catalyst immobilisation on the surface of silica gel, in which the silanol group of the silica gel can serve as the acid catalyst for the second step of the reaction. This method was reported in the synthesis of Artemisinin **1** using a batch reactor [66] and was applied here using PhotoVap reactor. The dual-action catalyst system as reported by Amara *et al.* to facilitate both photo-oxidation.

*Table 7: Results obtained for photo-oxidation of DHAA **3** using Silica-supported [Ru(bpy)$_3$]Cl$_2$ in PhotoVap Reactor at different catalyst loading.*



Entry	Solvent	Cat. (mol%)	Temp. (°C)	Time (min)	Conv. (%)	2A Yield (%)	2B Yield (%)	2C Yield (%)	Selectv. of 2A (%)
1	Toluene	0.5	20	15	75	47	8	5	63
2		0.5	-10	7.5	99	64	8	4	65
3	DCM	1.0	20	15	100	40	9	5	40
4		0.5	-10	15	100	60	9	2	60

Unless specified otherwise, the reaction was conducted in semi-continuous mode using 5 mL of solution in a 1 L round-bottom flask rotating at 175 rpm with O_2 bubbling through the solution at 60 sccm (sccm = standard cubic centimetres per minute). The yields and conversions were obtained from the corresponding integrals of proton-NMR chemical shifts of the DHAA **3** and the products, using 10 % biphenyl as internal standard, and the selectivity of **2A** was calculated from: conversion (%)/yield of **2A** (%).

The use of heterogeneous catalyst system for the synthesis of Artemisinin **1** has advantages as it can facilitate both photo-oxidation and acid catalysed reaction steps, allowing the production of **1** through a one-pot approach. Another advantage is the ease of isolation and recovery of **1**, without contamination by the highly coloured photosensitiser, which is difficult and costly to remove. Employing this approach Tambosco *et al.* reported the synthesis of **1** in a batch reactor achieving the recorded yield of up to 37 %.[66]

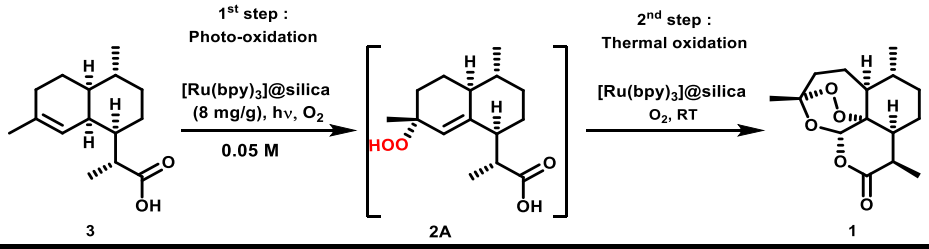
shows the results obtained from the photo-oxidation performed in the PhotoVap reactor using silica gel loaded with 2.5 mg/g and 8.0 mg/g $[Ru(bpy)_3]Cl_2$. After 15 minutes irradiation at 20 °C in toluene with 0.5 mol% of the supported catalyst, 75 % conversion of DHAA **3** was obtained with the yield of 47 % of the desired peroxide **2A** (, Entry 1). Running the reaction at a lower temperature of -10 °C for 7.5 min of irradiation in toluene, an excellent conversion of 99 % and a yield of **2A** of 64 % was achieved (, Entry 2).

Changing the solvent to DCM gave full conversion of **3** after 15 minutes irradiation, with the formation of 60 % of **2A** at low temperature of -10 °C (, Entry 4). Increasing the catalyst concentration to 1.0 mol% resulted in full conversion of **3**, with a decreased yield and selectivity of 40 % for **2A** (, Entry 3). After the photo-oxidation, the formation of Artemisinin **1** was not observed.

Because of the inability of the silica bound catalyst to facilitate immediate conversion to Artemisinin **1**, molecular oxygen was bubbled through the crude products of the photo-oxidation, in a round bottom flask, without removing the silica-supported catalyst. The conversion of the photo-oxidation product **2A** into Artemisinin **1** were monitored over time.

In toluene, oxygen was bubbled for 3 hours, and the yield of Artemisinin **1** obtained was calculated to be 1 % after 45 % conversion (Table 8, Entry 1). Similar results were obtained when the reaction was run in DCM, with only 2 % of Artemisinin **1** formed after one hour of bubbling oxygen at room temperature. Lowering the temperature to -10 °C does not improve the conversion after 1 hour (Table 8, Entry 3).

Table 8: Results obtained after bubbling of O_2 through to the photo-oxidation products in the presence of silica-supported.



Entry	Solvent	Temp. (°C)	Time (hours)	Conv. of 3 (%)	Art. (%)	δ-lactone (%)	γ-lactone (%)
1	Toluene	22	3	45	1	1	6
2	DCM	22	1	47	2	1	6
3		-10	1	47	3	0	4

Unless specified otherwise, the reaction was conducted in semi-continuous mode using 5 mL of solution in a 1 L round-bottom flask rotating at 175 rpm with O_2 bubbling through the solution at 60 sccm (sccm = standard cubic centimetres per minute). The yields and conversions were obtained from the corresponding integrals of proton-NMR chemical shifts of the DHAA **3** and the products, using 10 % biphenyl as internal standard.

Because of this, it was assumed that either the starting material or the product might have high affinity to silica resulting to their adsorption or a strong interaction with its surface. To probe this hypothesis, the solution of Artemisinin **1** of known concentration was prepared in toluene, after which silica supported catalyst was added and the solution left stirring for 1-hour. Proton NMR spectra were recorded before the addition of the supported catalyst and after stirring the mixture containing the supported catalyst (Figure 24).

The comparison between the proton NMR spectra before and after the addition of the supported catalyst shows that the amount of Artemisinin **1** decreased after the addition of the silica-catalyst system and stirring, hence supporting this hypothesis. Another limiting factor for the use of the silica supported catalyst, is that large amount of silica powder containing the photosensitiser of equivalent concentration required, even at higher photosensitiser loading, this could result in a large volume of waste as well as limiting the light penetration even in a batch reactor set-up. Because up to 0.374 g and

0.117 g of silica supported catalyst of 2.5 and 8.0 mg/g respectively are equivalent to 0.5 mol% of the photosensitiser in 5 mL solution.

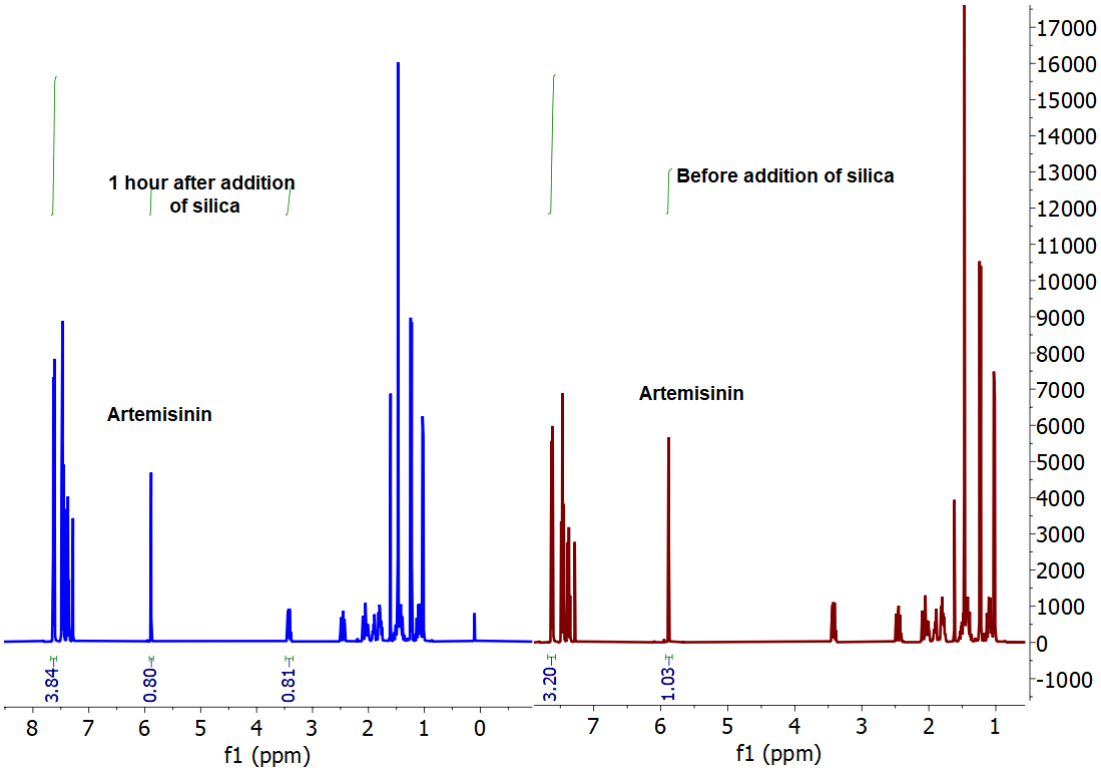


*Figure 24: ^{1}H-NMR spectrum of obtained before addition of silica gel and 1 hour after addition of silica gel to the solution of **1** in toluene.*

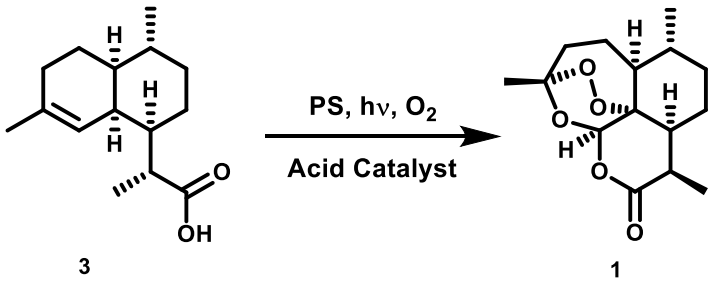
Although considerable yield of tertiary hydroperoxide **2A** was achieved in PhotoVap reactor with limited leaching of photosensitiser from the silica surface, the process is limited by the fact that it can only proceed manually on batch setup. It is practically difficult to pump a slurry of silica gel in the semi-continuous setup of the PhotoVap reactor and requires a large volume of solution and supported catalyst. A single batch will encounter decreased light penetration, which will ultimately reduce the productivity of the process according to the Beer-Lambert Law.

In summary, the results show low overall yield of the Artemisinin **1** encountered due to the complexity of the second step, which often involves prolonged bubbling of oxygen before the completion of the process, with the use of TFA as an acid catalyst lower overall

yield of Artemisinin **1** was obtained. However, when TMSTFA is used, the yield improved to 60 % with limited side products formed. The use of a silica based heterogeneous catalyst showed promise with the photo-oxidation step but failed to yield Artemisinin **1** in any significant amounts.

2.4.1. ONE-POT SYNTHESIS OF ARTEMISININ IN PHOTOVAP REACTOR

Another strategy for semi-synthesis of **1**, is through One-pot process which involves the addition of acid catalyst before photo-oxidation thereby allowing the acid catalysed thermal oxidation to proceed immediately after the photo-oxidation process. The following section will explore the synthesis of **1** through the one-pot process in the PhotoVap reactor using DHAA **3** as precursor (Scheme 40).



3 1

Scheme 40*: the one-pot synthesis of Artemisinin **1** using DHAA **3** as a starting material.*

The one-pot process was carried out in the PhotoVap reactor and was run semi-continuously under different conditions, to optimise the best method for improving the yield and productivity of **1**.

2.4.1.1 THE EFFECT OF VARYING THE PHOTOSENSITISER ON THE YIELD AND PRODUCTIVITY OF ARTEMISININ

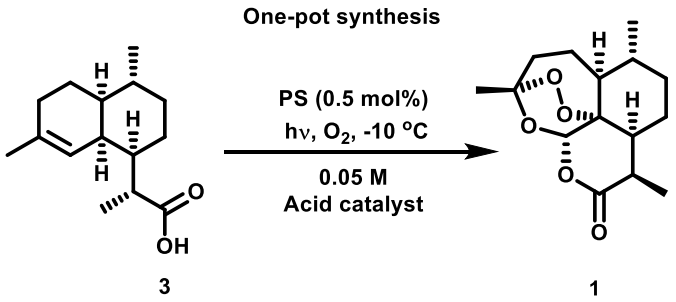
Although, other factors such temperature, nature of acid catalyst and solvents can influence the rate and selectivity of the reaction, photosensitisers play an important role in the overall conversion of DHAA **3**, which is the very start of the whole process. However, unlike in the two-step process where acid is added only after photo-oxidation, the presence of acid has potential to affect the photophysical properties of the photosensitiser. For example, the presence of acid will influence the singlet oxygen quantum yield (Φ_Δ) of free base TPP, through protonation of the nitrogen atoms.[158] The Φ_Δ measured for TPP with corresponding diacids; CF_3COOH, $Cl_2CHCOOH$, $HClO_4$ and H_2SO_4, show an increase in the Φ_Δ for CF_3COOH and ClCHCOOH compared to TPP, and decrease in Φ_Δ with $HClO_4$ and H_2SO_4. [158] This protonation often results in the shift of its maximum absorption wavelength from 420 to 435 nm,[3] shown visibly by the catalyst becoming a deep green colour, rather than reddish colour.

Unlike porphyrin photosensitisers, the presence of acid does not have much impact on the Φ_Δ of $[Ru(bpy)_3]Cl_2$. The Φ_Δ of $[Ru(bpy)_3]Cl_2$ arises from the interactions between the MLCT state of $[Ru(bpy)_3]^{2+}$ and oxygen molecule, which leads to an almost equal yield of energy transfer to the oxygen molecule. Any possible effect of acid Φ_Δ of $[Ru(bpy)_3]Cl_2$ is only observed at high acid concentration.[159]

shows the results obtained from the one-pot synthesis of Artemisinin **1** using TPP and $[Ru(bpy)_3]Cl_2$ as photosensitisers. In the PhotoVap reactor at -10 °C, the use of TPP in the presence of 0.5 equiv. of TFA in toluene provided full conversion of DHAA **3** within 7.5 min of irradiation with good yield and a projected productivity of Artemisinin **1** of respectively 64 % and 8.34 g/day. Running the reaction in DCM under the same

conditions resulted in a yield and productivity of 58 % and 7.56 g/day respectively (Table 9, Entries 1 and 2).

*Table 9: show the effect of nature of photosensitiser on the one-pot synthesis of Artemisinin **1**, at temperature of -10 °C, and 0.5 equiv. of acid catalyst, after full conversion of starting material (DHAA **3**), in different solvents.*



Entry	PS	Acid Cat. (0.5 equiv.)	Solvent	Time (min)	Conv. (%)	Art. Yield (%)	Prod. of 1 (g/day)
1	TPP	TFA	Toluene	7.5	100	64	8.34
2	TPP	TFA	DCM	7.5	100	58	7.56
3	TPP	TCA	DCM	5	100	46	8.82
4	TPP	TCA	Toluene	7.5	100	62	8.08
5	TPP	TMSTFA	Toluene	20	100	51	2.59
6	$[Ru(bpy)_3]Cl_2$	TFA	DCM	5	100	75	14.38
7	$[Ru(bpy)_3]Cl_2$	TCA	DCM	5	100	65	12.47

Unless specified otherwise, the reaction was conducted in semi-continuous mode using 5 mL of solution in a 1 L round-bottom flask rotating at 175 rpm with O_2 bubbling through the solution at 60 sccm (sccm = standard cubic centimetres per minute). Yields were calculated based on the relevant peaks in the ^1H NMR spectrum with reference to an internal standard (biphenyl), for all the yields calculated and all samples ran in triplicate. The productivity was calculated from [Conc. (DHAA)*(vol.(mL)/1000/time(min))*1440*Molecular weight of Art.*Yield (%)]. PS = Photosensitiser.

Changing the acid catalyst to trichloroacetic acid (TCA) gave a decrease in the yield of Artemisinin to 46 % after full conversion, but there is an improvement in the a projected productivity to 8.82 g/day (Table 9, Entry 3). The decrease in the yield of Artemisinin **1** might be because of side reactions involving some the generated reactive intermediates in DCM, because when the reaction was repeated in toluene full conversion resulted in an increase in the yield of Artemisinin **1** to 62 %.

Using TMSTFA there is a decrease in yield and productivity of Artemisinin **1**, because full conversion was achieved only after 20 min irradiation, with decreased yield of 51 % and projected productivity of 2.59 g/day (Table 9, Entry 5).

One-pot synthesis of Artemisinin **1** using this reactor with $[Ru(bpy)_3]Cl_2$ in DCM resulted in the improved yield and productivity compared to the previously described two-step process (Section 2.3.1), where the yield is limited by poor solubility of the catalyst especially for low temperature reactions. Here the highest and very good yield of 75 % Artemisinin **1** was obtained at low temperature of -10 °C and 0.5 equiv. of TFA but changing the acid catalyst to TCA only lead to the decrease in the yield of **1** under the same condition, although the two processes proceed with the same rate (Table 9, Entries 7 and 8).

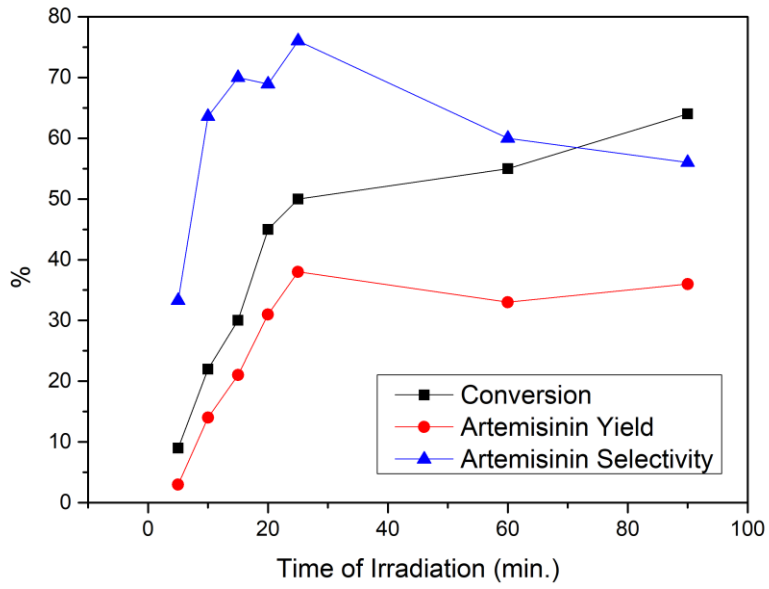


Figure 25*: Showing the relationship between irradiation time on the yield of Artemisinin* ***1*** *from DHAA* ***3****, for One-pot Synthesis in PhotoVap Reactor using 5.0 mol% of DCA as photosensitiser at low temperature in toluene. There is no significance attached to the lines connecting the points, as they are used to guide the eye.*

In Figure *25* Artemisinin **1** yield is plotted against the time of irradiation using DCA. The reaction proceeds with a slow increase in Artemisinin **1** yield with only 3 % of **1** produced after 5 min irradiation. The yield increased with prolonged irradiation, and after 38 min

where the Artemisinin **1** yield reached its peak, with no further increase in yield despite continuing consumption of DHAA **3**.

The slow rate of the reaction encountered was due to very low extinction coefficient of DCA even though higher concentration of 5 mol% is used compared to other photo-catalyst such as TPP and $[Ru(bpy)_3]Cl_2$, where mostly 0.5 mol% has been used to achieve good conversion. Despite slow rate of the reaction with DCA, there is noticeable improvement in selectivity to **1** before the reaction reaches equilibrium, as the selectivity of 75 % was achieved at 45 % conversion of the starting material and Artemisinin **1** yield of up to 35 % (Figure 25).

The one-pot synthesis of Artemisinin **1** in PhotoVap reactor proceed with very good yield and productivity, compared to the two-step approach. Very good yield of 75 % Artemisinin **1** was obtained at -10 °C using $[Ru(bpy)_3]Cl_2$ as photosensitiser. Using TPP as photosensitiser, the yield of **1** is not higher and the presence of acid catalyst resulted in protonation of the catalyst, the process that is thought to affect the efficiency of the photosensitiser. Because of the observed effect, in the following section, the effect of acid and solvents on the yield of Artemisinin **1** are studied.

2.4.1.2 Effect of the Acid Catalyst and Solvent on the yield of Artemisinin

The nature of the acid catalyst plays an important role for the acid catalysed Hock – cleavage, as described in Chapter 1. This process involves Brønsted or Lewis acid promoted rearrangement of hydroperoxides to form mostly alcohols and carbonyl compounds which depends on the reactivity of the compound containing the hydroperoxide group.[160] Aliphatic hydroperoxides are associated with the higher resistance toward acid-catalysed rearrangements compared to benzylic and allylic hydroperoxides, for the former Hock rearrangement is reported to proceeds readily in

concentrated Sulphuric acid (H_2SO_4),[161] or Superacids (FSO_4H).[162] The increase in the reactivity of the later hydroperoxides allows the rearrangement to proceed under mild acidic conditions, such as the very low concentration of TFA in the rearrangement of tertiary hydroperoxides **2A**.[48] Levesque and Seeberger tested different Bronsted and Lewis acid catalysts such as camphorsulfonic acid, copper(II) trifluoromethanesulfonate, DOWEX, p-toluenesulfonic acid, and trifluoroacetic acid (TFA) in various solvents to identify better condition for Hock cleavage of **2A** into the enol intermediate **5**, and TFA was identified as the best acid catalyst under the reaction condition.[83]

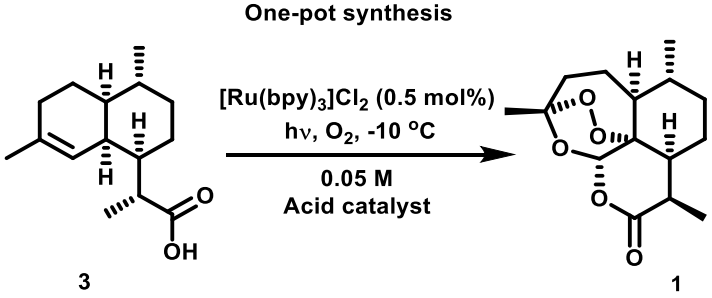
*The results for the one-pot synthesis of **1** in this reactor are shown in*
Table 10 and shows the effect of acid concentration on the reaction. As presented in the previous section the highest yield of 75 % of **1** was obtained from 0.5 equivalent of TFA in DCM at -10 °C. Increasing the acid concentration to 1.0 equiv. under the same conditions resulted in slight decrease in the yield of **1** to 71 % (

Table 10, Entry 1 and 2). A further decrease in the yield of Artemisinin **1** was observed. However, no decrease in the reaction rate was seen when TFA is replaced with TCA under the same condition, as 65 % of **1** was obtained after 5.0 minutes irradiation with projected productivity of 12.47 g/day, (

Table 10, Entry 3). For most of the reactions with TCA (as will be described later) changing the photo-oxidation catalyst does not seem to affect the yield and productivity of Artemisinin **1**. In ethyl acetate the process does not result in a significant yield of Artemisinin **1**, as only 15 % was obtained at 20 °C, using 0.5 equiv. of TFA. Doubling the acid concentration of acid to 1.0 equiv. improved the yield to 42 % under the same condition (

Table 10, Entries 4 and 5), this could be due to the decreased lifetime of singlet oxygen in ethyl acetate compared to DCM, coupled with an increase in temperature, which could also decrease the life span of $^1O_2$ through quenching.

*Table 10: Showing the effect of solvent and acid concentrations on the yield and productivity of Artemisinin **1**, after full conversion of DHAA **3**.*



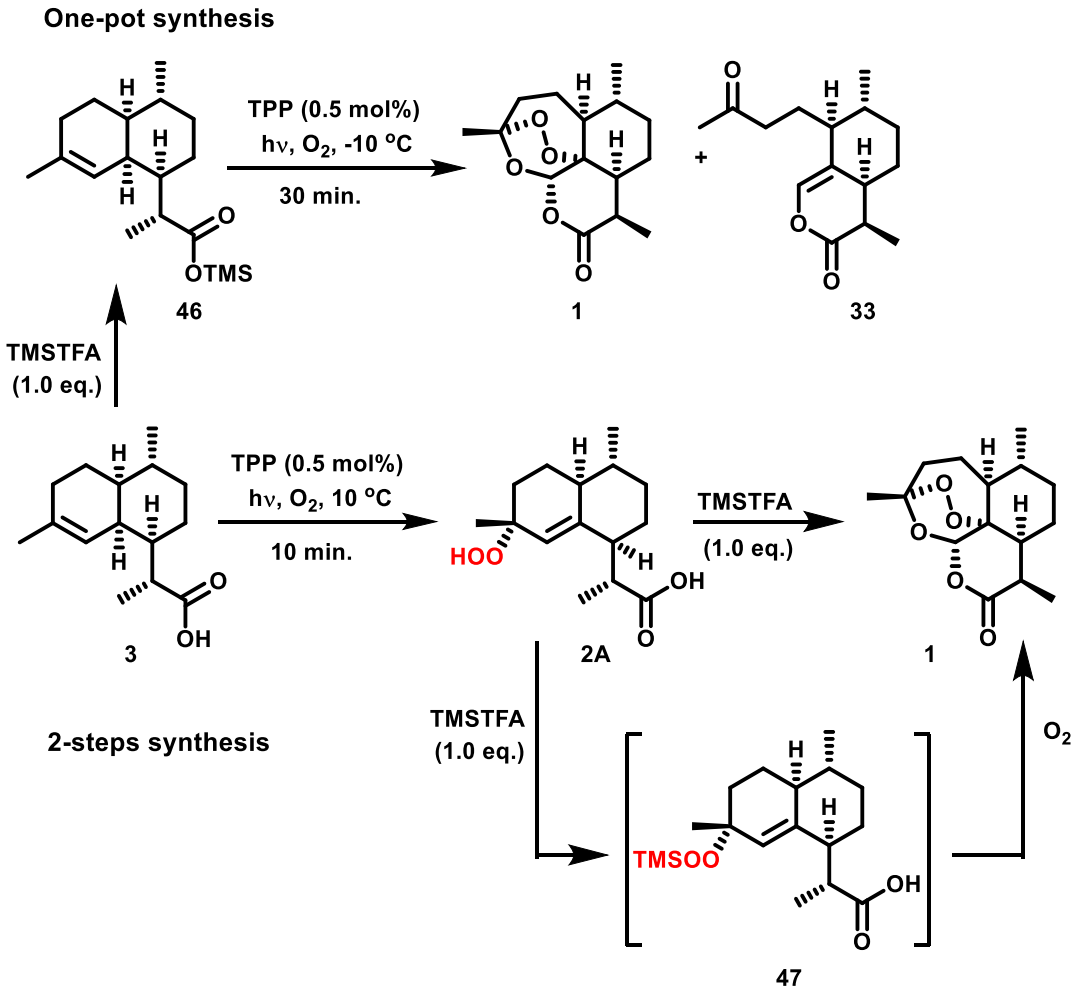
Entry	PS	Solvent	Acid Cat. (equiv.)	Temp. (°C)	Time (min)	Art. Yield (%)	Prod. (g/day)
1	$[Ru(bpy)_3]Cl_2$	DCM	TFA (0.5)	-10	5	75	14.38
2		DCM	TFA (1.0)	-10	5	71	13.62
3		DCM	TCA (0.5)	-10	5	65	12.47
4		EtOAc	TFA (0.5)	20	7.5	15	1.95
5		EtOAc	TFA (1.0)	20	7.5	42	5.47

Unless specified otherwise, the reaction was conducted in semi-continuous mode using 5 mL of solution in a 1 L round-bottom flask rotating at 175 rpm with O_2 bubbling through the solution at 60 sccm (sccm = standard cubic centimeters per minute). Yields were calculated based on the relevant peaks in the ^1H NMR spectrum with reference to an internal standard (biphenyl), for all the yields calculated and all samples ran in triplicate. The productivity was calculated from [Conc. (DHAA)*(vol.(mL)/1000/time(min)) *1440*Molecular weight of Art.*Yield (%)].

And possibility of acid catalysed hydrolysis of ethyl acetate, which will result in the formation of alcohol which is a quencher of singlet oxygen. Although there is full conversion of the starting material in ethyl acetate low yield of Artemisinin **1** was obtained with more than 50 % of it has been lost to the formation side products, from the ^1H-NMR of the crude mixture a high percentage yield of δ-lactone **33** was obtained, which is formed due to the trapping of enol intermediate by the carboxylic acid group at 12-position (Scheme 41). It was proposed that the use of TMSTFA as Lewis acid catalyst

will in introduce a bulky TMS to the enol intermediate **5** which could prevent the formation of **33** and other by-products by preventing the protonation of an internal hydroperoxide's oxygen, and ultimately preventing the loss of hydrogen peroxide

.

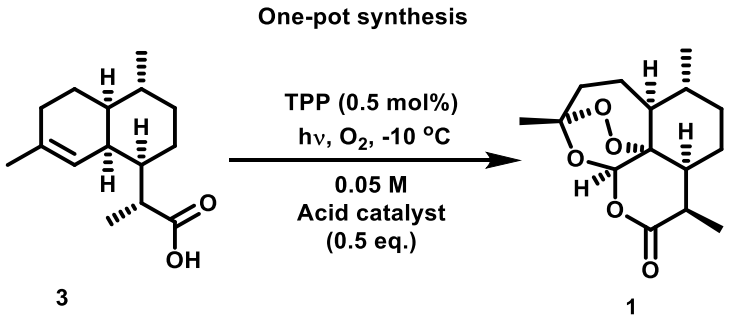


Scheme 41*: The synthesis of artemisinin **1** through both one-pot and 2-steps processes using TMSTFA as an acid catalyst.*

Table 11 compares the use of TFA and its chlorinated analogue (TCA) in facilitating the Hock rearrangement of **2A** under similar conditions. Using TPP as the photosensitiser, the one-pot synthesis of Artemisinin **1** was performed in toluene, varying the of temperature from -10 to 23 °C. With TFA as the acid a decrease in the yield and productivity of Artemisinin **1**, was observed from 64 to 46, and 8.34 to 5.99 g/day,

respectively (Table 11, Entries 1 to 3), at -10 °C a higher yield and productivity was obtained (Table 11, Entry 3). Changing the acid catalyst to TCA under similar conditions the yield does not significantly change when there is a decrease in temperature (Table 11, Entries 2 to 6), but productivities decreased significantly on lowering the temperature, from 11.51 to 8.08 g/day.

*Table 11: Showing the effect of solvent and acid catalyst (0.5 equiv.) on yield and productivity of Artemisinin **1**, after full conversion of DHAA **3**, using TPP as photosensitiser, at temperature of -10 °C.*



Entry	Solvent	Temp. (°C)	Acid (equiv.)	Time (min)	Artemisinin Yield (%)	Conversion (%)	Productivity (g/day)
1	Toluene	23	TFA	7.5	46	92	5.99
2		06	TFA	7.5	57	95	7.43
3		-10	TFA	7.5	64	100	8.34
4		23	TCA	5.0	60	100	11.51
5		-02	TCA	5.0	57	100	10.93
6		-10	TCA	7.5	62	100	8.08
7		-10	TMSTFA	10	25	100	1.29
8		-10	TMSTFA	20	51	100	2.59
9	DCM	-10	TFA	7.5	58	100	7.56
10		-20	TFA	7.5	48	100	6.25
11		-10	TCA	5.0	46	100	8.82
12	EtOAc	-5	TFA	7.5	12	100	1.56

Unless specified otherwise, the reaction was conducted in semi-continuous mode using 5 mL of solution in a 1 L round-bottom flask rotating at 175 rpm with O_2 bubbling through the solution at 60 sccm (sccm = standard cubic centimeters per minute). Yields were calculated based on the relevant peaks in the ^{1}H NMR spectrum with reference to an internal standard (biphenyl), for all the yields calculated and all samples ran in triplicate. The productivity was calculated from [Conc. (DHAA)*(vol.(mL)/1000/time(min))*1440*Molecular weight of Art.*Yield (%)].

Using TMSTFA gave a poor the selectivity of Artemisinin **1** as evidenced by the formation of up to 17 % of δ-lactone **33**, with very low yield and productivity of Artemisinin **1**. Only

90 % conversion was achieved after 10 minutes of irradiation at – 10 °C with 25 % of **1** obtained.

The catalyst seems to be effective in shifting the equilibrium of keto-enol tautomerism to favour the formation of TMS enol ether, because the ^{1}H-NMR show up to 14 % of enol intermediate and very low yield of its aldehyde tautomer, however, after 20 min irradiation full conversion of both starting material and TMS enol ether intermediate was achieved with improved yield of 51 % of Artemisinin **1** (Table 11, Entries 7 and 8). The unexpected decreased in the yield of **1** has been due to the initial displacement of the carboxylic acid proton by TMS resulting in the formation of an ester **46**, and released of TFA which catalysed the Hock-cleavage process (Scheme 41)

In DCM using TPP as photosensitiser for one-pot synthesis at -10 °C, yields 58 % of **1** and full conversion of DHAA **3** after 7.5 minutes irradiation (Table 11, Entry 9). However, decreasing the temperature to -20 °C resulted in the decrease in the yield of **1** to 48 % and productivity of 6.25 (Table 11, Entry 10). Repeating the reaction using TCA at -10 °C the yield of **1** decreased to 46 % with an improvement in the projected productivity to 8.82 g/day.

Comparing the yields of **1** in toluene and DCM using TCA as acid catalyst, at -10 °C showed the influence of solvent on yield of **1**, with toluene producing a better yield of 62 % of **1** (Table 11, Entries 6 and 11).The use of polar aprotic solvents such as ethyl acetate, results in decreased in the yield of **1** to 12 % at – 10 °C using TPP as a photosensitiser (Table 11, Entry 12), the yield improved to 42 % with the increase in temperature under the same condition. Toluene was also used for one-pot synthesis in Vortex reactor at higher temperatures from 20 to 30 °C, using both DCA and TPP as photosensitisers, like in continuous flow reactor, there is also decrease in the yield of **1** with increasing temperature, because 49 and 22 % yield were obtained at 25 and 30 °C respectively.

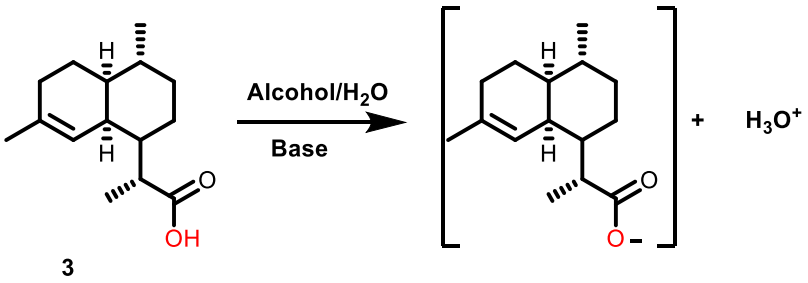
From these reported cases, coupled with what is observed in PhotoVap reactor we can point out that, although low and high temperatures are understood to favour photo-oxidation and acid catalysed thermal oxidation respectively when the two processes are performed separately, for one-pot process the yield depends more on the nature of the solvent, photosensitiser, and acid catalyst than the temperature. In these sections we discussed the synthesis of Artemisinin **1** in the PhotoVap reactor through a one-pot process, the process proceeds with the improved productivity compared to the two-step process, due largely to minimum concentration of photo-oxidation products and reactive intermediates present at any moment during the reaction, such that the two processes are taking place in a concerted manner, making one-pot process to proceed in the same rate as the photo-oxidation, with improved yield and productivity of **1**.

Aqueous solutions of organic solvents have been reportedly used as the solvent system in the synthesis of Artemisinin, as the water molecule is reported to assist in during the acid catalysed hock-cleavage and it facilitate ease of Artemisinin isolation and purification process.[2] In the following section we explore the use of aqueous solvents in the synthesis of Artemisinin **1** in PhotoVap reactor, using aqueous solvent which can affectively dissolve the reaction mixture as described from the initial solubility studies to identify the best condition for the for exploring the advantage of aqueous mixture in Artemisinin **1** synthesis, has been performed using different concentration of DHAA **3** for different alcohol/water mixture as described in the next section.

2.5.1. SOLUBILITY STUDIES OF DHAA, DIFFERENT AQUEOUS SOLVENT MIXTURES

The choice of a suitable solvent for the synthesis of important pharmaceutical active ingredients (API) such as Artemisinin **1** is an important step toward its industrial production, semi-synthetically using DHAA **3** and its derivatives as precursors.[136, 163]

DHAA **3** is an organic carbobicyclic, monocarboxylic acid compound, which belongs to the wide family of sesquiterpenoids. The compound ionises to its conjugate base Dihydroartemisinate a monocarboxylic acid anion resulting from the removal of a proton from its carboxylic group in solution. It dissolved efficiently in non-polar and moderately polar solvents due to the hydrophobic nature of its conjugate base, the presence of a polar carboxylic acid group allowed the aqueous solubility of this compound to be manipulated to some extent using the large proportion of water-miscible solvents such as ethanol, methanol, tetrahydrofuran and so on (Scheme 42).



*Scheme 42: water soluble carboxylate ion of DHAA **3** formed in Alcohol/water mixture.*

Like other hydrophobic carboxylic acids, the aqueous solubility of DHAA **3** can be achieved by making its carboxylate salt, through reaction with an aqueous base such as sodium hydroxides or the use of buffered solutions of TRIS (2-amino-2-hydroxymethyl-propane-1,3-diol) at pH of 8.2 as reported by Brown and Sy (2004),[164, 165] to effectively fix the carboxylate group at the 12-position of DHAA **3** in the more soluble conjugate base form, thereby enhancing its aqueous solubility for ejection into the *Artemisia annua* plant to study it's in vivo transformation into **1** at very low concentration.[164]

The solvent occupies a central position during chemical transformation in solution, in that it serves as the medium in which the chemical reaction occurs. It is mostly employed to ensure homogeneity of the reaction mixture, thereby influencing processes such as rate

of reaction and equilibrium, which chooses solvent very important task, leading to improvement of both the safety and productivity of a given synthetic route.[34]

However, most of the solvents used for synthetic applications in industrial and academic research are volatile organic compounds (VOCs), some of which are hazardous and highly volatile involving in processes of environmental pollution. Other problems such as non – renewable nature of VOCs and difficult synthetic route, difficulty in purification and scale-up, and cost of handling, are the factors limiting their applications.[34, 163] The recent attempts to tackle the problems associated with the use of VOCs as solvents, especially in the production of food and pharmaceutical products, is through the design of processes that proceed via green reaction media, in some instances under solvent-free condition or by minimising the amount of solvents used. One of the approaches frequently applied is the use of solvents mixture, such as water and water-miscible solvents (such as alcohols) mixture to dissolve weakly polar organic compounds such as DHAA **3** and its derivatives.[2] The use of water miscible solvent mixture is necessary because of the possible lactone derivative hydrolysis in aqueous base, thereby limiting its overall yield.

In this section, the objective is to find the solubilities of DHAA **3** and its carbonate derivatives in different polar and non-polar solvents, and different proportions of polar solvent and water mixtures, by changing the temperature and concentrations of the solutions. The use of large proportion of water can allow easy isolation and crystallisation of the desired product; Artemisinin **1** in high recovered yield. Therefore, the aims of this studies are:

- To know the solubility of the starting material in mixture of alcohol/water. Different type of alcohols will be used for this qualitative study ranging from

primary alcohols to tertiary alcohols and including diols, given emphasis for the mixture that will contain the highest amount of water.

- To find the suitable solvents or mixture of solvents that will allow us to explore the synthesise of Artemisinin **1** in the PhotoVap reactor, and "pre-selecting" the best conditions that will allow the optimisation step to proceed further.

- To hypothetically, recover **1** in an easier way, by evaporating organic solvent and Artemisinin **1** will precipitate in water. Because our lab has previously shown that mixture of ethanol/water mixture gave good/excellent results.

The data in this Chapter involving solubility of DHAA **3** were obtained in collaboration with Dr Hamza Boufroura who carried out some of the measurements at room temperature I then performed the measurements at lower temperatures. We have first studied the solubility of DHAA **3** in different alcohol/ water mixtures.

2.5.1.1 SOLUBILITY STUDY OF DHAA AT ROOM TEMPERATURE AND DIFFERENT CONCENTRATIONS IN ALCOHOL/WATER MIXTURES

The studies of the solubility of DHAA **3** in water are important because it was reported that presence of water is required during the acid catalysed thermal oxidation step of the Artemisinin **1** synthesis, and another benefit of using water mixture is the ease of recovery of the final product by simple evaporation of the organic phase allowing Artemisinin **1** to crystallise.[2]

Unlike DHAA **3**, there have been many reports of the solubility of **1** in different solvents with the aim of improving its extraction and recovery from *Artemisia annua* plants.[166, 167] The solubility of **3** in binary ethanol-water solvent mixtures was reported to be dependent on temperature, and a fraction of ethanol in the mixture.[168] Also, the solubility of Artemisinin **1** in pure methanol, ethyl acetate, acetone, acetonitrile, cyclohexane, toluene, and chloroform was reported to improve as the temperature increases.

*Table 12: DHAA **3** Solubility at 0.05 M in Alcohol/Water mixtures.*

Entry	Alcohols	Mixture composition of Alcohol/Water [v/v]									
		10:0	9:1	8:2	7:3	6:4	5:5	4:6	3:7	2:8	1:9	0:10
	Primary alcohols											
1	MeOH				NS							
2	EtOH						NS					
3	1-PrOH								NS			
4	1-Butanol			NM								
5	Isobutanol			NM								
6	1-Pentanol		NM									
7	1-Hexanol		NM									
8	1-nonanol		NM									
	Secondary alcohols											
9	*i*-PrOH							NM				
10	HFIP				NS							
11	2-Butanol					NM						
12	2-Heptanol		NM									
13	2-Octanol		NM									
14	(4-Methyl-2pentanol)		NM									
	Tertiary alcohols											
15	*tert*-Butanol								NM			
	Cyclic alcohols											
16	Cyclopentanol			Emulsion								
17	Cyclohexanol			Emulsion								
	Diols											
18	1,2-Propanediol	NS										
19	1,3-Propanediol	NS										
20	1,5-Pentanediol	NS										

In all cases the DHAA **3** was dissolved in the organic component first and then water was added and mixed with a vortex mixer. Not miscible (NM) = DHAA **3** soluble in the organic phase but water did not mix when added. Not Soluble (NS) = Precipitation of DHAA **3** upon addition of the water. Emulsion = Cloudy Emulsion formed upon addition of water.

The solubility of **3** in water-alcohol mixtures has been studied in various primary, secondary, and tertiary alcohols, by initially testing the alcohol/water miscibility prior to dissolving the solute, the alcohol used are selected from primary, secondary, and tertiary

alcohols. The primary alcohols used MeOH, EtOH and 1-PrOH (Table 12, Entries 1 to 3) were found to be miscible with water, but the solubility of **3** at 0.05 M decreases with the decrease in molecular weight of alcohol, because 0.05 M of **3** is found to be soluble in up to 60 % aqueous solution of 1-PrOH (Table 12, Entry 3).

The decrease in solubility of **3** with increase in the polarity of low molecular weight of alcohol is an indication of increased interaction of the solvent mixture with weakly polar organic solute. However, the higher molecular weight primary alcohols from 1-butanol to 1-nonanol exhibit decrease polarity, with reduced solubility in water. 1-butanol and iso-butanol are miscible with only 10 % of water, and **3** has been found to be soluble in the mixture (Table 12, Entries 4 and 5). Other primary alcohols studied which include 1-pentanol, 1-hexanol and 1-nonanol are completely immiscible with water although **3** can dissolve in them as expected due to their less-polar nature.

For secondary alcohol, the solubility of **3** was tested in *i*-propanol and highly polar hexafluoro isopropyl alcohol (HFIP), and good solubility with up to 50 % water has been recorded for the former, it however decreases for latter as **3** can only dissolve in the mixture with 20 % water (Table 12, Entries 9 and 10). Other secondary alcohol tested are totally immiscible with water and hence the solubility has been tested in without the presence of water.

Among the tertiary alcohols, only the solubility of *tert.*-butanol was studied and was found to be highly miscible with water for up to 60 % volume with **3** in the mixture (Table 12, Entry 15). The final category are cyclic alcohols, with only 10 % solubility (Table 12 Entries 16 and 17) and diols comprising 1,2- and 1,3-propanediol and 1,5-pentanediol although they miscible with water, due to the viscosity the solute did not dissolve in them.

*Table 13: DHAA **3** Solubility at 0.5 M in Alcohol/Water mixtures*

Entry	Alcohols	Mixture composition of Alcohol/Water [v/v]									
		10:0	9:1	8:2	7:3	6:4	5:5	4:6	3:7	2:8	1:9	0:10
Primary alcohols												
1	MeOH		NS									
2	EtOH				NS							
3	1-PrOH						NS					
4	1-Butanol			Emulsion								
5	Isobutanol			Emulsion								
Secondary alcohols												
6	*i*-PrOH					NS						
7	HFIP	NS										
8	2-Butanol			Emulsion								
Tertiary alcohols												
9	*tert*-Butanol						NS					
Cyclic alcohols												
10	Cyclopentanol			NS								
11	Cyclohexanol	NS										

In all cases the DHAA **3** was dissolved in the organic component first and then water was added and mixed with a vortex mixer. **Not miscible (NM)** = DHAA **3** soluble in the organic phase but water did not mix when added. **Not Soluble (NS)** = Precipitation of DHAA **3** upon addition of the water. **Emulsion** = Cloudy Emulsion formed upon addition of water.

The increase in the concentration of DHAA **3** to 0.5 M decreases its solubility, because for primary alcohols **3** was found to dissolved in MeOH, EtOH and 1-PrOH having 0, 20 and 40 % water respectively (

Table 13, Entry 1 to 3). While for secondary alcohol DHAA **3** was found to be only soluble in 30 % water/*i*-PrOH mixture which unlike for the previous concentration (0.05 M), the HFIP cannot dissolve the solute at this concentration. Also, for *tert.* butanol the solution containing only 40 % water can allow dissolution of 0.5 M of **3**. These observations indicate that this concentration is not ideal for the synthesis of **1** especially the photo-oxidation step, reported to favoured by low-temperature.

Apart from alcohol water mixture, the solubility has also been tested for water miscible organic solvents, which include dimethyl carbonate (DMC), THF, 2-MeTHF, 1,2-dioxane and 4-MTHP, Table 12. Because some of these polar organic solvents such as THF were proved to be promising in aqueous solution experiments previously reported.[2]

Tetrahydrofuran (THF) and 1,4-Dioxane are both miscible with water and can dissolve DHAA **3** in the presence of up to 40 % water (Table 14, Entry 2 and 4), owing to its less toxicity THF is preferable recommended by the Pfizer, Sanofi and RSC solvents guide.[2] other organic solvents tested that include DMC, 2-MeTHF, and 4-MTHP are not miscible with water, so they can only be used directly as they efficiently dissolve the substrates (Table 14, Entries 1, 3 and 5).

*Table 14: DHAA **3** Solubility at 0.05 mol/L in Organic solvent/Water mixtures*

Entry	Solvents	Mixture composition of Solvent/Water [v/v]										
		10:0	9:1	8:2	7:3	6:4	5:5	4:6	3:7	2:8	1:9	0:10
1	DMC		NM									
2	THF						NS					
3	2-MeTHF		NM									
4	1,4-Dioxane						NS					
5	4-MTHP		NM									

In all cases the DHAA **3** was dissolved in the organic component first and then water was added and mixed with a vortex mixer. **Not miscible (NM)** = DHAA **3** soluble in the organic phase but water did not mix when added. **Not Soluble (NS)** = Precipitation of DHAA **3** upon addition of the water. **Emulsion** = Cloudy Emulsion formed upon addition of water. DMC = Dimethyl carbonate; THF = Tetrahydrofuran; 2-MeTHF = 2-Methyl tetrahydrofuran; 4-MTHP = 4-Methyl tetrahydropyran.

2.6.1. SYNTHESIS OF ARTEMISININ IN AN ALCOHOL/WATER MIXTURE IN THE PHOTOVAP REACTOR

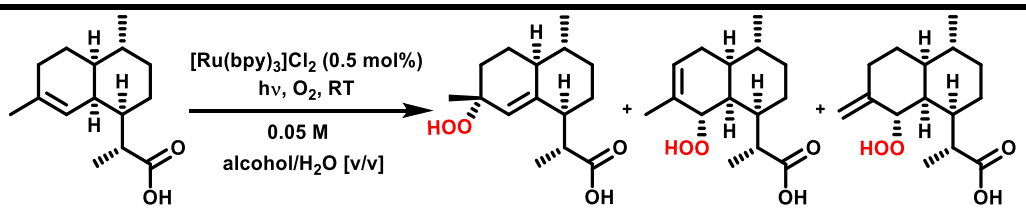
The used of water miscible solvents such as alcohols and THF, has been reported by Amara *et al.,* [2] in the synthesis of Artemisinin **1** to provide an alternative to the traditional organic solvents, most of which are highly volatile, thereby requiring energy intensive cooling even for room temperature experiments in the high power LEDs driving synthesis of valuable pharmaceutical compound Artemisinin **1.** Very encouraging results were obtained using THF/H_2O and EtOH/H_2O, which is surprising because of the potential quenching of singlet oxygen by large volume of water used for the process. To further explore the method for semi-synthesis of Artemisinin **1** from DHAA **3** under

different condition that could result in the improvement of its overall yield. The aqueous mixtures of alcohol with different proportion of water that had been first identified. For this strategy $[Ru(bpy)_3]Cl_2$ has been used as photo-catalyst because of its good solubility in water and reported good photocatalytic properties. The synthesis has been performed by considering both approach: two steps and one-pot in the PhotoVap reactor.

2.6.1.1 TWO-STEP APPROACH IN AN ALCOHOL/WATER MIXTURE IN PHOTOVAP REACTOR.

The studies of the solubility of 0.05 M of DHAA **3** in alcohol/water mixture discussed in Section 2.5.1, show that appreciable solubility of DHAA **3** in EtOH, *n*-propanol, *i*-propanol 2-butanol and *tert*-butanol. The work focused on EtOH and n-PrOH because of better solubility of DHAA **3** in these solvents as described in Section 2.5.1. The initial photo-oxidation has been performed in 60 % aqueous *n*-PrOH at room temperature using water soluble $[Ru(bpy)_3]Cl_2$.

Table 15: R*esults obtained from the experiments using alcohol/water mixtures in the PhotoVap reactor.*



Entry	Solvent	Time (min)	Conv. (%)	2A Yield (%)	2B Yield (%)	2C Yield (%)	Select. of 2A
1	*n*-PrOH/H_2O (60/40)	5	60	51	00	03	85
2		10	93	62	00	03	67
3		15	100	62	00	07	62
4	EtOH/H_2O (70:30)	20	100	57	04	05	57

Unless specified otherwise, the reaction was conducted in semi-continuous mode using 5 mL of solution in a 1 L round-bottom flask rotating at 175 rpm with O_2 bubbling through the solution at 60 sccm (sccm = standard cubic centimetres per minute). The yields and conversions were obtained from the corresponding integrals of proton-NMR chemical shifts of the DHAA 3 and the products, using 10 % biphenyl as internal standard, and the selectivity of **2A** was calculated from: conversion (%)/yield of **2A** (%).

The reaction proceeds with very good selectivity of 85 % after 5 minutes irradiation in the PhotoVap reactor (51 % yield of the tertiary hydroperoxide **2A**) 60 % conversion of starting material (Table 15, Entry 1). After prolonged irradiation, full conversion was achieved, but the yield of **2A** peaked at 62 % (Table 15, Entry 3). In 70 % aqueous ethanol full conversation was obtained after 20 min and yielded 57 % of the tertiary hydroperoxide **2A** at room temperature (Table 15, Entry 4). Considering the effect of solvent on the selectivity of photo-oxidation step, alcohols and water are good quenchers of singlet oxygen, because high vibrational energies of -OH and C-H groups, with water being more strongly deactivating toward singlet oxygen than alcohols and increase in molecular weight of alcohols decreases their singlet oxygen quenching rate.[16, 26, 28]

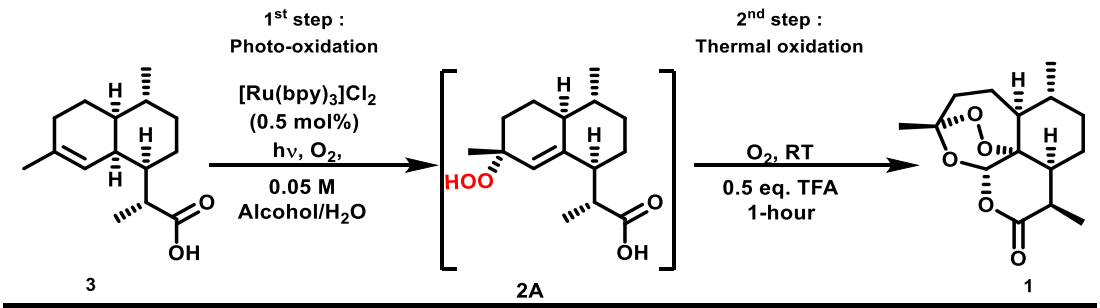
The accompanied decrease in the overall yield of the photo-oxidation the products in the aqueous solvent mixture was lower compared to those obtained from a protic organic solvent. For 70 % EtOH experiments there has been decreased yield and selectivity of the photo-oxidation product **2A**, which could be due to the higher quenching rate of singlet oxygen in EtOH, compared to the use of aqueous *n*-propanol solution.

At high quenching rates of singlet oxygen, there is the need for prolonged irradiation to reach full conversion of the starting material **3.** However, it is possible that a prolonged irradiation leads to a decrease in selectivity of the desired tertiary hydroperoxide **2A**, for instance after full conversion in both aqueous *n*-propanol and ethanol, only 62 % and 57 % of **2A** were obtained, indicating the loss of 38 % and 43 % of starting material respectively. Therefore, photo-oxidation in aqueous solvent mixtures does not result in the improvement of the yield of the desired tertiary hydroperoxide **2A**. A loss of yield of the desired peroxide **2A** at this stage of the process would have negative effect on the yield and productivity of Artemisinin **1**, because the photo-oxidation step is known to

procced with better selectivity than the latter stage of the process, i.e., the sequential Hock cleavage/thermal oxidation.

The crude products of photo-oxidation are subjected to acid catalysed thermal oxidation at room temperature. The yields and selectivities were calculated based on the yield of tertiary hydroperoxide **2A** obtained from the photo-oxidation step. Full conversion of **2A** was achieved after 1-hour of bubbling of oxygen, to the crude product using an oxygen filled balloon. This resulted in the formation of 60 % Artemisinin **1** based on the amount of **2A** present in the crude of the photo-oxidation products in 60 % aqueous PrOH. For 70 % aqueous EtOH the yield of Artemisinin **1** was 56 % (Table 16, Entry 1 and 2). The results for both solvent mixtures show that there is a decrease in the overall selectivity of Artemisinin to 37 and 32 % respectively. Considering the overall lost in selectivity from the two steps, which is about 63 and 68 % respectively of the starting material (DHAA **3**), most of which is lost during the processes of its conversion to Artemisinin **1**, in these two solvents mixture.

*Table 16: Acid catalysed oxidation of the crude products of DHAA **3** photo-oxidation*



Entry	Solvent	1 Yield (%)	δ-lactone 33 (%)	γ-lactone 37 (%)	Aldehyde 32. (%)	Select. of 2nd Step (%)	Overall select. to 3 (%)
1	PrOH/ H_2O (60/40)	60	00	19	10	60	37
2	EtOH/ H_2O (70:30)	56	2	27	15	56	32

Unless specified otherwise, the reaction was conducted in semi-continuous mode using 5 mL of solution in a 1 L round-bottom flask rotating at 175 rpm with O_2 bubbling through the solution at 60 sccm (sccm = standard cubic centimetres per minute). The yields and conversions were obtained from the corresponding integrals of proton-NMR chemical shifts of the DHAA **3** and the products, using 10 % biphenyl as internal standard, and the selectivity (select.) of **1** was calculated from: conversion (%)/yield (%).

Some of the side products obtained are a γ-lactone **37** and aldehyde **32**, unlike in organic solvent where more of δ-lactone **33** is produced depending on the solvent and condition, here higher yields of γ-lactone **37** were obtained in both solvent mixtures, with aqueous ethanol accounting for up to 27 % of the hydroperoxide intermediate converted to γ-lactone **37** (Table 16, Entry 2). Higher yield of this lactone indicates that the alcohol/water mixture provide enabling environment for proximal protonation of **2A** leading to the loss of hydrogen peroxide and attack by the 12-carboxylic acid group of the hydroperoxide on its allylic double leading to its lactonization as explained earlier. To overcome this loss in the productivity, encountered from both steps of the synthesis, the process in this reactor has been performed employing one-pot strategy.

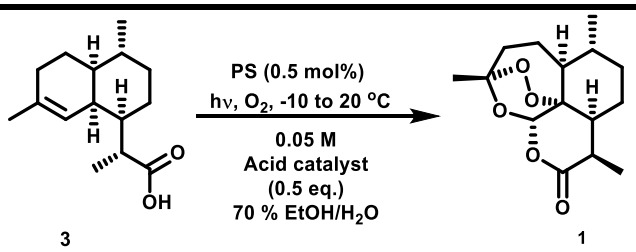
2.6.1.2 ONE-POT SYNTHESIS ARTEMISININ IN ALCOHOL/WATER MIXTURES

The one-pot synthesis was carried out using 70 % aqueous ethanol by addition of 0.5 equivalent of TFA at the beginning, 70 % of Ethanol was used to compare with the previous results obtained from 2-steps method. 7.5 minutes irradiation in PhotoVap reactor gave the yield of 27 % Artemisinin at – 10 °C (Table 17, Entry 1), increasing the temperature to 20 °C only resulted in the decrease of the reaction rate, with only 93 % conversion achieved after 7.5 minutes irradiation and small improvement in selectivity reaching 29 % (Table 17, Entry 1).

Changing the photo-oxidation catalyst to TPP using the same concentration only resulted in a small decrease of the yield of Artemisinin **1** to 25 % even though full conversion was achieved (Table 17, Entry 3). Like in the two-step process, higher yield of γ-lactone **37**, 11 – 12 % in this method, the expected improvement in the yield and selectivity to Artemisinin **1** was not observed, which is surprising because the one-pot synthesis using

hydrocarbon solvents described earlier resulted in better selectivities and yields of Artemisinin **1** compared to the two-steps approach.

*Table 17: The results for one-pot synthesis of Artemisinin **1** in 70 % Ethanol/H_2O.*



3 **1**

Entry	PS	Temp. (°C)	Time (min)	Conv. (%)	Art. Yield (%)	δ-lactone Yield (%)	γ-lactone Yield (%)	Art. Select. (%)
1	$[Ru(bpy)_3]Cl_2$	-10	7.5	100	27	06	11	27
2	$[Ru(bpy)_3]Cl_2$	20		93	27	05	10	29
3	TPP			100	25	05	12	25

Unless specified otherwise, the reaction was conducted in semi-continuous mode using 5 mL of solution in a 1 L round-bottom flask rotating at 175 rpm with O_2 bubbling through the solution at 60 sccm (sccm = standard cubic centimetres per minute). The yields and conversions were obtained from the corresponding integrals of proton-NMR chemical shifts of the DHAA **3** and the products, using 10 % biphenyl as internal standard, and the selectivity (select.) of **1** was calculated from: conversion (%)/yield (%).

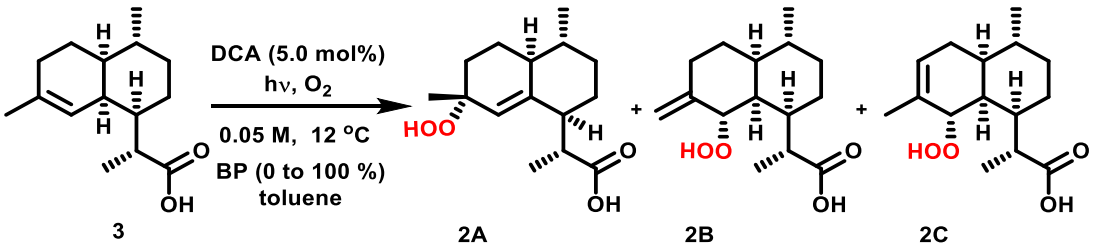
Although, the presence of water was reported to be necessary during Artemisinin **1** synthesis,[2] the one-pot synthesis of **1** in Water/THF was reported by Lee *et al.* with significantly lower initial conversion of DHAA **3** (46 %) and the yield of **1** was only 5 %. Screening of other conditions resulted in the full conversion of the starting material and an increase in yield to 22 % at 30 °C in a Vortex reactor.[79] This is an indication that the lower yield of Artemisinin **1** recorded is exclusive to this reactor. From these results we can conclude that other factors might be responsible for the decrease of yields and productivities of **1**. There is a need for further optimisation, considering the green nature of the solvent system and the ease of isolation and purification of the final product, by simple evaporation of organic portion.

STUDYING THE EFFECT OF BIPHENYL ON DHAA PHOTO-OXIDATION

Biphenyl has been used as an internal standard for quantitative ^{1}H-NMR, to determine the percentage yield of the reactants and products, under different conditions, with reference to the chemical shifts of its four equivalent aromatic protons, as described in previous sections. During the process 10 or 100 % of biphenyl has been used, for the ^{1}H-NMR chemical shifts integration to the factors of 0.4 and 4.0 respectively. In this section the effect of biphenyl in the DHAA **3** photo-oxidation process using DCA and $[Ru(bpy)_3]Cl_2$ as photosensitisers are discussed. The studies were performed by comparing the percentage yield of the photo-oxidation products at different concentrations of biphenyl, in different solvents.

2.3.1. EXPLORING PHOTO-OXIDATION OF DHAA, USING DCA-BIPHENYL.

The results obtained from the DHAA **3** photo-oxidation in toluene at 12 °C, using 5.0 mol% of DCA as photosensitiser, and addition of different percentages of biphenyl before irradiation, of the mixture in PhotoVap reactor are plotted in . It shows an increase in the percentage yields and selectivity of tertiary peroxide **2A**, with the increasing amount of biphenyl. The synthesis was initially performed without addition of biphenyl, which resulted in the yield and productivity of 46 % and 35 % of **2A**, respectively (Figure 26). The addition of biphenyl resulted in improvement of the yield and selectivity of the tertiary hydroperoxide **2A** because initial addition of 25 % of biphenyl resulted in an increased yield and selectivity of 54 % and 41 % of **2A**, respectively (Figure 26). Increasing the concentration of biphenyl to 50 %, further improves the yield of **2A** to 62 % and selectivity of 45 %.



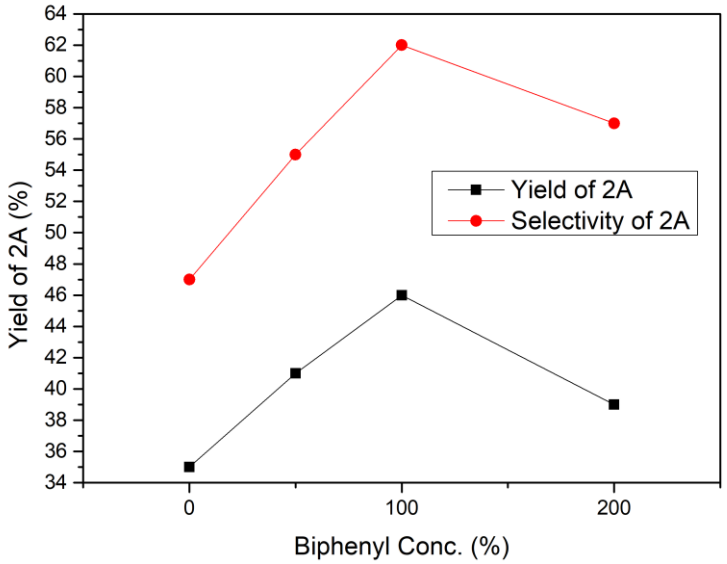
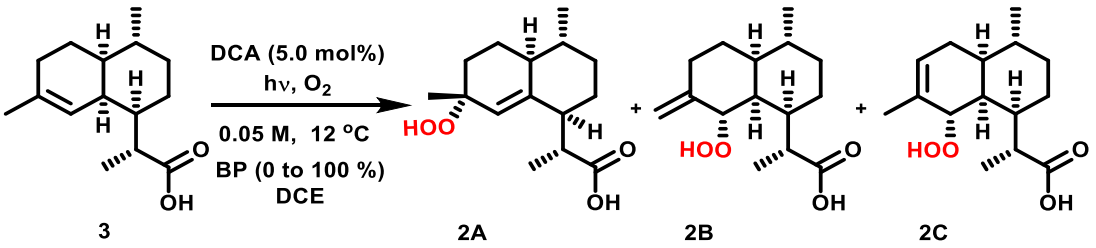


*Figure 26: 60 min photo-oxidation of DHAA **3** with DCA in toluene with variation of biphenyl concentrations.*

However, at stoichiometric concentration of biphenyl (BP) the yield and selectivity reduced to 37 and 55 % respectively (Figure 26), indicating the possible quenching of the excited DCA* by BP at higher concentration. Because of the observed changes in the yield and selectivity of **2A**, with the increase in concentration of biphenyl in toluene, the experiment was repeated using dichloroethane (DCE) with remaining parameters unchanged. As observed in toluene running the reaction in the absence of biphenyl, results in a low yield and selectivity of **2A**, (57 % and 62 % respectively) Figure 27.



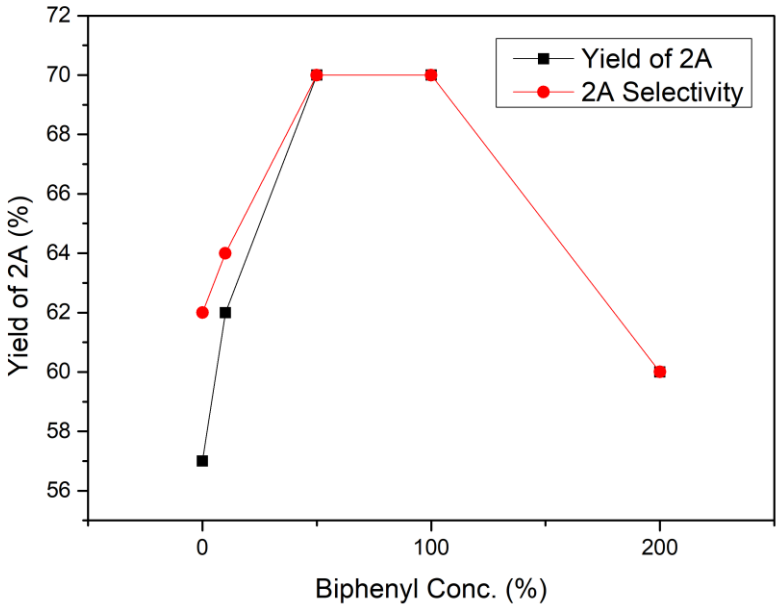
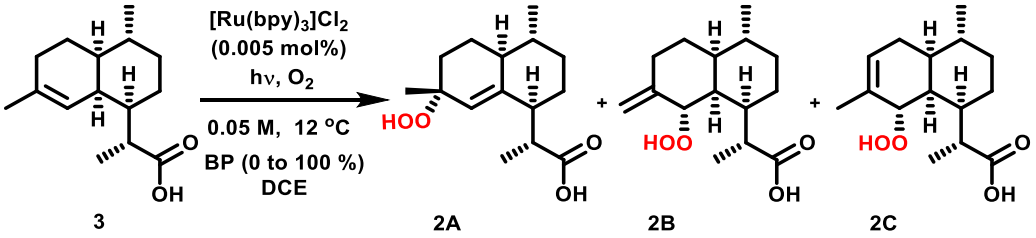


*Figure 27: The 30 minutes photo-oxidation of DHAA **3** using DCA in DCE with variation of biphenyl (0 – 200 % with respect to DHAA **3** concentrations)*

Addition of 10 % biphenyl improves the yield and selectivity to 62 and 64 % respectively. At higher concentrations of 22.5 and 50 % of biphenyl, the same yield and productivity of 70 % was obtained. Compared to the used of toluene as a solvent, there is improvement in yields and productivities of the tertiary hydroperoxide **2A** in DCE, with increasing concentration of biphenyl (Figure 27), and similar decrease in the yield and selectivity was obtained at stoichiometric concentration. To determine if this effect was exclusive to DCA or not, the conditions were repeated using $[Ru(bpy)_3]Cl_2$ as the photosensitiser.

2.7.2. PHOTO-OXIDATION OF DHAA USING $[Ru(bpy)_3]Cl_2$ - BIPHENYL SYSTEM

The chemistry of this catalyst is discussed in Chapter 1, of particular importance is its strong absorption in the visible region and formation of long lived excited state, with lifetime of 1100 ns,[169] which makes it a good catalyst for the photo-oxidation process involving generation of singlet oxygen. The effect of biphenyl on the DHAA photo-oxidation in dichloroethane (DCE) at 12 °C was studied using very low concentration of 0.005 mol% $[Ru(bpy)_3]Cl_2$, this is because of its very large extinction coefficient. For this study the low concentration has been used to decrease the reaction rate, which will allow us to follow the effect of biphenyl on the process.



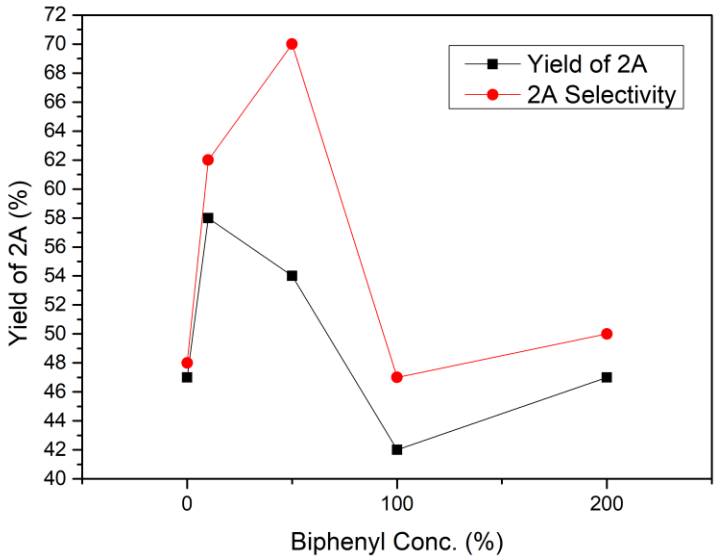


*Figure 28: the 60 minutes photo-oxidation of DHAA **3** using $[Ru(bpy)_3]Cl_2$ as photosensitiser at 12 °C in dichloroethane (DCE) in the presence of different concentrations of biphenyl, (0 – 200 % with respect to DHAA **3** concentrations)*

The initial reaction was performed in the absence of BP, decreased yield and selectivity of **2A** of 46 and 48 % respectively, were obtained after 1-hour irradiation. In the presence of 5 % biphenyl, 1-hour irradiation resulted in the yield of 55 % **2A** with about 60 % selectivity, increasing the amount of biphenyl to 25 % resulted in decreased yield of **2A**, with accompanied improvement of selectivity (Figure 28). It also shows that the yield of the tertiary hydroperoxide **2A** decreased further when increasing the amount of biphenyl to 50 %, these results indicate the possible effect of biphenyl to the yield of the photo-oxidation products using this catalyst, which include its influence in the possible quenching of the photo-excited catalyst, resulting in its deactivation at higher concentration.

2.7.3. ONE-POT SYNTHESIS OF ARTEMISININ USING $[Ru(bpy)_3]Cl_2$-BIPHENYL SYSTEM IN DCE.

$[Ru(bpy)_3]Cl_2$ biphenyl system was also used in the one-pot synthesis of Artemisinin **1**, like in the photo-oxidation process the studies were carried out using very low concentration of the catalyst at 12 °C in the presence of TFA as acid catalyst ().

Unlike during photo-oxidation, running the process in the absence of biphenyl proceeded with good a yield of Artemisinin **1**, and the yield was reduced with the increasing biphenyl concentration; at a stoichiometric concentration of biphenyl 60 minutes irradiation resulted in the yield of 47 % of Artemisinin **1**. This shows that while presence of acid at the beginning improves the yield and productivity of Artemisinin **1** in most of the conditions described earlier, addition of biphenyl at the beginning of the process could have negative effect on the yield and productivity of Artemisinin **1** under this reaction condition.

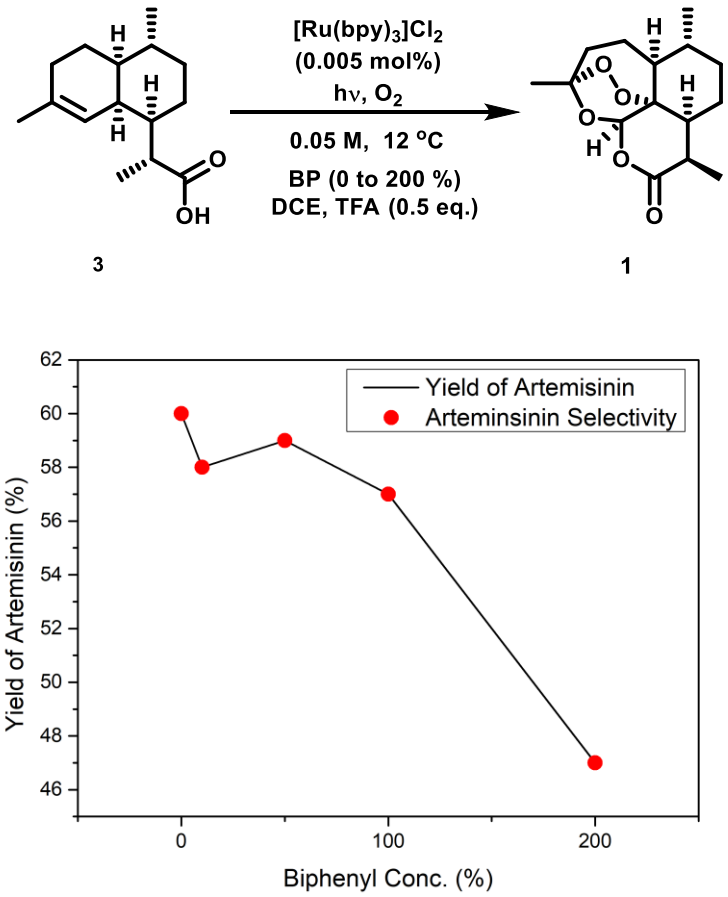


*Figure 29: 60 minutes irradiation of DHAA **3** using $[Ru(bpy)_3]Cl_2$ as photosensitiser at 12 °C in dichloroethane (DCE), by initial addition of TFA, in the presence of different concentrations of biphenyl (0 – 200 % with respect to DHAA concentrations)*

The presented results for the use of biphenyl from all the described cases, show possible the competing energy and electron transfer mechanisms. Which indicates that in the absence of biphenyl the photo-oxidation process could proceeds via energy transfer photosensitisation and because of very low extinction coefficient of DCA and low concentration of $[Ru(bpy)_3]Cl_2$, the rate of the reaction is rather very slow. Addition of biphenyl could result in the activation of electron transfer pathway because biphenyl is known to participate in an electron transfer photo-oxidation process, due to its low oxidation potential compared to the photosensitisers such as DCA.[18, 21, 170] This could occur through initial reduction of the singlet photo-excited photosensitiser into the

corresponding radical anion, which itself is oxidised to its radical cation ($BP^{+\cdot}$) that can activate the oxygen molecule, leading to the formation of the photo-oxidation products.

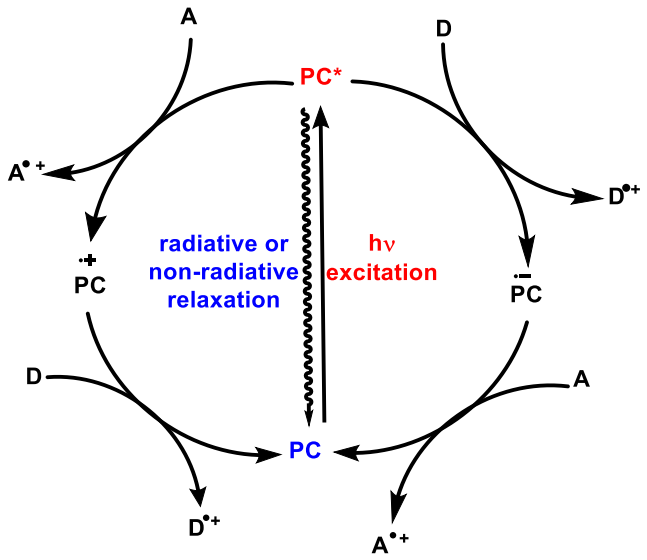
Exploring the ability of BP to co-sensitise the photo-oxidation of DHAA **3**, through electron transfer process, is important due to its very low oxidation potential, long life of biphenyl radical cation ($BP^{+\cdot}$), less cost and readily available. The potential application of BP in the synthesis of Artemisinin **1** can reduce its cost of production, through improvement in the yield and productivity at reduced concentration of expensive photosensitisers. Therefore, in the following sections we described the theory behind the use of BP as co-sensitiser, with reference to some reported applications, particularly involving the use of 9,10-dicyanoanthracene (DCA), which has been extensively studied because of its ability to catalysed both energy and electron transfer photo-oxidation processes. **COMPETING ELECTRONIC AND ENERGY TRANSFER PROCESSES DURING PHOTO-OXIDATION PROCESS**

In Chapter one, the processes involving energy transfer photosensitisation of molecular oxygen (O_2) to produced photochemically excited singlet oxygen $^1O_2$ and its application in the synthesis of Artemisinin **1** has been extensively discussed. Another competing process that could take place concurrently with energy transfer photo-oxidation process, is the electron transfer process, which involves transfer of an electron from electron rich donor to an acceptor.

Molecular chromophores commonly possessed useful redox properties in excited states, involving photoinduced promotion of an electron from the HOMO to its LUMO resulting in the formation of electronically exited state charge separated electron-hole pair. If the lifetime of this excited state is sufficiently long to engage in subsequent intermolecular reactions, it acts both as electron acceptor by filling its partially occupied

orbital through reaction with suitable electron donor (D), or electron donor by donation of its high-energy electron to an appropriate acceptor (A).

Which means the excited photocatalyst can participate in both reduction and oxidation processes, through the formation of electron-hole pair. Upon absorption of light photocatalyst can undergo photoinduced electron transfer process (PET) summarised in Scheme 43.

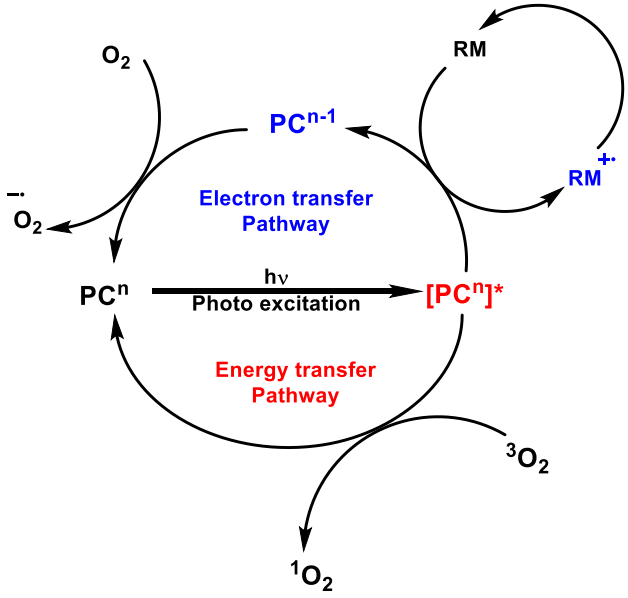


Scheme 43*: General mechanism of photoinduced electron transfer process.*[57]

The PET process involves generation of electronically excited state of a molecule due to light absorption, the excited molecule can undergo relaxation back to the ground state via several radiative and non-radiative pathways at relatively rapid rates. These transitions involve fast electron transfer to an electron-deficient acceptor species (**A**) or from an electron-rich donor species (**D**), via the processes of oxidative and reductive quenching, respectively. Regeneration of the photochemically active state requires a second electron-transfer process from a complementary donor or acceptor species. Thus, photoredox catalysis typically results in a formal transfer of an electron from one reagent to another, which produces a pair of reactive radical ions comprising the oxidized donor ($\mathbf{D}^{\bullet+}$) and

reduced acceptor ($\mathbf{A}^{\bullet-}$), these are referred to as reductive and oxidative quenchers, respectively.[18]

These photochemically generated radical cations and anions possessed different synthetic application than the sensitisers, because the radical ions can in most cases participate in single redox process and the regeneration of the photochemically active state requires a second electron-transfer process from complementary donor or acceptor known as balancing redox equivalent.



Scheme 44: showing the possible transitions taking place during photo-oxidation process, using photosensitiser (PC) in the presence of redox mediator (RM).

The photochemical redox processes can occur through two important pathways. The first is by the ability of substrate to directly quench the excited state of the photocatalyst, in which case the balancing redox equivalent is required to regenerate the photocatalyst, which occurs when the redox process between the substrate and excited photocatalyst is thermodynamically possible. The second pathway is using a secondary quencher to engage the excited state, thereby producing an oxidised or reduced ground-state catalyst that is more redox active than the excited state, which can perform broader range of

electron-transfer processes (Scheme 44). The second pathway involves the use of a substance known as a cocatalyst, co-sensitiser or redox mediator, that can influence the redox transformation by mediating the electron transfer process, through independent generation of intermediate substance which can undergo photocatalytic activation *in-situ*.[18, 20, 171]

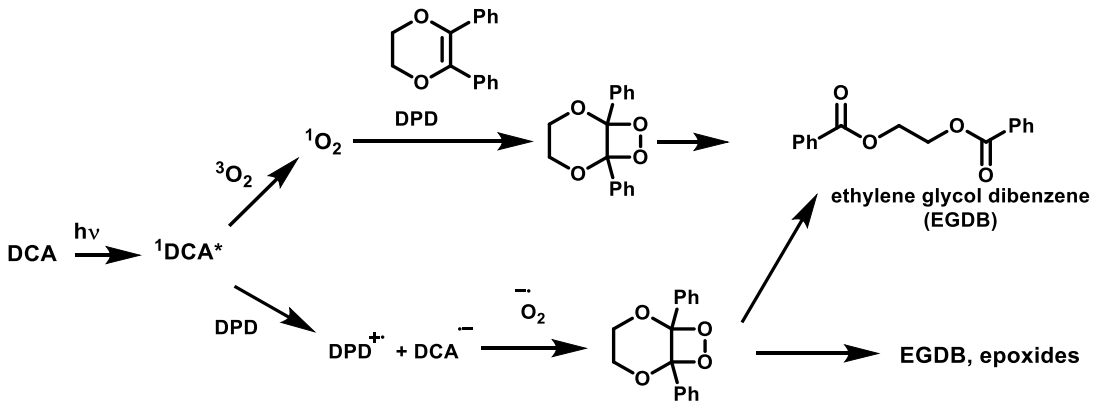
Cyano derivatives of anthracenes are well known photosensitizers, with wide applications for photo-induced energy transfer, and photo-induced electron transfer (PET) reactions.[21, 50] One of these compounds is 9,10-dicyanoanthracene (DCA),[51] the properties of which have been extensively studied due to its broad applications. This is particularly due to its absorption of light at wavelengths longer than 400 nm.[21]

Its reactions can proceed either through energy transfer, particularly efficient with ground state oxygen, leading to formation of singlet oxygen ($^1O_2$) with quantum yields ranging from 1.46 – 2.06 in acetonitrile and 1.71 in benzene at an infinite oxygen concentration.[50] Or alternatively, through PET depending on the reactants, giving rise to redox reactions. For PET process, presence of molecular oxygen ($^3O_2$) lead to an easy production of superoxide radical anion.[50, 52] Because of these properties DCA and other photosensitisers, sensitise photo-oxidation of a large number of molecules under mild conditions in solution,[53] with the contribution of each of these mechanisms depending on the solvents polarity, nature of substrate and its concentration, and temperature.

The effect of solvent polarity on the DCA-sensitized reactions can serve as guide to the possible mechanism of a given transformation, the electron-transfer photo-oxygenation can occur predominantly in polar solvents, such as acetonitrile and methanol.[21, 54] This is because an intermediate ion pair (exciplex) which is too poorly solvated to diffuse apart in a non-polar solvent.[52] In contrast, singlet oxygen reactions show only a very small response to changes in solvent polarity, which results for most of the DCA promoted

photo-oxidation in non-polar solvents to occur via energy transfer mechanisms (Scheme 8).[52] Apart from solvents, temperature and concentration of the substrate also affect the pathway of the photo-oxidation process, with high substrate concentration and temperature favouring the electron transfer process. For the PETs processes back electron transfer from acceptor to the donor can result in the inefficiency of products formation, as reported during DCA catalysed photo-oxidation process.[172]

These effects were demonstrated by Foote and Silverman[173], that at low concentration of 2,3-diphenyl-1,4-dioxetene (DPD), the products formation are entirely through energy transfer sensitisation to produce singlet oxygen ($^1O_2$) by the excited DCA, which was suggested to be due to relatively low rate of quenching of the ^{1}DCA* by the substrate, resulting in the rapid production of ethylene glycol dibenzene (EGDB), increasing the DPD concentration resulted in decrease in the reaction rate (Scheme 45).[174] The electron transfer mechanism is however favoured at the high temperature due to the separation of initially formed radical ion pair (DCA^{-}/DPD^{+}) to free ions DCA^{-} and DPD^{+} thereby forming large amount of epoxides. Therefore, under this condition the main pathway for the product is energy transfer process of singlet oxygen generation to give dioxetane which cleaves to EGDB.

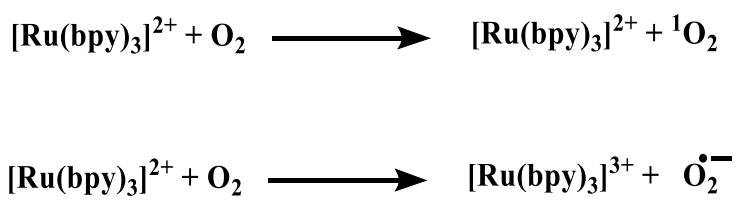


Scheme 45: reported mechanism to illustrate the competing energy transfer and electron transfer sensitisation catalysed by DCA.[174]

The inefficiency of product formation by electron transfer pathway suggests that back electron transfer from $DCA^{\cdot-}$ to $DPD^{\cdot+}$ in the initially formed ion pair is faster than ion pair separation in polar solvent. Alternatively, free ions are formed due to solvent effect in polar solvent such as acetonitrile, and the $O_2^{\cdot-}$ formed transfer its electron to the substrate ($DPD^{\cdot+}$) instead of given oxygenated products.[54]

However, using biphenyl (BP) as co-sensitiser, it reacts with ^{1}DCA* to produce biphenyl radical cation ($BP^{\cdot+}$), which in turn reacts with DPD to produce $DPD^{\cdot+}$ and change the reaction pathway to favour electron transfer mechanism. This indicates that co-sensitisation with BP is used to improve the efficiency of electron transfer pathway. Because a low concentration of substrate and a high loading of BP change the entire mechanism to favour electron transfer process[54].

Another group of photosensitisers that have been reported to catalysed both energy and electron transfer transitions are transition metals catalysts.[58] Some of the most important transition metal catalysts for PET processes are ruthenium and iridium based catalysts systems, the photophysical properties of which can be tuned depending on the nature of the ligand. For $[Ru(bpy)_3]Cl_2$ the relatively long-lived MLCT excited state can undergo both energy transfer and electron transfer processes,[57, 159] as described in Chapter 1. In the presence of molecular oxygen, energy transfer predominates which give rise to singlet oxygen ($^1O_2$). But in principle the quenching of $[Ru(bpy)_3]^{2+}$ by molecular oxygen ($^3O_2$) can take place via the aforementioned two mechanisms, with the energy transfer process generating $^1O_2$ and ground state sensitiser, while for electron transfer quenching, the excited sensitiser is oxidised as a results of electron transfer to molecular oxygen resulting in the formation of superoxide radical ($^{\cdot-}O_2$).[159]

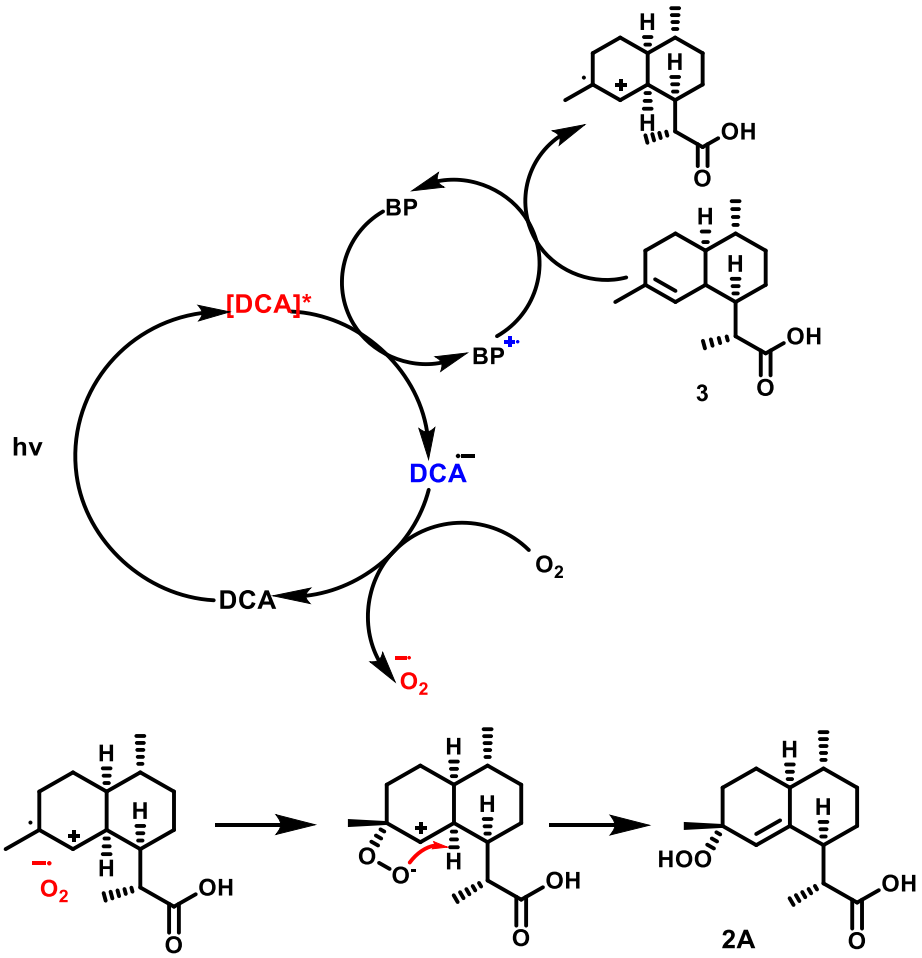


Scheme 46: energy and electron transfer mechanisms for ruthenium tris-bipyridine and molecular oxygen interactions.[159]

While the electron transfer pathway is sensitive to substrate and co-sensitiser (redox mediator) concentration, it was observed that the presence of biphenyl can have a negative effect on the processes that involve potential simultaneous energy and electron transfer. For example, in the DCA catalysed photo-oxidation of 2,3-diphenyl-1.4-dioxene (DPD) reported by Silverman and Foote, presence of biphenyl (1 M) trapped all singlet excited DCA (^{1}DCA*) and the observed products arise completely from electron transfer process.[21, 174, 175] Therefore, for the photochemical process involving photosensitiser that is capable of undergoing both energy transfer and electron transfer transitions such as DCA, and $[Ru(bpy)_3]Cl_2$ the presence of other reaction constituents capable of acting as co-sensitisers must to be given special consideration depending on the pathway that results in the production of desired product.

Using DCA as photosensitiser the competing energy and electron transfer photosensitisation for the photo-oxidation of DHAA **3** into tertiary hydroperoxide **2A** is illustrated according to proposed mechanism, Scheme 47. Addition of biphenyl resulted in the improvement of the percentage yield and selectivity of the tertiary hydroperoxide **2A**. This is an indication that addition of biphenyl helps to improve the yield and selectivity of the photo-oxidation products by co-catalysing the electron transfer pathway through possible interaction with excited singlet ^{1}DCA* and reducing it to DCA^{-} while it-self oxidised to $BP^{\cdot+}$, the electron rich DCA^{-} is then quench by O_2 and possible

formation of $^{\cdot}O_2$ making it to return to ground state. The electron rich $^{\cdot}O_2$ react with the oxidised DHAA **3** leading to the formation tertiary hydroperoxide **2A**.



Scheme 47: the proposed biphenyl assisted electron transfer mechanism for DCA catalysed DHAA **3** photo-oxidation process.

CHAPTER SUMMARY

In this Chapter the semi-synthesis of Artemisinin **1** from DHAA **3** was reported. Two strategies were employed with a semi-continuous PhotoVap reactor: two-step and one-pot. Various conditions were optimised which include photosensitiser, solvent, and temperature, with the view to finding the best possible route to improve the industrial production of Artemisinin 1, according to the stated aims.

The best conditions for the photo-oxidation of DHAA **3** in the PhotoVap reactor is using the polar aprotic solvent ethyl acetate at 22 °C to produce 90 % of **2A** after 7.5 minutes irradiation using TPP as photosensitiser. Although similar selectivity was obtained using DCM (with $[Ru(bpy)_3]Cl_2$) at -10 °C, the use of ethyl acetate was considered as the best option due to its green nature and reduced cost of production, as the process does not involve as much cooling.

The acid catalysed Hock-cleavage and the thermal oxidation cascade to Artemisinin **1** was performed in batch, through addition of an acid catalyst to the crude products of the photo-oxidation. A good yield was achieved in toluene using TMSTFA as the acid catalyst with a high yield of 60 % Artemisinin **1** and projected productivity of 0.64 g/day. The use of TMSTFA could be further optimised to realise the potential of this acid in the industrial production of Artemisinin **1.**

The potential of industrial production of **1** using a PhotoVap reactor could be realised through a one-pot approach, because after optimisation of various conditions, a high yield of 75 % Artemisinin **1** was obtained using DCM at -10 °C with $[Ru(bpy)_3]Cl_2$ and TFA as photosensitiser and acid catalyst respectively, this gave a projected productivity of 14.38 g/day.

The use of a heterogeneous catalyst system was explored but did not yield high amount of Artemisinin **1**. Alcohol/water mixtures were also explored because of their reported potentials for improving the recovery of the artemisinin during isolation and purification processes. This method resulted in a low overall yield and projected productivity of **1**.

TMSTFA and $[Ru(bpy)_3](TFA)_2$ were used as acid catalyst and photosensitiser respectively, very promising improvement in the yield of Artemisinin were recorded when TMSTFA was used to catalyse the second step of the process, while the use of $[Ru(bpy)_3](TFA)_2$ improved the solubility of $[Ru(bpy)_3]^{2+}$ in organic solvent which allows its use in DCM.

The effect of biphenyl on the outcome of each stage of the reaction was explored. The presence of biphenyl in the photo-oxidation step of DHAA **3** in DCE showed an increase in the yield of **2A** to 70 %, in the presence of 100 % biphenyl. When an excess of 200 % biphenyl was used the yield of **2A** dropped significantly to 60 %. For the one-pot synthesis of Artemisinin **1** using $[Ru(bpy)_3]Cl_2$ as photosensitiser, presence of biphenyl had a detrimental effect on the yield of **1**. Because in the absence of biphenyl 60 % of Artemisinin **1**, increasing the concentration of biphenyl only decreased the yield of **1** further.

CHAPTER 3: LACTONES DERIVED FROM THE SYNTHESIS OF ARTEMISININ AND THEIR ROLES IN ITS PRODUCTIVITY

INTRODUCTION AND MECHANISTIC STUDIES

The semi synthesis of Artemisinin **1** is a complex process accompanied by the production of different side products during the photo-oxidation, acid catalysed Hock cleavage and thermal oxidation steps. However, most of the side products are generated in the later steps, leading to a substantial decrease in the overall yield of Artemisinin **1**. In the previous Chapters the synthesis of Artemisinin **1** has been explored by optimizing various parameters that resulted in the improvement of its yield and productivity, using the PhotoVap reactor.

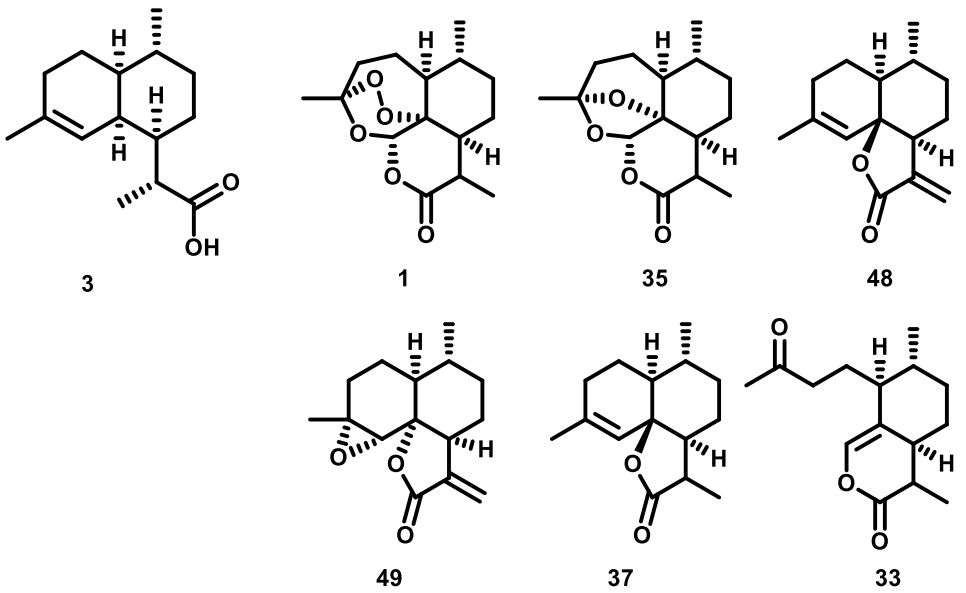


*Figure 30: structures of DHAA **3** and some sesquiterpene lactones isolated from A. annua.*[165]

The major limiting factor towards improving the productivity of Artemisinin **1** is the lactonization of the carboxylic acid group at 12-position of **3**; this process takes place during the thermal oxidation step, leading to the formation of lactone side products.

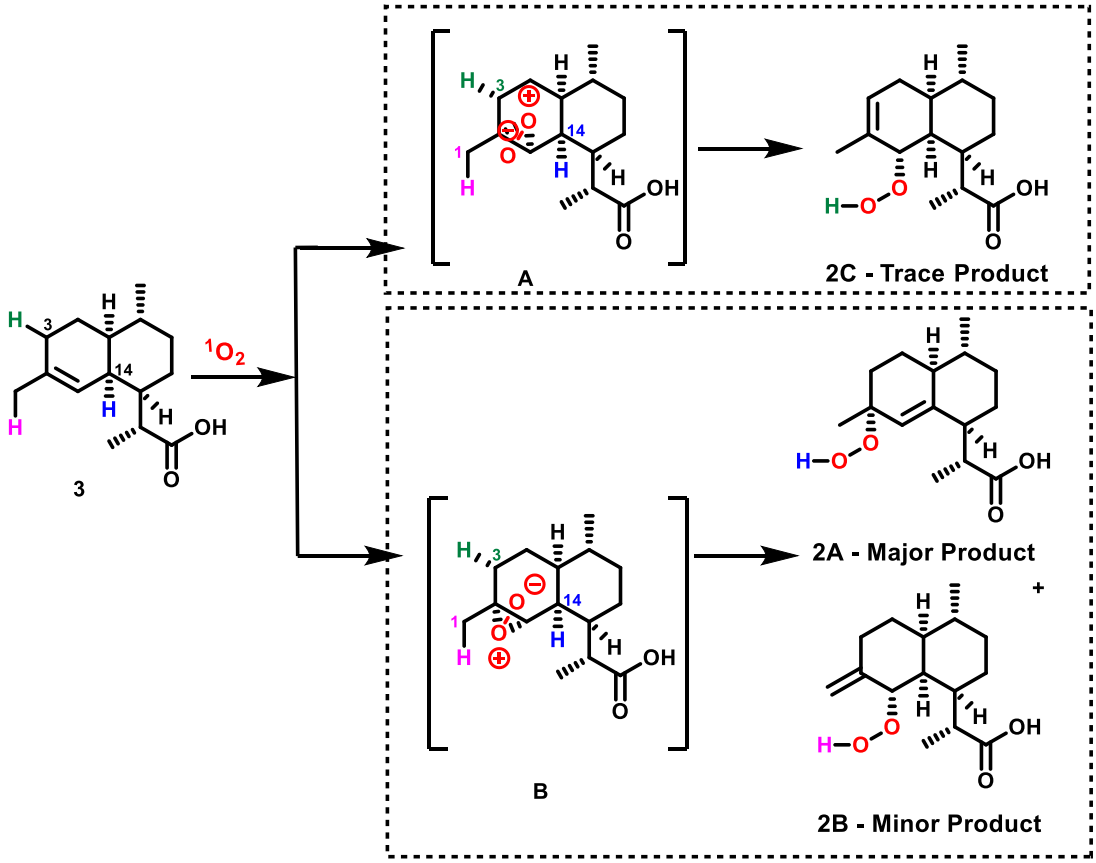
These by-products are also found in *A. annua* plant, which include deoxyartemisinin **35**, Arteannuin B **49**, and epideoxyarteanuin B **48**. (*Figure 30*). They are thought to be produced during the biosynthetic production of Artemisinin 1 in the plant as described by Brown and co-workers.[132, 164, 176, 177] The lactones **33** and **37** were reported as synthetic by-products encountered during the acid catalysed Hock-cleavage of the photo-oxidation product of DHAA **3**, as explained in the previous Chapters. Another side product mostly encountered is deoxy Artemisinin **1**, which also contributes to the decrease in overall yield of the desired product Artemisinin **1**.

MECHANISM AND SELECTIVITY IN THE SEMI-SYNTHESIS OF ARTEMISININ

In the previous Chapters the synthesis of Artemisinin **1** has been described as accomplished in three general steps namely, photo-oxidation, acid catalysed Hock-cleavage and the thermal oxidation cascade. In this section, the details of mechanistic processes during each step will be described, with ae report of the contribution of each step towards the selectivity, productivity, and overall yield of the final product.

3.2.1. MECHANISM AND SELECTIVITY OF DHAA PHOTO-OXIDATION PROCESS

The reaction of photochemically generated singlet oxygen ($^1O_2$) with the C-C double bond of **3** is governed by the stereochemistry and occurs through a sequence of highly selective Schenk-ene reactions.



*Scheme 48: The proposed stereochemistry of Schenk reaction of **3** with photochemically generated singlet oxygen, showing the formation of 2°-hydroperoxide **2C** via exo-per-epoxide (**A**), 3°-hydroperoxide **2A** and 2°-hydroperoxide (**2B**) via the endo-per-epoxide (**B**).*

As shown in Scheme 48, the Ene-reaction involving photochemically generated singlet oxygen ($^1O_2$) and DHAA **3**, result in the formation of the two per-epoxide intermediates, **A** and **B**, with *exo* and *endo* geometry, respectively. The *endo* geometry is favoured due to increased stability arising from a favourable interaction between the per-epoxide tail oxygen and allylic double bond, leading to easier hydro gen abstraction.[25, 178, 179] These per-epoxide intermediates are the precursors of the hydroperoxides **2A** – **C**, with the tertiary hydroperoxide **2A** produced as the major product due to a *cis*-effect, and the ease of hydrogen abstraction at the bulky terpene ring of DHAA **3**. Leading to the production of **2A** with very good yield and selectivity.[2, 48, 83 97, 179, 180] The hydrogen abstraction occurs on the same side as the bulky terpene ring, and from the shape of the per-epoxide

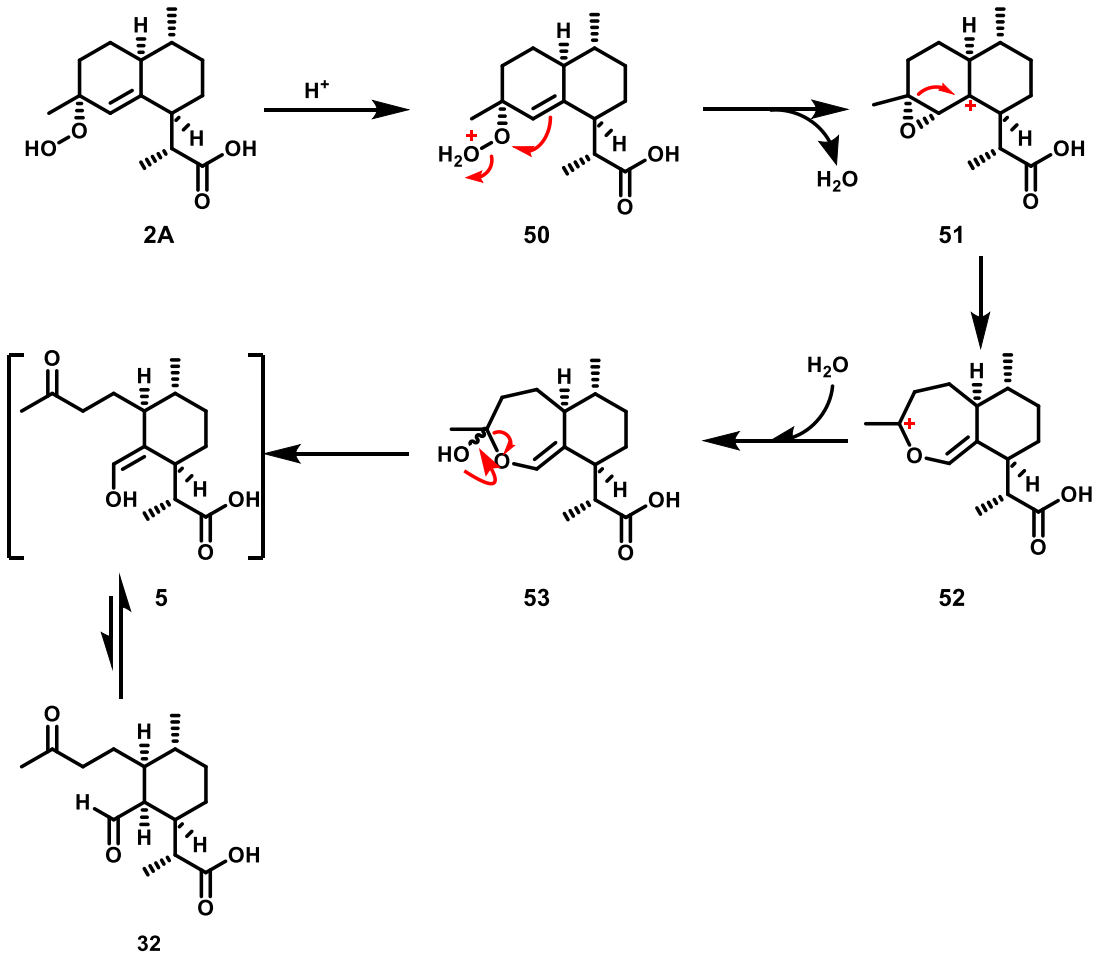
intermediate, it seems unlikely that there is a strong steric interaction between the per-epoxide group and the terpene ring, which is folded away from the face of attack.[25]

The chiral feature of DHAA **3**, allows the photo-oxidation process to proceed with facial selectivity, a diastereoselective process which involves back-side attack on the allylic double by the $^1O_2$. This results in the formation of all the hydroperoxide intermediates having the -OOH group on the same face of the molecule, while other possible products that could result from $^1O_2$ attack from the opposite face of the alkene are not seen.[25]

The reported semi synthesis of Artemisinin **1** shows that tertiary hydroperoxide **2A** is produced in good yield.[1, 48] The results discussed in Chapter 2 showed that a yield and selectivity of up to 90 % of **2A** can be obtained in ethyl acetate, which indicates only 10 % of the starting material is lost to the formation of other hydroperoxide side products (**2B** and **C**).

3.5.2.2 MECHANISM OF THE ACID CATALYSED HOCK-CLEAVAGE PROCESS

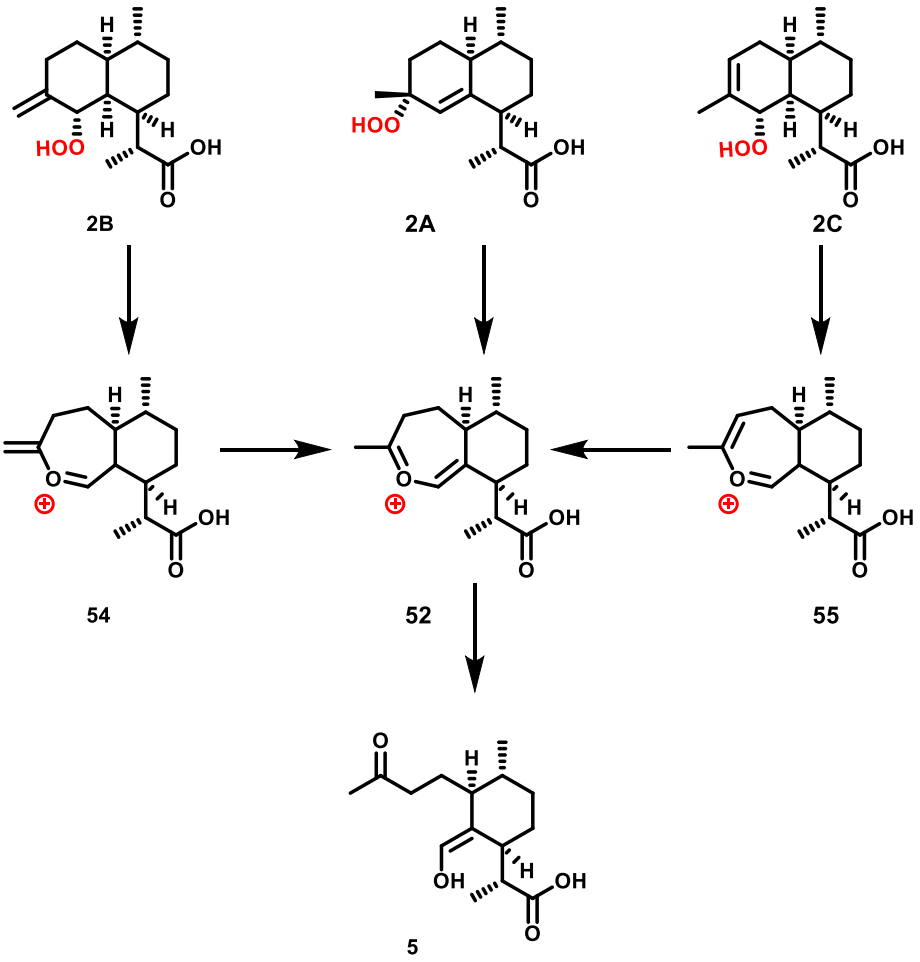
Following the production of the tertiary hydroperoxide **2A**, the next step in the synthesis of Artemisinin **1** consists of the acid catalysed Hock cleavage. This cleavage and the thermal oxidation are in general the step that generates more side products resulting in a significant decrease in the selectivity and yield of Artemisinin **1**. The allylic tertiary hydroperoxide **2A** is converted to an aldehyde **32** via enol **5** through an acid catalysed Hock cleavage, Scheme 49. The addition of an acid results in the protonation of the distal oxygen of the hydroperoxide of **2A**, which then triggers the elimination of a molecule of water and subsequently giving rise to the α-epoxide carbocation **51** which is then involved in an intramolecular rearrangement to form a more stable oxocarbenium ion (also called oxonium ion) **52**.



*Scheme 49: The Hock cleavage mechanism for the acid catalysed rearrangement of the allylic tertiary hydroperoxide **2A** to keto-enol species **32**.*[25]

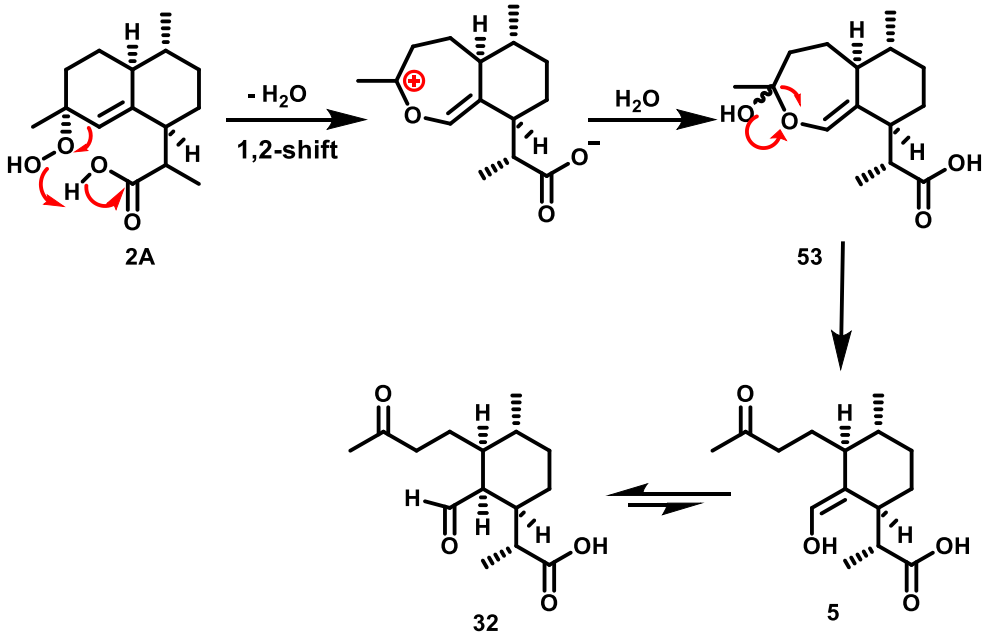
Finally, the attack of a molecule of water on the oxocarbenium **52** generates the hemi-acetal **53**, which ring opens to form **5**.

Recently, Yoshimoto and co-workers reported isotopic studies on the mechanism of endoperoxide formation and proposed the conversion of all the allylic hydroperoxides (**2A – C)** to the same oxonium ion intermediate **52**, through in-situ rearrangement of the corresponding oxonium to **52**, which opened to enol intermediate **5** (Scheme 50).[181, 182]



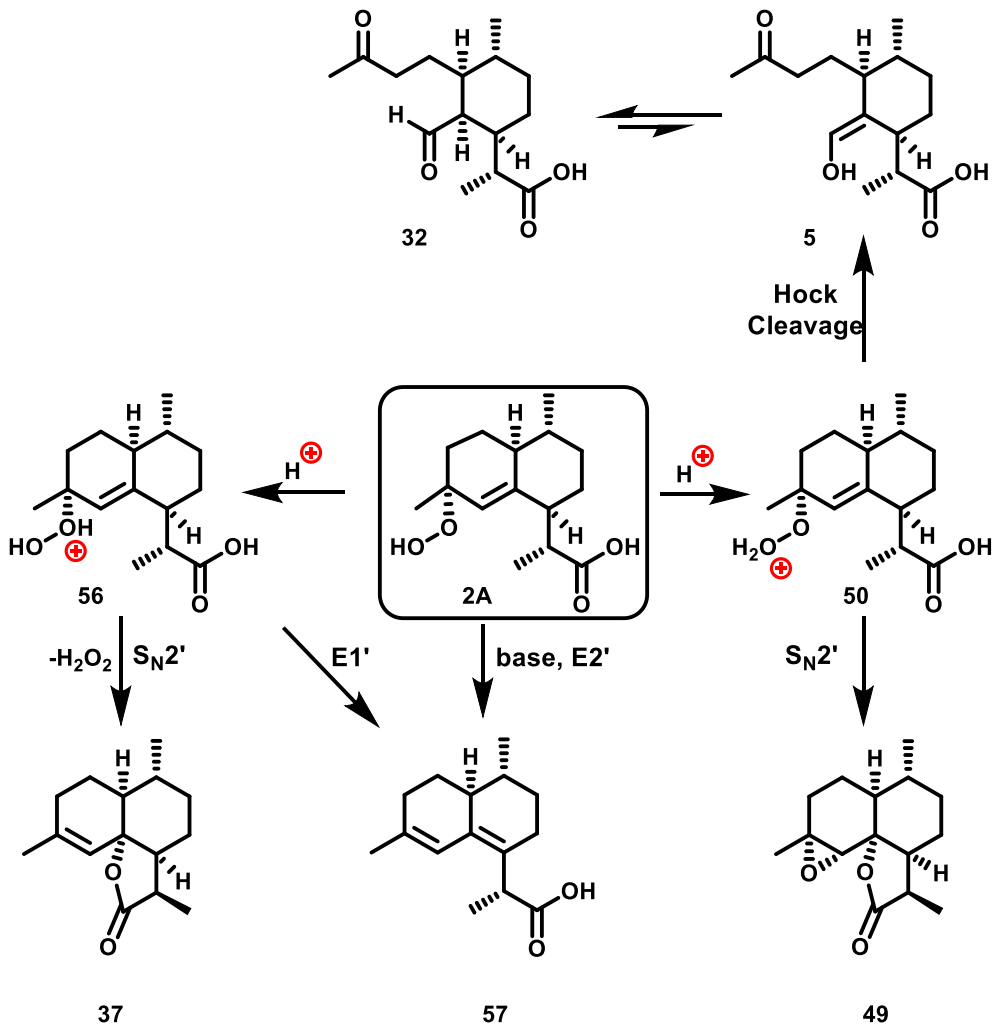
*Scheme 50: the proposed conversion of secondary hydroperoxides (**2B** and **C**), to their corresponding oxonium ions each of which rearranges to common oxonium ion **52** believed to opened to enol intermediate **5**.*[181]

The proposed mechanism by Yoshimoto and Co-workers on the semi synthesis of Artemisinin **1**, does not agree with the known mechanism, that the secondary hydroperoxides **2B** and **C** are stable under conditions of the acid catalysed Hock-cleavage and thermal oxidation cascade, and the two hydroperoxides only contributed to the decrease in selectivity of **2A**. The Hock-cleavage also occur spontaneously catalysed by the proton of the carboxylic acid group at the 12-position of **2A** (Scheme 51).[182]



Scheme 51: proposed mechanism by which the 12-carboxylic acid group catalyses the spontaneous Hock cleavage reaction of tertiary hydroperoxide ***2A****.*[157]

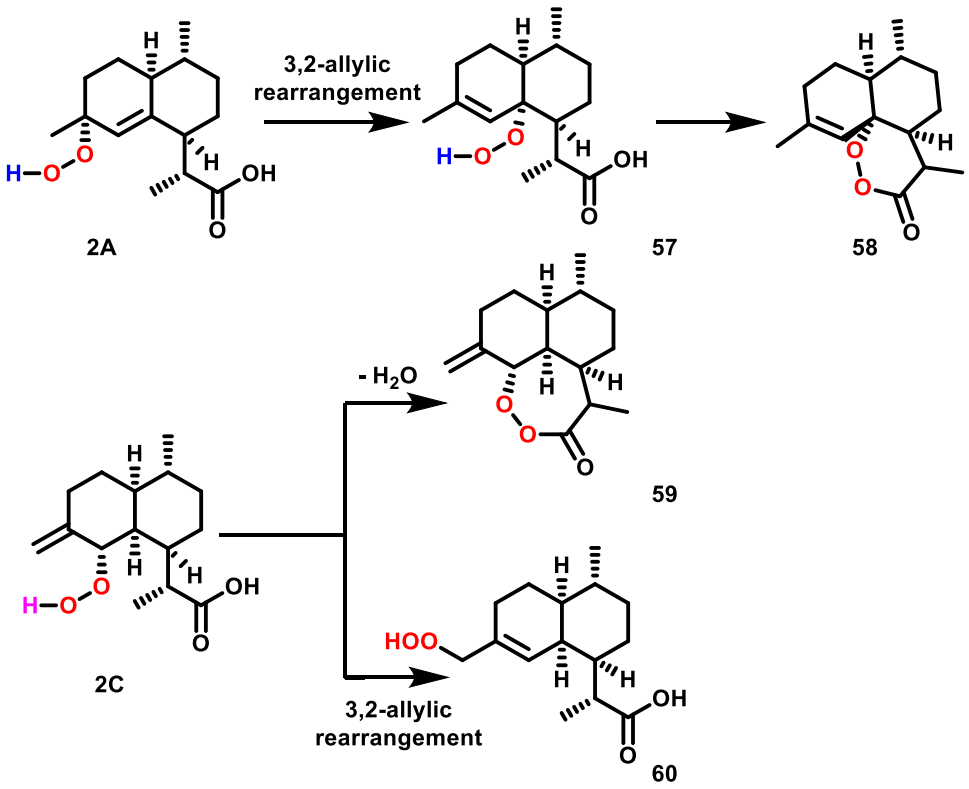
The addition of acid can also result in the protonation of the proximal oxygen atom of the tertiary hydroperoxide **2A**, leading to the loss of a molecule of hydrogen peroxide instead of water, and the formation of the γ-lactone **37** *via* an intermolecular S_N2' mechanism as proposed by Brown *et al.* the γ-lactone **37** was also reported during the semi-synthesis of Artemisinin **1** as one of the side products, with further confirmation of its mode of formation.[48, 83, 183] A wide range of other sesquiterpenes have been isolated from *A. annua* and characterized, which might help in probing the mechanism of their formation. These compounds include an epoxy lactone **49** and diene **57**, formed through E1 and S_N2' mechanisms respectively (see Scheme 52).



Scheme 52: Brown's mechanisms proposed pathway for the formation of side product formation during the Hock cleavage process.[157]

Subsequent work on the semi-synthesis of Artemisinin **1** probed the proposed mechanism for the formation of these side products particularly the γ-lactone **37**. A lactone endoperoxide **58** was also reported by Brown and Sy to form *via* a 3,2-allylic rearrangement of the tertiary hydroperoxide **2A**. According to their proposed mechanism, the process involved trapping of the rearranged allylic hydroperoxide by the 12-carboxylic acid group (Scheme 53).[106] This mechanism is related to the trapping of the secondary hydroperoxide **2C** to form the allylic lactone endoperoxide **59** with the loss of a water molecule, or the 3,2-allylic rearrangement of the peroxide to form compound related to

DHAA **3** with a hydroperoxide group at 15-position.[48, 177] The formation of this side products further demonstrate the complexity of this step, which result in the formation of various side products, thus reducing the overall yield of Artemisinin **1**.

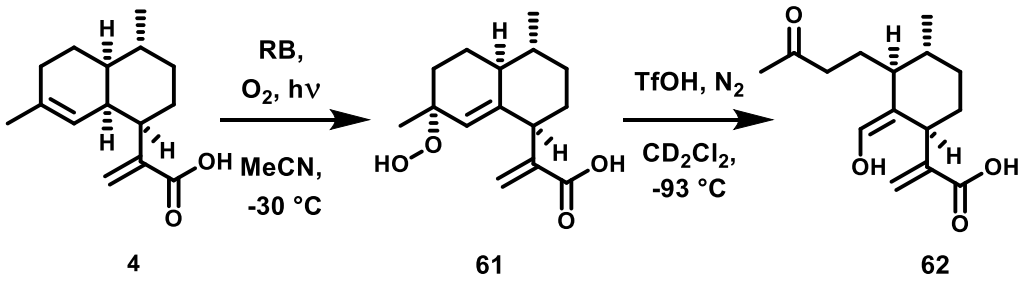


*Scheme 53: mechanism for the formation of lactone endoperoxide from tertiary and secondary hydroperoxides (**2A** and **2C**).*[157]

In 1997 Haynes and Vonwiller designed an experiment to demonstrate the formation of the intermediate enol **62**, *via* photo-oxygenation of artemisinic acid **4** by treatment with trifluoromethanesulfonic acid (TfOH) under an inert atmosphere (Scheme 54), the intermediate was thought to form from the tertiary hydroperoxide **2A** of artemisinic acid **4**, in a similar fashion to that described earlier for DHAA **3.**[140]

The dependence of Hock cleavage on the nature and concentration of acid was studied by Seeberger and co-workers who revealed that very strong acids, such as sulfonic (pKa -7) and triflic (pKa -14.7) acids, did not result in an improved yield of Artemisinin **1**.

Changing the acids to the weaker, but still quite strong trifluoroacetic acid (TFA), pK_a = -0.25, outperformed all the sulfonic acids, as well as the Lewis acid Cu(II) trifluoromethanesulfonate $Cu(OTf)_2$.



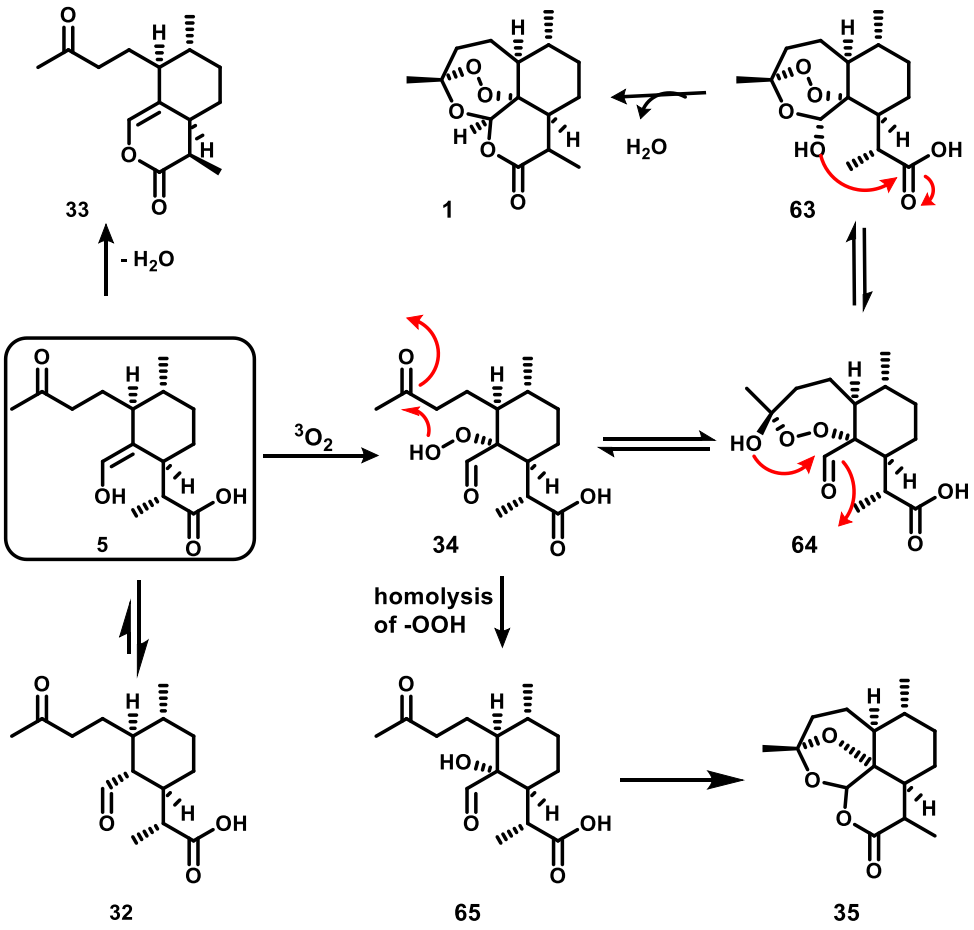
Scheme 54: Haynes and Vonwiller's low temperature ^{1}H-NMR study showing the formation of keto-enol, supporting the Hock cleavage mechanism.[140]

However, increasing the pK_a further led to a loss of selectivity, as shown by the low yield of **1** when using acetic acid, (pK_a = 4.75). Seeberger and Co-workers also found that low concentrations of TFA gave a large relative increase in Artemisinin **1** yield when the temperature was raised, an effect which was not observed for higher concentrations.[83, 85, 154]

The mechanism of the Hock-cleavage described above shows the formation of different products, among which, only the keto-enol intermediate **5** has been reported to undergo thermal oxidation and eventual cyclisation to form the desired Artemisinin **1**. The formation of products other than the keto-enol, only contribute to the decrease in the overall yield of Artemisinin **1**. Therefore, the reaction conditions will have an impact on improving its yield. As explained in Chapter 2, among these possibilities, a one-pot synthesis proved to significantly improve the yield of Artemisinin **1**. Although, the quantitative yield of enol intermediate **5** cannot be easily ascertained because of its reactivity, this step remains one of the main challenges for increasing the overall yield of Artemisinin **1**, and thus the productivity of the process.

3.5.2.2 Mechanism of the Thermal Oxidation and Final Cyclisation Cascade

The final step in the mechanism of Artemisinin **1** formation is the thermal oxidation of the enol intermediate **5**. This thermal oxidation involves the addition of triplet oxygen to the reactive enol intermediate **5** obtained from the acid-catalysed Hock-cleavage. The initial studies on the mechanism of Hock-cleavage by Brown *et al.* were conducted in the absence of oxygen (in nitrogen atmosphere), but surprisingly some thermal oxidation products such as Artemisinin **1** and deoxyartemisinin **35** was also produced; the oxidation was believed to be facilitated by the hydrogen peroxide produced by the proximal protonation of tertiary hydroperoxide **2A** leading to the production of the γ-lactone **37**.



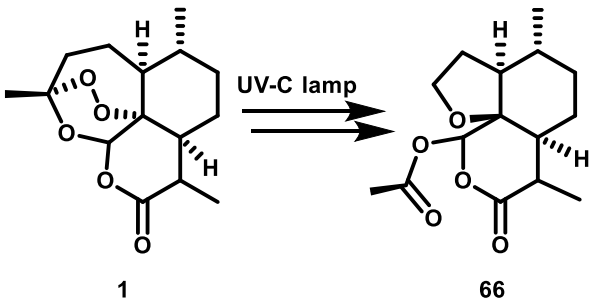
*Scheme 55: The cascade of ring closures leading to Artemisinin **1**, deoxyartemisinin **35**, and tautomerisation to 6α-aldehyde **32**.*[25]

In the presence of oxygen, the thermal oxidation proceeds with the formation of the hydroperoxyl aldehyde **34**, and a final ring closure cascade to produce Artemisinin **1** as shown in Scheme 55. There is a sequence of two ring closures each of which is stereospecific, leading to either Artemisinin **1**, or homolysis of hydroperoxide from hydroperoxyl aldehyde **34** and ring closure to deoxyartemisinin **35**.

The formation of **63** and **64** is likely to be reversible, with the driving force for the reaction being the elimination of water to form the lactone ring in Artemisinin **1**. In the presence of water and under acidic condition, lactone formation is reversible and could lead to lower yields. Whilst the acetal formation steps can form diastereomers of **63** and **64**, only structure **64** with the stereochemistry shown has the correct geometry for lactone ring formation, explaining the stereospecificity of the cascade.

The keto-enol intermediate can undergo tautomerisation to produce more stable 6α-aldehyde **32**. The aldehyde is less reactive toward oxygen and was not converted to a 1,2,4-trioxalane ring system, it was reported to instead undergo spontaneous autoxidation to 6α-carboxylic acid, after several weeks with no detectable Artemisinin **1**.[106] The δ-lactone **33** is formed by the condensation of water molecule, other possible side products produce include polymers[106] and oligomers[2] believed to form as a result of self-condensation of generated enol radical, leading to further decrease in the overall yield of Artemisinin **1**.

One of the most important aspects of Artemisinin **1** synthesis is the endoperoxide formation, because it is the group that confer anti-parasitic properties to **1**, through the release of reactive oxygen species which lead to the death of the parasite. Because of that, there is growing interest in determining how the endoperoxide formed in nature,[184] and synthetically through deuteration studies.[133, 181, 182]



Scheme 56: The reported mechanism of light induced rearrangement of Artemisinin ***1.***[181]

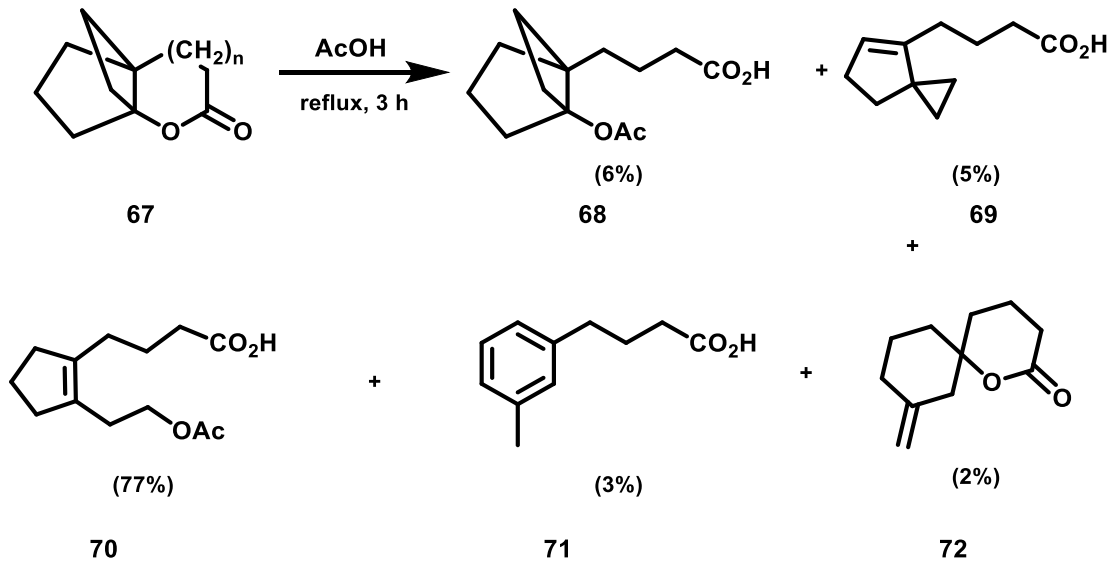
In their studies Yoshimoto and co-workers synthesised dideuterated and trideuterated dihydroartemisinic acid isotope at C3 and C15 and $^{18}O_2$ incorporated into the endoperoxide bridge of Artemisinin **1**.[181] The studies revealed a slower rate of conversion of deuterated DHAA **3** to Artemisinin **1** than for non-deuterated, which revealed a kinetic isotope effect in the initial ene-reaction toward endoperoxide formation. They also revealed that irradiation with high power Ultraviolet-C (UV-C) initially increased the rate of Artemisinin formation, but prolonged irradiation resulted in the homolytic cleavage of the trioxolane (O-O) bond and rearrangement to THF derivative **66** (Scheme 56).[181] This indicates that high power UV-irradiation is suitable for the photo-oxidation process, and prolong irradiation can often result in the degradation of desired products.

3.2.2. REACTIONS OF LACTONES

The well-known reactions of lactones are acid and base catalysed hydrolysis processes which occur at high temperature to give its parent carboxylic acids. Unlike their corresponding esters, lactones are more stable making the equilibrium of the hydrolysis to favour the reactant rather than the products. The most common processes of lactone hydrolysis are catalysed by base, because of the high susceptibility of lactones toward nucleophilic attack.[181]

Many acid-catalysed hydrolysis of lactones has also been reported, such as isomerization, and recyclization are often observed. An example of hydrolysis of a lactone accompanied

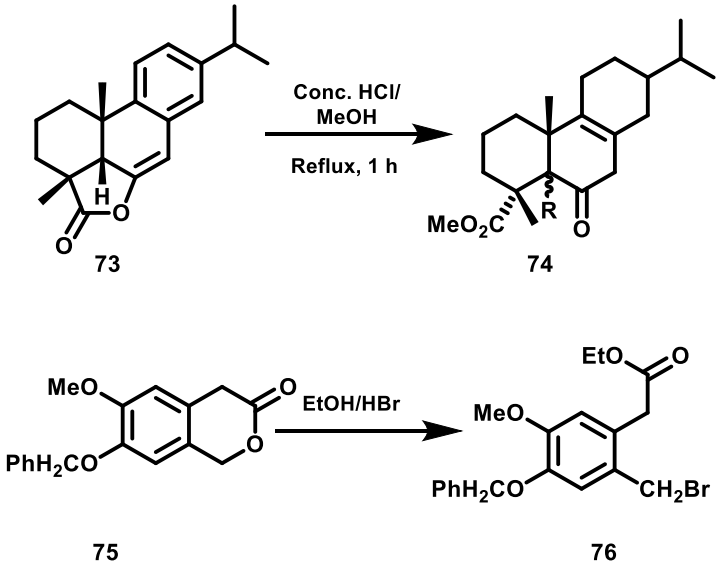
by extensive isomerization is the cleavage of an ε-lactone [5.3.2]propella-ε-lactone **67 (n = 2)** which reacts under refluxing acetic acid (Scheme 57).[185, 186]



Scheme 57: acid catalysed hydrolysis of lactone accompanied by poor selectivity.[186]

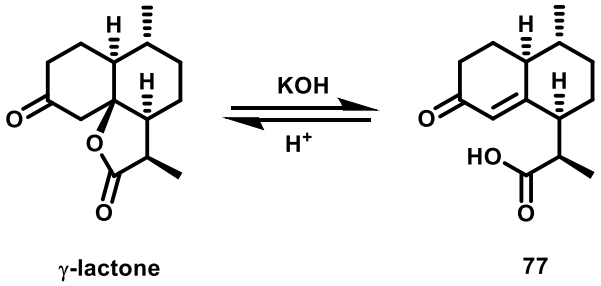
The poor selectivity of the process results in the formation of five products with a combined yield of 93%; the thermodynamically most stable 1,2-disubstituted cyclopentene **70** was the major product (77 %). The formation of **70** was suggested to proceed by the formation of a cyclopropylcarbinyl cation intermediate followed by a nucleophilic attack on the cyclopropane ring, concerted with ring cleavage and/or rearrangement. Unlike **67**, its corresponding the δ-lactone does not react when subjected to similar reaction conditions.[185] The acid catalysed hydrolysis of the lactone was reported by Mutsomoto *et al.* involving the use of concentrated HCl in methanol under reflux to hydrolyse the γ-lactone into 81 % of keto ester **74**. [187] Another reaction was catalysed by Bronsted or Lewis acids such as zinc bromide and chloride resulting in the cleavage of the δ-lactone ring to produce the ω-bromoester. Addition of HBr in an alcoholic solution of the *N*-benzyltetrahydroisoquinoline alkaloid corgoine **76** was produced from the δ-

lactone **75** (Scheme 58). This method was reported to have been employed in the synthesis of naturally occurring *N*-benzyltetrahydroisoquinoline alkaloids.[186]



Scheme 58: Mineral acid catalysed hydrolysis of lactones in alcoholic solutions.[186]

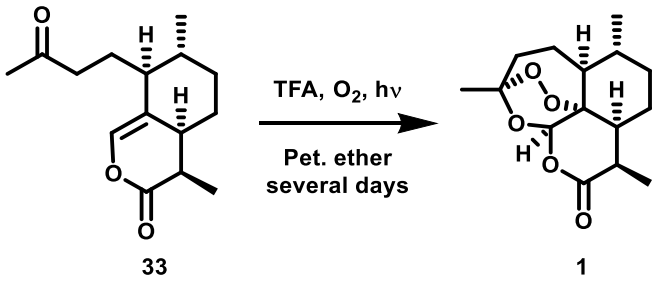
The base catalysed hydrolysis of the γ-lactone was reported upon treatment with KOH to produce decalenone **77** which, upon treatment with acid, will convert back to its lactone form, the alkali process is often employed to synthesize **77** in high overall yield (Scheme 59).[188]



Scheme 59: base catalysed hydrolysis of γ-lactone.[188]

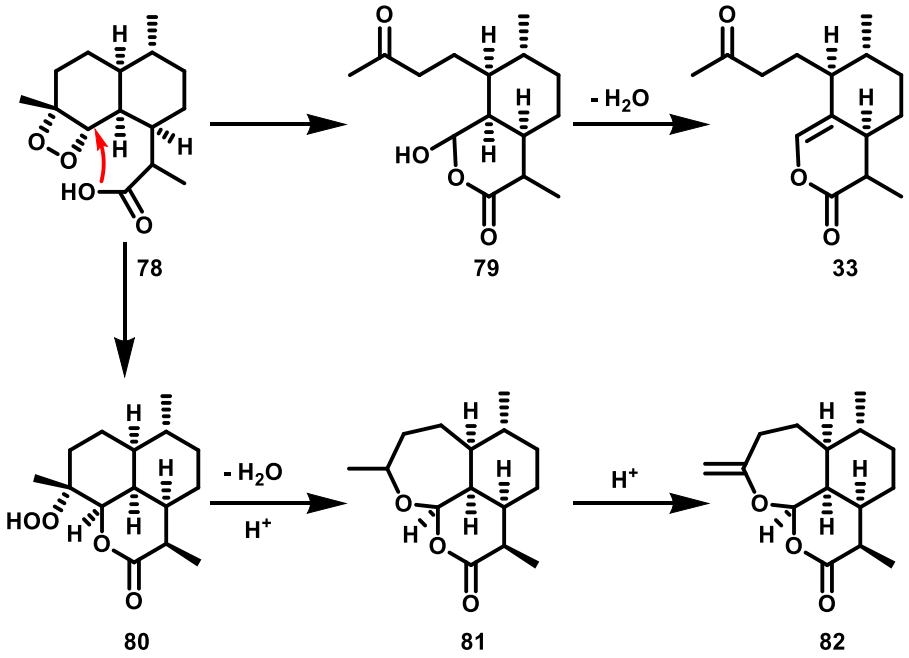
Studies by Acton and Ruth suggested that the δ-lactone **33** is readily photo-oxidized to yet unidentified material. Because the petroleum ether solution of the δ-lactone **33**

containing TFA is stable in air for several days, and when it was subjected to photo-oxidation, and the products allowed to stand in solution, no more than 1-2% of Artemisinin **1** could be detected by liquid chromatography using an electrochemical detector (Scheme 60).[133, 134]



*Scheme 60: the conversion of the δ-lactone **33**, into Artemisinin **1** reported by Acton and Roth.*[133]

Other products isolated included the well-known δ-lactone **33** and other sesquiterpene lactones **80** and **82**, Scheme *61*.



Scheme 61*: the proposed mechanism for the formation of the δ-lactone **33** reported by Acton and Roth.*[133]

It has been observed that, during the synthesis of Artemisinin **1** using ethyl acetate as the solvent described in Chapter Two, there is an increase in the percentage yield of **1** with a

corresponding decrease in the amount of one of the side-products (**33**). As a result, it has been assumed that the enol-lactone ring of the **33** opens under certain conditions to allow addition of molecular oxygen, and eventually convert to Artemisinin **1**.

The semi synthesis of Artemisinin is a complex process which is always accompanied by several side products during both the photo-oxidation and acid catalysed thermal oxidation steps, with the most of them appearing in the later step, leading to the reduction in the overall product yield. Therefore, the aim of this Chapter is to increase our understanding of the side products that can be generated in the conversion of the endoperoxide to the final product. The objectives of this Chapter are:

(i) to increase our understanding of these side products, with emphasis on the δ-lactone **33**, one of the compounds generated during the conversion of the enol intermediate to the final product.

(ii) To study the yield of various side products of thermal oxidation step of Artemisinin **1** synthesis and identify best conditions for their formation in higher yield.

(iii) To explore the possible method of isolation and studying their reactivity under various conditions.

(iv) To identify possible ways of preventing their formation or possible conversion to other important intermediates that can be converted to Artemisinin **1**.

LACTONES AS BY-PRODUCTS OF THE ARTEMISININ SYNTHESIS

The semi-synthesis of Artemisinin **1** has been described as accompanied by the formation of various side products most of which are generated during the acid catalysed Hock-cleavage/thermal oxidation step. These by-products largely form due to the reactivity of the carboxylic acid group at 12-position of the starting material **3**, which in most cases reacts at intramolecular position to form different type of lactone rings. The synthesis of **1** through a one-pot strategy has advantages that include improved yield, productivity, and better selectivity than a two-step approach. Because close monitoring of the process shows that addition of acid from the beginning to activate immediate acid catalysed thermal oxidation, can reduce the chances of the formation of side products, most of which possess a lactone ring.

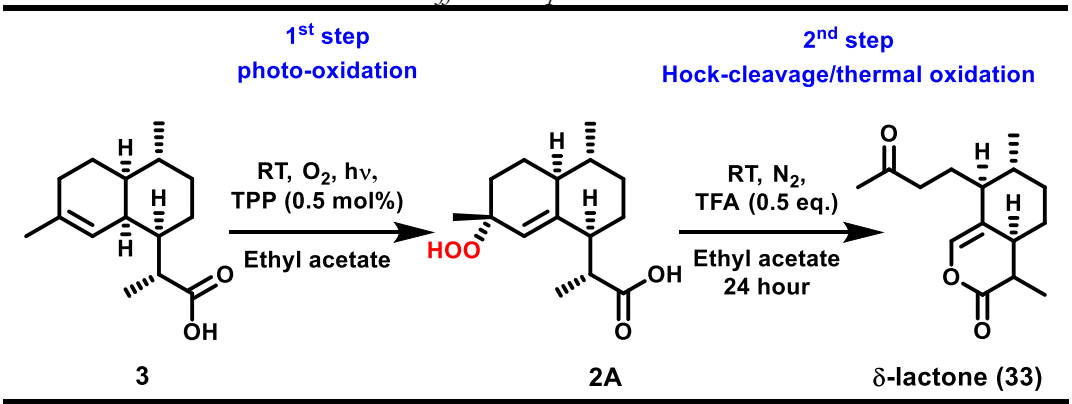
As explained in Section 2.3.1, the γ-lactone **37** is formed due to proximal protonation of the hydroperoxide intermediate, which triggers the immediate loss of hydrogen peroxide and subsequent trapping of 12-carboxyl group to the γ-lactone **37**. This lactone is very stable, but it is mostly produced at a very small overall yield. Therefore, it is not considered as a limiting factor for the improvement in the Artemisinin **1** yield and productivity. The two step approach has been accompanied by a decrease in Artemisinin **1** yield, with the increase in production of the δ-lactone **33** during thermal oxidation step. For example, in ethyl acetate, the yield of the δ-lactone **33** is obviously higher than that of Artemisinin **1**. It has been also observed that, there is an increased yield of Artemisinin **1** with the decrease in the δ-lactone's yield with prolonged bubbling of oxygen gas, signifying its possible conversion to Artemisinin **1**. The following sections described the synthesis, isolation, and characterization of the δ-lactone **33**.

3.3.1. SYNTHESIS OF Δ-LACTONE IN THE PHOTOVAP REACTOR

We describe how the δ-lactone **33** has been synthesised by initial photo-oxidation of DHAA **3** in ethyl acetate using the PhotoVap reactor, followed by the addition of TFA to the crude photo-oxidation products under the atmosphere of N_2, to convert all the tertiary hydroperoxide **2A** into the δ-lactone **33**, the γ-lactone **37**, Artemisinin **1**, and enol **5**.

The reaction was completed after 24 hours under N_2, with the conversion of all the enol intermediate to the δ-lactone **33**. The yield has been calculated using 10 % biphenyl as internal standard; different temperatures were screened to find the optimum condition for the best yield of the δ-lactone **33** (Table 18).

*Table 18: the results for the Synthesis of the δ-lactone from the DHAA **3** photo-oxidation products at different temperatures.*

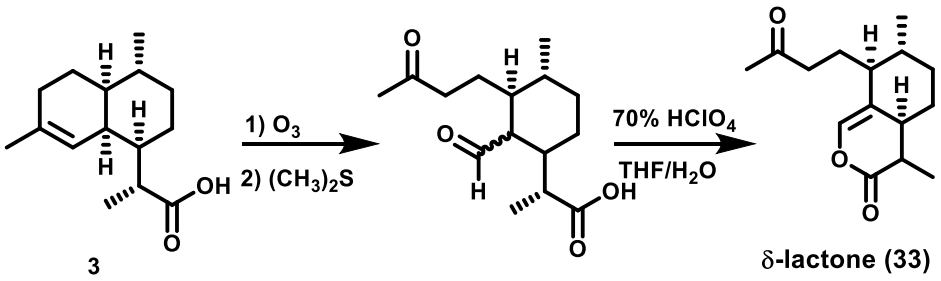


Entry	Temp. (°C)	Art. (%)	δ-lactone 33 (%)	γ-lactone 37 (%)
1	10	10	63	4
2	20	22	49	5
3	30	19	28	8

At the relatively low temperature of 10 °C, the highest yield of the lactone **33**, 63 %, (Table 18, Entry 1) was obtained with low yields of Artemisinin **1** (10 %) and γ-lactone **37** (4 %) respectively. Increasing the temperature to 20 °C resulted in a decrease in yield to 49 %

with an increase in the yield of Artemisinin **1** to 22 % while that of the γ-lactone **37** remains relatively unchanged. (Table 18, Entry 2) Further increase in temperature to 30 °C, decreases the yield of δ-lactone **33** to 28 %.

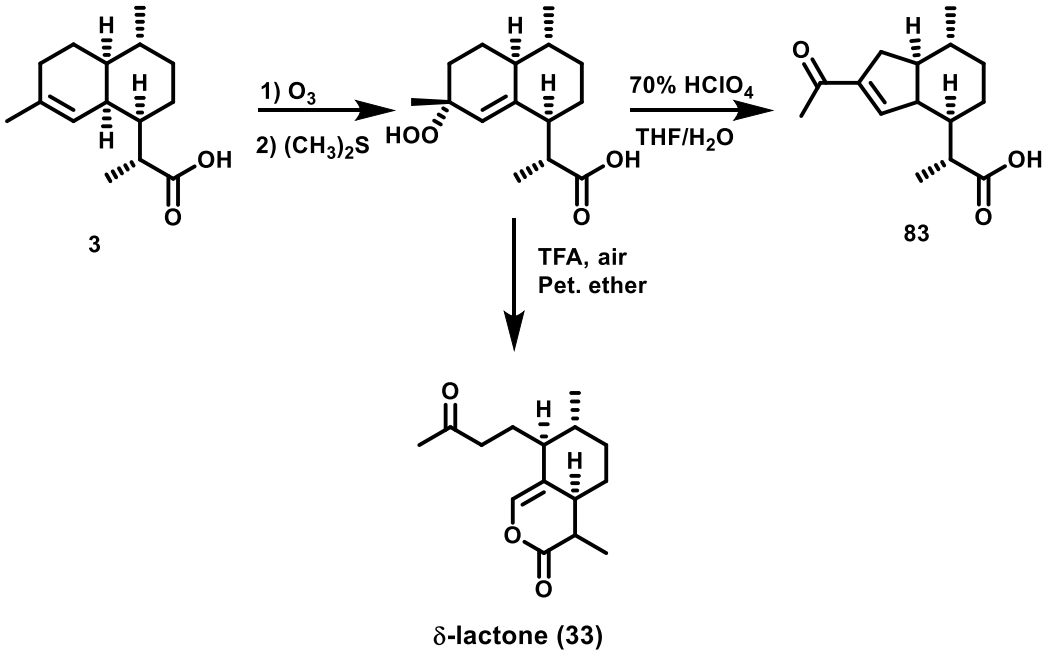
The formation of the δ-lactone **33** was accompanied by the formation of Artemisinin **1** under all the conditions but, at 20 °C, a higher yield of 22 % of Artemisinin **1** (Table 18, Entry 2) was produced with a correspondingly decreased overall yield of the δ-lactone **33**. Although the thermal oxidation was carried out under an atmosphere of N_2, the formation of Artemisinin **1** is thought to arise, as explained earlier, from the decomposition of some of the unreacted hydroperoxide intermediates, and the hydrogen peroxide produced during the formation of some by-products such as the γ-lactone **37**. At higher temperatures, which favour the thermal oxidation of the enol intermediate, more Artemisinin **1** is produced, indicating that the best condition for optimal yield of the δ-lactone is at a temperature of 10 °C.



*Scheme 62: conversion of DHAA **3** to compound **33** instead of the δ-lactone initially reported by Jung et al.* [148]

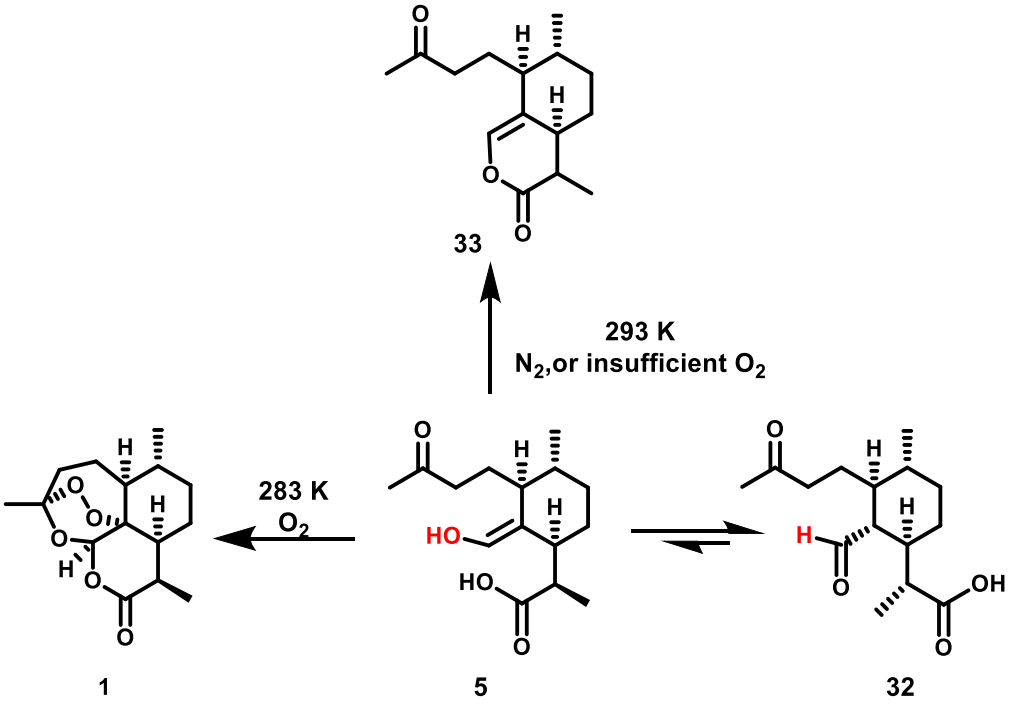
The synthesis of the δ-lactone **33** was previously reported during the conversion of **3** into deoxyartemisinin **35** reported by Jung *et al.,* [148] the process was accompanied by the formation of various intermediates and side products including the δ-lactone **33** with a yield up to 52 %. The lactone was reportedly obtained from the cyclisation of the keto aldehyde at room temperature in THF/H_2O solution and 70 % perchloric acid ().[148]

Although, Acton and Ruth were able to synthesize the δ-lactone **33**, only trace amounts of it have been isolated on treatment of the photo-oxidation product with TFA in petroleum ether, using air as an oxidant.[133, 135] Under limited amounts of triplet oxygen, **83** was produced and detected using infrared spectroscopic measurements, two carbonyl peaks were detected at 1756 and 1713 cm^{-1} for the δ-lactone **33** and keto groups respectively, as well as double bond absorption at 1676 cm^{-1}.[3]



*Scheme 62: conversion of DHAA **3** to δ-lactone **33**, and a ketone **83** as reported by Acton and Ruth.[133]*

Comparing what is reported in this Chapter with the work of Acton and Roth,[133] and Jung *et al.*[148] none of their work was able to achieve a high yield of the δ-lactone. The following sections describe the scale-up of its synthesis with the intention of having enough for the onward study of its reactivity and exploring its conversion to Artemisinin **1**.

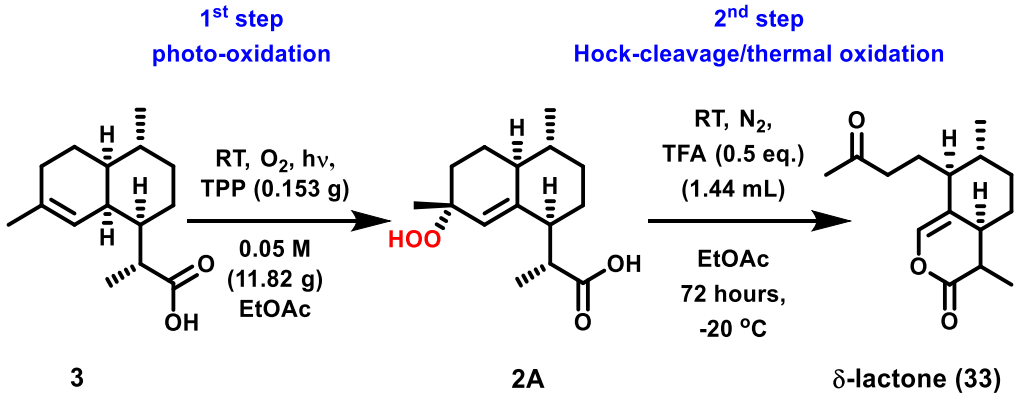


Scheme 63: transformations of an enol intermediate into various products, depending on the experimental condition.[157]

The scale-up of the synthesis of the δ-lactone **33** was performed by Dr Darren Lee using the Vortex reactor exploiting the conditions screened by myself in PhotoVap reactor. The process was achieved by initial photo-oxidation of DHAA **3**, in the Vortex reactor using TPP as photosensitiser in ethyl acetate Scheme 64, as described in the previous Chapter.

Proceeding with good selectivity of up to 90 % of the desired hydroperoxide **2A**, using the kilogram scale Vortex Reactor described in Chapter 1.

A solution of the photo-oxidation products was initially purged with N_2 for 20 minutes at – 20 °C, after which 0.5 equiv. of TFA was added while stirring the solution. The solution was left stirring for ca. 72 hours to reach full completion. The ^{1}H-NMR of the crude mixture using biphenyl as an internal standard showed the formation of 62 % of the δ-lactone **33**, and ca. 6.3 g of crude product was isolated; that is a 53 % isolated yield of the δ-lactone was obtained.



*Scheme 64: the scale-up for the synthesis of the δ-lactone **33**, in kg-scale Vortex reactor*

White flocculent crystals of the δ-lactone **33** were obtained by recrystallization from diethyl ether/*n*-heptane solution by drying out the solvent using a rotary evaporator.

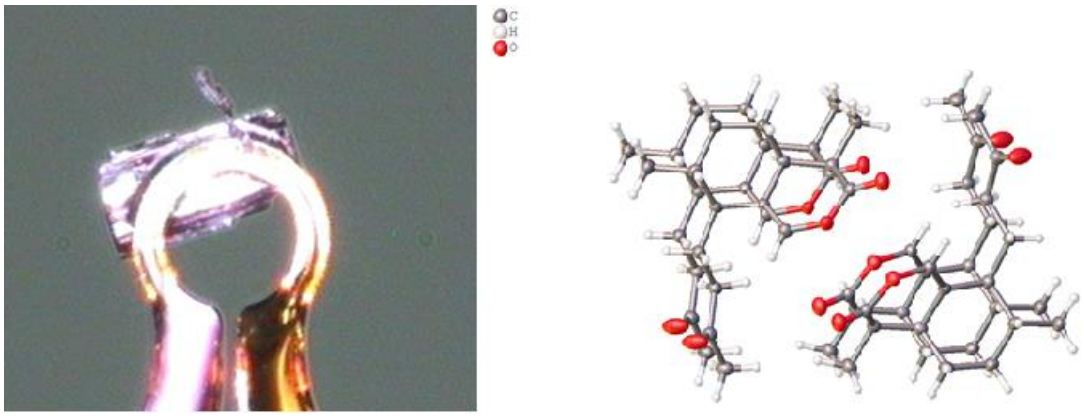
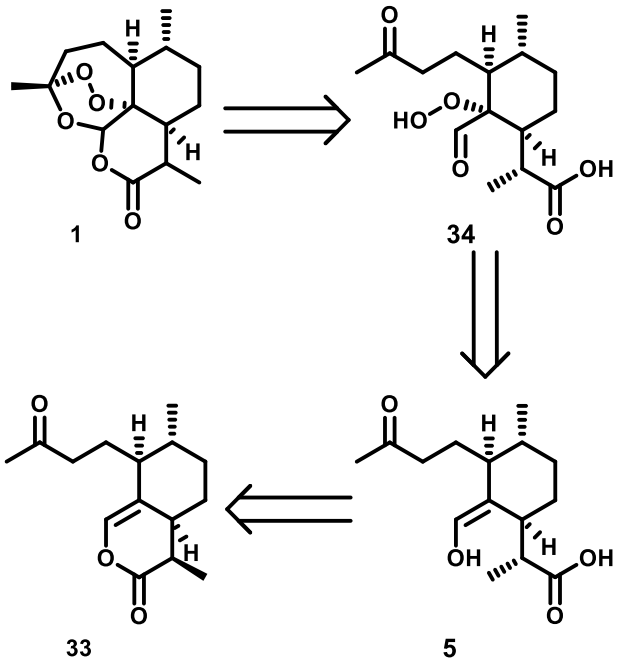


*Figure 31: Show the picture of the needles of δ-lactone **33** (left) and its ORTEP structure obtained for the first time.*

X – ray crystallography was performed by Dr Stephen Argent on the fine crystals obtained by dissolving the isolated powder in a vial of ethyl acetate, followed by careful addition of highly non-polar solvent *n*-hexane using a glass pipette. The mixture was left undisturbed for two days, after which very nice needle like crystals of the δ-lactone 33to formed, the ORTEP picture of the δ-lactone **33** crystal and picture of its needle is shown in (Figure 31). This is the first reported crystal structure of this compound.

SYNTHESIS OF ARTEMISININ FROM Δ-LACTONE

In principle, the synthesis of Artemisinin **1** from the δ-lactone **33** could be achieved through initial ring opening of the lactone ring under acidic conditions, to give the enol intermediate **5** in the absence of oxygen. Addition of oxygen gas would result in spontaneous thermal oxidation to hydroperoxyl aldehyde **34**, which could eventually cyclise to Artemisinin **1** (Scheme 65).



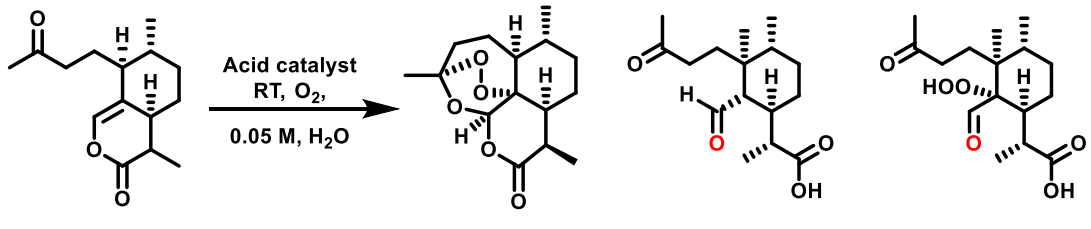
*Scheme 65: Retrosynthetic analysis of Artemisinin from the δ-lactone **33**.*

3.4.1. ACID CATALYSED HYDROLYSIS OF 6-MEMBERED LACTONE IN MEOH/H_2O SOLUTION

This section describes how the reactivity of the δ-lactone **33**, has been studied under different condition to find best route for its efficient conversion to Artemisinin **1**, with the aim of enhancing the yield from the current route, because the δ-lactone **33** has been considered one of the side products, responsible for a decrease in the yield and productivity of Artemisinin **1**.

The initial studies of the ring opening reaction of the δ-lactone **33** were carried out in a mixture of the highly polar solvents (MeOH and H_2O (1 equiv.)) and 0.5 equiv. of TFA. Under these conditions, the lactone ring opens, to regenerate the reactive enol intermediate **5** which can undergo thermal oxidation to **34** in the presence of molecular oxygen, to produce 15 % of Artemisinin **1** (Table 19, Entry 3).

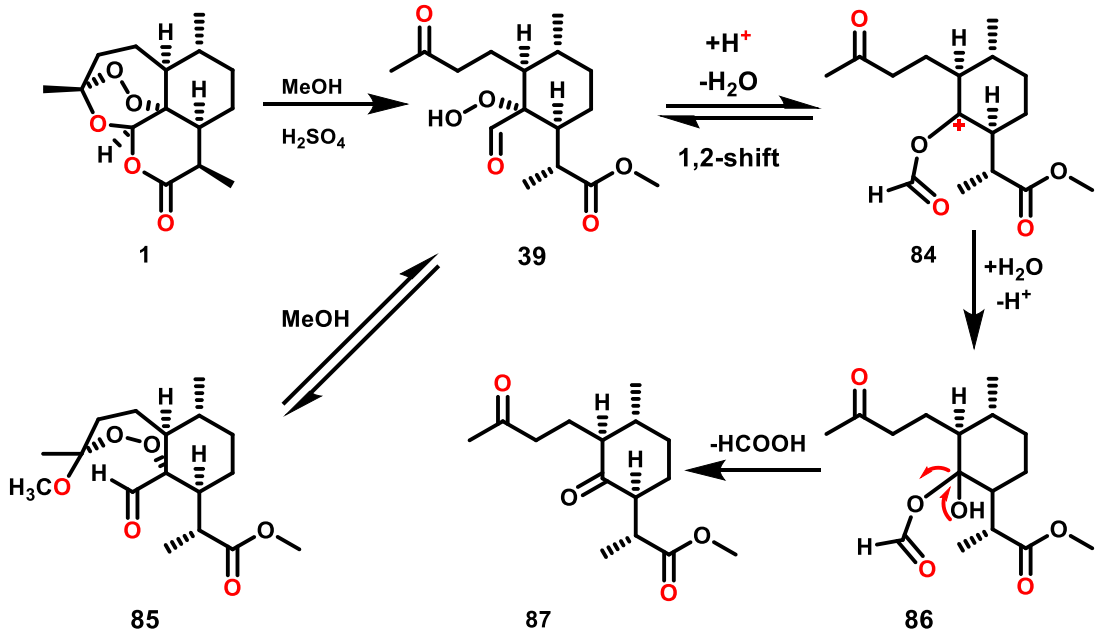
*Table 19: Results for the reactions of **33** under different conditions, of 0.5 eq. of TFA*



33 **1** **32** **peroxyaldehyde (34)**

Entry	Solvent	H_2O (equiv.)	Time (hour)	Aldehyde 32 (%)	Artemisinin (%)	34
1	EtOAc	0	24	0	0	0
2	DCM	0	24	0	0	0
3	MeOH	1.0	1	24	15	0
4	MeOH	1.0	48	9	0	17

Prolonged bubbling of oxygen up to 48 hours (Table 19, Entry 4) results in the decrease in its yield, due to further hydrolysis of the lactone ring in Artemisinin **1** leading to formation of 17 % of hydroperoxyaldehyde **34** (is identified from the aldehyde doublet at 9.93 ppm as reported by Singh *et al.*[189]) and possible polymerization of these hydrolysis products, and other side reactions.[2, 189] In both ethylacetate and DCM (Table 19, Entry 1 and 2), no reaction was observed even after 24 hours of bubbling of oxygen in the presence of TFA.



*Scheme 66: The acid catalysed degradation of Artemisinin **1** in Methanol.*[188]

The hydrolysis of the lactone ring may be responsible for the increased yield of hydroperoxyaldehyde **34**, with the disappearance of Artemisinin's proton-NMR chemical shift at 5.89 ppm (Scheme 66). This is not in line with our initial observation of the possibility of converting the δ-lactone **33** into **1** during prolonged bubbling of oxygen in ethyl acetate. So other factors may be responsible for the observed effect, because in ethylacetate solution of the δ-lactone **33**, in the presence of TFA no reaction has been observed (Table 19, Entry 1).

The acid catalysed degradation of Artemisinin **1** has been reported using methanol solution of sulfuric acid, involving the formation of a hydroperoxyaldehyde **39** in the presence of high concentration of acid. The aldehyde produced can either add MeOH to form a more stable endoperoxyaldehyde **85** (Scheme 66) or otherwise it undergoes 1,2-shft of an aldehyde group to the internal oxygen atom of a tertiary hydroperoxide **2A** intermediate, and loss of the second oxygen atom of the hydroperoxide group as water and 5-aldehyde group as formic acid to form stable ketoester **87**.[188, 190]

The acid catalysed hydrolysis of the δ-lactone **33** was also performed in deuterated chloroform solution with 1.0 equiv. of MeOH and 0.5 equiv. of TFA. The process was performed in an NMR tube with initial bubbling of oxygen, and the reaction was monitored by recording the proton-NMR spectra periodically. The results showed an increase in the yield of aldehyde **32**, from proton-NMR chemical shift, and a very limited yield of Artemisinin **1** (Figure 32).

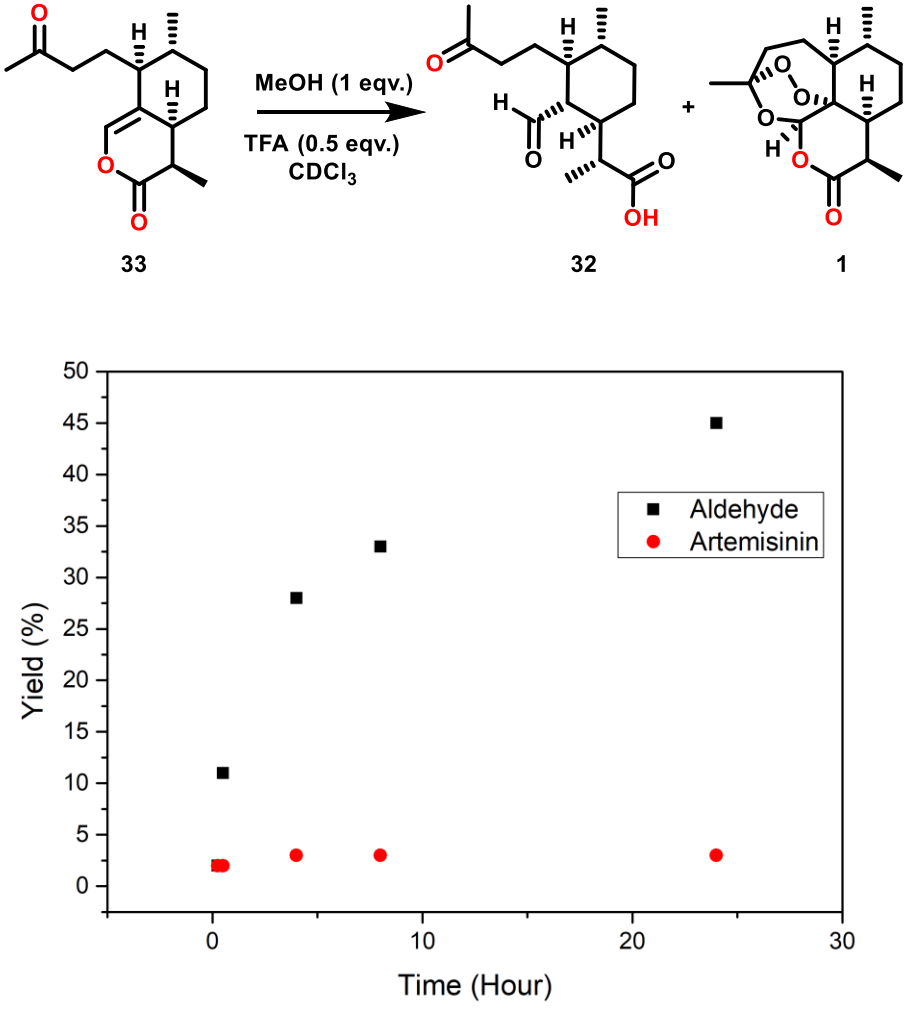


*Figure 32: the yield of aldehyde plotted against time of a deuterated chloroform solution of **33**, using 1.0 equiv. of MeOH and 0.5 equiv. of TFA at room temperature.*

The acid catalysed hydrolysis of the δ-lactone **33** in MeOH/H_2O solution appears to be ineffective for the synthesis of Artemisinin **1,** through hydrolysis of the lactone ring of the δ-lactone **33**. This is due to the limitation caused by the possible simultaneous ring

opening of the desired product **1** in the solution**.** To overcome this limitation, the reaction was carried out in a mixture of THF/H_2O, this is because of the influence of H_2O in the formation of **1** and the role of MeOH in opening the lactone ring of Artemisinin **1** in presence of acid, as discussed in the following section.

3.4.2. THE ACID CATALYSED HYDROLYSIS OF THE Δ-LACTONE IN THF/H_2O SOLUTION

The studies in THF-d_8:D_2O (60:40) solution of the δ-lactone **33** was performed in an NMR tube, the sample was initially purged with nitrogen gas, after which TFA was added, and the reaction was monitored through periodic ^{1}H-NMR measurements.

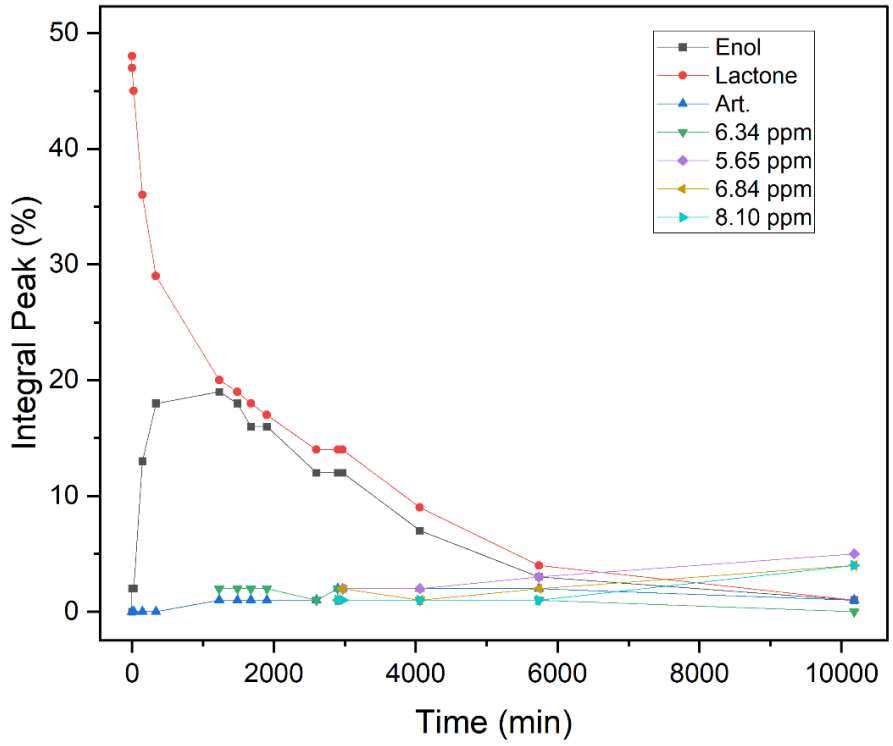


*Figure 33: follow up the degradation of the δ-lactone **33** into reactive enol intermediate in THF-d_8:D_2O solution*

The spectra show only one signal grew in 5 hours, which was assigned to the enol **5** with the concurrent degradation of the δ-lactone **33**, as observed by the corresponding decrease in its characteristic proton-NMR peak at 6.10 ppm. The solution was left for seven days with regular NMR monitoring. The peak due to reactive enol intermediate **5** began to decay, with the appearance of other side products peak including that of the γ-lactone **37** at 5.65 ppm and other unidentified side products peaks (Figure *33*), and very low yield of Artemisinin **1** has been obtained. This shows the total degradation of both δ-lactone **33** and the enol intermediate **5**, with no formation of any observable product, thus implying the possibility of involvement of δ-lactone **33** and the enol intermediate **5** in the polymerisation process as reported by Brown and Sy.[157]

Unlike in the mixture of MeOH/H_2O experiments where the δ-lactone **33** was initially converted into the more stable and relatively unreactive aldehyde **32** because enol-keto tautomerism favours its formation. In THF/H_2O, the lactone is converted into an enol intermediate **5**, showing a possible reverse of the equilibrium towards the enol intermediate **5**, which could then undergo thermal oxidation to Artemisinin **1**. Because of these observations the experiment was repeated in the presence of O_2, with the aim of converting the reactive enol **5** into Artemisinin **1**. Bubbling of oxygen into the solution for 1 hour resulted in the formation of Artemisinin **1**, as witnessed by the appearance of a peak at 5.89 ppm in the proton-NMR spectra. Prolonged bubbling of O_2 lead to complete decay of the δ-lactone's ^{1}H-NMR peak at 6.10 ppm and the increase of that of Artemisinin **1**, deoxyartemisinin **35** as well as several other multiplets. However, the other multiplets are thought to arise because of activation of the THF molecules by the enol intermediate, resulting to the formation of adduct, as shown in .

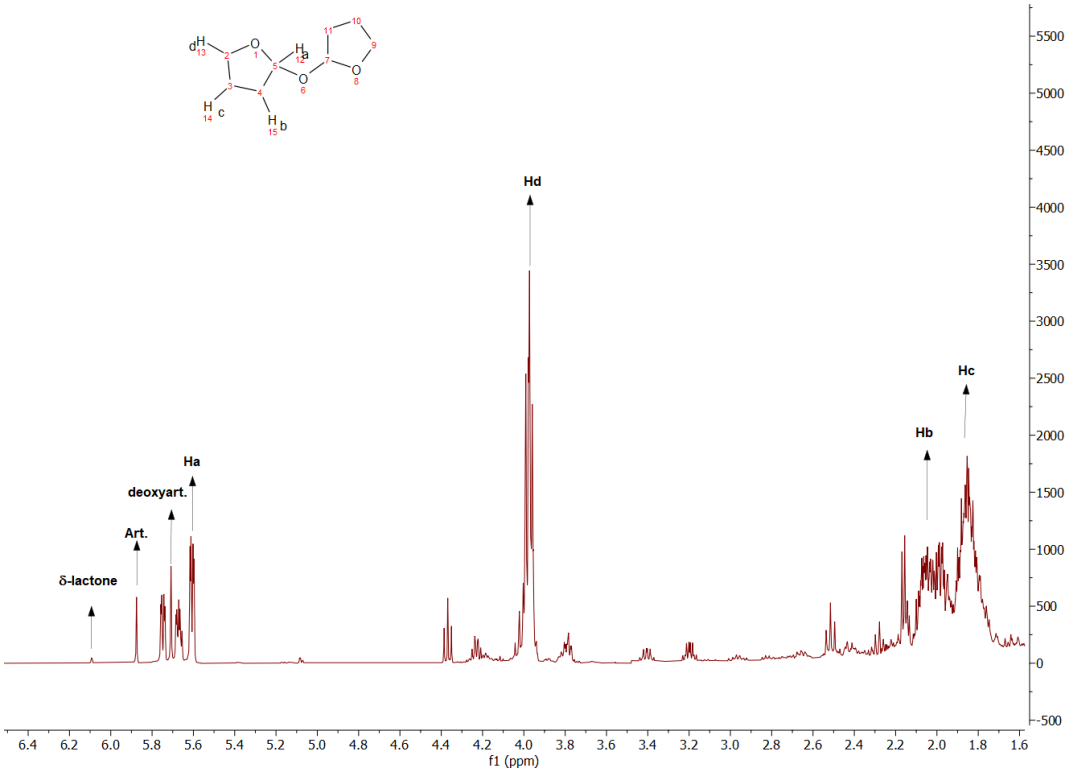
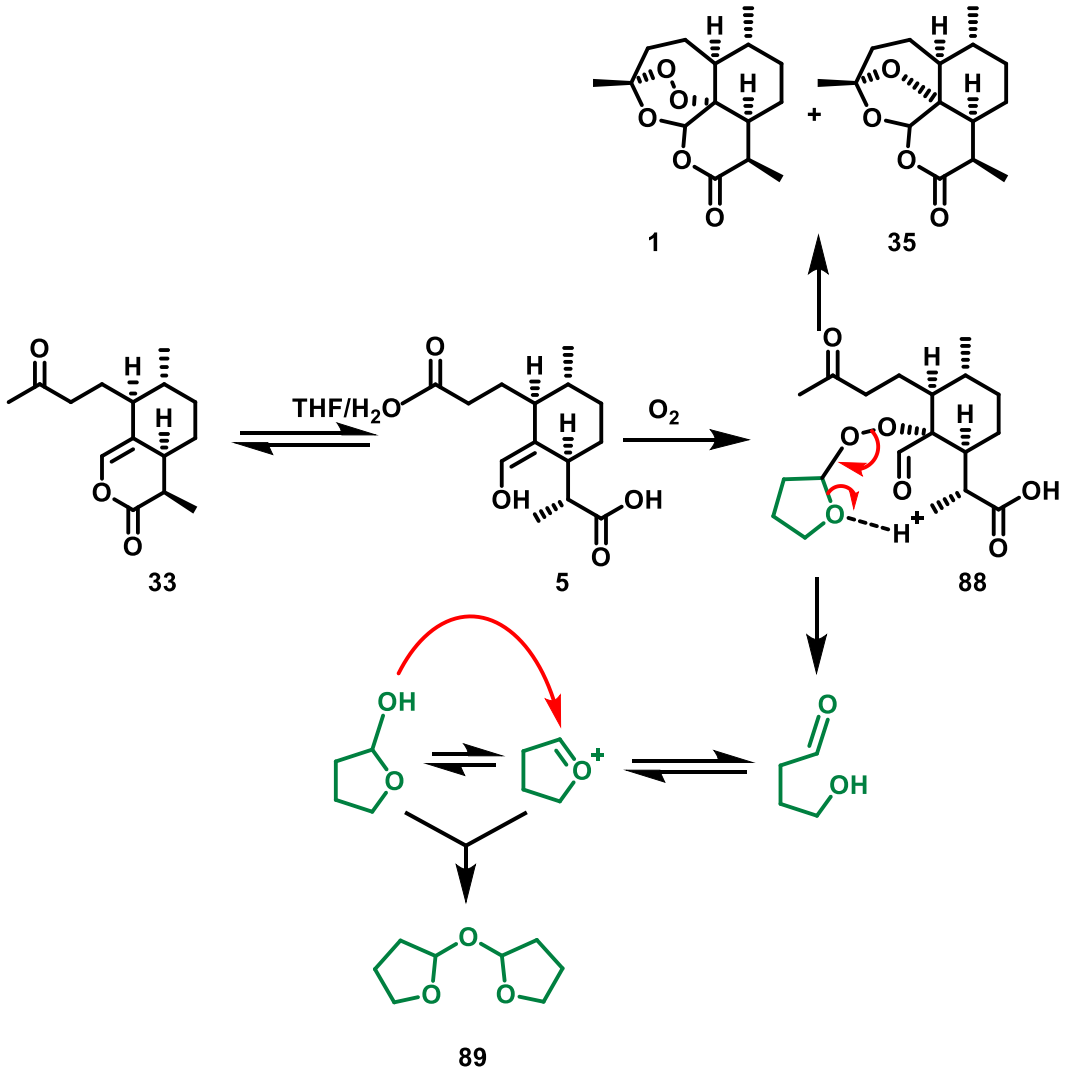


*Figure 34: the ^{1}H-NMR spectrum obtained from the studies of the reactivity of the δ-lactone **33** in THF/H_2O solution, after prolonged bubbling of oxygen gas at room temperature. Showing the formation of Art. = Artemisinin **1**, deoxyart. = deoxyartemisinin **35**, and the THF adduct as by-product.*

The δ-lactone **33** has been synthesised in ethylacetate by addition of TFA to the photo-oxidation products of DHAA **3** in absence of oxygen. The δ-lactone **33** was produced in 62 % yield as observed through quantitative proton-NMR, from its peak at 6.10 ppm using biphenyl as an internal standard. The isolated compound was subjected to different conditions to explore the possibility of opening the lactone ring back to the enol intermediate which can further undergo thermal oxidation to form Artemisinin **1**.

The acid catalysed hydrolysis in MeOH, using 0.5 equiv. of TFA resulted in the opening of the δ-lactone **33** ring, and its subsequent conversion to Artemisinin **1**. However, under the same conditions, the Artemisinin's lactone ring also opened to corresponding hydroperoxyl aldehyde **34**. In THF/H_2O experiments, the lactone was opened with the

formation of Artemisinin **1** and other side products believed to be THF adducts **89** (Scheme 67).



*Scheme 67: The proposed mechanism for the ring opening reaction of δ-lactone **33**, in THF/H_2O solution to enol intermediate **5**, which interact with THF in the presence of oxygen molecules to form both THF-adduct **89** and the thermal oxidation products **1** and **35**.*

The above studies have shown that the δ-lactone **33** can be converted into Artemisinin **1** through acid catalysed hydrolysis, but due to competing side reactions and the susceptibility of Artemisinin **1** to acid hydrolysis, the amount of Artemisinin produced is not significant enough to serve as an alternative route toward its synthesis. Therefore, the best alternative is to further optimize the route of Artemisinin **1** synthesis to minimize

the amount of the δ-lactone **33** and other side products produced, as this could maximized the amount of Artemisinin formed.

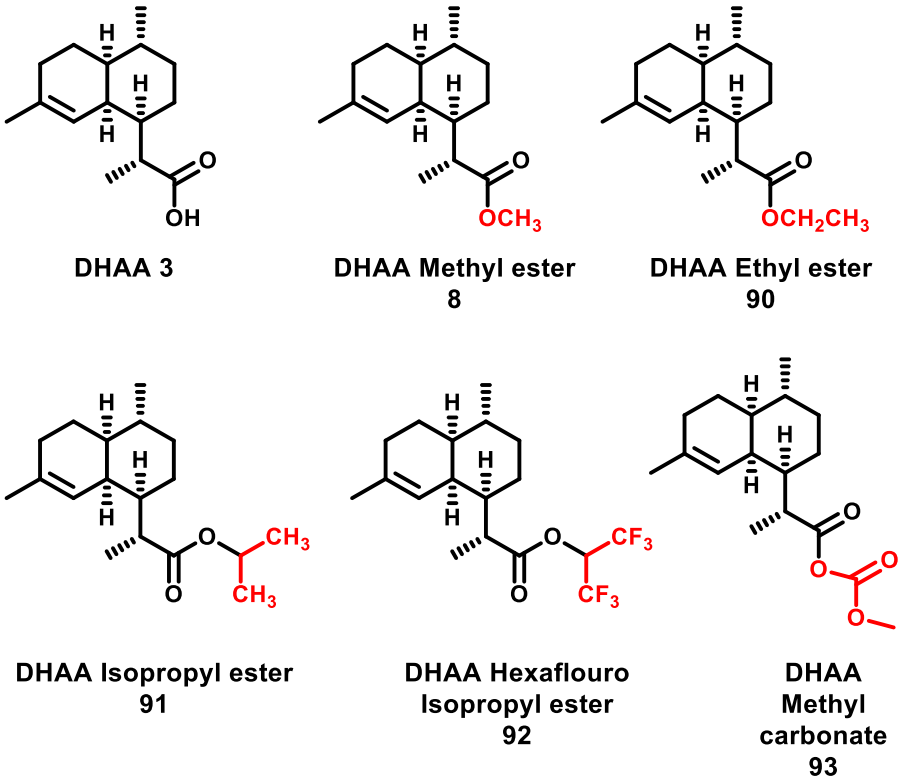


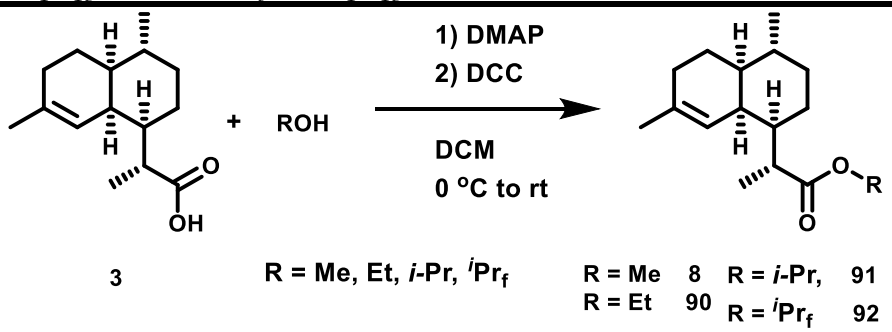
*Figure 35: Structures of DHAA **3** and its derivatives used for the synthesis of Artemisinin **1**.*

The well-known method of preventing the lactonization of carboxylic acids is derivatization to the corresponding ester and carbonates. [1, 3, 157] This method was employed by Sanofi for their industrial production of Artemisinin **1**. In the next sections, the synthesis, and application of various DHAA derivatives (Figure *35*) toward the semi-synthesis of Artemisinin **1** is described, with the aim of finding the best possible route of synthesising Artemisinin **1** in higher yield using the PhotoVap reactor.

SYNTHESIS OF DHAA DERIVATIVES AND THEIR APPLICATION IN THE SYNTHESIS OF ARTEMISININ

DHAA derivatives including esters; DHA Methyl, Ethyl, Isopropyl and Hexafluoroisopropyl esters, and carbonates; DHA Methyl and Ethyl carbonates, (Figure *35*). The ester derivatives were synthesised by treatment of the mixture of DHAA **3**, and the corresponding alcohol in DCM, with dicyclohexylcarbodiimide (DCC) and an acyl transfer agent dimethylaminopyridine (DMAP) at 0 °C to room temperature. The syntheses were performed by Dr Hamza Boufroura adapting the reported procedure[191] and the studies of their reactions were carried out by me.

*Table 20: The results for the synthesis of DHAA derivatives comprising of esters; DHA Methyl **8**, Ethyl **90**, Isopropyl **91** and Hexafluoroisopropyl **92** esters.*

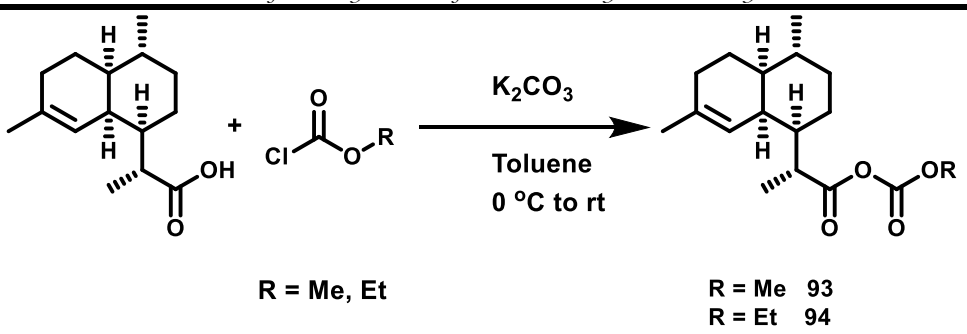


Entry	DHAA Derivatives	Yield (%)
1	Me	97
2	Et	95
3	*i*-Pr	92
4	*i*-Pr$_f$ (HFIP)	82

The results for the synthesis of DHAA ester derivatives, shown in the Table 20, indicate a decrease in the yield of the derivative with increase in the molecular weight of the alkyl group of the corresponding ester (Table 20, Entries 1 to 4). With the highest yield of 97 % obtained for the DHA methyl ester **8** derivative (Table 20, Entry 1). The DHAA carbonates derivatives, comprising of methyl **8**, and ethyl **90** derivatives were synthesised from the mixtures of DHAA and corresponding alkyl chloroformate derivative in toluene at 0 °C to room temperature.

The results in Table 20 show that, unlike for ester derivatives, the yield increases with increase in the molecular weight of the carbonate, with ethyl carbonate having a higher yield of 93 % compared to the methyl carbonate, 85 % yield (Table 21, Entries 1 and 2).

*Table 21: The results for the synthesis of DHA Methyl **8** and Ethyl **90** carbonates.*



Entry	DHAA Derivatives	Yield (%)
1	Me	85
2	Et	93

The results presented for the esterification of DHAA **3**, to the corresponding esters and carbonate derivatives, show that the process proceeds with very good selectivity and near quantitative yields. This is promising because of the potential of these derivatives in improving the yield and productivity of Artemisinin **1**, through possible prevention of the formation of lactone side products, according to the stated aims. These derivatives were then used for the synthesis of Artemisinin **1** in the PhotoVap reactor, following solubility screening as described in the next sections.

3.5.1. SOLUBILITY STUDY OF DHAA DERIVATIVES AT ROOM TEMPERATURE AND DIFFERENT CONCENTRATIONS IN ALCOHOL/WATER MIXTURES

The solubilities of DHAA methyl **93** and ethyl carbonate **94** derivatives were studied in different water/alcohol mixtures adapting the strategy employed for **3** as described in Chapter 2 and selecting the alcohols which showed promising dissolution of the solutes

3 with a large proportion of water mixture. The alcohols used include ethanol, *n*-PrOH, and *tert*-butanol at different concentrations of the substrate. For 0.05 M of DHAA methyl carbonate (DHAMC) **93**, the solubility has been studied in EtOH, PrOH and *tert*-butanol, in the aqueous mixtures of these solvents. The solvents mixture containing 30, 50 and 60 % water respectively, were found to dissolve DHAMC **93**.

The solubility of DHAMC **93** in aqueous solution decreased compared to that of **3** in the same solvent as described in Chapter 1. This could be attributed to the decreased polarity of the carbonate compared to the acidic DHAA **3**. For DHAA ethyl carbonate (DHAEC) **94** at both 0.05 and 0.5 M concentrations, there is uniform decrease in the solubility in all the solvents mixtures tested of the ethyl carbonate **94**. In *tert*-butanol DHAEC **94** is soluble in the solvent mixture with up to 50 % water, the solubility also decreased for n-propanol and ethanol solutions as the solute can only dissolved in the solvent with 30 and 20 % water respectively. For higher concentration of DHAEC **94,** there is decrease in the solubilities in the aqueous mixtures of three solvents, with *tert*-butanol having higher solubility at increased amount of water in the solution. The detailed results for the solubility of these derivatives are included in the appendix section of this Chapter.

3.5.2. DHAA DERIVATIVES AS PRECURSORS TO ARTEMISININ

The DHAA derivatives synthesised were then employed for the semi-synthesis of Artemisinin **1** in the PhotoVap reactor, with the aim of preventing the formation of side products, especially the lactones. The semi-synthetic approach using DHAA **3** has already been described in Chapter 2. While the reactivity of the DHAA **3** is governed by the carboxylic acid at 12 – position, its esters and carbonates used herein contain different leaving groups, the reactivity of each leaving group depends on the acidity of its conjugate acid; this factor determines the rate of the final cyclisation of their vicinal hydroperoxyl

aldehyde **34** into Artemisinin **1**, and formation of the corresponding alcohol by the leaving group.

3.5.2.1. THE SEMI-SYNTHESIS OF ARTEMISININ FROM THE DHAA DERIVATIVES: 2 STEP PROCESS

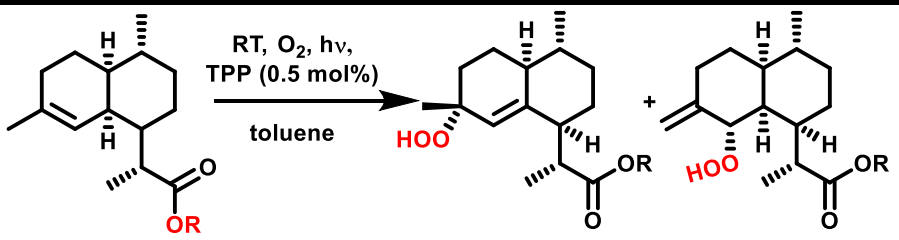
The 2-step approach to the synthesis of Artemisinin **1** using DHAA derivatives was performed in a similar way to that described in Chapter 2, i.e., by running the photo-oxidation semi-continuously in the PhotoVap reactor, while the acid catalysed Hock-cleavage/thermal oxidation step was subsequently performed by bubbling oxygen gas with the aid of balloon through the crude photo-oxidation products in a round bottom flask following the addition of an acid catalyst. Two DHAA derivatives namely, DHAMC **93** and DHAME **8** as representative carbonate and ester, were used for this process to further optimise the synthesis of Artemisinin **1**.

3.5.2.1.1. 1ST STEP: PHOTO-OXIDATION

The photo-oxidation was performed at room temperature (22 °C) in toluene, using TPP as the photosensitiser. When DHAMC **93** was used as the precursor, 90 % of the tertiary hydroperoxide **96A** was obtained after 5 minutes of irradiation, while only 2.5 min irradiation were needed when using DHAME **8** as the precursor to obtain 95 % of **95A** (Table 22, Entry 1 and 2).

The photo-oxidation of these derivatives proceed with very good yield and selectivity compared to what has been reported in the previous Chapter using DHAA as a precursor. 5 minutes irradiation of DHAEE **90** solution resulted in the formation 89 % yield of **96A**, and 9 % of the secondary hydroperoxide **96B**, under the same condition as the other derivatives. The improved selectivity of the tertiary hydroperoxide is promising, and that the second step might proceed with better selectivity and productivity of Artemisinin **1**.

Table 22: the photo-oxidation of DHAA derivatives in toluene at 22 °C, using 0.5 mol% of TPP as photosensitiser.



R = - CH_3 (DHA Methylester) 8 — 94A — 94B
R = -$OCOOCH_3$ (DHA Methyl carbonate) 93 — 95A — 95B
R = - CH_2CH_3 (DHA Ethylester) 90 — 96A — 96B

Entry	Starting Material	Time (min)	A Yield (%)	B Yield (%)
1	DHAMC **93**	5	90	9
2	DHAME **8**	2.5	95	3
3	DHAEE **90**	5	89	9

Unless specified otherwise, the reaction was conducted in semi-continuous mode using 5 mL of solution in a 1 L round-bottom flask rotating at 175 rpm with O_2 bubbling through the solution at 60 sccm (sccm = standard cubic centimetres per minute). Yields were calculated based on the relevant peaks in the ^1H NMR spectrum with reference to an internal standard (biphenyl), for all the yields calculated and all samples ran in triplicate.

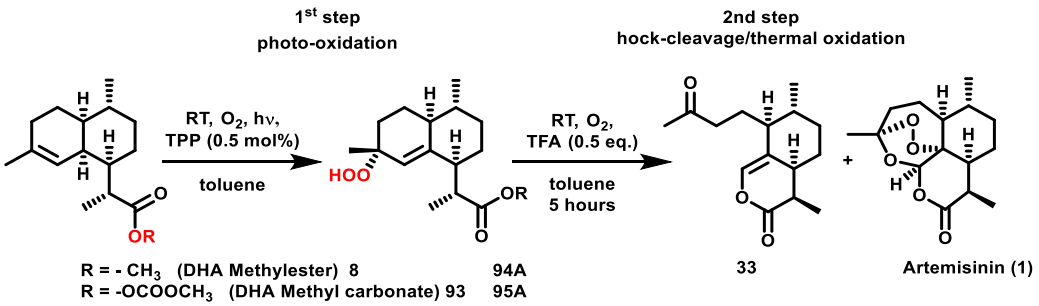
Another advantage achieved from the use of these derivatives is that the process was performed at room temperature, which is good because it would further reduce the production cost associated with cooling, compared to the use of DHAA **3**, where better yield of photo-oxidation product was often obtained at low temperature. The industrial production of Artemisinin **1** by Sanofi was achieved using activated DHA ethyl-carbonate in a batch reactor, but the process was performed as one-pot by addition of acid catalyst at the beginning of the process.[1] Burgard *et al.* reported the use of DHAA methyl **93** and ethyl **43** carbonates in the synthesis of Artemisinin **1**, through both 2-steps and one-pot but the yields of photo-oxidation products were not reported.[3]

3.5.2.1.2. 2ND STEP: HOCK CLEAVAGE / THERMAL OXIDATION

The crude products of the photo-oxidation were subjected to acid catalysed Hock-cleavage and thermal oxidation cascade without isolation of the desired tertiary hydroperoxide from the photo-oxidation products. Full conversion of the tertiary

hydroperoxide was achieved immediately after addition of acid catalyst to oxygen saturated solution.

*Table 23: Results for the acid catalysed Hock-cleavage/ thermal oxidation of the photo-oxidation products obtained from carbonate and methyl ester of DHAA **3**.*



Entry	Starting Material	Artemisinin 1 (%)	δ –lactone 33 (%)	enol 5 (%)	Productivity of Art. (g/day)
1	DHAMC **93**	13	54	11	0.04
2	DHAME **8**	21	34	5	0.07
3	DHAEE **90**	18	40	9	0.06

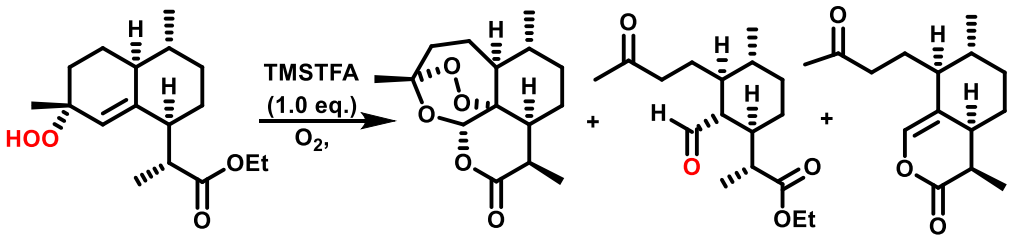
Unless specified otherwise, the reaction was conducted in semi-continuous mode using 5 mL of solution in a 1 L round-bottom flask rotating at 175 rpm with O_2 bubbling through the solution at 60 sccm (sccm = standard cubic centimetres per minute). Yields were calculated based on the relevant peaks in the ^{1}H NMR spectrum with reference to an internal standard (biphenyl), for all the yields calculated and all samples ran in triplicate. The productivity was calculated from [Conc.(starting material)*(vol.(mL)/1000/time(min))*1440*Molecular weight of Art.*Yield (%)].

The ^{1}H-NMR spectrum taken of the sample immediately show total disappearance of peak attributed to hydroperoxide and appearance of peaks attributed to Artemisinin **1**, the δ-lactone **33**, and enol intermediate **5** at 5.89, 6.10 and 5.32 ppm, respectively. When the mixture was left for some time longer under the same conditions, there was a slow but non-linear disappearance of the enol **5** and the δ-lactone **33**, with an increase in the percentage yield of Artemisinin **1**, as shown by the decay of their peaks and growth in that of Artemisinin **1**, and deoxyartemisinin **35**.

Although, good yields and selectivity were accomplished during the photo-oxidation from these DHAA derivatives, especially with DHAME **8** where 95 % of **94A** was obtained. The Artemisinin **1** yield is low compared what was obtained from DHAA **3**, and there was an unexpectedly high yield of the δ-lactone **33** of 54, 40 and 34 % for DHAMC **93**,

DHAEE **90**, and DHAME **8** respectively, (Table 23), based on the corresponding tertiary hydroperoxide in the crude products from photo-oxidation step.

*Table 24: the results for TMSTFA catalysed Hock-cleavage of the photo-oxidation products obtained from DHAEE **90**, after bubbling of oxygen gas for 0.5, 1.5, and 19 hours.*



96A **1** **98** **33**

Entry	Time (hours)	Enol (%)	6α-aldehyde 98 (%)	Artemisinin (%)	δ-lactone (%)	Productivity of Art.(g/day)
1	0.5	08	36	11	7	0.32
2	1.5	02	36	29	3	0.02
3	19.0	00	03	70	0	0.06

Unless specified otherwise, the reaction was conducted in semi-continuous mode using 5 mL of solution in a 1 L round-bottom flask rotating at 175 rpm with O_2 bubbling through the solution at 60 sccm (sccm = standard cubic centimetres per minute). Yields were calculated based on the relevant peaks in the ^1H NMR spectrum with reference to an internal standard (biphenyl), for all the yields calculated and all samples ran in triplicate. The productivity was calculated from [Conc.(starting material) *(vol.(mL)/1000/time(min))*1440*Molecular weight of Art.*Yield (%)].

Therefore, disappointingly, the use of these derivatives did not prevent the formation of the δ-lactone **33**, as stated earlier addition of acid catalysts converted all the tertiary hydroperoxide to the δ-lactone **33**, enol intermediate **5**, and prolonged bubbling of oxygen up to 5-hours did not increase the amount of Artemisinin **1**, even though all the enol **5**, and most of the δ-lactone **33** have been consumed. Because of the low yield of Artemisinin **1** and higher yield of the δ-lactone, the second step was performed using TMSTFA.

The aim of using TMSTFA as acid catalyst is to prevent the formation of lactone by-products, by introduction of bulky TMS as a protecting group to displace hydrogen atom of the tertiary hydroperoxide **96A**. Because the TMSTFA is a Lewis acid it can facilitate the Hock-cleavage process and its presence will hopefully prevent the attack of the proton on the proximal peroxide's oxygen, which can result in the loss of hydrogen peroxide and

trapping of the enol **5** by the carboxylic acid or ester group at the 12-position leading to the formation of the δ-lactone **33**.

The use of TMSTFA as the acid catalyst has been observed to result in the improved yield of Artemisinin **1**, as shown in Chapter 2, from two-steps approach using DHAA **3** as precursor. The results obtained by addition of 1.0 equiv. of TMSTFA to the photo-oxidation products of DHAEE **90** are presented in Table 24. Bubbling oxygen into the solution of photo-oxidation products for 30 minutes resulted in an 11% yield of Artemisinin **1**, with higher yield of up to 36 % of the 6α-aldehyde **98**, based on the amount of the tertiary hydroperoxide **96A** obtained from the photo-oxidation step. While for the enol **5** and the δ-lactone **33** the lower yields of 8 and 7 % respectively, were obtained (Table 24, Entry 1).

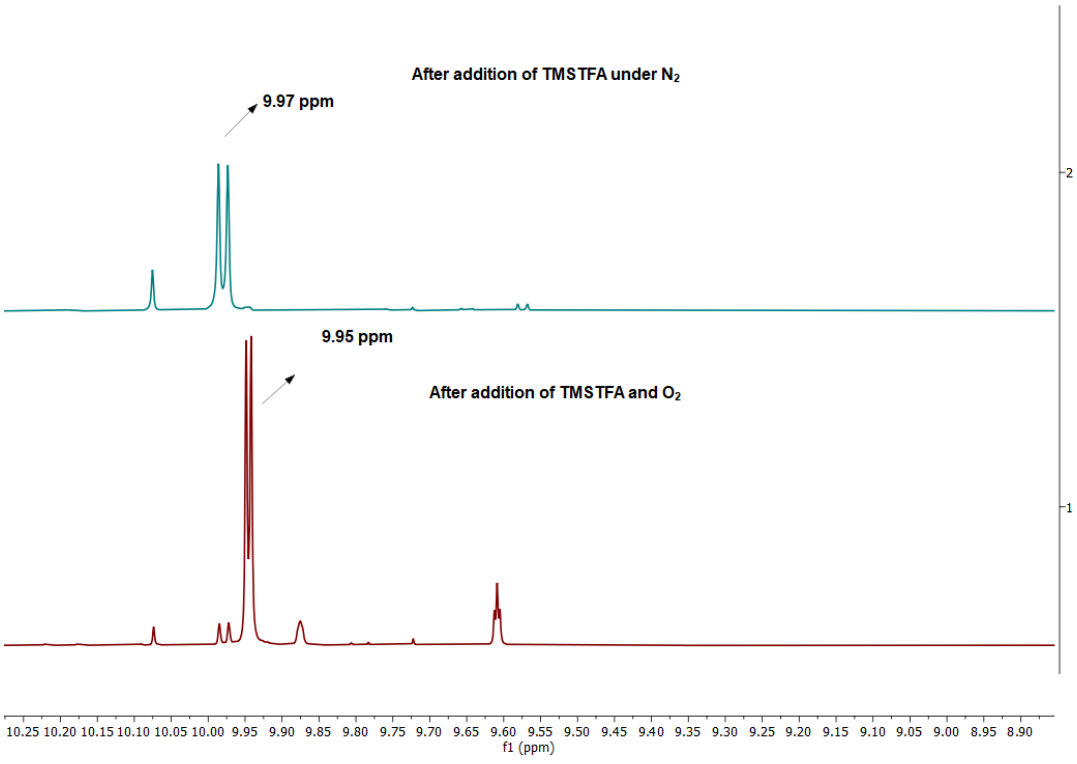


Figure 36: ^{1}H-NMR spectra comparing the aldehyde chemical shift obtained after addition of TMSTFA under N_2 and O_2.

Continued bubbling of oxygen for 90 minutes resulted in the decay of the proton-NMR chemical shift attributed to the enol-intermediate **5** and an increase in the yield of Artemisinin **1** up to 29 %, while the resonances of 6α-aldehyde **98** and the δ-lactone **33** do not decrease (Table 24, Entry 2).

Figure 36 shows the ^{1}H-NMR spectrum showing the changes in the percentage yield of Artemisinin **1** and other side products with bubbling of oxygen. However, prolonged bubbling of oxygen for 19-hours resulted in the total decay of proton-NMR chemical shifts characteristic of 6α-aldehyde **98** at 9.97 ppm and the δ-lactone **33** at 6.10 ppm, with an increase in the yield of Artemisinin **1** to 70 % (Table 24, Entry 3), based on the amount of tertiary hydroperoxide **96A** obtained from the photo-oxidation step. The 6α-aldehyde 98 was identified to be similar to that obtained from DHAA **3** as reported by Brown and Sy.[157] This yield of Artemisinin **1** (70%) was higher than the 62% obtained previously when DHAA **3** was used as the precursor and TMSTFA as the acid catalyst. However, the conversion DHAA **3** to Artemisinin was faster compared to DHAEE **90**, and 6α-aldehyde **98** was not produced from DHAA **3**, although there was very low yield of the δ-lactone **33**.

To further understand the mechanism of the TMSTFA action, the Hock-cleavage process was performed under N_2 gas with the aim of either trapping the enol intermediate **5** or the 6α-aldehyde **98** because, in the absence of oxygen, that could facilitate the subsequent thermal oxidation to Artemisinin **1**, and presence of bulky TMS could prevent the trapping of enol intermediate **5** to the δ-lactone **33**. After using Schlenk line for the initial removal of air from the photo-oxidation products generated from DHAEE **90**, addition of TMSTFA to the solution under N_2 gas and stirring for 19 hours, resulted in the formation of up to 40 % of the δ-lactone **33**, 22 % of an aldehyde **98** with the proton-NMR chemical shift at 9.97 ppm, which had not been reported, as shown in Figure *37*,

and 25 % Artemisinin **1**. The formation of Artemisinin **1** is unsurprising because it has been previously observed under N_2 during the synthesis of the δ-lactone **33** probably forming from the loss of the peroxide group in solution, possibly due the formation of lactone.

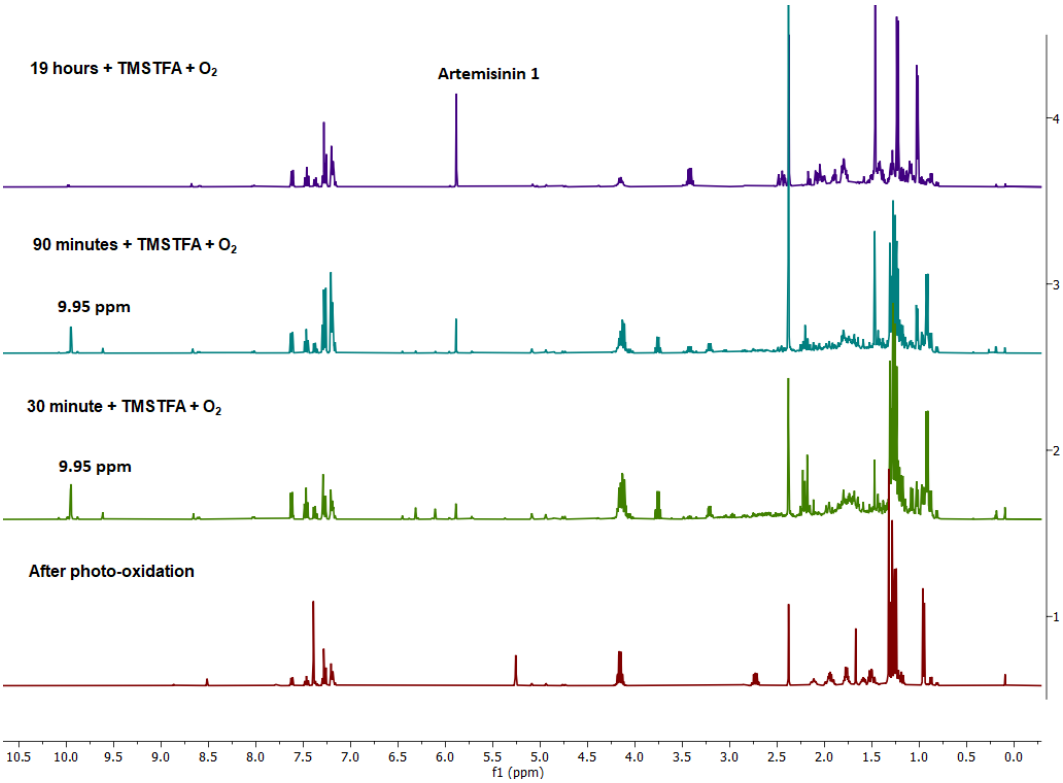


*Figure 37: the ^{1}H-NMR spectra for synthesis of Artemisinin **1** from DHAEE, using TMSTFA as acid catalyst. Showing the growth of Artemisinin **1** chemical shift with the decay of aldehyde's chemical shift at 9.95 ppm, with prolonged bubbling of oxygen.*

The results presented, show that the derivatisation technique does not prevent the formation of the δ-lactone **33**, but it has been effective in preventing the formation of the γ-lactone **37**, in most of the cases.

These results show that the use of TMSTFA can effectively prevent the formation of the γ-lactone **37**. It also influences the shift in the keto-enol tautomerization equilibrium to favour the more stable 6α-aldehyde **98**, than the reactive enol intermediate **5**, and prolonged bubbling of oxygen is assumed to reverse the position of the equilibrium by

continuous elimination of the reactive enol **5**, through thermal oxidation to Artemisinin **1**, which take place at slow rate.

These DHAMC **93**, DHAME **8** and DHAEE **90**, and other derivatives were then employed in the one-pot synthesis of Artemisinin **1** in the PhotoVap reactor under different conditions. To further optimize the use these derivatives in the synthesis of Artemisinin **1** and their potential in preventing the formation of these lactone side products, believed to be responsible in the reduction of the overall yield of Artemisinin **1**.

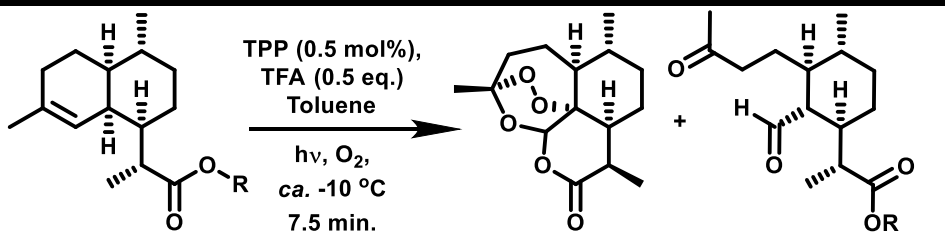
3.5.2.2. ONE-POT SYNTHESIS OF ARTEMISININ 1 USING DHAA DERIVATIVES.

Following the screening of DHAMC **93** and DHAME **8** for the synthesis of Artemisinin following a two-step approach in the PhotoVap reactor, the ester and methyl carbonate were screened under different temperatures observing their ability or otherwise to prevent the formation of side products, especially the δ-lactone **33** and the possible improvement in the yield and productivity of Artemisinin **1.** This could be achieved using DHAME **8**, DHAEE **90**, DHAIP **91**, and DHAHFIP **92**, (Figure *35*) with the aim of studying the influence of leaving group in the reactivity and ability of the given ester to delay the intramolecular esterification of the reactive enol intermediate **5**, before the addition of molecular oxygen, leading to the formation of the highly stable δ-lactone **33**, which cannot add oxygen necessary for the formation of trioxolane ring of Artemisinin **1**. The screening has been performed through one-pot process using TPP and TFA as photosensitiser and acid catalyst respectively at different temperatures in toluene.

Low temperature experiments were performed at -10 °C, for DHAME **8**, 61 % of **1** has been obtained after 7.5 min irradiation in the PhotoVap reactor, with the projected productivity of 8.0 g/day (Table 25, Entry 1). Interestingly, none of the lactone side

products were produced, suggesting that the ester group is efficient in esterification in delaying the transesterification with the enol intermediate **5** before thermal oxidation process. However, the yield of Artemisinin **1** is not significantly different from those obtained using DHAA **3** and described in the previous Chapter under similar conditions.

*Table 25: the results for synthesis of Artemisinin **1** using DHAA derivatives at low temperature.*



DHAA Derivatives
R = Me 8 *i*-Pr 91
R= Et 90 $^{i}Pr_f$ 92

Artemisinin (1)

Aldehydes
R = Me 99 *i*-Pr 101
R= Et 100 $^{i}Pr_f$ 102

Entry	SM	Aldehyde Yield (%)	Artemisinin 1 Yield (%)	Productivity (g/day)
1	DHAME	03	61	8.0
2	DHAEE	04	57	7.4
3	DHAIP	25	20	2.6
4	DHAHFIP	28	23	3.0

Unless specified otherwise, the reaction was conducted in semi-continuous mode using 5 mL of solution in a 1 L round-bottom flask rotating at 175 rpm with O_2 bubbling through the solution at 60 sccm (sccm = standard cubic centimetres per minute). Yields were calculated based on the relevant peaks in the ^{1}H NMR spectrum with reference to an internal standard (biphenyl), for all the yields calculated and all samples ran in triplicate. The productivity was calculated from [Conc. (starting material) *(vol.(mL)/1000/time(min))*1440*Molecular weight of Art.*Yield (%)]. TPP = Tetraphenyl porphyrin, Methyl carbonate (DHAMC **93**), Methyl ester (DHAME **8**), Ethyl ester (DHAEE **90**), Isopropyl ester (DHAIPE **91**) and Hexafluoro isopropyl ester (DHAHFIP **92**)

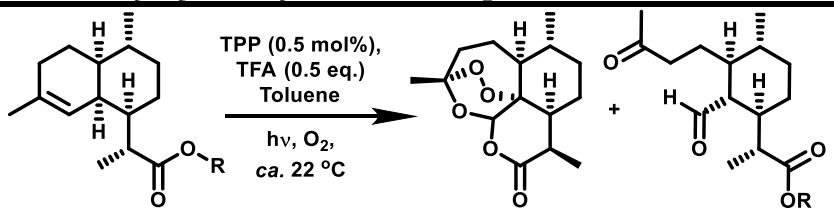
For DHAEE **90,** there is a decrease in the yield and productivity of Artemisinin 1 to 57 % and 7.4 g/day respectively, compared that of **8**. The decrease in the yield is accompanied by the formation of 4 % of a by-product which appears to be 6α-aldehyde **100** based on the chemical shift observed on the proton-NMR spectrum (Table 25, Entry 2). The formation of an aldehyde by-product can be explained as arising from tautomerism of the enol intermediate **5**, which is thought to reduce the amount of the enol intermediate **5** produced, and that of Artemisinin **1**, because the aldehyde is more stable than the enol **5,** and hence cannot easily undergo thermal oxidation process. The formation of 6α-aldehyde increased significantly when the DHAIP **91** and DHAHFIP **92**

were used as precursors under the same condition, with yields of 25 and 28 % of 6α-aldehydes **101** and **102** respectively, and corresponding decrease in the yield of Artemisinin **1** to 20 and 23 % respectively (Table 25, Entry 3 and 4).

The increase in the yield of the 6α-aldehyde, with decrease in the reactivity of the ester leaving group from methyl (DHAMC **93**) to isopropyl (DHAIP **91**), indicates that the reduction in the rate of intramolecular esterification of the esters. This might be because of an increased stability of the leaving group which results in the shift of the equilibrium of the keto-enol tautomerism to favour more stable 6α-aldehyde, which causes drastic reduction in the rate of thermal oxidation, with accompanied by higher yield of 6α-aldehyde.

When the synthesis was performed at 22 °C, the yield and productivity of Artemisinin **1** were relatively similar for DHAME **8** compared to the low temperature experiment, with 63 % yield of **1** (Table 26, Entry 1). For DHAEE **90**, the increase in temperature has negatively affected the yield and productivity with only 42 % of **1** produced and accompanied with an increase in the yield of the 6α-aldehyde **100** to 9 %.

Table 26: the results for synthesis of Artemisinin using DHAA derivatives at room temperature.

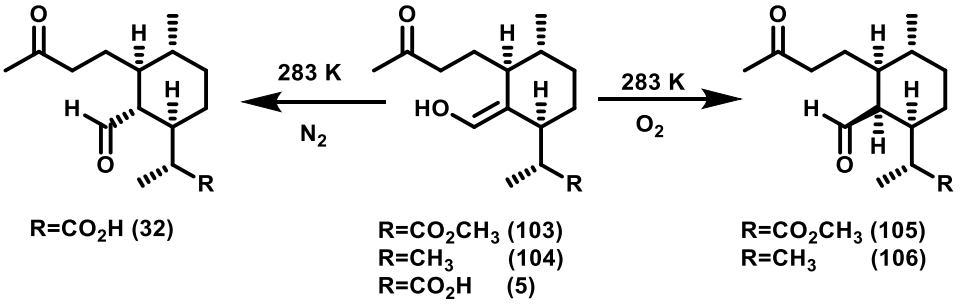


Entry	Starting Material	Time (min..)	Aldehyde yield (%)	Artemisinin Yield (%)	Productivity (g/day)
1	DHAME	7.5	03	63	8.2
2	DHAEE	7.5	09	42	5.5
3	DHAIP	5.0	37	22	4.2
4	DHAHFIP	7.5	33	17	2.2

Yields were calculated based on the relevant peaks in the ^{1}H NMR spectrum with reference to an internal standard (biphenyl), for all the yields calculated in this work and all samples ran in triplicate. The productivity was calculated from [Conc. (starting material) *(vol.(mL)/1000/time(min))*1440*Molecular weight of Art.*Yield (%)]. TPP = Tetraphenyl porphyrin, Methyl carbonate (DHAMC **93**), Methyl ester (DHAME **8**), Ethyl ester (DHAEE **90**), Isopropyl ester (DHAIPE **91**) and Hexafluoro isopropyl ester (DHAHFIP **92**)

Moreover, for DHAIP **91** and DHAHFIP **92**, the yield of **1** decreased with an increase in the yield of the aldehyde to 37 and 33 % respectively, (Table 26, Entry 3 and 4).

The pK_a of the conjugate acid each of ester can be taken as a measure of the leaving ability of these leaving groups based on their basicity. Thus, for methyl-, ethyl-, and isopropyl esters the pK_a are 15.20, 15.50 and 15.70 respectively, indicating an increase in basicity from methyl to isopropyl ester.



*Scheme 68: the conversion of enols obtained from DHAA **3** and some derivatives to different aldehydes under atmosphere of N_2 gas.*

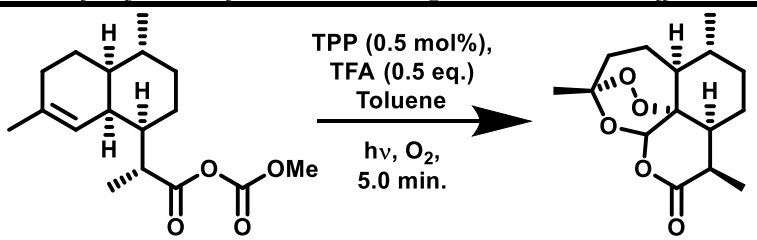
However, the HPIP ester has the lowest pK_a, 9.30, due to the increase in the electronegativity of the substituent, which could potentially improve the yield of Artemisinin 1, because of possible improvement in the leaving ability of the alkoxide group. The observed decrease in yield may be due to the steric effects hindering protonation of the carbonyl group, a condition necessary for the nucleophilic attack for the hydroxyl group of the enol **5**.

Brown *et al.* observed that, when the functional group at 12-position of DHAA **3** was replaced by $-CO_2CH_3$ or $-CH_3$ and corresponding enols (**103** and **104**) were kept under O_2 and N_2 (Scheme 68).[106, 157] In the presence of oxygen, the enols from **103 (R = CO_2CH_3)** or **104 (R = CH_3)** preferentially underwent tautomerization to 6β-aldehydes **105** and **106** respectively. This competes with the oxygenation to vicinal hydroperoxyl aldehyde, which was observed for the enol obtained from DHAA **3** that undergoes

spontaneous auto-oxidation to produce predominantly Artemisinin **1**.[106] Under N_2 different aldehyde (6α-aldehyde **32**) was obtained when the corresponding enol from DHAA **3** was treated under the same conditions.[106] The authors suggested that these differences in the kind of aldehyde arose because of intramolecular proton transfer from the 12-CO_2H of the DHAA **3** to the 6-position of the enol restricted to the α-face of the molecule considering its geometry. For the **103 (R = CO_2CH_3)** or **104 (R = CH_3)**, intermolecular transfer of proton occurs from the organic acid in the reaction medium to the less sterically hindered 6β-position of the molecule.[157]

Using DHAMC **93,** the process was optimized by changing the temperature from room temperature to -10 °C, while maintaining the same concentrations of starting material, acid and photocatalyst, At c*a.* 6 °C the highest yields of 66 % of **1** was obtained after full conversion, running the process at higher and lower temperatures of 22 °C and *ca.* -10 °C respectively, similar yields of *ca.* 60 % of **1** were obtained (Table 27, Entry 1), which implies that using DHAMC **93** the best condition for the synthesis of Artemisinin **1** is at the intermediate temperature of 6 °C using toluene as a solvent.

*Table 27: Results for synthesis of Artemisinin using DHAMC **93** at different temperatures*



DHAMC (93) 1

Entry	Temp. (°C)	Artemisinin Yield (%)	Productivity (g/day)
1	22	60	11.5
2	6	66	12.7
3	-10	59	11.3

Yields were calculated based on the relevant peaks in the ^{1}H NMR spectrum with reference to an internal standard (biphenyl), for all the yields calculated in this work and all samples ran in triplicate. The productivity was calculated from [Conc. (DHAA)*(vol.(mL)/1000/time(min))*1440*Molecular weight of Art.*Yield (%)]. TPP = Tetraphenyl porphyrin.

The better yield and productivity of **1** from DHAMC **93**, may be due to its ability to prevent the formation of both lactone and aldehyde side product, due its increased reactivity compared to the esters derivatives, and results in an increase in the productivity of Artemisinin **1**, up to nearly 13 g/day. (Table 27, Entry 2). The results presented for the yields of 6α-aldehyde obtained from esters and carbonate are plotted in Figure 38, it compares the yield of **32** against the all the derivatives, it shows no formation of the 6α-aldehyde from DHAMC **93**, for DHAME **8** only low yield of the aldehyde was obtained. The highest yield an aldehyde has been realised form DHAIP **91** give the highest yield of 36 % 22 °C.

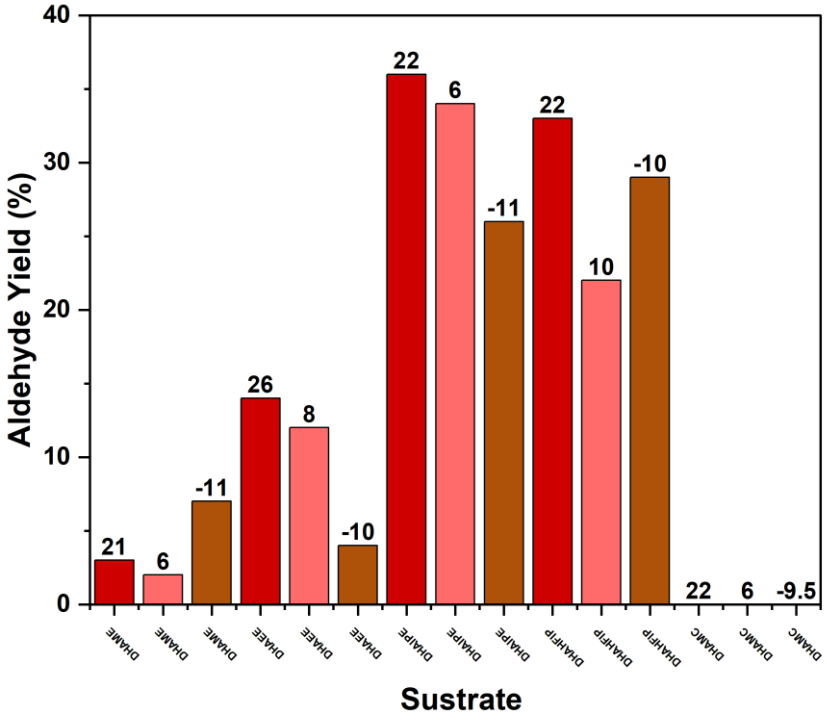


*Figure 38: Comparing the yield of 6α-aldehyde from different DHAA derivatives at different temperatures (°C) (the temperatures are shown at the top of each bar), for DHAA derivatives that include Methyl carbonate (DHAMC **93**), Methyl ester (DHAME **8**), Ethyl ester (DHAEE **90**), Isopropyl ester (DHAIPE **91**) and Hexafluoro isopropyl ester (DHAHFIP **92**)*

SUMMARY OF THE CHAPTER

Our primary aim has been achieved, namely using these esters in preventing the formation of lactone side products believed to be one of the reasons for the decreased yield of **1** was achieved. Although an unexpectedly high yield of aldehyde **32** was obtained from some of the esters, the methyl ester and carbonate performed well by preventing the formation of lactones, very low yield of aldehyde **32** (Figure 38), with improved yield of **1** at moderate temperature. For methyl carbonate, a high yield of **1** has been recorded, with no production of aldehyde under all the conditions, showing that carbonates tend to behave in similar way as DHAA **3**, with both producing similar yield of **1**.

In accordance with the stated aims, most of the side products responsible for a reduction in the overall yield, selectivity, and productivity of Artemisinin 1, are obtained during and after the acid catalysed Hock-cleavage process, largely arise from reactive nature of the enol intermediate. These side products include the aldehyde **32**, the γ- and δ-lactones (**37** and **33**), deoxyartemisinin **35**, polymers and unidentified oligomers.

The δ-lactone **33** has been synthesized, isolated and its crystal information have been reported for the first time. The reactivity of the isolated compound has been studied under various conditions to explore the possibility of opening its ring back to the enol intermediate, which could then undergo thermal oxidation to Artemisinin **1**. The acid catalysed hydrolysis in MeOH, using 0.5 equiv. of TFA resulted in the opening of the δ-lactone **33** ring, and subsequent conversion to Artemisinin **1**. However, under the reaction conditions, the Artemisinin's lactone ring has also been opened to the corresponding hydroperoxyl aldehyde. In experiments with THF/H_2O, the lactone ring was opened with the formation of Artemisinin **1** and other side products believed to be THF adducts. The studies of the δ-lactone **33** reactivity show that although the compound has been

converted to Artemisinin **1**, the yield and productivity of Artemisinin **1** through this route could not compete with its current route from DHAA **3**, especially one-pot strategy. Therefore, the best option is to explore further and optimize the possible ways of preventing its formation, through the well-known derivatization to DHAA esters and carbonates.

Various esters and carbonates have been synthesized, these include DHAME **8**, DHAEE **90**, DHAIPE **91**, DHAMC **93**, and DHAEC **94**. The process was optimized, and isolated esters and carbonates have been employed in the synthesis of Artemisinin through one-pot and two-step processes. The results show an improved yield of Artemisinin **1** using DHAMC **93** and DHAME **8** as precursors. A decrease in yield encountered with other esters is probably due to steric effects, which enable the tautomerization of the enol intermediate **5** to favour the keto-form, resulting in the formation of higher yields of the aldehyde **32** (Figure 38)**,** and a decrease in the yield of Artemisinin **1**.

For the two-step approach, the initial photo-oxidation of DHAME **8** and DHAMC **93** proceeded with good yield of the tertiary hydroperoxide at room temperature, better than what was achieved from DHAA **3** at lower temperatures, but the second step of the process has led to low yields of Artemisinin **1** and relative higher yield of side products, especially the δ-lactone **33**. However, the δ-lactone's proton-NMR chemical shift decayed with a nonlinear growth of the peak due to **1** after prolong bubbling of oxygen gas.

These observations show that, while derivatisation could serve as a technique for preventing lactonisation of carboxylic acid due to intramolecular esterification processes, an appropriate choice of the leaving group and further optimisation of various condition, employing one-pot strategy in the PhotoVap reactor could provide the best route for the sustainable production of Artemisinin **1**.

CHAPTER 4: CONCLUSIONS AND FURTHER WORK

In the chapter **1** the aims of the thesis have been stated as to identify the best possible starting material and the most productive conditions for converting various starting materials to Artemisinin **1** using PhotoVap reactor. By identifying the various side-products responsible for the decrease in the overall yield of **1** and explore their reactivities and possible method of preventing their formation. To achieve the stated aims the following four objectives were put forward:

(i) To optimise the semi-synthesis of Artemisinin **1** in both a sequential two-step and one-pot approach using the PhotoVap reactor. Moreover, the use of a previously reported silica immobilised photo-catalyst will be studied in the one-pot approach.

(ii) To determine the solubilities of the starting materials, and the photosensitisers, at different temperatures and concentrations in different solvent that will allow us to optimise of the onward semi-synthesis of Artemisinin, in aqueous solvents using the PhotoVap reactor.

(iii) To explore and exploit the use of a photosensitiser-biphenyl system through a redox mediation process to produce peroxides and to measure the effects that this will have on the formation of Artemisinin **1**.

(iv) To study the yield of various side products of thermal oxidation step of Artemisinin **1** synthesis and identify best condition for their formation in higher yield. Explore the possible method of isolation and studying their reactivity under various conditions and identify possible ways of preventing their formation or possible conversion to other important intermediates that can be converted to Artemisinin **1**.

CONCLUSIONS

1. The objectives 1, 2 and 3, were put forward toward the optimisation of the semi-synthesis of Artemisinin **1** through both a sequential two-step and one-pot approach using the PhotoVap reactor, the strategies employed in achieving these objectives were presented and discussed in chapter 2 and following conclusions were drawn.

i) The synthesis of Artemisinin **1** in PhotoVap reactor has been accomplished at both low and room temperatures, with the observed improvement in the yield of the photo-oxidation products at low temperatures. Both two-step and one-pot approaches have been performed in the PhotoVap reactor at low temperature, with the highest yield of 75 % Artemisinin **1** recorded through one-pot process at -10 °C.

However, the control of temperature is one of the difficult tasks of running low temperature experiment in PhotoVap reactor. The cooling process involve the use of recirculating chiller for the water-cooled LEDs and the reactor's water bath used to cool the reaction flask, for low temperature experiments the bath is equipped with the immersion probe of a chiller which is set at the desired temperature of the process. despite the use of two-chillers the temperature is difficult to be optimised to a particular point, because of large surface area between the rotating flask and the cooling bath and recurring temperature build-up between runs, as shown in the Figure 39.

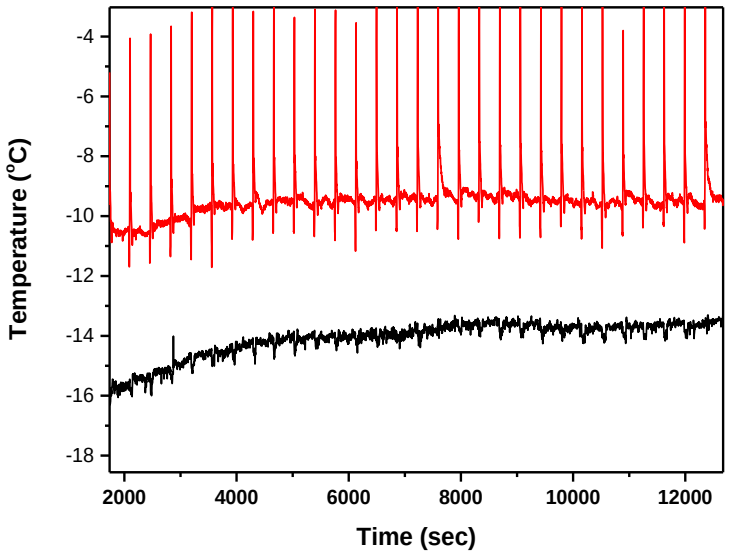


Figure 39: The change in temperature with LEDs irradiation during photolysis at low temperature. Red and black lines represent, solution and water bath temperatures respectively.

The temperature build-up was also encountered during room temperature experiments, which often result in the loss of volatile organic solvents, as described in chapter **2** for room temperature reaction in DCM. Another limiting factor is the high surface area to volume ratio of the PhotoVap flask and volume of the solution that could allow generation of thin film for photochemistry, which was optimised to be only 5 mL in a 1 L round bottom flask, this also contributed to the loss of volatile solvent especially during prolonged irradiation.

ii) The use of heterogenous catalyst system, made of $[Ru(bpy)_3]Cl_2$ supported on silica gel is practically very difficult or even impossible in PhotoVap reactor. Because in each batch large amount of silica is required to give the desired amount of catalyst needed for better productivity even at higher catalyst loading, compared to the volume of solution that could ensure generation of thin film for maximum light absorption. The semi-continuous process in PhotoVap reactor is practically

impossible because it is difficult to pump the slurry of silica-gel in and out of the reactor.

iii) The initial solubility screening allows the selection of aqueous ethanol and n-propanol (70:30 and 60:40 respectively) for the synthesis of Artemisinin **1** in PhotoVap reactor. However, the used of aqueous alcohols resulted in the lower overall yield of Artemisinin **1** for all the conditions screened.

iv) Biphenyl has been used throughout the studies as an internal standard for the determination of quantitative yield of Artemisinin **1** and other side products with reference to its ^{1}H-NMR chemical shift. Biphenyl has been used as internal standard because it does not react with any of the reaction mixture or products under the reaction condition. But evidence from the literature show that it can undergo electron transfer redox processes in the presence of suitable acceptor such as DCA at excited state.[21, 170] We described the effect of biphenyl in promoting photoinduced electron transfer oxidation process, in the presence of DCA, in which it can serve as co-catalyst or redox mediator

The highest inefficiency in the synthesis of Artemisinin **1** has been observed using aqueous solvent mixtures, especially during the auto-oxidation of enol intermediate **5** with the molecular oxygen (O_2).

2. The 4th objective has been put forward to study the yield of various side products of thermal oxidation step of Artemisinin **1** synthesis and identify best condition for their formation in higher yield. Also, to explore the possible method of isolation and studying the reactivities of these side products under various conditions and identify possible ways of preventing their formation or

possible conversion to other important intermediates that can be converted to Artemisinin **1**. The following conclusions were drawn.

i) The synthesis, isolation, and crystallisation of δ-lactone **33** allow the studies of its reactivity under different conditions with the aim of opening its ring and converting it to Artemisinin **1**. Various methods have been evaluated, one of which is the use of MeOH/H_2O mixture as the solvent, this led to the opening of the ring, but resulted in the production of limited amount of Artemisinin **1**. The limitation is due to subsequent ring opening of the lactone ring of Artemisinin **1** under the same condition. Because of this problem, it has been concluded that this side product cannot convert to Artemisinin **1** efficiently.

Various DHAA derivatives has been synthesised with the aim of improving the yield and productivity of Artemisinin **1** through prevention of the formation of Lactones. Among the derivatives studied only DHAME and DHAMC show promising yield of Artemisinin **1**, while for other derivatives studied higher yield of the aldehyde tautomer **32** has been observed through one-pot approach in PhotoVap reactor.

ii) This aldehyde **32** side product has been observed to decay during prolonged bubbling of oxygen at the second step (thermal oxidation) of the process, with the growth of Artemisinin **1**. Therefore, further optimisation is required through both one-pot and two-step approaches, to find the route with improved yield and productivity of Artemisinin **1**.

FURTHER WORK

The synthesis of Artemisinin **1** in PhotoVap reactor, discussed in this thesis described the contribution toward sustainable synthesis of Artemisinin **1**, using an accessible reactor. The results reported could be used for the optimisation of its synthesis using kilo-scale vortex reactor developed by this group. Based on the described results the following recommendations are made.

1. For easier and more efficient optimisation of the photochemical process in PhotoVap reactor, the temperature control system of the reactor needs to be enhanced. One of the proposed methods is through automatic control system in which the LEDs could be turned off during the emptying and filling of the reactor's flask after each run, which could prevent the temperature build-up between successive runs. And proper containment of the irradiation and cooling section of the reactor to prevent heating from the surrounding.
2. Because of the limitations described, for the synthesis of Artemisinin **1**, using silica-supported $[Ru(bpy)_3]^{2+}$, the heterogenous process can be optimised in a batch or fixed bed continuous flow set-up, to properly harness its potential benefit.
3. The use of $[Ru(bpy)_3](TFA)_2$ and TMSTFA as photosensitiser and acid catalyst respectively, should be explored further. For the former there is evident improvement in solubility of $[Ru(bpy)_3]^{2+}$ in the organic solvent such as DCM, compared to its chloride $[Ru(bpy)_3]Cl_2$, which will allow the photocatalytic ability of the photosensitiser to be studied in different organic solvents. Also, the photosensitiser could serve in preventing the possible generation of strong acid (HCl) in situ, which could lead to the possible degradation of the hydroperoxides and causing the decrease in the overall yield of the Artemisinin **1**. For the later (TMSTFA) the primary aim of its use was to introduce bulky TMS to the tertiary

hydroperoxide **2A** intermediate which could prevent the proximal protonation and formation of lactone side products, during Hock-cleavage process.

4. The use of TMSTFA was accompanied with the improvement in the yield of Artemisinin **1** during two-step process, which is surprising because in most of the results described herein for two-step process there is low yield and productivity of Artemisinin **1**. Therefore, there is need to further explore the use of TMSTFA for the synthesis of Artemisinin **1** through two-step approach.
5. Further exploration of the co-catalytic property of biphenyl is recommended, due to the observed potentials of improving the productivity of the synthesis of Artemisinin **1** through photo-redox catalysis, involving biphenyl this simple and less costly approach.
6. And it is likely that the rate of the auto-oxidation could be enhanced by exploring electron-transfer mechanisms through the generation of superoxide ($O_2^{\cdot-}$) promoted using biphenyl as redox mediator. Therefore, because of the potential benefits of using aqueous solution in the synthesis of Artemisinin **1**, the process should be explored further using different photosensitisers and the alcohol-water mixtures.

CHAPTER 5: EXPERIMENTAL

GENERAL ANALYTICAL METHODS

All the purchased chemicals and solvents were supplied from standard suppliers such as Sigma-Aldrich, Fischer Scientific or Fluorochem and were used as received without further purification. Oxygen gas cylinder was supplied by BOC.

5.1.1. NMR SPECTROSCOPIC ANALYSIS

The NMR spectra were obtained using a Bruker 400 MHZ or HD-400 MHZ spectrometer at the University of Nottingham NMR facility. The chemical shifts for protons were reported in parts per million (ppm), and all the samples were prepared at room temperature. The quantitative ^{1}H NMR yields were determined using biphenyl as an internal standard, and the values were calculated relative to residual ^{1}H nuclei in $CDCl_3$ (δ = 7.26, singlet) using Mestre Nova software. The multiplicity of signals was designated by the following abbreviations: (s) singlet; (bs) broad singlet; (d) doublet; (dd) doublet of doublets; (ddd) doublet of doublets of doublets; (dt) doublet of triplets; (t) triplet; (appt), apparent triplet; (td) triplet of doublets; (q) quartet; (qd) quartet of doublets; (qu) quintet; (hept) heptet; (heptd) heptet of doublets; and (m) multiplet. The 13C NMR spectra were recorded using the same NMR spectrometer with ^{1}H NMR decoupling, the chemical shifts were reported relative to ^{13}C nuclei in $CDCl_3$ (δ = 77.16) using Mestra Nova.

5.1.1.1 QUANTITATIVE PROTON-NMR MEASUREMENTS

The quantitative proton-NMR measurements were performed using biphenyl as an internal standard, with reference to its four equivalent protons. The calculations for the integral values were carried out through either of the following methods.

1. Addition of known percentage (10 or 100 %) of the biphenyl, with respect to the concentration of the starting material (DHAA or its derivatives) before the reaction. In this case the percentage yields of all the products, were computed based on the integral of the characteristic proton of the compound in question with reference to the four hydrogen atoms of the biphenyl.
2. Addition of the known mass (g) of the biphenyl to the sample, and the integral value of the internal standard (biphenyl) is calculated using the following relationship.

$$Integral\ value = \frac{number\ of\ protons\ of\ the\ internal\ standard}{\frac{moles\ of\ sample}{moles\ of\ the\ internal\ standard}}$$

- Level of error in the integration process

The integration of the peak area for the determination of concentration for each NMR spectrum was generally performed using MestreNova software for each of the peak of interest, using manual integration function of the software. As reported by Bharti and Roy,[192] to include 100% of the peak area, the integration should be extended to a region at least 20 times the peak width in both directions of the spectrum. This method is limited because of the possibility of resonances from the impurities such as carbonates, chlorides, salts, metal ions, phosphates, or moisture present in the sample.[192, 193] Because of these uncertainties the level of error of ±5 % is assumed to exist for each of the results reported herein.

5.1.1.2 Calculations of the productivity of Artemisinin

The projected Productivities of Artemisinin **1** in grams per day has been calculated from the percentage yield of Artemisinin **1**, as described by the following equation.

$$projected\ prodcutivity\ of\ Artemisinin\ (gday^{-1})$$

$$= \frac{DHAA\ Conc(molL^{-1}) * vol(L)}{time\ (min.)} * 1440\ (\text{min})$$

$$* Artemisinin\ yield\ (\%)$$

Yields were calculated based on the relevant peaks in the ^{1}H NMR spectrum with reference to an internal standard (biphenyl), for all the yields calculated and all samples ran in triplicate.

5.1.2. MASS SPECTROSCOPY AND X-RAY DIFFRACTION ANALYSIS

The mass spectrometry measurements were conducted using a Bruker MicroTOF mass spectrometer with electrospray ionisation (ESI-MS). Samples were prepared in acetonitrile. The X-ray diffraction (XRD) structure determinations were performed by Dr S. Argent at the University of Nottingham using an Agilent SuperNova Atlas S2 diffractometer.

5.1.3. UV-VISIBLE AND INFRA-RED ABSORPTION SPECTROSCOPY

The Ultraviolet-Visible (UV-vis) absorption spectra were recorded on the miniature Ocean Optics Flame-S-UV-VIS-ES spectrometer with a Deuterium-Halogen light source and GP400-2-SR fibres in a 1 cm quartz cuvette. The analyses were carried out using an OceanView software.

The FTIR Spectra were collected with a Nicolet™ Avatar 370 (Thermo Scientific™) FT-IR spectrometer, the spectrophotometer connected to a computer equipped with Thermo-Nicolet's OMNIC 7 software, set to an average of 32 scans per spectrum and resolution of 2 cm^{-1} each was spectrum monitored over the wavenumber range of 400-4000 cm^{-1}.

PHOTOVAP REACTOR SETUP

PhotoVap reactor; a modified rotary evaporator that can operate in both batch and semi continuous modes using a variety of different size flasks. Thin Polytetrafluoroethylene (PTFE) tubes thread through the neck of the rotating flasks to convey reactants in both gaseous and solution phase into and out of the reactor with the aid of peristaltic pumps as shown in Figure 12.

5.2.1 LIGHT SOURCE FOR PHOTOVAP REACTOR

The light source for the reactor is equipped with an Asynt water cooled LEDs having an electrical consumption of *ca.* 360 W (Figure 40), emitting high power polychromatic light of wavelengths between 400 – 800 nm, with two absorptions maximum at 456 and 595 nm measured at 100 % power output and distance of 13 cm from the lamp (Figure 40; left). The LEDs are located at the right hand of the water bath at approximately 13 cm from the rotating flask (Figure 40; right). The entire setup of the reactor is enclosed in a single fume hood, where the LEDs light can be fully contained by hood's walls and coloured Perspex sheeting, during irradiation process.

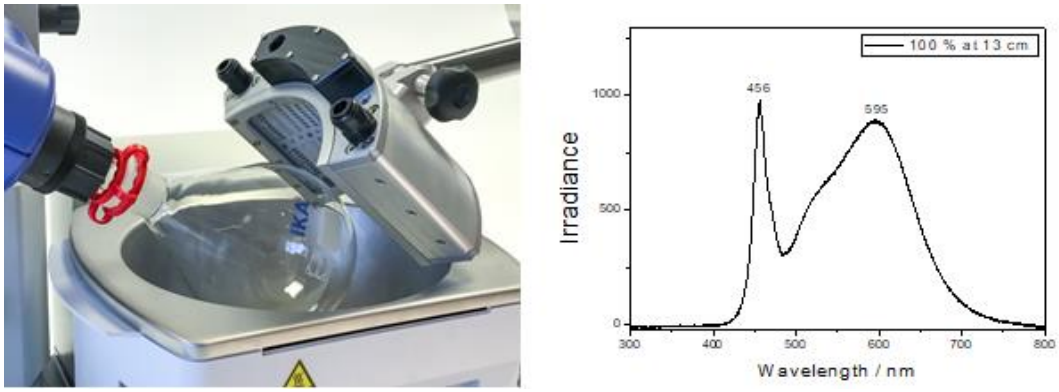


Figure 40: Right if the picture of Asynt water cooled LEDs showing how it's positioned during Irradiation. Left is its irradiance spectrum.

5.2.2 PHOTOVAP REACTOR STANDARD OPERATION PROCEDURE

The PhotoVap reactor is a modified IKA RV10-Control rotary evaporator fitted with the 1 L flask round-bottomed flask. The pumps used are Masterflex peristaltic pumps with PTFE tubing used throughout. Oxygen was dosed into the reaction flask using a Bronkhorst EL-Flow mass-flow controller set at a fixed rate of 60 sccm at a pressure of 1.015 bar. Automated PC control of the reactor was achieved via a control board, built at Nottingham, which uses an Arduino Uno microcontroller. All commands to the microcontroller were written and uploaded using Arduino 1.6.5. For low temperature reactions, cooling liquid consisting of 50 % ethylene glycol/water mixture has been used, and the mixture is cooled using RP100CD Chiller equipped with immersion probe, for each low temperature process the chiller is set to a given temperature and allowed to stabilise before irradiation.

5.2.3 GENERAL PROCEDURE FOR THE SEMI-CONTINUOUS PHOTO-CHEMICAL PROCESS IN PHOTOVAP REACTOR

- Switch-on the recirculating chiller for the PhotoVap LEDs set at 15 °C.
- Check the reactor's water bath to make sure 2/3 of the bath is filled with cooling liquid (depending on the temperature of the experiment), insert the cooled finger of the immersion well chiller into the bath, switch on the chiller and set to the temperature for the experiment. Allow the liquid in the water bath to reach at least 5 °C below the desired temperature, as recorded by the external thermocouple immersed into the reactor's bath.
- Connect the PhotoVap's round bottom flask and immerse it to the reactor's bath at the distance of 13 cm from the PhotoVap LEDs to allow maximum penetration of light to the solution in the flask (usually at the distance of 13 cm away from

the flask), and push the input, output and oxygen PTFE tubes, and the internal thermocouple, so that each can touch the lowest level of the flask.

- Switch on the reactor, the pumps, and PC containing the program settings for the Arduino and mass flow controller.

- Connect the USB cables for the Arduino control box and mass flow controller. Set the pumps at the specific flow rates for the input and output lines, open the flow dynamic data exchange (DDE) program and set the oxygen flow rate 60 sccm.

- Connect the bottle containing the solution to the input PTFE tube and the empty one to the output PTFE tube, each of which should be firmly held with clamp and wrapped with foil to prevent light penetration.

  Enclose the fume hood with the perplex sheeting, start the Arduino program, allow the temperature to equilibrate by monitoring both the internal and external thermocouples and finally switch-on the PhotoVap LEDs (100 % Power) to start the photochemical process.

SYNTHESIS OF ARTEMISININ IN PHOTOVAP REACTOR

The process was performed through either a two-step or a one-pot process as described in the previous Chapters, for the two-step process the initial photo-oxidation was performed in the PhotoVap reactor employing semi-continuous approach described in section 2.1.0, while the second step was carried out in a round bottom flask, by bubbling oxygen gas with the aid of a balloon.

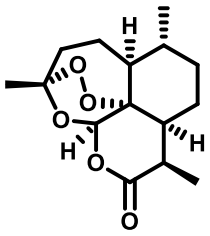
5.3.1 PHOTO-OXIDATION OF DHAA IN PHOTOVAP REACTOR

Synthesis of (2S)-2-((4R,4aS,7R)-7-hydroperoxy-4,7-dimethyl-1,2,3,4,4a,5,6,7 octahydronaphthalen-1-yl) propanoic acid **2A** from Dihydroartemisinic acid (DHAA). Different sequence of photo-oxidation experiments has been performed to optimise the process, in each case 50 mM of the DHAA and 10 % biphenyl, with varied concentrations of photosensitiser were dissolved in a given solvent, the solution was kept in an amber bottle to prevent the penetration of light before the process, the solution and oxygen gas were dosed into the reaction flask according to the procedure explained in section 2.1.0 using peristaltic pump and Bronkhorst EL-Flow, mass-flow controller set at a fixed rate of 60 sccm at a pressure of 1.015 bar, respectively. In all the experiments in the PhotoVap, a 1 L flask was used, rotating at 175 rpm and LEDs ran at 100 % power and cooled by a recirculating chiller kept at 15 ^{o}C. After each process three aliquots of 1 mL were collected and dried by using Nitrogen gas (N_2), the dried sample was dissolved in 0.7 mL of $CDCl_3$, and the resulting solution was submitted for ^{1}H NMR analysis. The percentage yield of the tertiary hydroperoxide was quantitatively determined from its ^{1}H-NMR chemical shift at 5.25 ppm using biphenyl as internal standard.

5.3.2 ACID CATALYSED HOCK-CLEAVAGE AND THERMAL OXIDATION

The DHAA **3** crude photo-oxidation products obtained following the experimental procedure described in Section 5.3.1, were transferred into round bottom flask with a stirrer bar, the flask was closed with Suba seal, after which oxygen gas bubbled into the solution with the aid of balloon for 5 minutes before addition of desired equivalent of the acid catalyst to the mixture while stirring, until the reaction is completed. After each process three aliquots of 1 mL were collected and dried by using N_2, and samples were dissolved in 0.7 mL of $CDCl_3$, and the resulting solution was submitted for ^{1}H NMR analysis. The percentage yield of Artemisinin **1** and other reaction products were

determined quantitatively from their respective ^{1}H-NMR chemical shifts by using biphenyl peak as internal standard.



Artemisinin **1** structure

^{1}H NMR (400 MHz, $CDCl_3$) 5.88 (s, 1H), 3.42 (dq, *J* = 6.9 Hz, 1H), 2.46 (td, *J* = 13.8, 3.9 Hz, 1H), 2.13 – 1.98 (m, 2H), 1.94 – 1.86 (m, 1H), 1.80 (dd, *J* = 12.3, 7.4 Hz, 2H), 1.56 – 1.37 (m, 3H), 1.46 (s, 3H), 1.23 (dd, *J* = 7.3, 1.4 Hz, 3H), 1.10 (q, *J* = 10.2 Hz, 2H), 1.02 (d, *J* = 5.6 Hz, 3H).

^{13}C NMR (101 MHz, $CDCl_3$) δ 172.60, 105.29, 93.71, 79.52, 50.11, 44.98, 37.57, 35.93, 33.61, 32.91, 25.24, 24.86, 23.41, 19.88, 12.62.

HRMS (ESI) m/z calculated [$C_{15}H_{22}O_5Na^+$] (M + Na^+) = 305.1359, found [$C_{15}H_{22}NaO_5$] (M + Na) = 305.1395

5.3.3 GENERAL PROCEDURE FOR THE ONE-POT SYNTHESIS OF ARTEMISININ IN PHOTOVAP REACTOR

The starting material, photosensitiser and 10 % biphenyl were dissolved in 50 mL of a given solvent, followed by the addition of the required amount of acid catalyst to the solution prepared in an amber bottle to avoid light penetration before irradiation, the solution and oxygen gas were dosed into the reaction flask according to the procedure explained in section 2.1.0 using peristaltic pump and Bronkhorst EL-Flow, mass-flow controller set at a fixed rate of 60 sccm at a pressure of 1.015 bar, respectively. In all the experiments done in the PhotoVap, a 1 L flask was used, rotating at 175 rpm and LEDs ran at 100 % power and cooled by a recirculating chiller kept at 15 °C. After each process

three aliquots of 1 mL were collected and dried using N_2, and samples were dissolved in 0.7 mL of $CDCl_3$, and the resulting solution was submitted for ^1H NMR analysis. The percentage yield of Artemisinin **1** and other products were determined quantitatively using biphenyl as internal standard, according to specific ^1H-NMR chemical shift.

5.3.4 OPTIMISING THE SYNTHESIS OF ARTEMISININ IN PHOTOVAP REACTOR

As explained in Chapter 2, the optimisation of the synthesis of Artemisinin **1** in PhotoVap reactor were performed through variation of different parameters such as temperature, nature of solvent, photosensitiser, and acid catalyst, employing either a two-step or one-pot approach in PhotoVap reactor, as explained in sections 2.2.1 and 2.2.3 respectively. These procedures were adopted during all the processes by simply varying the solvents, the concentrations of the reactants and conditions for the process.**SYNTHESIS OF $[Ru(bpy)_3](TFA)_2$**

$[Ru(bpy)_3](TFA)_2$ has been synthesised by slowly adding an aqueous solution of AgTFA (0.295 g, 1.34 mmol) to an aqueous solution of the $[Ru(bpy)_3]Cl_2$ (0.59 g, 0.67 mmol) in a 500 mL round bottom flask while stirring the solution, the compounds react in a 2:1 mole ratio according to the equation below.

$$[Ru(bpy)_3]Cl_{2(aq)} + 2AgTFA_{(aq)} \longrightarrow [Ru(bpy)_3](TFA)_{2(aq)} + 2AgCl_{2(aq)}$$

The resulting white precipitate of AgCl was removed by filtration, and the filtrate was concentrated in vacuo until the $[Ru(bpy)_3](TFA)_2$ crystals began to form. After which the solution was cooled to 0 °C to effect further crystallisation, the dark red crystals of $[Ru(bpy)_3](TFA)_2$ were washed with cold ether, dried in a suction pump, and dried in an oven at 60 °C. The resulting crystals were analysed using UV-Visible and ^{19}F NMR spectroscopy.

^{19}F NMR (376 MHz, D_2O) δ -75.59.

5.4.1 SYNTHESIS OF ARTEMISININ USING $[Ru(bpy)_3](TFA)_2$

The process was performed through in two-step process, with the initial photo-oxidation performed in the PhotoVap reactor as described in section 2.2.1, by dissolving (0.591 g, 5.0 mM) of DHAA **3** and (0.02 g, 0.025 mM) of $[Ru(bpy)_3](TFA)_2$ in 50 mL of toluene, the solution was connected to the reactor for the photo-oxidation after setting the temperature to – 10 °C, the photo-oxidation. The yield of the product was determined from its ^{1}H-NMR chemical shifts using biphenyl as an internal standard, by taking three aliquots of 1 mL each from the products, dried by using N_2, 0.1 mL of 10 % biphenyl in $CDCl_3$ and 0.6 mL of $CDCl_3$ were added, and the resulting solution was submitted for ^{1}H NMR analysis.

The acid catalysed reaction step was performed in the batch setup described in Section 5.3.2, by initial addition of (0.19 mL, 0.5 mM) of TFA. The solution was left stirring for 2 days, ^{1}H NMR spectrum were obtained from the sample, one taken immediately after addition of TFA in the oxygen saturated solution and another one after 2 days bubbling of oxygen. The yield of the products yield was determined from its ^{1}H-NMR using biphenyl as internal standard, using three aliquots of 1 mL collected and dried by using N_2, 0.1 mL of 10 % biphenyl in $CDCl_3$ and 0.6 mL of $CDCl_3$ were added, and the resulting solution was submitted for ^{1}H NMR analysis.

THE IMMOBILISATION OF $[Ru(bpy)_3]Cl_2$ CATALYST ON SILICA

The silica supported $[Ru(bpy)_3]Cl_2$ was prepared by the method reported by Tambosco et al. in which 2.5 mL ethanol/water (80:20) solution of $[Ru(bpy)_3]Cl_2$ (1 g/L) was added to a slurry of 1 g of silica in 47.5 mL of ethanol/water (80:20) at room temperature. The mixture was stirred for 2 hours at room temperature and then filtered, washed 3 times

with 15 mL ethanol/water (80:20), and the solid was dried in an oven at 60 °C overnight, the catalyst loading was determined as described elsewhere.

5.5.1 SYNTHESIS OF ARTEMISININ USING SILICA SUPPORTED CATALYST

The reactions using immobilised catalyst were performed in batch using PhotoVap reactor, each batch consist of 10 mL solution of DHAA (0.05 M) added in 1 L round bottom flask (of the reactor), after which 0.374 g of the immobilised catalyst of 2.5 mg/g was added and oxygen gas was bubbled for 2 minutes before light irradiation, the slurry was irradiated in the PhotoVap reactor for 15 minutes at 175 rpm to facilitate the photo-oxidation process. The yield of the products was determined from its ^{1}H-NMR using biphenyl as internal standard, and by collecting three aliquots of 1 mL collected and dried using N_2, 0.1 mL of 10 % biphenyl in $CDCl_3$ and 0.6 mL of $CDCl_3$ were added, and the resulting solution was submitted for ^{1}H NMR analysis.

The second step of the process was performed by continuous bubbling of oxygen gas to the crude photo-oxidation products in PhotoVap reactor for 2 hours under the same condition after switching off the PhotoVap LEDs, to facilitate the process, TFA is not added because the Hock-cleavage was reported elsewhere to be facilitated by the silanol group on the surface of the silica.

SOLUBILITY STUDIES OF DHAA IN AQUEOUS SOLUTION

5.6.1 SOLUBILITY STUDIES OF 50 AND 500 MM DHAA IN ALCOHOL/WATER SOLUTION AT ROOM TEMPERATURE

Different proportions of alcohol/water ranging from 100 % alcohol to 80 % water were used to test the solubility of DHAA **3** at room temperature. In all cases a specific amount of DHAA **3** (depending on the concentration) was dissolved in the organic component first and then water was added and mixed with a vortex mixer. The results were recorded

as; Not miscible = DHAA **3** soluble in the organic phase but water did not mix with the organic phase when added. Not Soluble = Precipitation of DHAA **3** upon addition of the water. Emulsion = Cloudy Emulsion formed upon addition of water. The alcohols tested are Methanol, Ethanol, Propanol, 1-Butanol, Isobutanol, 1-Pentanol, 1-Hexanol, *i*-Propanol, HFIP, 2-Butanol, 2-Heptanol, 2-Octanol, 4-Methyl-2-pentanol, *tert*-Butanol, Cyclopentanol, Cyclohexanol, 1,2-Propendiol, 1,3-Propendiol, and 1,5-Propendiol.

5.6.2 SCREENING OF THE SOLUBILITY OF DHAA AND PHOTOSENSITISER MIXTURES AT DIFFERENT TEMPERATURES

Solubility screening was performed using the mixtures of DHAA (50 mM) with TPP, $[Ru(bpy)_3]Cl_2$, and DCA at 0.5 mol% using different solvents and solvent mixture, by changing the temperatures from room temperature, 0, - 10, - 20, -30, and – 40 °C, using mixtures of freezing liquids; Ice/acetone (1:1) for -10 °C, Ice/NaCl (3:1) for -20 °C, liquid N_2/Bromobenzene – 30 °C, and Ice/Calcium chloride hexahydrate (0.8:1) – 40 °C. In all cases, the DHAA was dissolved in the organic component first and then water was added and mixed with a vortex mixer, to note the precipitation of substrate upon addition of the water or the complete dissolution of the substrate.

STUDYING THE EFFECT OF BIPHENYL ON DHAA PHOTO-OXIDATION

5.7.1 STUDYING THE EFFECT OF BIPHENYL ON DHAA PHOTO-OXIDATION USING DCA AS PHOTOSENSITISER

To study the effect of biphenyl concentration on the DHAA photo-oxidation at 12 °C, the solutions were prepared by dissolving a set amount of biphenyl, DHAA (50 mM) and DCA (2.5 mM) in Toluene or Dichloroethane (DCE), each reaction was performed as a single batch described in Section 5.3.1 in PhotoVap reactor , but here only single run was performed by injecting 5 mL of the solution into the PhotoVap 1L round bottom flask, after which the flask is mounted to the reactor, oxygen gas was initially bubbled for 2

minutes to saturate the solution while rotating the flask at 175 rpm, after which the reactor's LEDs are switch-on for the a specified irradiation time. The resulting photo-oxidation products were dried using N_2 and analysed with ^{1}H-NMR spectroscopy.

5.7.2 Studying the effect of biphenyl on DHAA photo-oxidation using $[Ru(bpy)_3]Cl_2$ as Photosensitiser

To study the effect of biphenyl concentration on the DHAA photo-oxidation at 12 ^oC, the solutions were prepared by dissolving (0 – 100 mM) biphenyl, DHAA (50 mM) and $[Ru(bpy)_3Cl_2]$ (0.025 mM) in Dichloroethane (DCE), each reaction was performed as a single batch in the PhotoVap reactor as described in Section 5.3.1, but here only single run was performed by injecting 5 mL of the solution into the PhotoVap 1L round bottom flask, after which the flask is mounted to the reactor, oxygen gas was initially bubbled for 2 minutes to saturate the solution while rotating the flask at 175 rpm, after which the reactor's LEDs are switch on for the specified irradiation time. The resulting photo-oxidation products were dried using argon and analysed with ^{1}H-NMR spectroscopy using biphenyl as internal standard.

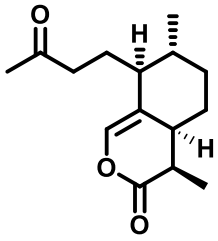
Synthesis of δ– Lactone

The δ-lactone is synthesised from the DHAA photo-oxidation product obtained using Ethyl acetate as solvent (Section 5.3.1). After photo-oxidation the crude products solution is mounted on Schlenk-line, the oxygen atmosphere was replaced with Nitrogen using freeze, pump – thaw method, the freezing was performed with liquid Nitrogen contained in a dewer flask. The process was repeated three times to ensure complete removal of oxygen, after which 0.5 equivalent of triflouroacetic acid (TFA) was added. The reaction was allowed to go to completion after 24 hours under N_2 at room temperature, resulting

in the conversion of all the enol into δ-lactone, as shown by the ^{1}H-NMR chemical shift of the crude products.

5.8.1 ISOLATION AND CRYSTALLISATION OF δ-LACTONE

The crude products are initially separated using Thin Layer Chromatography (TLC), with cyclohexane/diethyl ether (1:1) as mobile phase, products development using Anisaldehyde, reveals clear separation of the products. The crude mixture was finally separated using automatic column set at elution rate of 2 mL/min, using silica gel and cyclohexane/diethyl ether as stationary and mobile phase respectively, the desired product was identified by taking the ^{1}H – NMR of each fraction obtained. The white flocculent crystals of δ-lactone **33** were obtained by drying out the solvent using rotary evaporator and identified from its ^{1}H, ^{13}C-NMR techniques, FTIR and Mass Spectroscopy.



The structure of δ-lactone

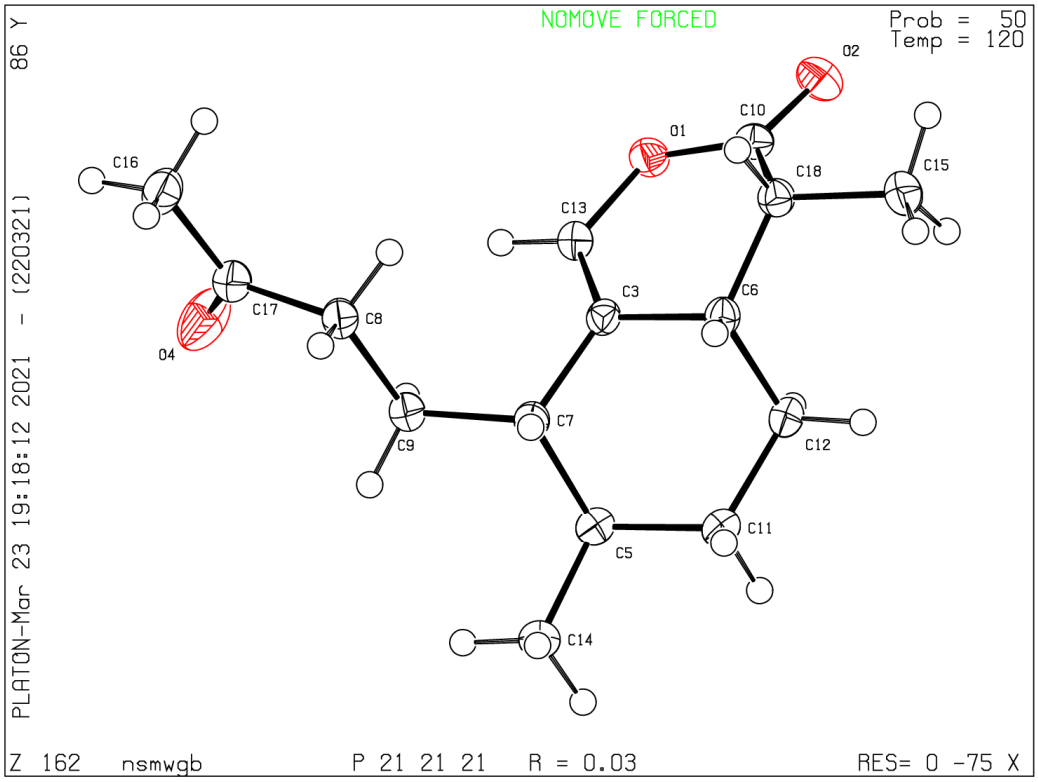
^{1}H NMR (400 MHz, $CDCl_3$) δ 6.10 (d, *J* = 1.5 Hz, 1H), 2.96 (qu, *J* = 7.1 Hz, 1H), 2.66 (ddd, *J* = 17.8, 9.2, 4.9 Hz, 1H), 2.47 (ddd, *J* = 17.9, 8.8, 6.7 Hz, 1H), 2.18 (s, 2H), 2.23 – 2.01 (m, 1H), 1.93 – 1.79 (m, 2H), 1.69 (ddt, *J* = 10.7, 9.2, 1.9 Hz, 1H), 1.54 – 1.43 (m, 1H), 1.25 (d, *J* = 7.0 Hz, 3H), 1.25 – 1.13 (m, 1H), 1.17 – 0.94 (m, 3H).

^{13}C NMR (101 MHz, $CDCl_3$) δ 208.40, 171.62, 131.90, 124.47, 47.25, 42.67, 41.71, 41.20, 36.58, 35.44, 30.08, 28.54, 20.88, 19.99, 11.53.

HRMS (ESI) m/z calculated [$C_{15}H_{22}O_3$] (M + Na^+) = 273.1461, found [$C_{15}H_{22}NaO_3$] (M + Na) = 273.1465

FTIR absorption peak; 1714 and 1756 cm^{-1}.

Fine crystals of this compound were obtained by dissolving the isolated compound in highly non – polar solvent such as n-hexane in a vial and carefully adding a drop of polar solvent, ethyl acetate after which the vial is kept in an upright undisturbed position for two days, for the crystals to grow. The crystals obtained were submitted for X – ray crystallographic analysis.



Crystal data for $C_{15}H_{22}O_3$ (250.34 g/mol): orthorhombic, space group $P2_12_12_1$, a = 4.88251(12) Å, b = 12.4849(3) Å, c = 22.5754(7) Å, β = 90°, α = 90°, γ = 90°, V = 1376.15(6) $Å^3$, Z = 4, T = 120 (2) K, ϱ_{calc} = 1.198 g/cm^3, Crystal size = 0.276 × 0.139 × 0.046 mm^{-3}, Radiation = Cu Kα (λ = 1.54184), Reflection collected = 15406, Independent

reflection = 2728 [R_{int} = 0.0253, R_{sigma} = 0.0153]. The final R_1 was 0.0347 (I>=2σ(I)) and wR_2 was 0.0993

5.8.2 SCALE-UP OF THE SYNTHESIS OF Δ-LACTONE IN LARGE VORTEX REACTOR

The general set-up for the Kilogram scale Vortex reactor and its standard operation procedure were described elsewhere.[96] The scale-up was performed by initial photo-oxidation in Vortex reactor, 1.0 L solution containing 50 mM (11.82 g) of DHAA and 0.5 mol% (0.153 g) of TPP were dissolved in 1.0 L of ethyl acetate, the process was performed at – 20 °C, full conversion was realized when the reactor was set at 10 mL/min input, 45 mL/min output and the oxygen dose of 25 mL/min, 750 mL of the crude photo-oxidation products was recovered from the Vortex into 1L round bottom flask. The photo-oxidation products were initially purged with N_2 for 20 min cooled to – 20 °C in ice bath (NaCl), after which 0.5 equiv. (1.44 mL) of TFA was added while stirring the solution, the solution was left stirring for 72 hours for the reaction to complete.

5.8.3 REACTIONS OF Δ-LACTONE

5.8.3.1 ACID CATALYSED HYDROLYSIS OF Δ-LACTONE IN MEOH/H_2O SOLUTION

To the solution δ-lactone (50 mM, 250 mg) prepared in 20 mL of methanol in a round bottom flask (50 mL), 1.0 equivalent of H_2O (18 μl) and 0.5 equiv. of TFA (0.038 mL) has been added to the solution. After which oxygen gas was bubbled with the aid of balloon for the initial 1.0 hour, and prolong bubbling for 48 hours, in each case products yield was determined from its ^{1}H-NMR, by monitoring the changes in the integral values of δ-lactone **33** at 6.10 ppm, with that of the possible products, using biphenyl as internal standard. Three aliquots of 1 mL each were collected and dried by using N_2, 0.1 mL of

10 % biphenyl in $CDCl_3$ and 0.6 mL of $CDCl_3$ were added, and the resulting solution was submitted for ^1H NMR analysis

5.8.3.2 ACID CATALYSED HYDROLYSIS OF Δ-LACTONE IN THF/H_2O SOLUTION

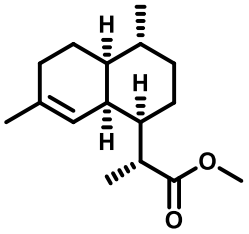
The acid catalysed hydrolysis was performed by dissolving (50 mM, 125 mg) of δ-lactone **33** in 10 mL of THF-d_8:D_2O in a vial, 0.7 mL of the solution were transferred into the NMR tube, the sample solution was purged with nitrogen gas, after which TFA (0.5 equiv. 0.019 mL) was added, and the process was monitored through regular ^1H-NMR measurements. Each product was determined by its specific ^1H-MNR peak in the spectrum.

SYNTHESIS OF DHAA DERIVATIVES

5.9.1 GENERAL PROCEDURE FOR THE SYNTHESIS OF THE DHAA ESTER DERIVATIVES

To a stirred suspension of DHAA (1 equiv.), DMAP (0.1 equiv.) and the desired alcohol (1 equiv.) in dichloromethane, was added dicyclohexylcarbodiimide (1 equiv.). The mixture was stirred at room temperature overnight until completion, determined by TLC analysis. The solution was then filtrated to remove the dicyclohexylurea formed and the filtrate was washed with HCl aqueous solution (1M). The combined organic layers were dried over anhydrous magnesium sulphate, filtered, and concentrated under reduced pressure. The crude product was purified by flash chromatography on silica gel eluting with a mixture of pentane/Et_2O to afford the desired product as colourless oils.

1. DHAA Methyl ester was isolated as colourless oil



The structure of DHAA methyl ester (**8**)

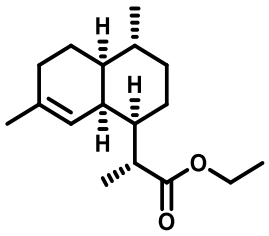
^{1}H NMR (400 MHz, $CDCl_3$) δ 5.14 (s, *J* = 1.5 Hz, 1H), 3.69 (s, 3H), 2.52 (dq, *J* = 10.9, 6.9 Hz, 2H), 2.02 – 1.76 (m, 3H), 1.70 – 1.56 (m, 5H), 1.60 – 1.36 (m, 2H), 1.27 (dqd, *J* = 12.0, 2.9, 1.3 Hz, 2H), 1.15 (d, *J* = 6.9 Hz, 3H), 1.12 – 0.99 (m, 1H), 1.03 – 0.89 (m, 1H), 0.88 (d, *J* = 6.5 Hz, 3H).

^{13}C NMR (101 MHz, $CDCl_3$) δ 177.94, 135.87, 119.45, 51.40, 43.97, 42.16, 41.72, 36.41, 35.26, 27.68, 27.46, 26.62, 25.78, 23.83, 19.71, 15.12.

HRMS (ESI) m/z calculated [$C_{16}H_{26}O_2$] (M + H) = 251.20, found [$C_{16}H_{26}O_2$] (M + H) = 251.1979

FTIR absorption peak; 1734 cm^{-1}.

2. DHAA Ethyl ester was isolated as colourless oil



The structure of DHAA ethyl ester (**90**)

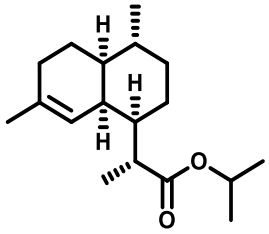
^{1}H NMR (400 MHz, $CDCl_3$) δ 5.15 (s, *J* = 1.6 Hz, 1H), 4.15 (q, *J* = 7.1 Hz, 2H), 2.55 – 2.42 (m, 2H), 2.02 – 1.76 (m, 3H), 1.71 – 1.58 (m, 6H), 1.55 (ddd, *J* = 11.1, 7.4, 4.3 Hz, 1H), 1.52 – 1.36 (m, 1H), 1.28 (t, *J* = 7.1 Hz, 5H), 1.18 – 1.06 (m, 4H), 1.06 – 0.94 (m, 1H), 0.88 (d, *J* = 6.5 Hz, 3H).

^{13}C NMR (101 MHz, $CDCl_3$) δ 177.48, 135.80, 119.56, 60.04, 43.91, 42.24, 41.72, 36.43, 35.29, 27.70, 27.40, 26.62, 25.79, 23.83, 19.72, 15.13, 14.30.

HRMS (ESI) m/z calculated for [$C_{17}H_{28}NaO_2$] (M + Na^+) = 287.1982, found for [$C_{17}H_{28}NaO_2$] (M + Na^+) = 287.1970.

FTIR absorption peak; 1723 cm^{-1}.

3. DHAA Isopropyl ester was isolated as colourless oil



The structure of DHAA Isopropyl ester (**91**)

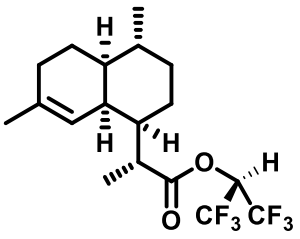
^{1}H NMR (400 MHz, $CDCl_3$) δ 5.15 (s, *J* = 1.5 Hz, 1H), 5.04 (qu, *J* = 6.3 Hz, 1H), 2.55 – 2.47 (m, 1H), 2.44 (dq, *J* = 11.0, 6.9 Hz, 1H), 2.01 – 1.76 (m, 3H), 1.64 (s, *J* = 1.1 Hz, 4H), 1.65 – 1.56 (m, 1H), 1.60 – 1.50 (m, 1H), 1.50 – 1.36 (m, 1H), 1.36 – 1.25 (m, 1H), 1.26 (s, 2H), 1.27 – 1.19 (m, 5H), 1.22 – 1.03 (m, 4H), 1.03 – 0.92 (m, 1H), 0.88 (d, *J* = 6.5 Hz, 3H).

^{13}C NMR (101 MHz, $CDCl_3$) δ 176.95, 135.73, 119.64, 67.12, 43.85, 42.38, 41.72, 35.31, 27.71, 27.32, 26.62, 25.79, 23.82, 23.79 21.93, 21.78, 19.73, 15.12.

HRMS (ESI) m/z calculated [$C_{18}H_{30}NaO_2$] (M + Na) = 301.2138, found [$C_{18}H_{28}NaO_4$] (M + Na) = 301.2131

FTIR absorption peak; 1712 cm^{-1}.

4. DHAA Hexafluoroisopropyl ester was isolated as colourless oil



The structure of DHAA Hexafluoroisopropyl ester (**92**)

^{1}H NMR (400 MHz, $CDCl_3$) δ 5.80 (hept, *J* = 6.1 Hz, 1H), 5.12 (s, *J* = 1.5 Hz, 1H), 2.72 (dq, *J* = 11.1, 7.0 Hz, 1H), 2.55 (qt, *J* = 4.4, 2.2 Hz, 1H), 2.04 – 1.93 (m, 1H), 1.97 – 1.82 (m, 1H), 1.85 – 1.71 (m, 1H), 1.74 – 1.61 (m, 3H), 1.64 – 1.55 (m, 1H), 1.58 – 1.39 (m, 1H), 1.35 – 1.22 (m, 4H), 1.14 (qd, *J* = 12.6, 3.2 Hz, 1H), 1.04 – 0.87 (m, 3H).

^{13}C NMR (101 MHz, $CDCl_3$) δ 173.87, 136.50, 118.70, 66.61, 65.92, 44.85, 43.52, 42.12, 41.63, 36.25, 35.04, 27.63, 27.18, 26.57, 25.70, 23.78, 19.60, 14.87.

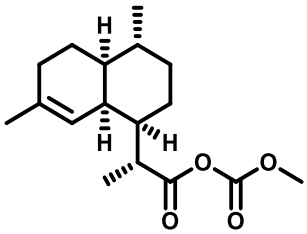
^{19}F NMR (376 MHz, $CDCl_3$) δ -73.16 (dq, *J* = 12.4, 6.1 Hz), -73.21 – -73.47 (m).

FTIR absorption peak; 1781 cm^{-1}.

5.9.2 GENERAL PROCEDURE FOR THE SYNTHESIS OF DHAA CARBONATES DERIVATIVES:

To a stirred suspension of DHAA and triethylamine in toluene, was added dropwise at 0 °C the corresponding chloroformate. The mixture was stirred for further 45 min The solution was then washed twice with water. The combined organic layers were dried over anhydrous magnesium sulphate, filtered, and concentrated under reduced pressure. The products were obtained as a pale yellow solid and has been used as such.

1. DHAA Methyl carbonate



The structure of DHAA methyl carbonate (**93**)

^{1}H NMR (400 MHz, $CDCl_3$) δ 5.10 (s, *J* = 1.5 Hz, 1H), 3.92 (s, 3H), 2.70 – 2.48 (m, 2H), 2.37 (d, *J* = 0.7 Hz, 1H), 2.02 – 1.77 (m, 3H), 1.76 – 1.65 (m, 1H), 1.69 – 1.61 (m, 4H),

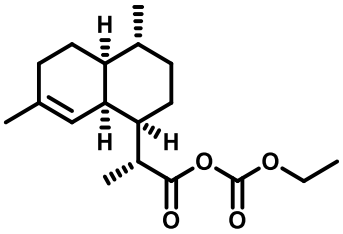
1.64 – 1.53 (m, 1H), 1.57 – 1.37 (m, 2H), 1.33 – 1.20 (m, 4H), 1.15 (td, *J* = 12.6, 3.2 Hz, 1H), 1.01 (ddd, *J* = 13.1, 11.7, 3.4 Hz, 1H), 0.89 (d, *J* = 6.5 Hz, 3H).

^{13}C NMR (101 MHz, $CDCl_3$) δ 171.39, 150.01, 136.40, 118.84, 55.83, 43.71, 42.62, 41.67, 36.31, 35.11, 27.61, 27.30, 26.59, 25.72, 23.83, 19.64, 14.67.

HRMS (ESI) m/z calculated [$C_{17}H_{26}NaO_4$] [M + Na] = 317.1702, found [$C_{17}H_{26}NaO_4$] [M + Na] = 317.1709.

FTIR absorption peak; 1755 cm^{-1}.

2. DHAA Ethyl carbonate



The structure of DHAA ethyl carbonate (**45**)

^{1}H NMR (400 MHz, $CDCl_3$) δ 5.10 (s, *J* = 1.4 Hz, 1H), 4.34 (q, *J* = 7.1 Hz, 2H), 2.60 (dq, *J* = 11.0, 6.9 Hz, 1H), 2.52 (d, *J* = 5.2 Hz, 1H), 2.02 – 1.88 (m, 1H), 1.82 (dd, *J* = 17.7, 7.0 Hz, 0H), 1.77 – 1.35 (m, 10H), 1.35 – 1.20 (m, 4H), 1.16 (qd, *J* = 12.7, 3.2 Hz, 1H), 0.99 (tdd, *J* = 13.0, 11.7, 3.4 Hz, 1H), 0.89 (d, *J* = 6.5 Hz, 3H).

^{13}C NMR (101 MHz, $CDCl_3$) δ 171.57, 149.34, 136.36, 118.88, 65.56, 43.69, 42.61, 41.67, 36.32, 35.11, 27.61, 27.29, 26.58, 25.72, 23.82, 19.64, 14.68, 13.94.

HRMS (ESI) m/z calculated [$C_{18}H_{28}NaO_4$] $[M + Na]^+$ = 331.1880, found [$C_{18}H_{28}NaO_4$] (M + Na) = 331.1875.

FTIR absorption peak; 1750 cm^{-1}.

5.9.3 SYNTHESIS OF ARTEMISININ USING DHAA DERIVATIVES

5.9.3.1 PHOTO-OXIDATION

Photo-oxidation process using DHAA methyl carbonate (**93**) (50 mM, 294 mg) and DHAA methyl ester (**8**) (50 mM, 250 mg) were performed in PhotoVap Reactor as described in Section 5.3.1. After each process three aliquots of 1 mL were collected and dried by using nitrogen gas, and sample was dissolved in 0.7 mL of $CDCl_3$, and the resulting solution was submitted for ^1H NMR analysis. The percentage yield of tertiary hydroperoxides were determined quantitatively using biphenyl as internal standard, according to the ^1H-NMR chemical shifts at 5.28 ppm of the hydroperoxides from the crude photo-oxidation products.

5.9.3.2 ACID CATALYSED HOCK-CLEAVAGE AND THERMAL OXIDATION

Acid catalysed thermal oxidation was performed as by addition of TFA (0.5 equiv.) to the crude products of photo-oxidation as described in Section 5.3.2. After the process three aliquots of 1 mL were collected and dried by using nitrogen gas, and sample was dissolved in 0.7 mL of $CDCl_3$, and the resulting solution was submitted for ^1H NMR analysis. The percentage yield of Artemisinin **1** and other products were determined quantitatively using biphenyl as internal standard, according to specific ^1H-NMR peak of each.ONE-POT METHOD

For each of the derivatives (50 mM), TPP (0.5 mol%) and biphenyl (10 %) were dissolved in a given Solvent (50 mL), followed by the addition of TFA (0.5 equiv.) to the solution, which was prepared in an amber bottle to avoid light penetration before irradiation, as described in Section 5.3.3. After each process three aliquots of 1 mL were collected and dried by using nitrogen gas, and sample was dissolved in 0.7 mL of $CDCl_3$, and the resulting solution was submitted for ^1H NMR analysis. The percentage yield of

Artemisinin **1** and other products were determined quantitatively using biphenyl as internal standard, according to specific ^{1}H-NMR peak of each.

REFERENCES

1. J. Turconi, F. Griolet, R. Guevel, G. Oddon, R. Villa, A. Geatti, M. Hvala, K. Rossen, R. Göller and A. Burgard, *Org. Process Res. Dev.*, 2014, **18**, 417-422.
2. Z. Amara, J. F. Bellamy, R. Horvath, S. J. Miller, A. Beeby, A. Burgard, K. Rossen, M. Poliakoff and M. W. George, *Nat. Chem.*, 2015, **7**, 489-495.
3. A. Burgard, T. Gieshoff, A. Peschl, D. Hörstermann, C. Keleschovsky, R. Villa, S. Michelis and P. M. Feth, *Chem. Eng. J.*, 2016, **294**, 83-96.
4. D. Zhao, Y. Wang, Y. Xu, N. Wang and J. Li, *J. Mat. Sci.*, 2018, **53**, 14241-14249.
5. C. A. Clark, D. S. Lee, S. J. Pickering, M. Poliakoff and M. W. George, *Org. Process Res. Dev.*, 2018, **22**, 595-599.
6. I. Newton, *Opticks: or, A treatise of the reflections, refractions, inflexions and colours of light*, Printed for Sam. Smith, and Benj, Walford, London.
7. C. A. and K. T.J., *Introductory photochemistry :J. Mol. Structure*, McGraw-Hill, London, 1972.
8. H. D. Roth, *Angew. Chem. Int. Ed.*, 1989, **28**, 1193-1207.
9. H. D. Roth, *Pure Appl Chem*, 2001, **73**, 395-403.
10. G. Nebbia and G. Kauffman, *Chem. Educcator*, 2007, **12**, 362-369.
11. G. Ciamician, *Science*, 1912, **36**, 385-394.
12. M. Sender and D. Ziegenbalg, *Chemie Ingenieur Technik*, 2017, **89**, 1159-1173.
13. M. Oelgemöller, *Chemical Reviews*, 2016, **116**, 9664-9682.
14. N. J. Turro, V. Ramamurthy and J. C. Scaiano, *Modern Molecular Photochemistry of Organic Molecules*, Viva Books, 2010.
15. M. S. Baptista, J. Cadet, P. Di Mascio, A. A. Ghogare, A. Greer, M. R. Hamblin, C. Lorente, S. C. Nunez, M. S. Ribeiro, A. H. Thomas, M. Vignoni and T. M. Yoshimura, *Photochem. Photobiol.*, 2017, **93**, 912-919.
16. P. R. Ogilby, *Chem. Soc. Rev.*, 2010, **39**, 3181-3209.
17. K.-H. Pfoertner and T. Oppenländer, *Photochemistry*, Ullmann's Encyclopedia of Industrial Chemistry, Weinheim, 2012.
18. K. L. Skubi, T. R. Blum and T. P. Yoon, *Chem. Rev.*, 2016, **116**, 10035-10074.
19. T. Tamai, K. Mizuno, I. Hashida and Y. Otsuji, *J. Org. Chem.*, 1992, **57**, 5338-5342.
20. T. Tamai, N. Ichinose, T. Tanaka, T. Sasuga, I. Hashida and K. Mizuno, *J. Org. Chem.*, 1998, **63**, 3204-3212.
21. C. S. Foote, *Tetrahedron*, 1985, **41**, 2221-2227.
22. A. Paul Schaap, S. Siddiqui, G. Prasad, E. Palomino and M. Sandison, *Tetrahedron*, 1985, **41**, 2229-2235.
23. J. Dabrowski, B. Pucelik, A. Regiel-Futyra, M. Brindell, O. Mazuryk, A. Kyzioł, G. Stochel, W. Macyk and L. Arnaut, *Coord. Chem. Rev.*, 2016, 67–101.
24. E. Coyle, PhD, Dublin City University, 2010.
25. S. J. Miller, PhD Thesis, University of Nottingham, 2017.
26. C. Schweitzer and R. Schmidt, *Chem. Rev.*, 2003, **103**, 1685-1758.
27. R. Dědic, M. Kořínek, A. Molnár, A. Svoboda and J. Hála, *J. Lum.*, 2006, **119-120**, 209-213.
28. R. L. Jensen, J. Arnbjerg and P. R. Ogilby, *J. Am. Chem. Soc.*, 2010, **132**, 8098-8105.
29. C. S. Foote and R. W. Denny, *J. Am. Chem. Soc.*, 1968, **90**, 6233-6235.
30. A. Barik, P. Indira, M. Hari, P. Bajaj, A. Sapre, J. Mittal and T. Mukherjee, *Singlet oxygen: photosensitized generation, detection and reaction with organic molecules*, Bhabha Atomic Research Centre, 2006.
31. A. Singh, G. W. Koroll and S. A. Antonsen, *J. Photochem.*, 1984, **25**, 99-104.
32. C. Michelin and N. Hoffmann, *ACS Catal.*, 2018, **8**, 12046-12055.

33. M. C. DeRosa and R. J. Crutchley, *Coord. Chem. Rev.*, 2002, **233-234**, 351-371.
34. J. F. B. Bellamy, Ph.D., University of Nottingham, 2014.
35. J. C. Barona-Castano, C. C. Carmona-Vargas, T. J. Brocksom and K. T. de Oliveira, *Molecules*, 2016, **21**, 310.
36. K. Kalyanasundaram and M. Neumann-Spallart, *J. Phys. Chem.*, 1982, **86**, 5163-5169.
37. M. M. El-Nahass, H. M. Zeyada, M. S. Aziz and M. M. Makhlouf, *Spectrochimi. Acta A.*, 2005, **62**, 11-15.
38. D. Mohammad Reza, M.-M. Ali Akbar and D. Mohammad Saaid, *Protein Peptide Lett.*, 2010, **17**, 473-479.
39. S. Aronoff and G. Mackinney, *J. Am. Chem. Soc.*, 1943, **65**, 956-958.
40. D. Wróbel, I. Hanyż, R. Bartkowiak and R. M. Ion, *J. Fluoresc.*, 1998, **8**, 191-198.
41. S. Callaghan and M. O. Senge, *Photochem. Photobio. Sci.*, 2018, **17**, 1490-1514.
42. L. M. G. Jansen, *Photochemistry and Photophysics of Azo Dyes*, Loughborough University, 1997.
43. D. K. Deda, C. Pavani, E. Caritá, M. S. Baptista, H. E. Toma and K. Araki, *J. Porphyr. Phthalocya.*, 2012, **16**, 55-63.
44. M. Kořinek, R. Dědic, A. Svoboda and J. Hála, *J. Fluoresc.*, 2004, **14**, 71-74.
45. J. Olmsted, *J. Am. Chem. Soc.*, 1980, **102**, 66-71.
46. E. Zenkevich, E. Sagun, V. Knyukshto, A. Shulga, A. Mironov, O. Efremova, R. Bonnett, S. P. Songca and M. Kassem, *J. Photochem. Photobio. B.*, 1996, **33**, 171-180.
47. X.-l. Zhang and X.-h. Chen, *Optoelectronics Letts.*, 2019, **15**, 135-138.
48. D. Kopetzki, F. Levesque and P. H. Seeberger, *Chem. Eur.*, 2013, **19**, 5450-5456.
49. R. W. Redmond and J. N. Gamlin, *Photochem. photobio.*, 1999, **70**, 391-475.
50. S. Blanc, T. Pigot, C. Cugnet, R. Brown and S. Lacombe, *Phys. Chem. Chem. Phys.*, 2010, **12**, 11280-11290.
51. Y. Shiraishi, Y. Taki, T. Hirai, I. Komasawa and I. Komasawa, *Chem. Commun.*, 1998, 2601-2602.
52. I. N. Lykakis, S. Lestakis and M. Orfanopoulos, *Tetrahedron Lett.*, 2003, **44**, 6247-6251.
53. S. M. Bonesi, M. Fagnoni and A. Albini, *Eur. J. Org. Chem.*, 2008, **2008**, 2612-2620.
54. R. C. Kanner and C. S. Foote, *J. Am. Chem. Soc.*, 1992, **114**, 678-681.
55. Q. Q. Zhou, Y. Q. Zou, L. Q. Lu and W. J. Xiao, *Angew. Chem.*, 2019, **58**, 1586-1604.
56. C. S. Brian, *Fundamentals of Fourier Transform Infrared Spectroscopy*, CRC Press, London, Second edn., 2011.
57. Y. Xi, H. Yi and A. Lei, *Org. Biomol. Chem.*, 2013, **11**, 2387-2403.
58. T. J. Meyer, *Acc. Chem. Res.*, 1989, **22**, 163-170.
59. T. P. Yoon, M. A. Ischay and J. Du, *Nat. Chem.*, 2010, **2**, 527.
60. K. Zeitler, *Angew.*, 2009, **48**, 9785-9789.
61. J. Van Houten and R. J. Watts, *J. Am. Chem. Soc.*, 1976, **98**, 4853-4858.
62. J. N. Demas, D. Diemente and E. W. Harris, *J. Am. Chem. Soc.*, 1973, **95**, 6864-6865.
63. S. Fukuzumi, S. Mochizuki and T. Tanaka, *J. Phys. Chem.*, 1990, **94**, 722-726.
64. G. J. Hutchings, *J. Mater. Chem.*, 2009, **19**, 1222-1235.
65. G. Zhang, I. Y. Song, T. Park and W. Choi, *Green Chem.*, 2012, **14**, 618.
66. B. Tambosco, K. Segura, C. Seyrig, D. Cabrera, M. Port, C. Ferroud and Z. Amara, *ACS Cat.*, 2018, **8**, 4383-4389.
67. V. Blanchard, Z. Asbai, K. Cottet, G. Boissonnat, M. Port and Z. Amara, *Org. Process Res. Dev.*, 2020, DOI: 10.1021/acs.oprd.9b00420.

68. A. E. Cassano, C. A. Martin, R. J. Brandi and O. M. Alfano, *Ind. Eng. Chem.*, 1995, **34**, 2155-2201.
69. S. Meyer, D. Tietze, S. Rau, B. Schäfer and G. Kreisel, *J. Photochem. Photobiol. A*, 2007, **186**, 248-253.
70. J. P. Knowles, L. D. Elliott and K. I. Booker-Milburn, *Beilstein J. Org. Chem.*, 2012, **8**, 2025-2052.
71. E. N. DeLaney, D. S. Lee, L. D. Elliott, J. Jin, K. I. Booker-Milburn, M. Poliakoff and M. W. George, *Green Chem.*, 2017, **19**, 1431-1438.
72. E. Speckmeier and K. Zeitler, *Journal*, 2019, **2018**, 101-132.
73. M. Oelgemöller and O. Shvydkiv, *Molecules*, 2011, **16**, 7522-7550.
74. T. H. Rehm, *Chem. Photo. Chem.*, 2020, **4**, 235-254.
75. R. Zavaleta Mercado, *Acta Nova*, 2015, **7**, 3-27.
76. C. A. Clark, D. S. Lee, S. J. Pickering, M. Poliakoff and M. W. George, *Org. Process Res. Dev.*, 2016, **20**, 1792-1798.
77. E. S. a. K. Zeitler, in *Photocatalysis in Organic Synthesis*, ed. B. König, Georg Thieme Verlag, Stuttgart, 2019 edn., 2019, DOI: 10.1055/sos-SD-229-00059.
78. M. Di Filippo, C. Bracken and M. Baumann, *Molecules*, 2020, **25**, 356.
79. D. S. Lee, Z. Amara, C. A. Clark, Z. Xu, B. Kakimpa, H. P. Morvan, S. J. Pickering, M. Poliakoff and M. W. George, *Org. Process Res. Dev.*, 2017, **21**, 1042-1050.
80. R. A. Maurya, C. P. Park and D.-P. Kim, *Beilstein J. Org. Chem.*, 2011, **7**, 1158-1163.
81. K. S. Elvira, R. C. R. Wootton, N. M. Reis, M. R. Mackley and A. J. deMello, *ACS Sustain. Chem. Eng.*, 2013, **1**, 209-213.
82. D. Ziegenbalg, G. Kreisel, D. Weiß and D. Kralisch, *Photochem. Photobio. Sci.*, 2014, **13**, 1005-1015.
83. F. Levesque and P. H. Seeberger, *Angew. Chem. Int. Ed.*, 2012, **51**, 1706-1709.
84. D. Kopetzki and P. H. Seeberger, *Nachrichten Aus Der Chemie*, 2012, **60**, 714-717.
85. D. T. McQuade and P. H.Seeberger, *J. Org. Chem.*, 2013, **78**, 6384-6389.
86. R. C. R. Wootton, R. Fortt and A. J. de Mello, *Org. Process Res. Dev.*, 2002, **6**, 187-189.
87. G. I. Ioannou, T. Montagnon, D. Kalaitzakis, S. A. Pergantis and G. Vassilikogiannakis, *Chem. Photo. Chem.*, 2017, **1**, 173-177.
88. A. A. Ghogare and A. Greer, *Chem. Rev.*, 2016, **116**, 9994-10034.
89. C. Sambiagio and T. Noël, *Trends Chem.*, 2020, **2**, 92-106.
90. E. E. Coyle and M. Oelgemöller, *Photochem. Photobio. Sci.*, 2008, **7**, 1313-1322.
91. D. Cambié and T. Noël, *Topics Curr. Chem.*, 2018, **376**, 1-27.
92. T. Carofiglio, P. Donnola, M. Maggini, M. Rossetto and E. Rossi, *Adv. Synth. Catal.*, 2008, **350**, 2815-2822.
93. T. K. Sengupta, M. F. Kabir and A. K. Ray, *Ind. Eng. Chem.*, 2001, **40**, 5268-5281.
94. E. Dłuska, S. Wroński and R. Hubacz, *Chem. Eng. Sci.*, 2001, **56**, 1131-1136.
95. D. Reay, C. Ramshaw and A. Harvey, in *Process Intensification (Second Edition)*, Butterworth-Heinemann, Oxford, 2013, DOI:

, pp. 121-204.
96. D. S. Lee, M. Sharabi, R. Jefferson-Loveday, S. J. Pickering, M. Poliakoff and M. W. George, *Org. Process Res. Dev.*, 2020, **24**, 201-206.
97. M. Prein and W. Adam, *Angew. Chem.Int. Ed.*, 1996, **35**, 477-494.
98. M. Yoshioka, Y. Sakuma and M. Saito, *J. Org. Chem.*, 1999, **64**, 9247-9250.
99. S. Cao, S. Zhong, L. Xin, J. P. Wan and C. Wen, *Chem. Cat. Chem.*, 2015, **7**, 1478-1482.
100. S. Sharma and A. Sharma, *Org. Biomol. Chem.*, 2019, **17**, 4384-4405.

101. C.-C. Chang, Y.-T. Yang, J.-C. Yang, H.-D. Wu and T. Tsai, *Dyes Pigments*, 2008, **79**, 170-175.
102. L. Ludvíková, P. Friš, D. Heger, P. Šebej, J. Wirz and P. Klán, *Phys. Chem. Chem. Phys.*, 2016, **18**, 16266-16273.
103. P. Bayer, J. Schachtner, M. Májek and A. Jacobi von Wangelin, *Org. Chem. Front.*, 2019, **6**, 2877-2883.
104. L. Burchill and J. H. George, *J. Org. Chem.*, 2020, DOI: 10.1021/acs.joc.9b02968.
105. D. Kopetzki, F. Levesque and P. H. Seeberger, *Chemistry*, 2013, **19**, 5450-5456.
106. L. K. Sy and G. D. Brown, *Tetrahedron*, 2002, **58**, 897-908.
107. E. G. Tse, M. Korsik and M. H. Todd, *Malar. J.*, 2019, **18**, 1-21.
108. M. Z. Abdin, M. Israr, R. U. Rehman and S. K. Jain, *Planta Med*, 2003, **69**, 289-299.
109. J. Achan, A. O. Talisuna, A. Erhart, A. Yeka, J. K. Tibenderana, F. N. Baliraine, P. J. Rosenthal and U. D'Alessandro, *Malar. J.*, 2011, **10**, 1-12.
110. N. White, P. Chanthavanich, S. Krishna, C. Bunch and K. Silamut, *Br. J. Clinical Pharmac.*, 1983, **16**, 399-403.
111. Y. Tu, *Nat. Med.*, 2011, **17**, 1217-1220.
112. J. K. Aronson, in *Meyler's Side Effects of Drugs (Sixteenth Edition)*, Elsevier, Oxford, 2016, pp. 701-710.
113. X.-Y. Chen, Y. Yin, J. Xi, Y. Yuan, Y. Li, Q. Li, R.-X. Wang, Z.-J. Yao and G.-L. Tang, *Chin. J. Chem.*, 2018, **36**, 1197-1201.
114. T. Nguyen Le, W. M. De Borggraeve, P. Grellier, V. C. Pham, W. Dehaen and V. H. Nguyen, *Tetrahedron Lett.*, 2014, **55**, 4892-4894.
115. K. R. Bonepally, N. Takahashi, N. Matsuoka, H. Koi, H. Mizoguchi, T. Hiruma, K. Ochiai, S. Suzuki, Y. Yamagishi, H. Oikawa, A. Ishiyama, R. Hokari, M. Iwatsuki, K. Otoguro, S. Ōmura, N. Kato and H. Oguri, *J. Org. Chem.*, 2020, **85**, 9694-9712.
116. P. M. O'Neill, V. E. Barton and S. A. Ward, *Molecules*, 2010, **15**, 1705-1721.
117. J. Wang, C.-J. Zhang, W. N. Chia, C. C. Y. Loh, Z. Li, Y. M. Lee, Y. He, L.-X. Yuan, T. K. Lim, M. Liu, C. X. Liew, Y. Q. Lee, J. Zhang, N. Lu, C. T. Lim, Z.-C. Hua, B. Liu, H.-M. Shen, K. S. W. Tan and Q. Lin, *Nat. Commun.*, 2015, **6**, 1-11.
118. Z. Wang, L. Yang, X. Yang and X. Zhang, *Synth. Commun.*, 2014, **44**, 1987-2003.
119. D. Chaturvedi, A. Goswami, P. P. Saikia, N. C. Barua and P. G. Rao, *Chem. Soc. Rev.*, 2010, **39**, 435-454.
120. T. E. Wallaart, N. Pras, A. C. Beekman and and W. J. Quax, *Planta. Med.*, 2000, **66**, 57-62.
121. L. Nahar, M. Guo and S. D. Sarker, *Phytochem. Anal.*, 2020, **31**, 5-14.
122. L. Baldino and E. Reverchon, *J. Chem. Technol. Biotech.*, 2018, **93**, 3171-3175.
123. M. Sixt and J. Strube, *Processes*, 2017, **5**, 86.
124. Y. Zhang, P. Prawang, C. Li, X. Meng, Y. Zhao, H. Wang and S. Zhang, *Green Chem.*, 2018, **20**, 713-723.
125. V. A. Vil, I. A. Yaremenko, A. I. Ilovaisky and A. O. Terent'ev, *Molecules*, 2017, **22**.
126. Y. Liang, X. Zhou, J. Z. Guo, M. Zhang, H. G. Jiang, C. Q. Fu, Y. X. Fu, Z. W. Shi, Y. Liu, Z. J. Xin, X. H. Lu, J. P. Liang, B. C. Hao, X. H. Li and Z. Wang, *Chin. J. Chinese materia medica*, 2019, **44**, 5363-5367.
127. C. J. Paddon, P. J. Westfall, D. J. Pitera, K. Benjamin, K. Fisher, D. McPhee, M. D. Leavell, A. Tai, A. Main, D. Eng, D. R. Polichuk, K. H. Teoh, D. W. Reed, T. Treynor, J. Lenihan, M. Fleck, S. Bajad, G. Dang, D. Dengrove, D. Diola, G. Dorin, K. W. Ellens, S. Fickes, J. Galazzo, S. P. Gaucher, T. Geistlinger, R. Henry,

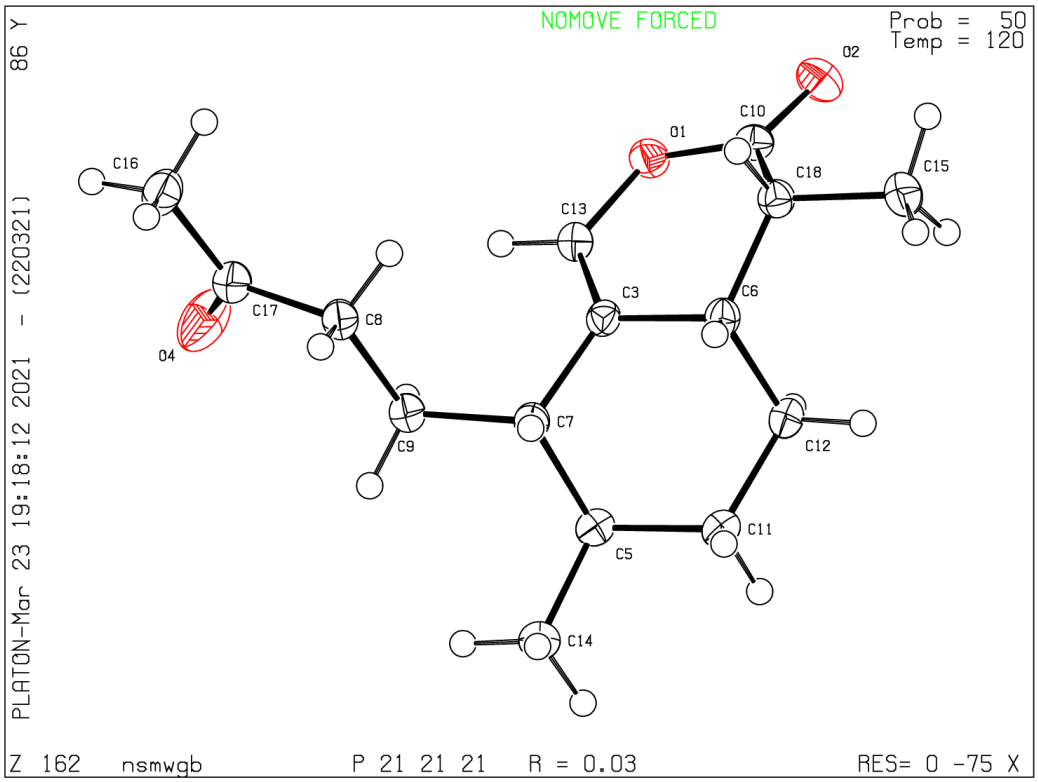
M. Hepp, T. Horning, T. Iqbal, H. Jiang, L. Kizer, B. Lieu, D. Melis, N. Moss, R. Regentin, S. Secrest, H. Tsuruta, R. Vazquez, L. F. Westblade, L. Xu, M. Yu, Y. Zhang, L. Zhao, J. Lievense, P. S. Covello, J. D. Keasling, K. K. Reiling, N. S. Renninger and J. D. Newman, *Nature*, 2013, **496**, 528-532.
128. J. S. Yadav, B. Thirupathaiah and P. Srihari, *Tetrahedron*, 2010, **66**, 2005-2009.
129. T. Ravindranathan, M. Anil Kumar, R. B. Menon and S. V. Hiremath, *Tetrahedron Lett.*, 1990, **31**, 755-758.
130. M. A. Avery, W. K. M. Chong and C. Jennings-White, *J. Am. Chem. Soc.*, 1992, **114**, 974-979.
131. C. Zhu and S. P. Cook, *J. Am. Chem. Soc.*, 2012, **134**, 13577-13579.
132. R. J. Roth and N. Acton, *J. Nat. Prod.*, 1989, **52**, 1183-1185.
133. N. Acton and R. J. Roth, *J. Org. Chem.*, 1992, **57**, 3610-3614.
134. N. Acton and R. J. Roth, *J. Am. Chem. Soc.*, 1990, **200**, 287-290.
135. R. J. Roth and N. Acton, *J. Chem. Ed.*, 1991, **68**, 612-613.
136. R. A. Bourne, X. Han, M. Poliakoff and M. W. George, *Angew.*, 2009, **48**, 5322-5325.
137. R. K. Haynes and S. C. Vonwiller, *Acc. Chem. Res.*, 1997, **30**, 73-79.
138. J. Kong, Y. Yang, W. Wang, K. Cheng and P. Zhu, *RSC Advances*, 2013, **3**, 7622-7641.
139. X. Xing-Xiang, Z. Jie, H. Da-Zhong and Z. Wei-Shan, *Tetrahedron*, 1986, **42**, 819-828.
140. S. C. Vonwiller, J. A. Warner, S. T. Mann and R. K. Haynes, *J. Am. Chem. Soc.*, 1995, **117**, 11098-11105.
141. G. Schmid and W. Hofheinz, *J. Am. Chem. Soc.*, 1983, **105**, 624-625.
142. M. G. Constantino, M. Beltrame, G. V. J. da Silva and J. Zukerman-Schpector, *Syn. Comm.*, 1996, **26**, 321-329.
143. L. Hsing-Jang, Y. Wen-Lung and Y. C. Sew, *Tetrahedron Lett.*, 1993, **34**, 4435-4438.
144. P. J. Westfall, D. J. Pitera, J. R. Lenihan, D. Eng, F. X. Woolard, R. Regentin, T. Horning, H. Tsuruta, D. J. Melis, A. Owens, S. Fickes, D. Diola, K. R. Benjamin, J. D. Keasling, M. D. Leavell, D. J. McPhee, N. S. Renninger, J. D. Newman and C. J. Paddon, *Proc. Natl. Acad. Sci.*, 2012, **109**, E111-118.
145. D. Singh, D. McPhee, C. J. Paddon, J. Cherry, G. Maurya, G. Mahale, Y. Patel, N. Kumar, S. Singh, B. Sharma, L. Kushwaha, S. Singh and A. Kumar, *Org. Process Res. Dev.*, 2017, **21**, 551-558.
146. G. Schwertz, A. Zanetti, M. N. de Oliveira, M. A. G. Fernandez, Z. Amara and J. Cossy, *J. Org. Chem.*, 2020, **85**, 9607-9613.
147. C. J. Paddon and J. D. Keasling, *Nature reviews. Microbiology*, 2014, **12**, 355-367.
148. M. Jung, H. N. ElSohly, E. M. Croom, A. T. McPhail and D. R. McPhail, *J. Org. Chem.*, 1986, **51**, 5417-5419.
149. R. K. Haynes and S. C. Vonwiller, *J. Chem. Soc. Chem. Commun.*, 1990, 451-453.
150. H. D. Hao, Y. Li, W. B. Han and Y. Wu, *Org. Lett.* , 2011, **13**.
151. K. Boehme and H. D. Brauer, *Inorg. Chem.*, 1992, **31**, 3468-3471.
152. H.-J. Chen, W.-B. Han, H.-D. Hao and Y. Wu, *Tetrahedron*, 2013, **69**, 1112-1114.
153. S. Karki, T. Friščić, L. Fábián and W. Jones, *Cryst. Eng. Comm.*, 2010, **12**, 4038-4041.
154. K. Gilmore, D. Kopetzki, J. W. Lee, Z. Horvath, D. T. McQuade, A. Seidel-Morgenstern and P. H. Seeberger, *Chem. Commun.*, 2014, **50**, 12652-12655.
155. M. Bregnhøj, M. Westberg, F. Jensen and P. R. Ogilby, *Phys. Chem. Chem. Phys.*, 2016, **18**, 22946-22961.
156. K. A. Zaklika, B. Kaskar and A. P. Schaap, *J. Am. Chem. Soc.*, 1980, **102**, 386-389.
157. L. K. Sy and G. D. Brown, *Tetrahedron*, 2002, **58**, 909-923.

158. A. G. Mojarrad and S. Zakavi, *Catal. Sci. Technol.*, 2018, **8**, 768-781.
159. X. Zhang and M. A. Rodgers, *J. Phys. Chem.*, 1995, **99**, 12797-12803.
160. I. A. Yaremenko, V. A. Vil, D. V. Demchuk and A. O. Terent'ev, *Beilstein J. Org. Chem.*, 2016, **12**, 1647-1748.
161. N. C. Deno, W. E. Billups, K. E. Kramer and R. R. Lastomirsky, *J. Org. Chem.*, 1970, **35**, 3080-3082.
162. G. A. Olah, D. G. Parker and N. Yoneda, *Angew. Chem. Int. Ed.*, 1978, **17**, 909-931.
163. D. Prat, J. Hayler and A. Wells, *Green Chem.*, 2014, **16**, 4546-4551.
164. G. D. Brown and L.-K. Sy, *Tetrahedron*, 2004, **60**, 1139-1159.
165. G. D. Brown and L.-K. Sy, *Tetrahedron*, 2007, **63**, 9548-9566.
166. Y. Liu, H. lu and F. Pang, *J. Chem. Eng Data*, 2009, **54**, 762-764.
167. N. Tian, J. Li, S. Liu, J. Huang, X. Li and Z. Liu, *Biomed. Chromatogr.*, 2012, **26**, 708-713.
168. L.-H. Wang, Y.-T. Song, Y. Chen and Y.-Y. Cheng, *J. Chem. Eng.*, 2007, **52**, 757-758.
169. C. K. Prier, D. A. Rankic and D. W. C. MacMillan, *Chem. Rev.*, 2013, **113**, 5322-5363.
170. A. P. Schaap, K. A. Zaklika, B. Kaskar and L. W. M. Fung, *J. Am. Chem. Soc.*, 1980, **102**, 389-391.
171. I. R. Gould, D. Ege, J. E. Moser and S. Farid, *J. Am. Chem. Soc.*, 1990, **112**, 4290-4301.
172. F. D. Lewis, A. M. Bedell, R. E. Dykstra, J. E. Elbert, I. R. Gould and S. Farid, *J. Am. Chemical Soc.*, 1990, **112**, 8055-8064.
173. R. Bonnett, D. J. McGarvey, A. Harriman, E. J. Land, T. G. Truscott and U.-J. Winfield, *Photochem. Photobio.*, 1988, **48**, 271-276.
174. S. K. Silverman and C. S. Foote, *J. Am. Chem. Soc.*, 1991, **113**, 7672-7675.
175. A. Greer, *Acc. Chem. Res.*, 2006, **39**, 797-804.
176. Z. Guo, *Acta Pharm. Sin. B*, 2016, **6**, 115-124.
177. L. K. Sy, K. S. Ngo and G. D. Brown, *Tetrahedron* 1999, **55**, 15127-15140.
178. K. N. Houk, J. C. Williams, P. A. Mitchell and K. Yamaguchi, *J. Am. Chem. Soc.*, 1981, **103**, 949-951.
179. I. Satoshi, F. Hiroshi and F. Kenichi, *Chem. Lett.*, 1976, **5**, 749-752.
180. L. B. Harding and W. A. Goddard, *J. Am. Chem. Soc.*, 1980, **102**, 439-449.
181. K. Varela, H. D. Arman and F. K. Yoshimoto, *J. Nat. Prod.*, 2021, **84**, 1967-1984.
182. K. Varela, H. D. Arman and F. K. Yoshimoto, *J. Nat. Prod.*, 2020, **83**, 66-78.
183. D. T. McQuade and P. H. Seeberger, *J. Org. Chem.*, 2013, **78**, 6384-6389.
184. L. Bryant, B. Flatley, C. Patole, G. D. Brown and R. Cramer, *BMC Plant Biol.*, 2015, **15**, 175.
185. K. Kakiuchi, T. Tsugaru, Y. Tobe and Y. Odaira, *J. Org. Chem.*, 1981, **46**, 4204-4208.
186. Z. Paryzek and I. Skiera, *Org. Prep. Proced. Int.*, 2007, **39**, 203-296.
187. M. Takashi, I. Sachihiko, O. Kenji, T. Nobuaki, K. Hideo, Y. Yasuhiro and F. Kenji, *Bull. Chem. Soc. Jpn.*, 1982, **55**, 891-898.
188. L.-K. Sy, N.-Y. Zhu and G. D. Brown, *Tetrahedron*, 2001, **57**, 8495-8510.
189. C. Singh, S. Chaudhary, R. Kanchan and S. K. Puri, *Org. Lett.*, 2007, **9**, 4327-4329.
190. S.-M. Hui, K.-S. Ngo and G. D. Brown, *J. Chem. Soc. Perkin Trans. 1*, 1997, 3435-3442.
191. H. Boufroura, R. Plais, S. Poyer, A. Gaucher, J. Marrot, G. Clavier, F.-X. Legrand, C. Huin, P. Guégan, D. Prim and J.-Y. Salpin, *RSC Advances*, 2020, **10**, 31670-31679.

192. S. K. Bharti and R. Roy, *Trends Anal. Chem.*, 2012, **35**, 5-26.
193. G. F. Pauli, B. U. Jaki and D. C. Lankin, *J. Nat. Prod.*, 2005, **68**, 133-149.

APPENDIX

Crystal Data for δ-lactone **33**



Crystal data for $C_{15}H_{22}O_3$ (250.34 g/mol): orthorhombic, space group $P2_12_12_1$, a = 4.88251(12) Å, b = 12.4849(3) Å, c = 22.5754(7) Å, β = 90°, α = 90°, γ = 90°, V = 1376.15(6) Å^3, Z = 4, T = 120 (2) K, ϱ_{calc} = 1.198 g/cm^3, Crystal size = 0.276 × 0.139 × 0.046 mm^{-3}, Radiation = Cu Kα (λ = 1.54184), Reflection collected = 15406, Independent reflection = 2728 [R_{int} = 0.0253, R_{sigma} = 0.0153]. The final R_1 was 0.0347 (I>=2σ(I)) and wR_2 was 0.0993

Empirical formular	$C_{15}H_{22}O_3$
Formula weight	250.34
Temperature/K	120(2)
Crystal system	Orthorhombic
Space group	$P2_12_12_1$
a/Å	4.88251(12)
b/Å	12.4849(3)
c/Å	22.5754(7)
α/°	90
β/°	90
γ/°	90
Volume/Å^3	1376.15(6)
Z	4
ϱ_{calc}g/cm^3	1.198
μ/mm^{-1}	0.661
F(000)	536.0
Crystal size/mm^3	0.276 × 0.139 × 0.046
Radiation	Cu Kα (λ = 1.54184)
2Θ range for data collection/°	7.832 to 146.338
Index ranges	-5 ≤ h ≤ 6, -15 ≤ k ≤ 15, -26 ≤ l ≤ 27
Reflections collected	15406
Independent reflections	2728 [R_{int} = 0.0253, R_{sigma} = 0.0153]
Data/restraints/parameters	2728/0/244
Goodness-of-fit on F^2	1.071
Final R indexes [I>=2σ (I)]	R_1 = 0.0347, wR_2 = 0.0993
Final R indexes [all data]	R_1 = 0.0359, wR_2 = 0.1009
Largest diff. peak/hole / e Å^{-3}	0.56/-0.17
Flack parameter	-0.08(6)

Table 1 Fractional Atomic Coordinates ($\times 10^4$) and Equivalent Isotropic Displacement Parameters ($Å^2 \times 10^3$) for 33. U_{eq} is defined as 1/3 of the trace of the orthogonalised U_{IJ} tensor.

Atom	*x*	*y*	*Z*	U(eq)
O1	-10690(3)	-7372.2(10)	-5510.1(6)	22.8(3)
O2	-11059(3)	-5750.6(11)	-5145.5(6)	28.7(3)
O3	-9297(4)	-11582.4(14)	-6239.7(8)	45.1(5)
C30	-7598(4)	-7781.3(13)	-6314.0(8)	18.2(4)
C23	-7032(4)	-6092.5(14)	-5732.8(8)	20.3(4)
C31	-9470(4)	-8069.7(14)	-5920.1(8)	20.4(4)
C32	-9738(4)	-6352.4(14)	-5448.5(8)	21.0(4)
C33	-6697(4)	-8475.7(14)	-6828.0(8)	19.7(4)
C34	-6616(4)	-6638.0(14)	-6335.1(8)	19.7(4)
C35	-7969(4)	-6119.2(15)	-6876.4(8)	22.4(4)
C36	-7899(4)	-7958.0(14)	-7396.3(8)	21.3(4)
C37	-7453(4)	-9660.9(14)	-6757.8(9)	22.2(4)
C24	-5671(5)	-11811.9(16)	-5551.7(10)	31.5(5)
C25	-5922(4)	-10202.9(14)	-6252.8(8)	22.2(4)
C26	-6904(5)	-8503.9(16)	-7966.5(9)	28.5(4)
C27	-7208(4)	-6758.7(14)	-7431.4(9)	24.0(4)
C28	-7169(4)	-11240.1(14)	-6039.2(9)	24.4(4)
C29	-6529(5)	-4882.8(15)	-5737.6(10)	27.7(4)

Table 2 Anisotropic Displacement Parameters ($Å^2 \times 10^3$) for NSMWGB. The Anisotropic displacement factor exponent takes the form: $-2\pi^2[h^2a^{*2}U_{11}+2hka^*b^*U_{12}+\ldots]$.

Atom	U_{11}	U_{22}	U_{33}	U_{23}	U_{13}	U_{12}
O1	23.4(6)	22.6(6)	22.3(6)	-0.7(5)	4.7(5)	-1.5(5)
O2	28.1(7)	29.8(7)	28.0(7)	-6.7(6)	3.8(6)	2.0(6)
O3	42.8(9)	39.3(8)	53.1(10)	17.5(7)	-18.9(9)	-17.9(7)
C30	19.0(8)	17.0(7)	18.5(8)	1.3(6)	-1.9(6)	0.6(6)
C23	20.3(8)	19.0(7)	21.7(9)	0.3(7)	0.3(7)	-1.0(7)
C31	20.6(8)	18.8(8)	21.8(9)	0.1(6)	1.0(7)	-0.4(7)
C32	22.4(8)	22.2(8)	18.4(8)	-0.4(7)	-1.8(7)	0.2(7)
C33	20.7(8)	18.1(8)	20.4(9)	-0.2(6)	1.9(7)	0.2(7)
C34	18.6(8)	18.2(8)	22.3(9)	1.1(6)	1.0(6)	-1.3(6)
C35	27.3(9)	17.1(8)	22.7(9)	2.6(7)	1.0(8)	0.4(7)
C36	22.8(9)	21.3(8)	19.9(9)	1.4(7)	1.1(7)	-0.6(7)
C37	24.4(9)	18.5(8)	23.7(9)	0.4(7)	-0.7(8)	-0.3(7)
C24	40.9(11)	24.4(9)	29.3(10)	5.3(8)	-4.2(10)	-2.9(9)
C25	25.5(9)	18.4(8)	22.6(9)	-0.1(7)	-0.5(8)	-0.6(7)
C26	39.7(12)	25.5(9)	20.3(9)	-0.8(7)	3.1(8)	1.7(9)
C27	30.3(10)	21.5(8)	20.2(9)	3.0(7)	1.8(8)	-0.4(7)
C28	28.2(9)	20.6(8)	24.6(9)	1.1(7)	-0.3(8)	-1.9(7)

Table 2 Anisotropic Displacement Parameters ($Å^2×10^3$) for NSMWGB. The Anisotropic displacement factor exponent takes the form: $-2\pi^2[h^2a^{*2}U_{11}+2hka^*b^*U_{12}+\ldots]$.

Atom	U_{11}	U_{22}	U_{33}	U_{23}	U_{13}	U_{12}
C29	34.1(11)	20.0(8)	28.9(10)	-2.1(8)	0.7(8)	-2.9(8)

Table 3 Bond Lengths for 33.

Atom	Atom	Length/Å	Atom	Atom	Length/Å
O1	C31	1.403(2)	C33	C36	1.552(2)
O1	C32	1.362(2)	C33	C37	1.533(2)
O2	C32	1.203(2)	C34	C35	1.533(3)
O3	C28	1.211(3)	C35	C27	1.531(3)
C30	C31	1.325(3)	C36	C26	1.535(3)
C30	C33	1.514(2)	C36	C27	1.537(2)
C30	C34	1.506(2)	C37	C25	1.522(3)
C23	C32	1.504(3)	C24	C28	1.502(3)
C23	C34	1.534(2)	C25	C28	1.510(2)
C23	C29	1.530(2)			

Table 4 Bond Angles for 33.

Atom	Atom	Atom	Angle/°	Atom	Atom	Atom	Angle/°
C32	O1	C31	120.17(14)	C30	C34	C23	110.52(15)
C31	C30	C33	124.00(15)	C30	C34	C35	106.77(15)
C31	C30	C34	119.87(16)	C35	C34	C23	117.52(15)
C34	C30	C33	115.22(15)	C27	C35	C34	109.12(15)
C32	C23	C34	113.49(15)	C26	C36	C33	112.86(15)
C32	C23	C29	110.92(15)	C26	C36	C27	108.64(15)
C29	C23	C34	114.24(15)	C27	C36	C33	111.43(15)
C30	C31	O1	124.52(16)	C25	C37	C33	112.85(15)
O1	C32	C23	117.22(15)	C28	C25	C37	115.00(16)
O2	C32	O1	117.31(16)	C35	C27	C36	114.35(15)
O2	C32	C23	125.35(16)	O3	C28	C24	121.59(18)
C30	C33	C36	106.58(14)	O3	C28	C25	121.94(18)
C30	C33	C37	113.80(15)	C24	C28	C25	116.45(17)
C37	C33	C36	113.36(15)				

Table 5 Torsion Angles for 33.

A	B	C	D	Angle/°	A	B	C	D	Angle/°
C30	C33	C36	C26	173.78(16)	C33	C37	C25	C28	161.85(16)
C30	C33	C36	C27	51.22(19)	C34	C30	C31	O1	0.9(3)

Table 5 Torsion Angles for 33.

A	B	C	D	Angle/°	A	B	C	D	Angle/°
C30	C33	C37	C25	-66.7(2)	C34	C30	C33	C36	-60.87(19)
C30	C34	C35	C27	-57.55(19)	C34	C30	C33	C37	173.44(15)
C23	C34	C35	C27	177.72(16)	C34	C23	C32	O1	38.0(2)
C31	O1	C32	O2	171.16(16)	C34	C23	C32	O2	-146.14(18)
C31	O1	C32	C23	-12.7(2)	C34	C35	C27	C36	55.0(2)
C31	C30	C33	C36	108.15(19)	C36	C33	C37	C25	171.30(15)
C31	C30	C33	C37	-17.5(3)	C37	C33	C36	C26	-60.3(2)
C31	C30	C34	C23	24.3(2)	C37	C33	C36	C27	177.17(15)
C31	C30	C34	C35	-104.57(19)	C37	C25	C28	O3	-3.2(3)
C32	O1	C31	C30	-8.0(3)	C37	C25	C28	C24	178.46(17)
C32	C23	C34	C30	-42.1(2)	C26	C36	C27	C35	-177.29(16)
C32	C23	C34	C35	80.7(2)	C29	C23	C32	O1	168.21(15)
C33	C30	C31	O1	-167.65(16)	C29	C23	C32	O2	-16.0(3)
C33	C30	C34	C23	-166.16(15)	C29	C23	C34	C30	-170.65(15)
C33	C30	C34	C35	64.93(19)	C29	C23	C34	C35	-47.8(2)
C33	C36	C27	C35	-52.3(2)					

Table 6 Hydrogen Atom Coordinates (Å×10^4) and Isotropic Displacement Parameters (Å^2×10^3) for 33.

Atom	*x*	*Y*	*Z*	U(eq)
H36	-9870(50)	-8046(19)	-7380(11)	22(6)
H35A	-10050(50)	-6106(18)	-6815(10)	20(5)
H24A	-3660(70)	-11910(20)	-5694(14)	50(8)
H26A	-4900(60)	-8460(20)	-8002(13)	41(7)
H34	-4700(50)	-6628(18)	-6412(10)	19(5)
H27A	-5280(60)	-6660(20)	-7502(12)	30(6)
H35B	-7310(60)	-5400(20)	-6934(12)	33(7)
H37	-9390(60)	-9710(20)	-6713(12)	34(7)
H25A	-4000(70)	-10360(20)	-6366(13)	41(7)
H25B	-5690(60)	-9750(20)	-5908(11)	31(6)
H29A	-6530(60)	-4600(20)	-5342(12)	31(6)
H31	-10210(50)	-8769(18)	-5889(9)	18(5)
H23	-5760(50)	-6422(19)	-5464(10)	20(5)
H29B	-4740(60)	-4750(20)	-5914(12)	34(7)
H26B	-7410(60)	-9300(20)	-7984(12)	39(7)
H29C	-8130(60)	-4510(20)	-5941(14)	41(7)
H24B	-5720(60)	-11400(20)	-5188(13)	42(7)
H33	-4680(50)	-8413(19)	-6859(10)	18(5)
H26C	-7570(70)	-8150(30)	-8321(16)	56(9)
H27B	-8120(60)	-6480(20)	-7787(13)	38(7)

NMR Data

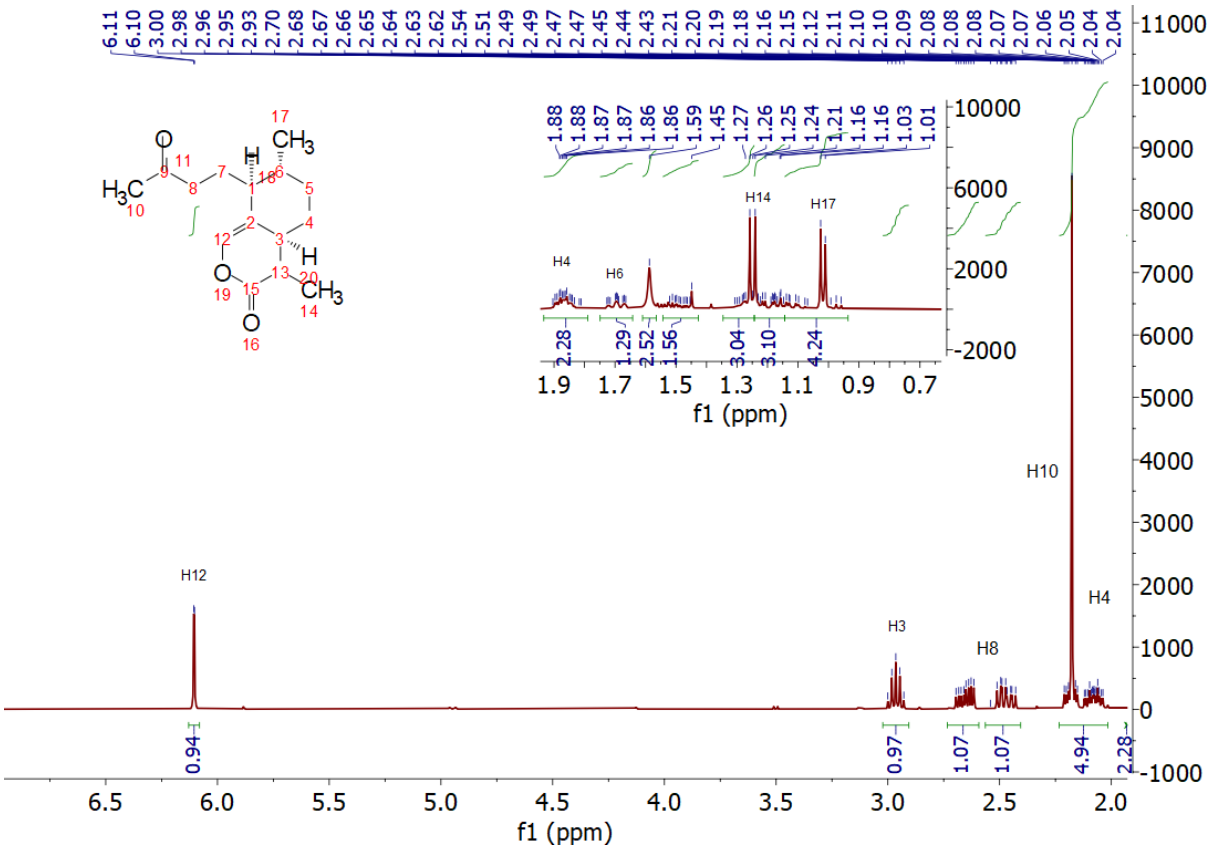


Figure 1: ^{1}H-NMR spectrum of δ-lactone **33** in $CDCl_3$

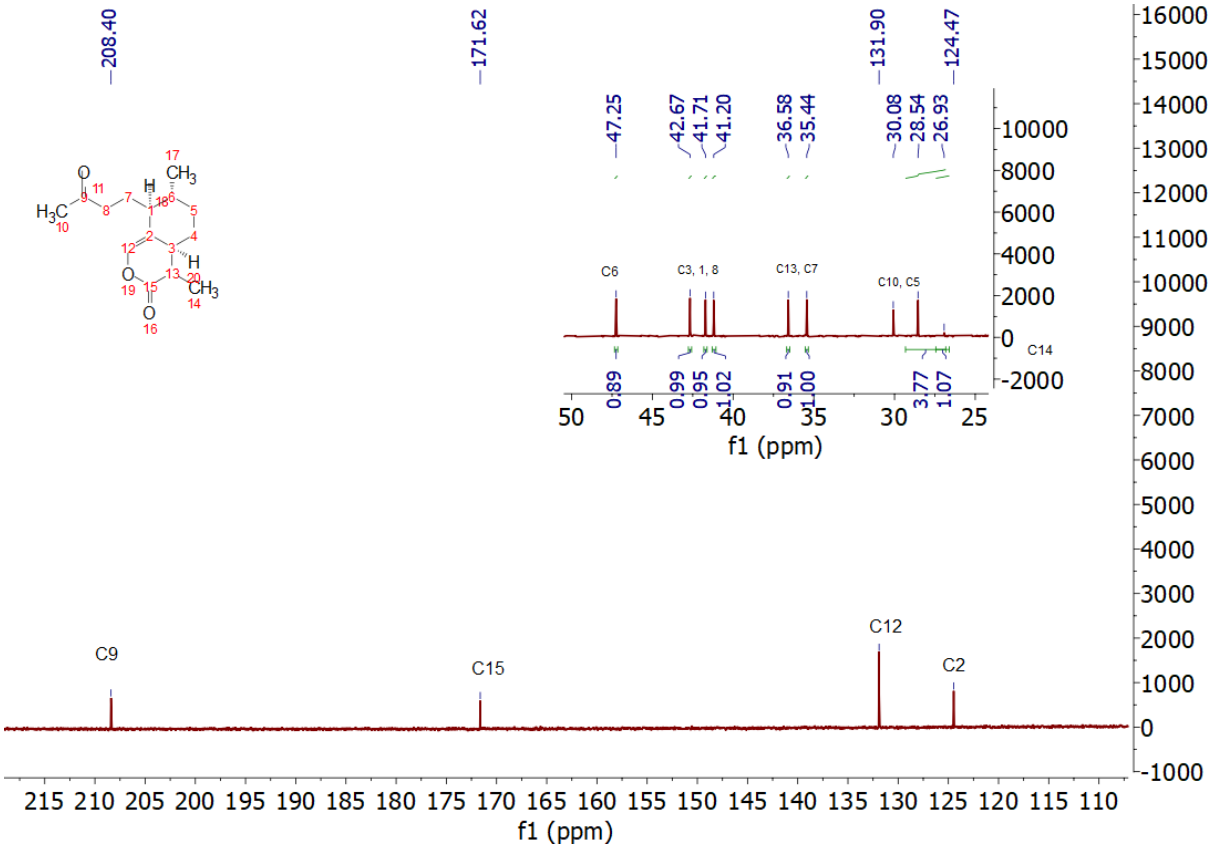


Figure 2: ^{13}C-NMR spectrum of δ-lactone **33** in $CDCl_3$

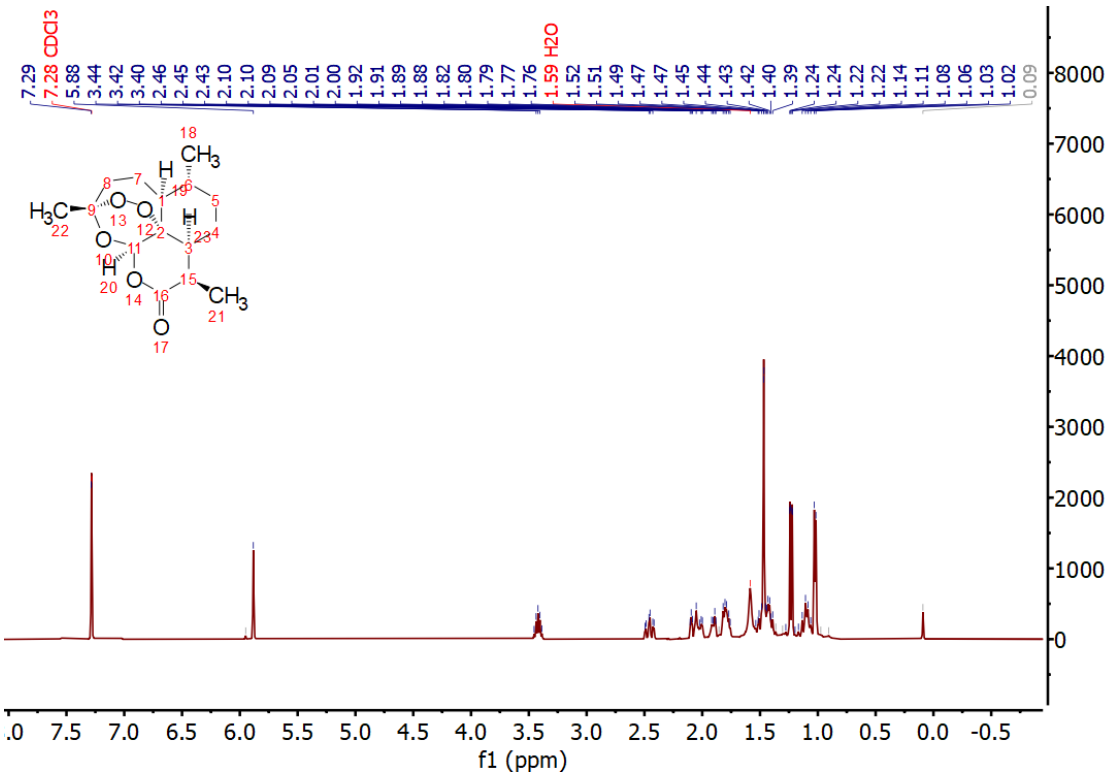


Figure 3: ^{1}H-NMR spectrum of Artemisinin **1** in $CDCl_3$

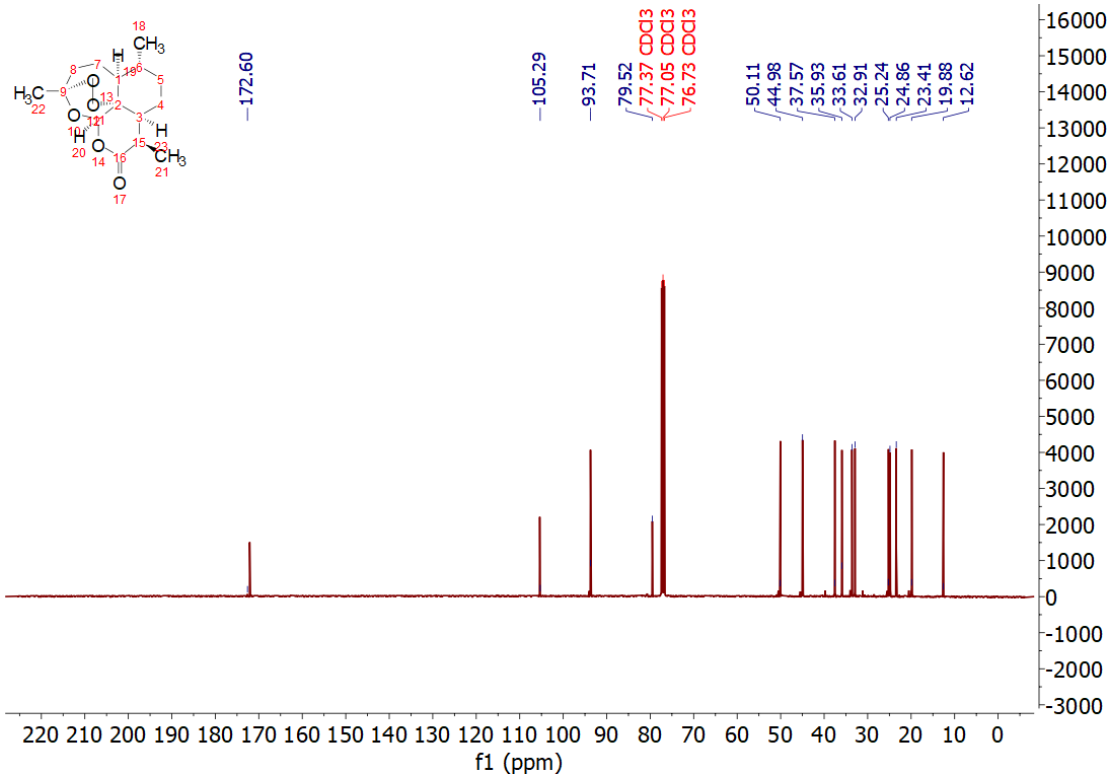


Figure 4: ^{13}C-NMR spectrum of Artemisinin **1** in $CDCl_3$

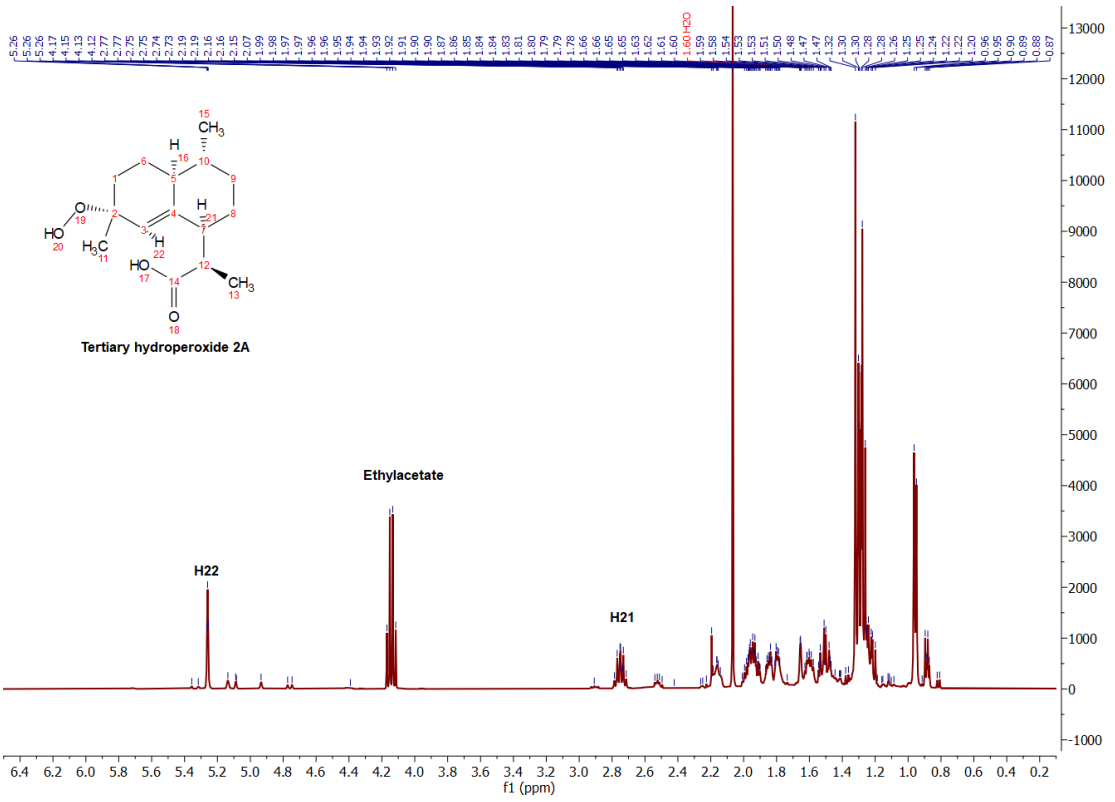


Figure 5: ^{1}H-NMR spectrum of tertiary hydroperoxide **2A** obtained during the synthesis of Artemisinin **1** in ethylacetate, the NMR measurement was done in $CDCl_3$.

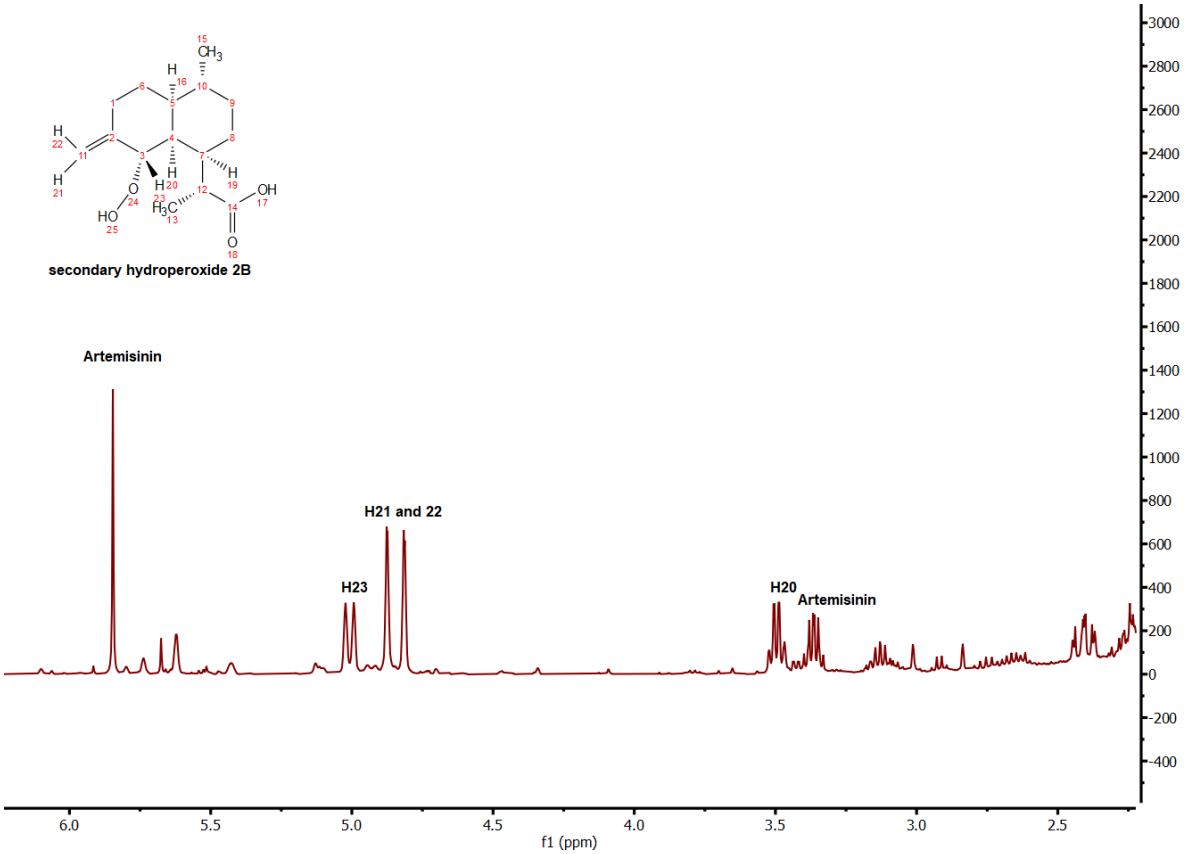


Figure 6: ^{1}H-NMR spectrum of secondary hydroperoxide **2B** obtained during the synthesis of Artemisinin **1** in ethylacetate, the NMR measurement was done in $CDCl_3$.

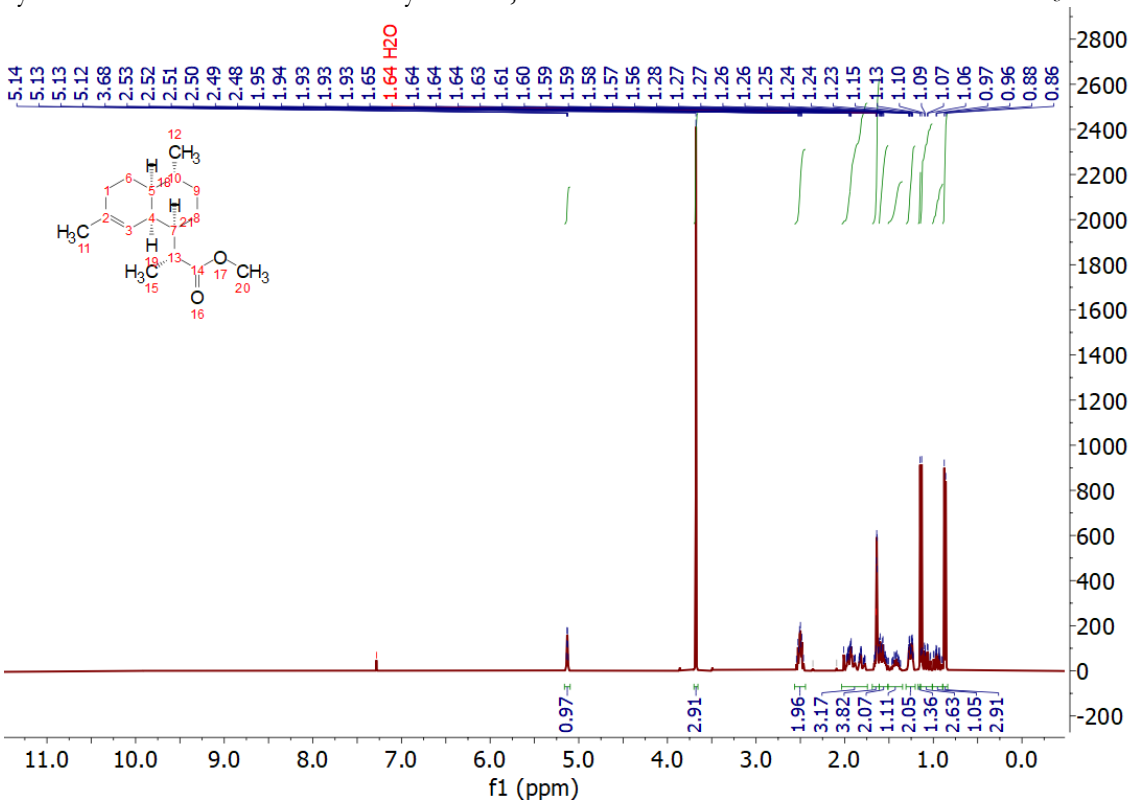


Figure 7: ^{1}H-NMR spectrum of DHAA methyl ester **8** in $CDCl_3$

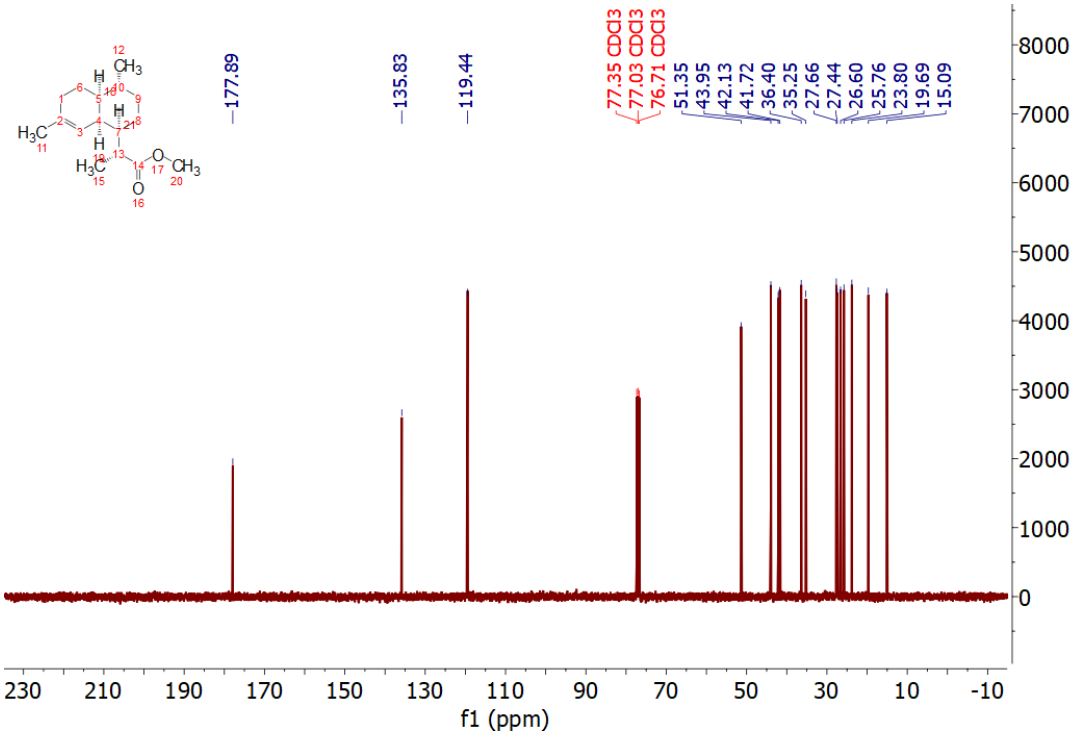


Figure 8: ^{13}C-NMR spectrum of DHAA methyl ester **8** in $CDCl_3$

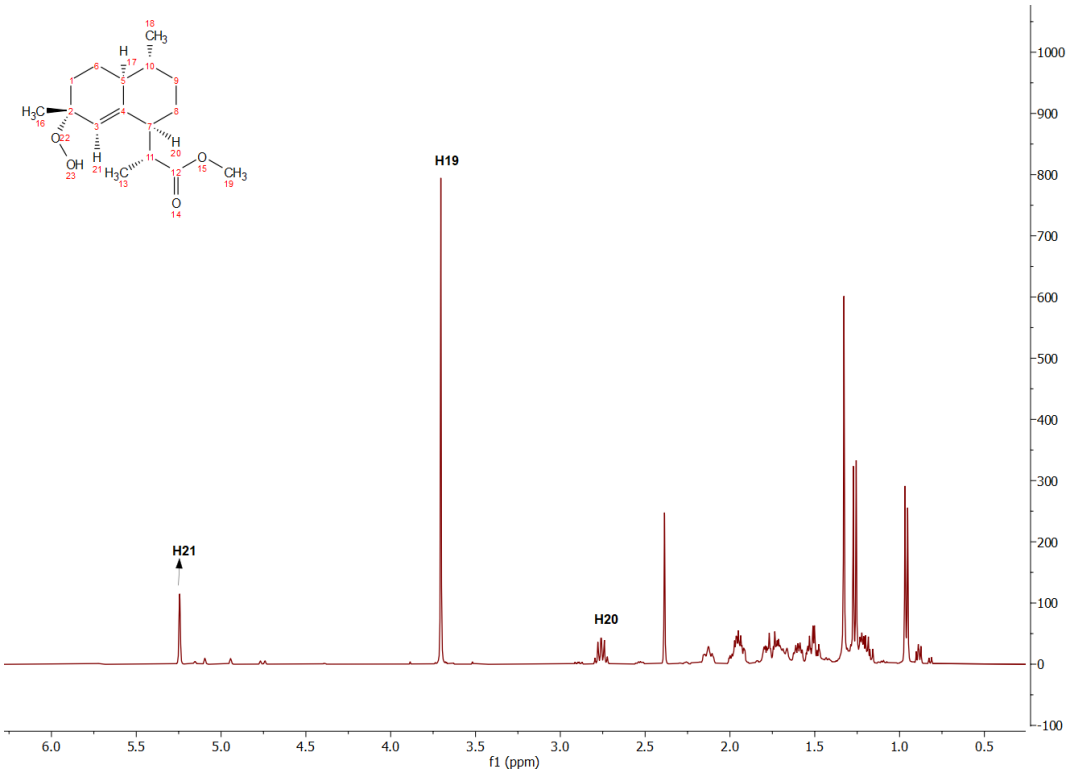


Figure 9: ^{1}H-NMR spectrum showing some peaks of tertiary hydroperoxides **94A** of DHAA methylester.

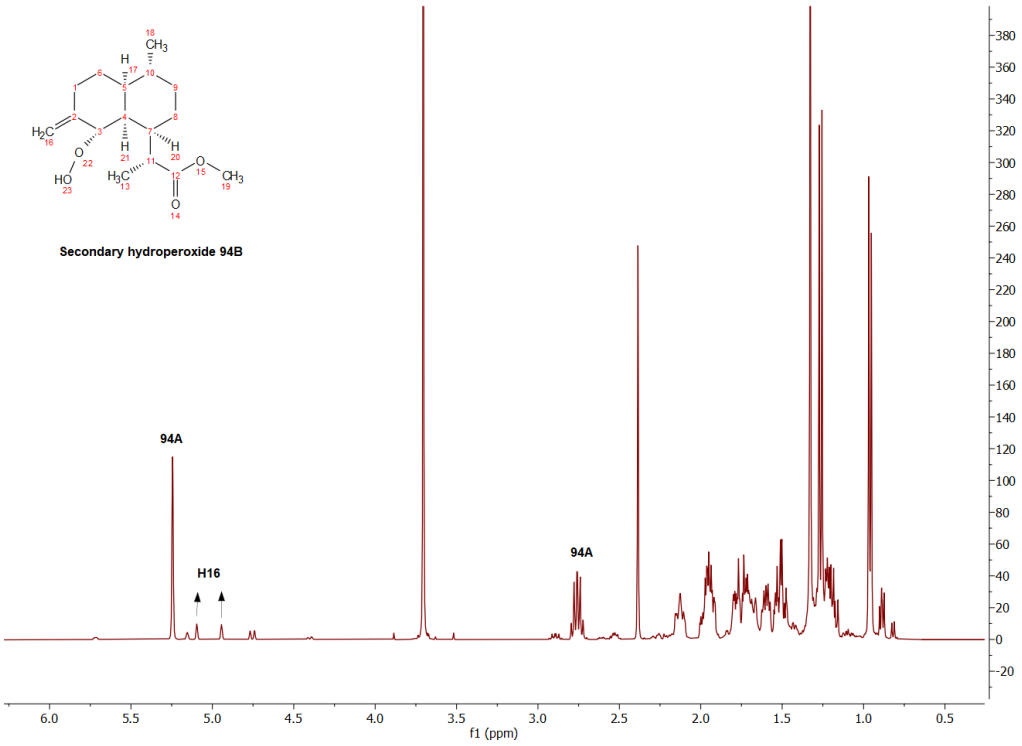


Figure 10: ^{1}H-NMR spectrum showing some peaks of secondary hydroperoxides **94B** of DHAA methylester.

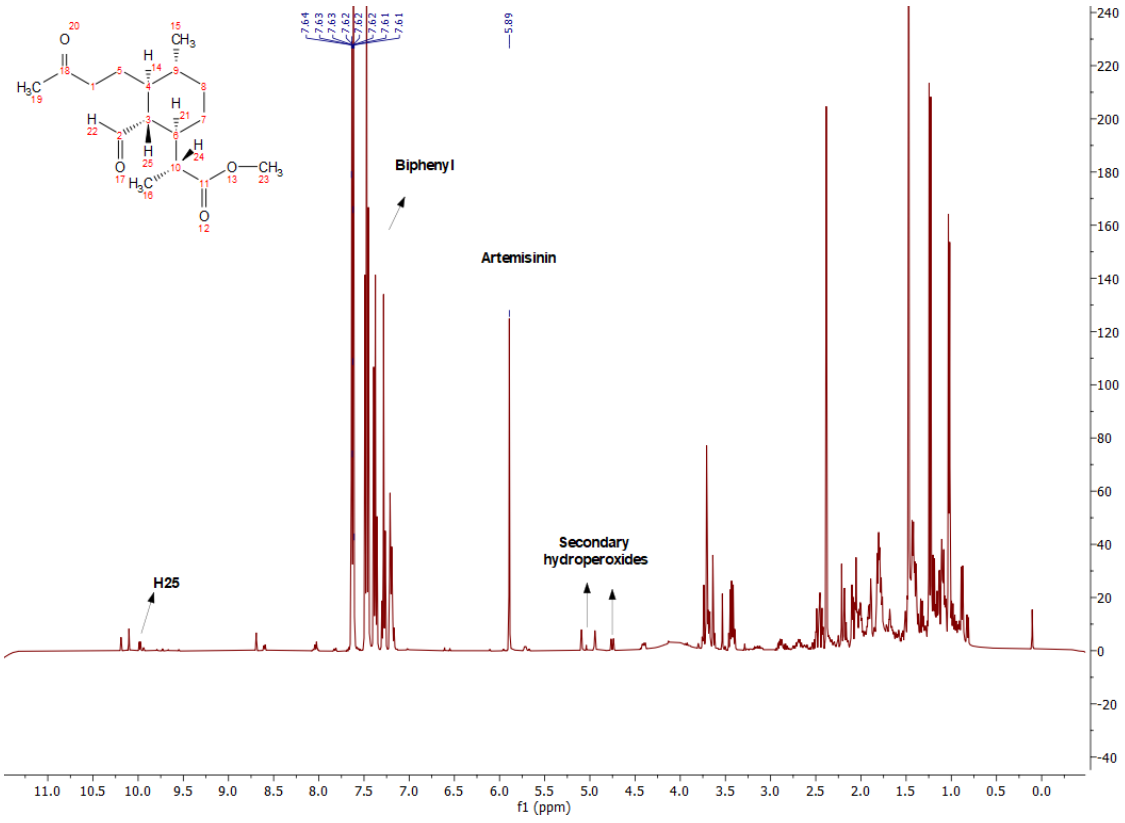


Figure 11: ^{1}H-NMR spectrum showing some peaks and aldehyde (**99**) and secondary hydroperoxides (**94B** and **C**) of DHAA methylester.

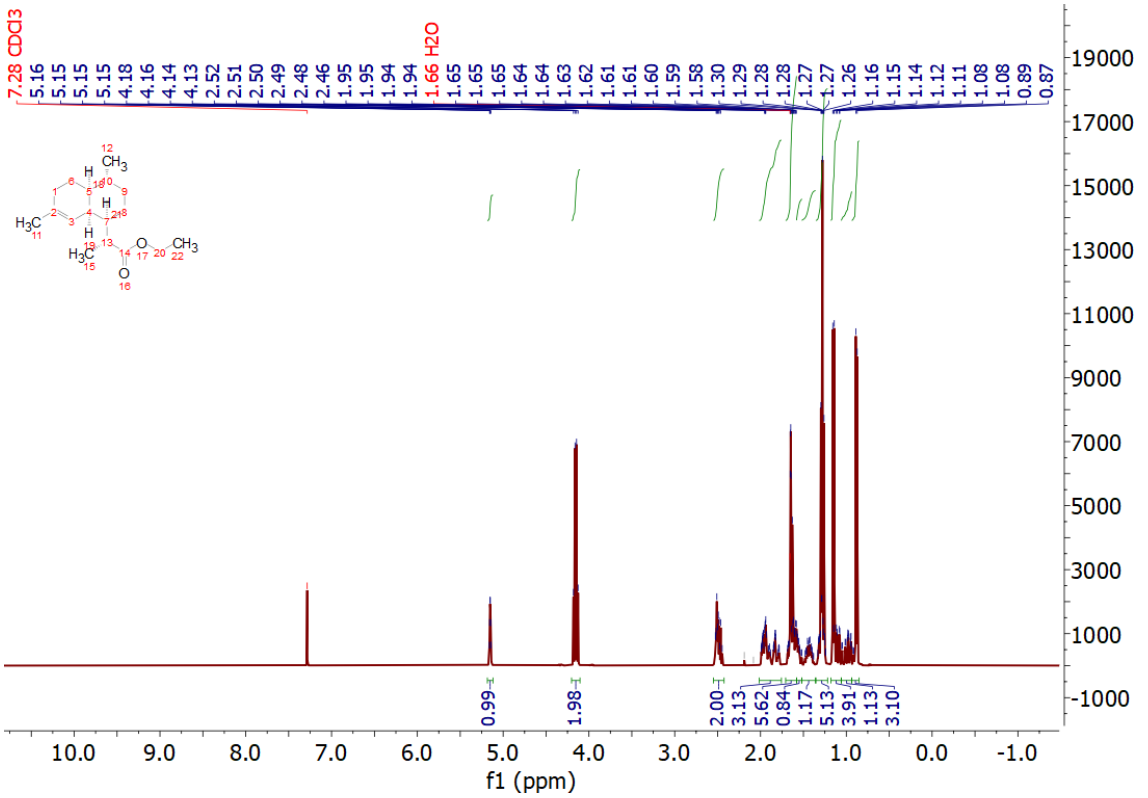


Figure 12: ^{1}H-NMR spectrum of DHAA ethyl ester **90** in $CDCl_3$

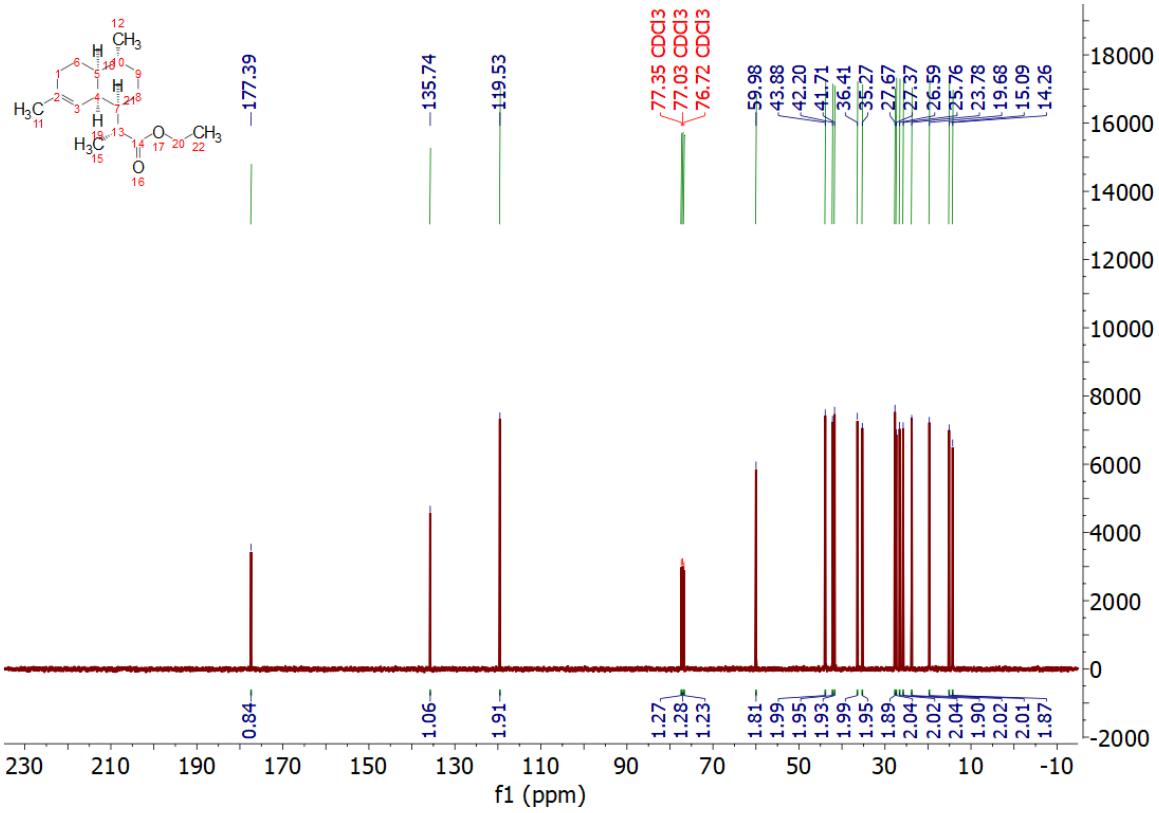


Figure 13: ^{13}C-NMR spectrum of DHAA ethyl ester **90** in $CDCl_3$

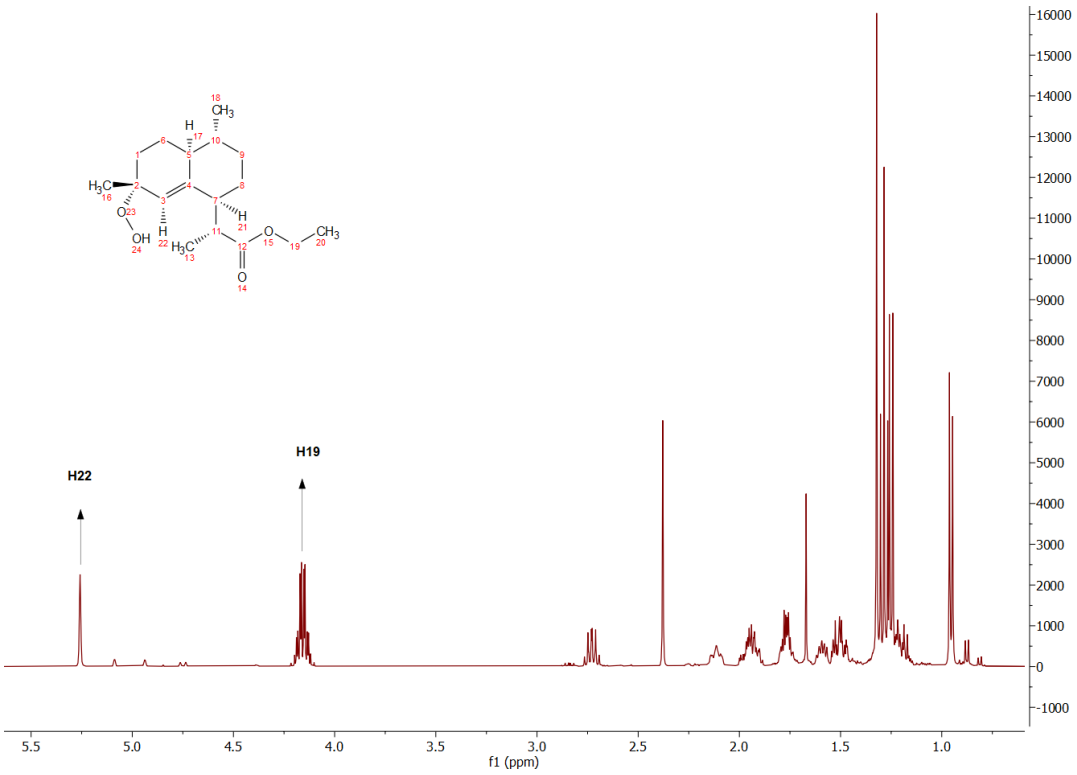


Figure 14: ^{1}H-NMR spectrum showing some peaks of tertiary hydroperoxides **96A** of DHAA ethylester.

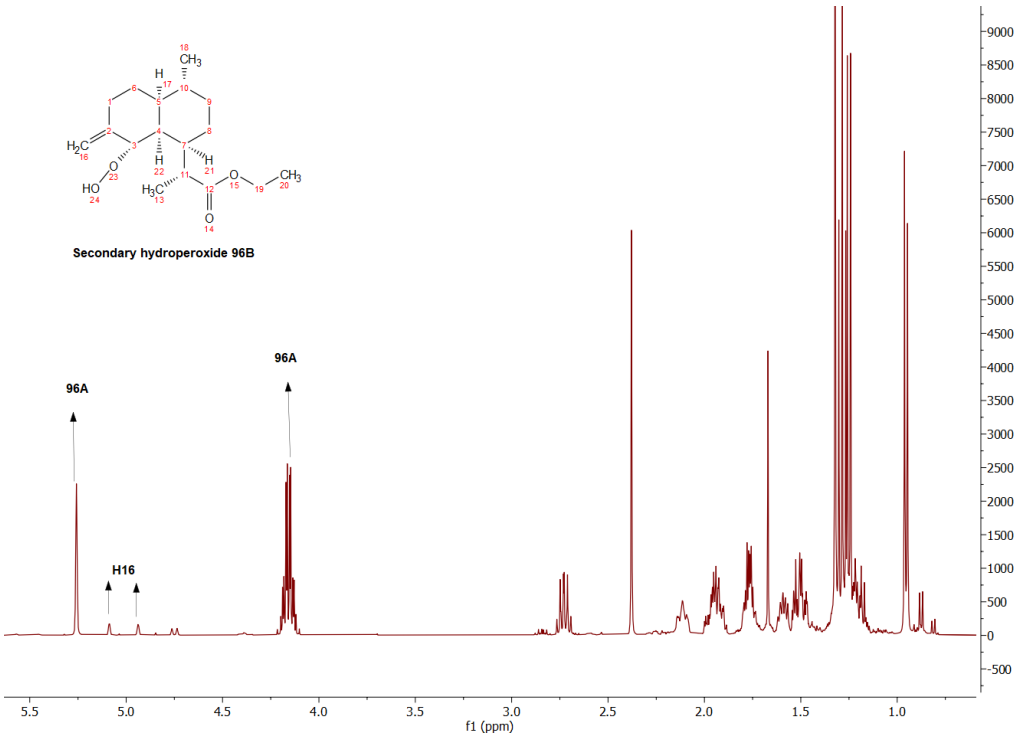


Figure 15: ^{1}H-NMR spectrum showing some peaks of secondary hydroperoxides **96B** of DHAA ethylester.

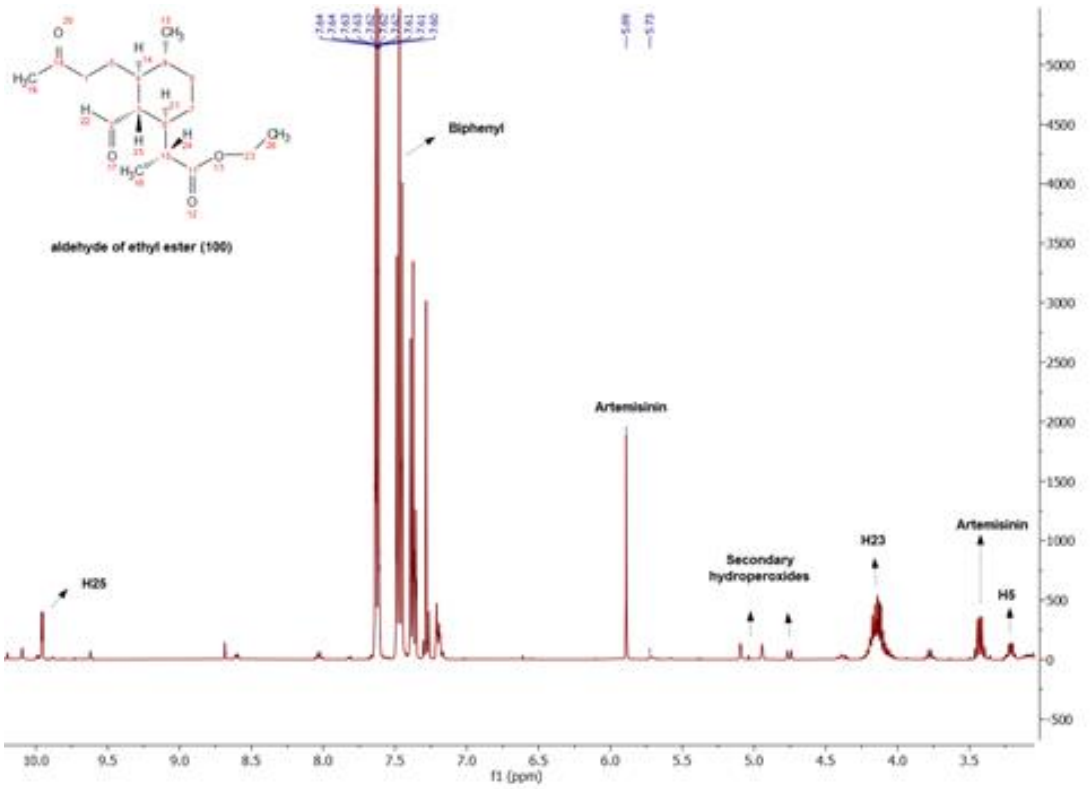


Figure 16: proton-NMR spectrum showing some peaks and aldehyde (**100**) and secondary hydroperoxides (**96B** and **C**) of DHAA ethylester.

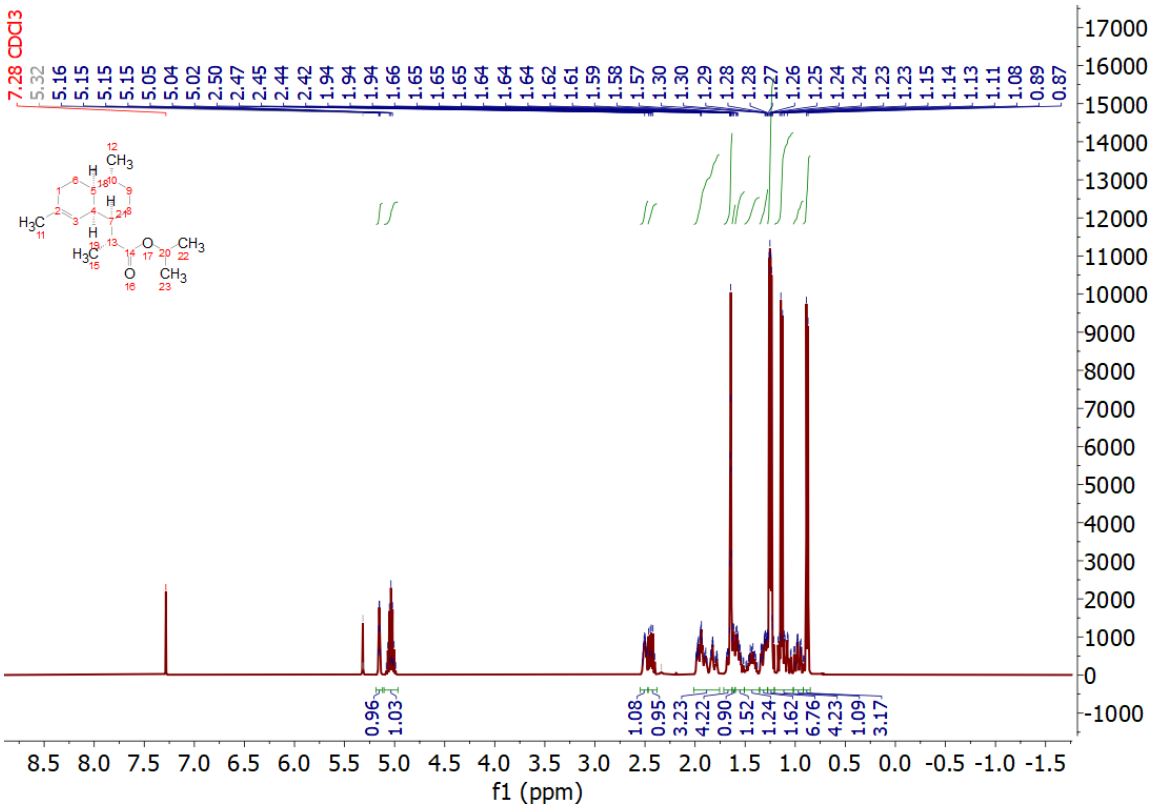


Figure 17: ^{1}H-NMR spectrum of DHAA isopropyl ester **91** in $CDCl_3$

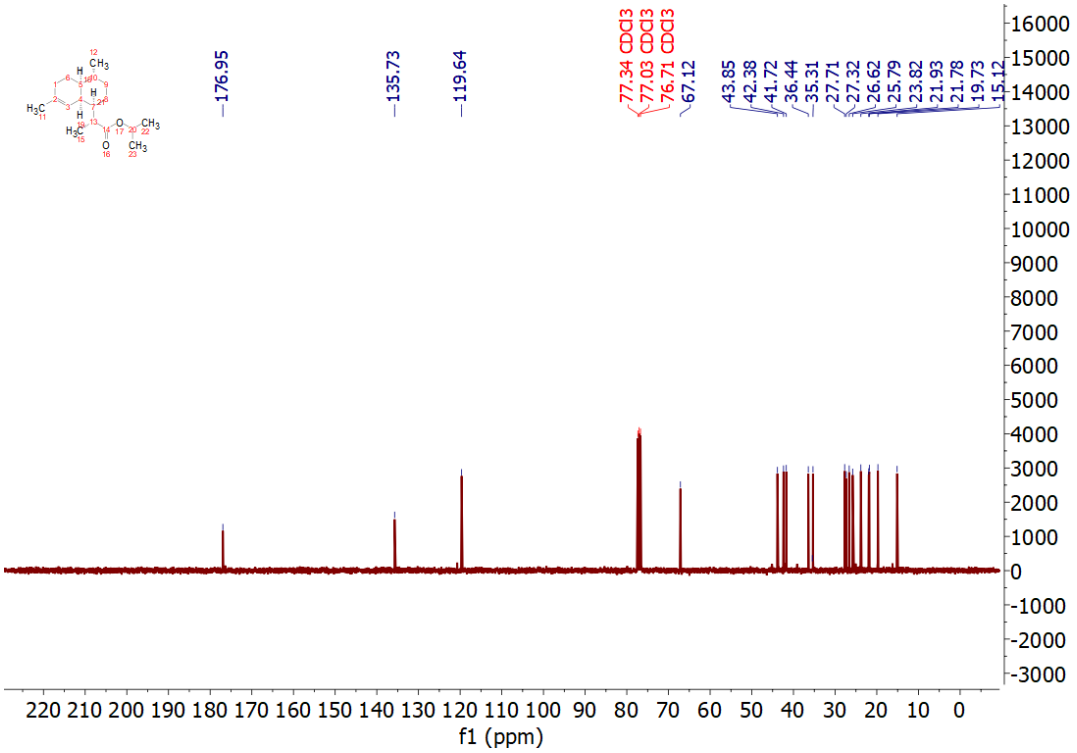


Figure 18: ^{13}C-NMR spectrum of DHAA isopropyl ester **91** in $CDCl_3$

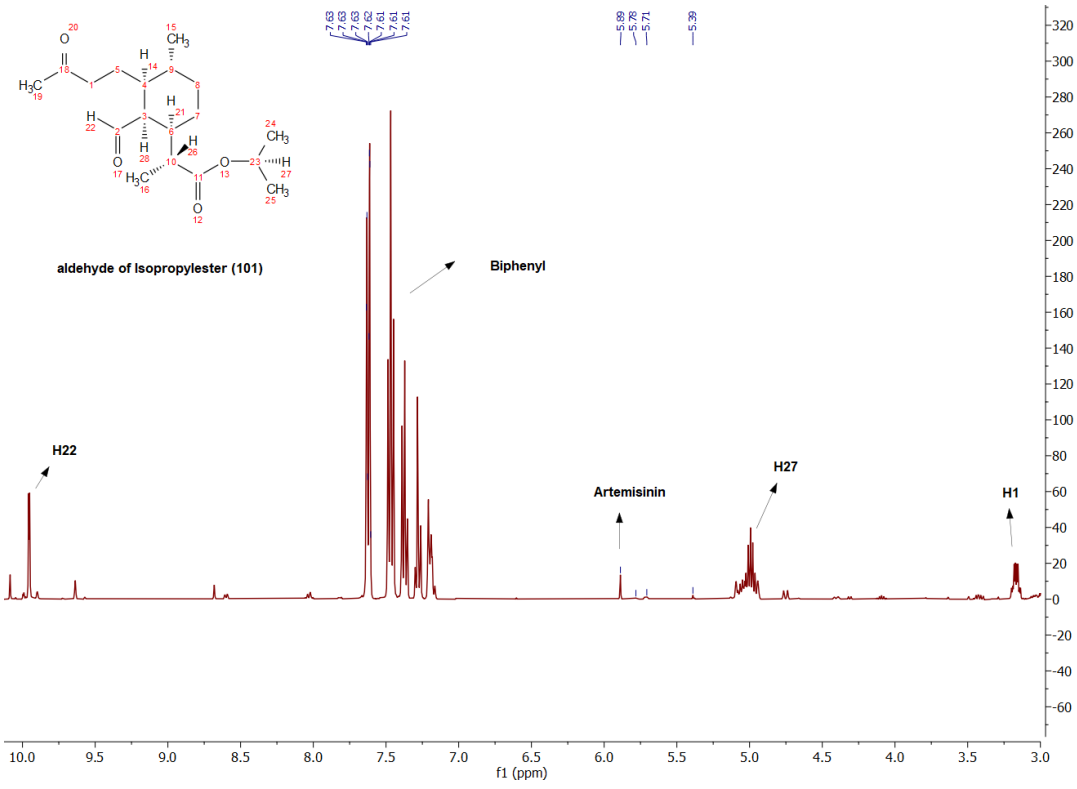


Figure 19: ^{1}H-NMR spectrum showing some peaks of an aldehyde (**101**) of DHAA isopropylester.

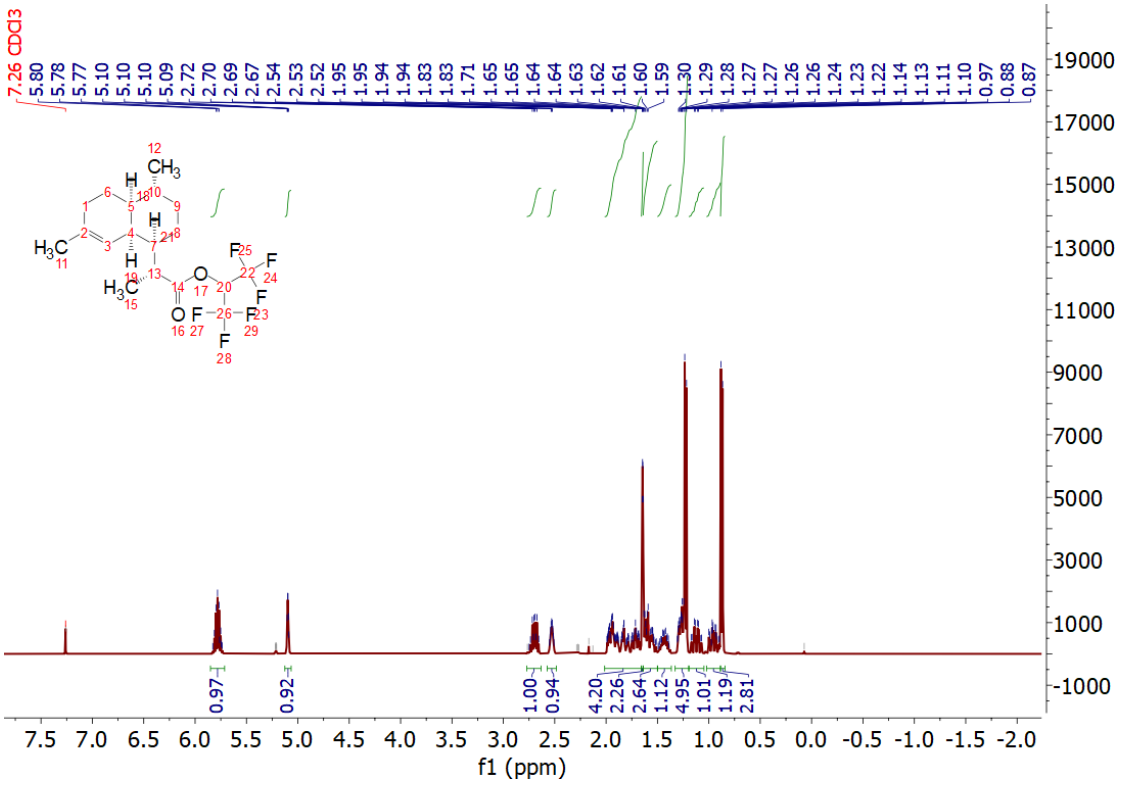


Figure 20: ^{1}H-NMR spectrum of DHAA hexafluoro isopropyl ester **92** in $CDCl_3$

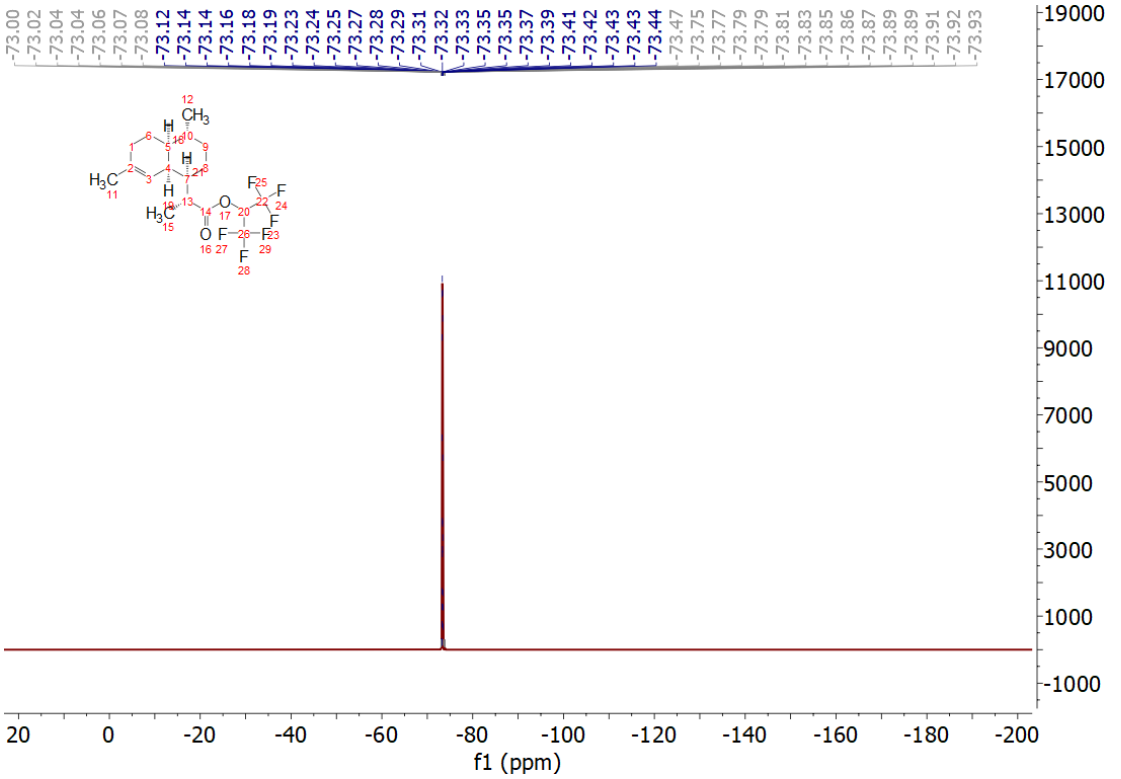


Figure 21: ^{19}F-NMR spectrum of DHAA hexafluoro isopropyl ester **92** in $CDCl_3$

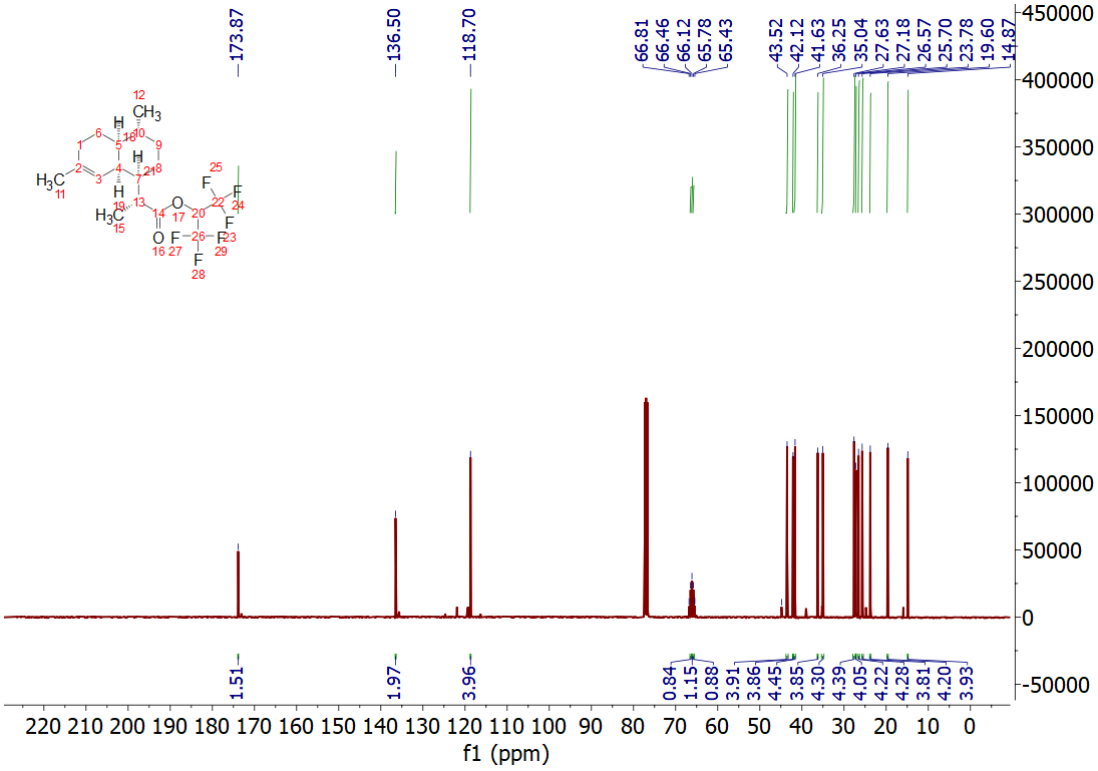


Figure 22: ^{13}C-NMR spectrum of DHAA hexafluoro isopropyl ester **92** in $CDCl_3$

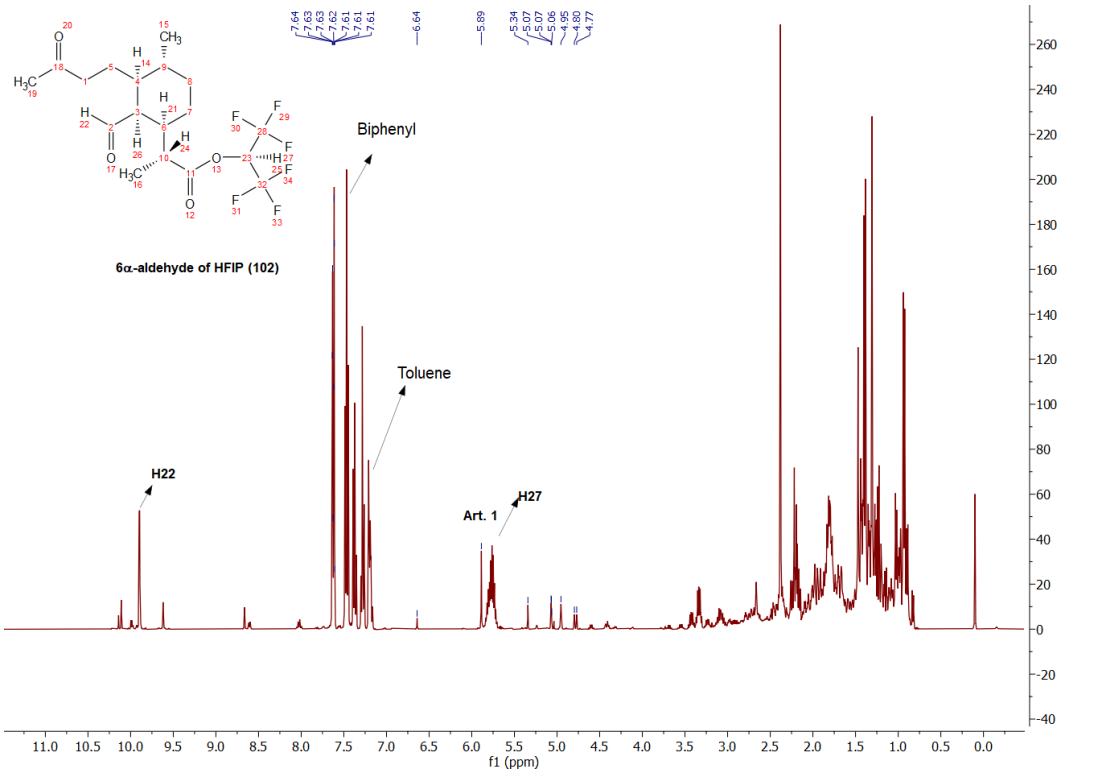


Figure 23: ^{1}H-NMR spectrum showing some peaks of an aldehyde (**102**) of DHAA hexaflouroisopropylester.

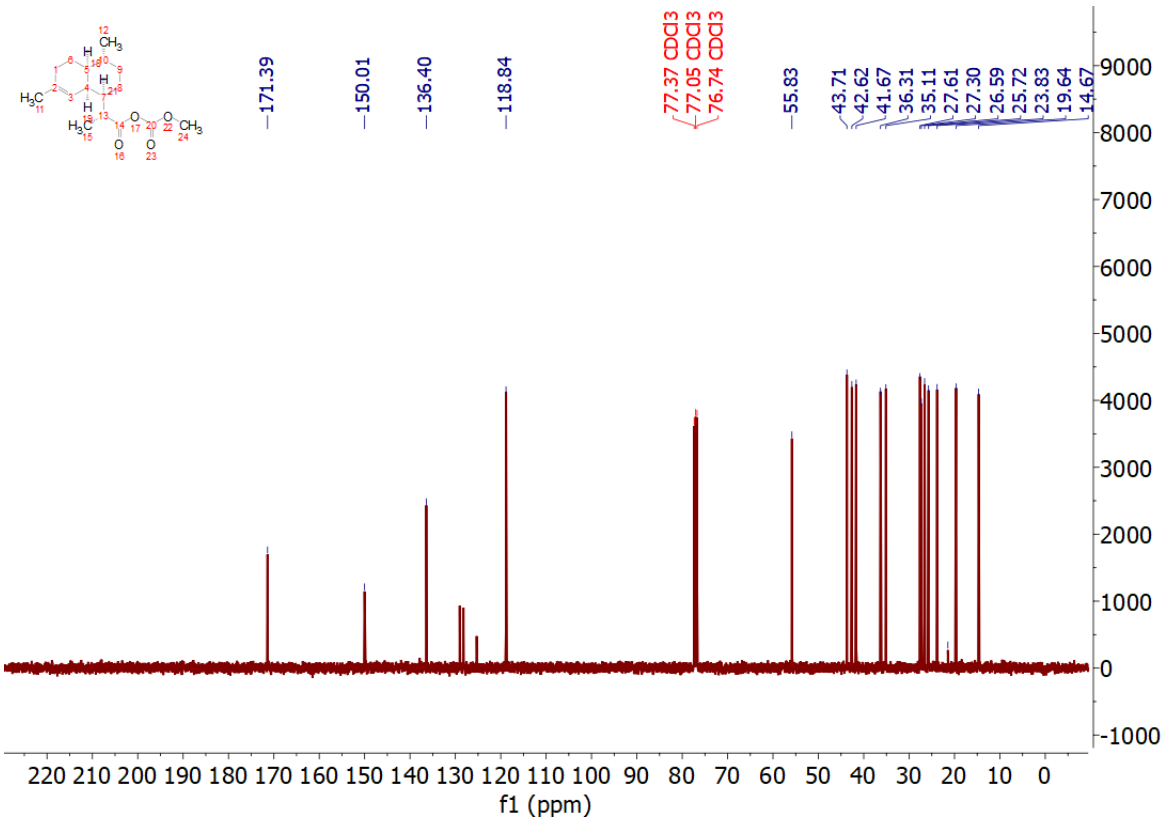


Figure 24: ^{13}C-NMR spectrum of DHAA methyl carbonate **93** in $CDCl_3$

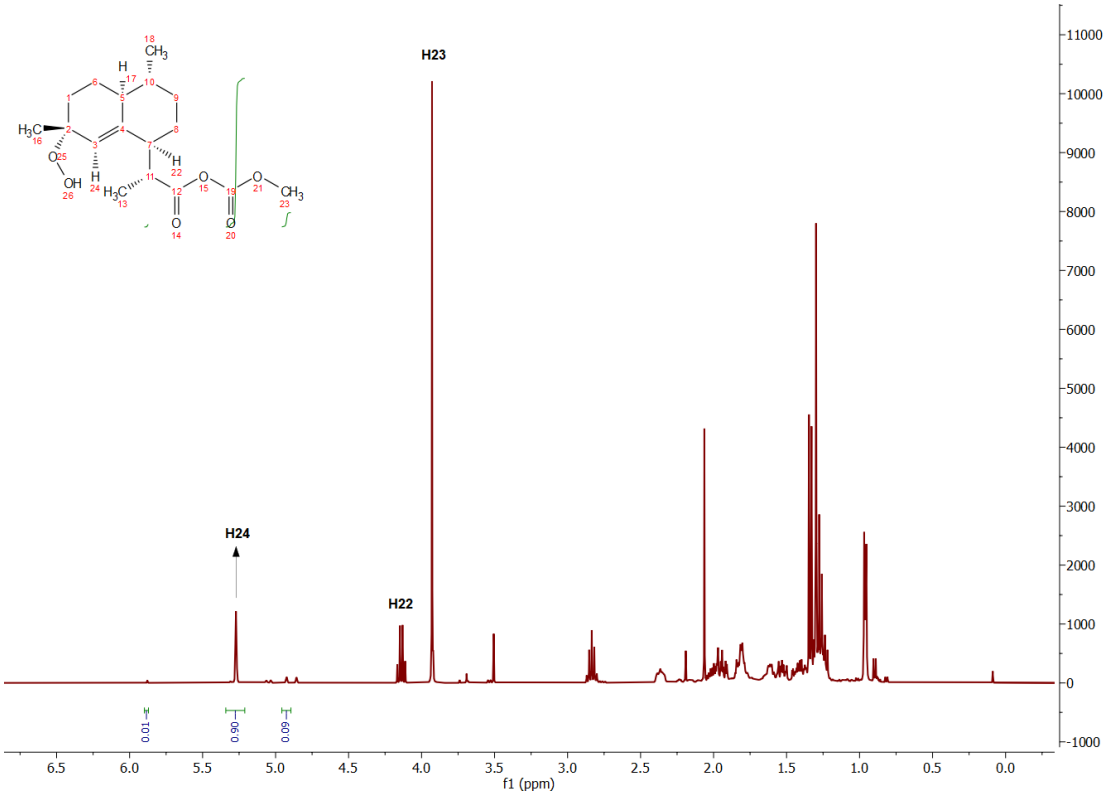


Figure 25: ^{1}H-NMR spectrum showing some peaks tertiary hydroperoxide (**95A**) of DHAA methylcarbonate.

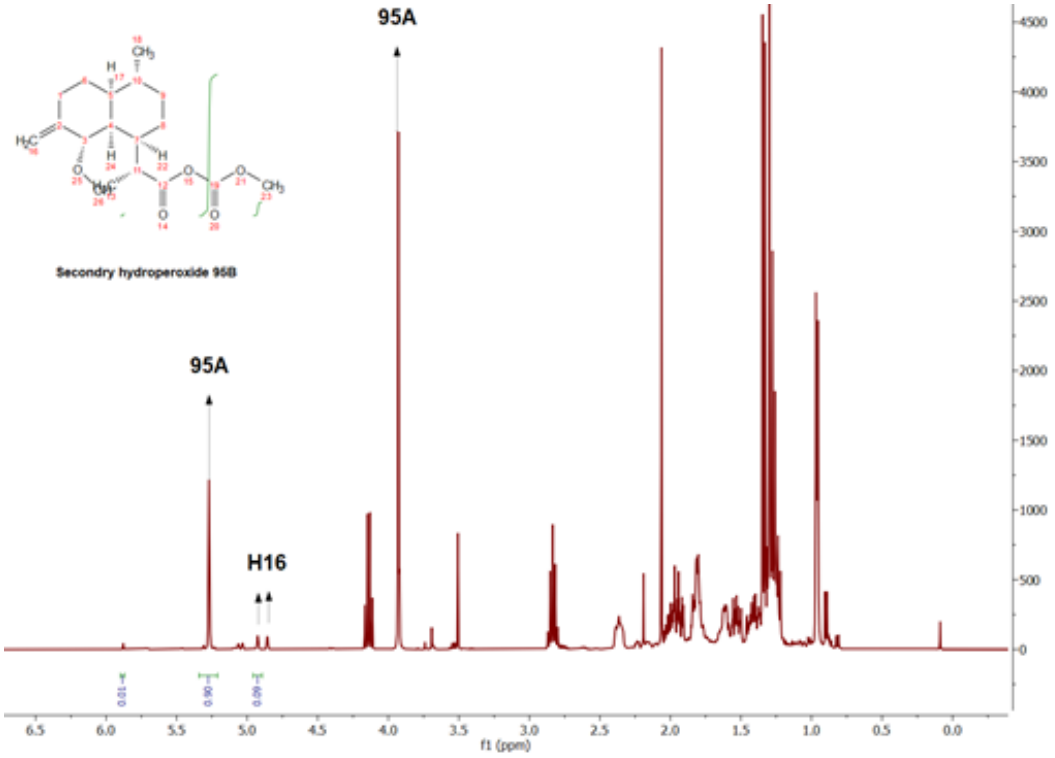


Figure 26: proton-NMR spectrum showing some peaks secondary hydroperoxide (**95B**) of DHAA methylcarbonate.

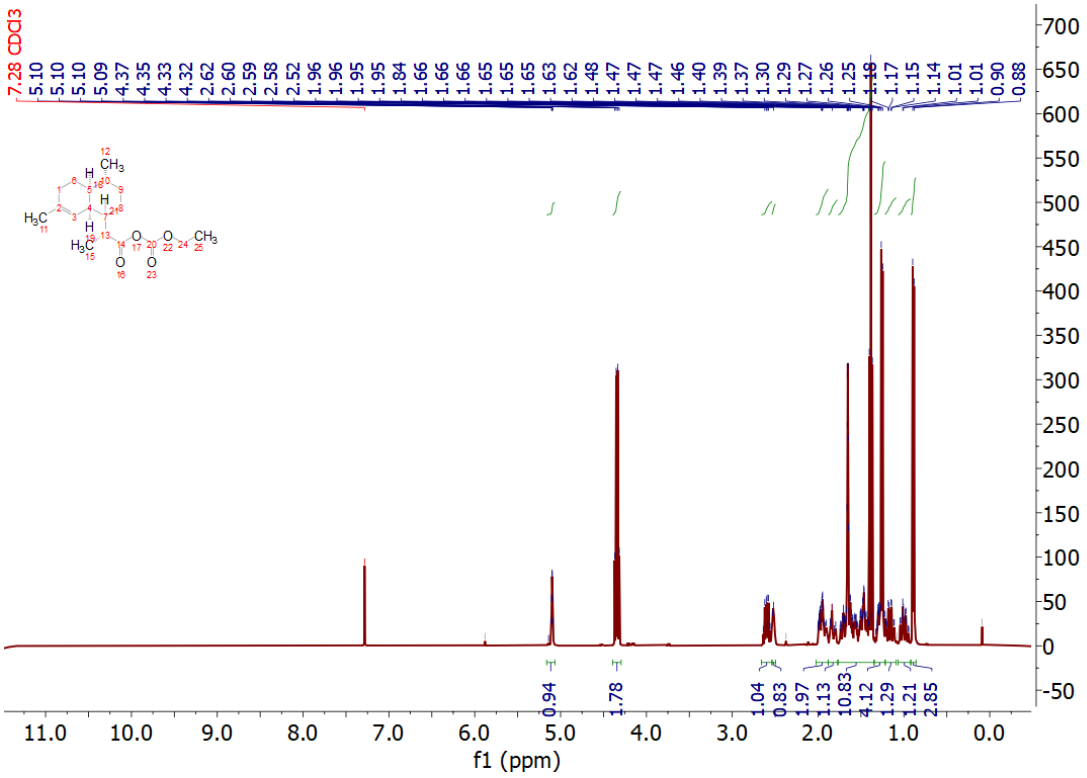


Figure 27: proton-NMR spectrum of DHAA ethyl carbonate **43** in $CDCl_3$

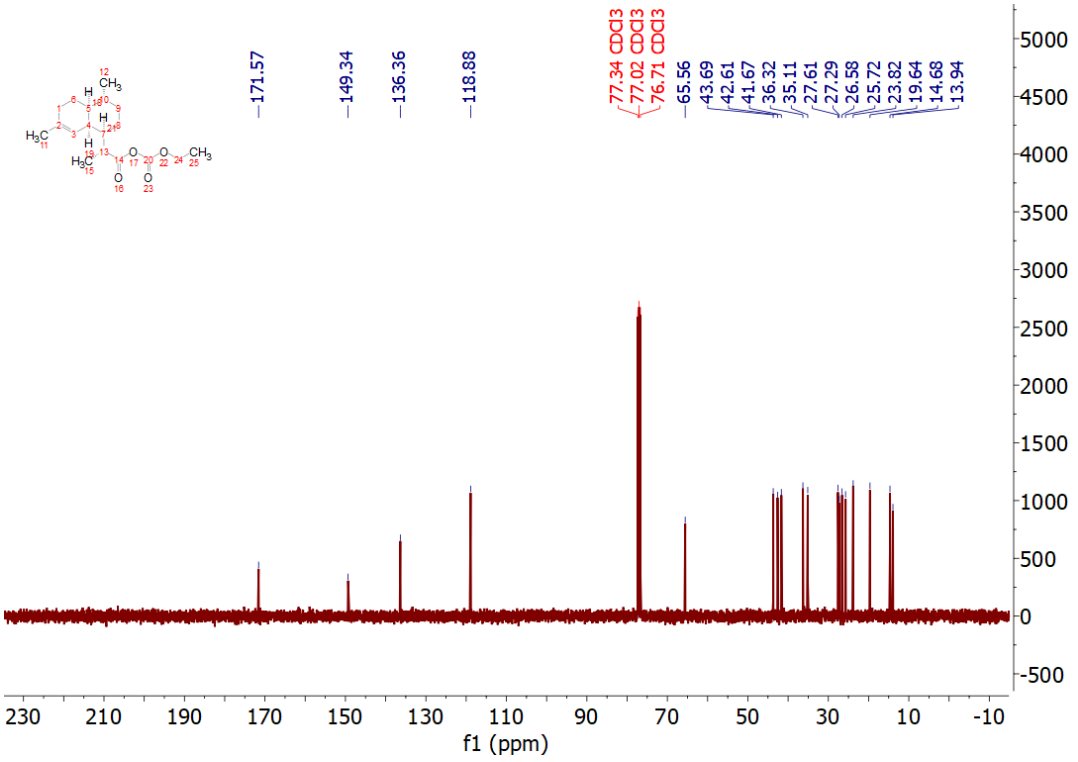


Figure 28: ^{13}C-NMR spectrum of DHAA ethyl carbonate **43** in $CDCl_3$

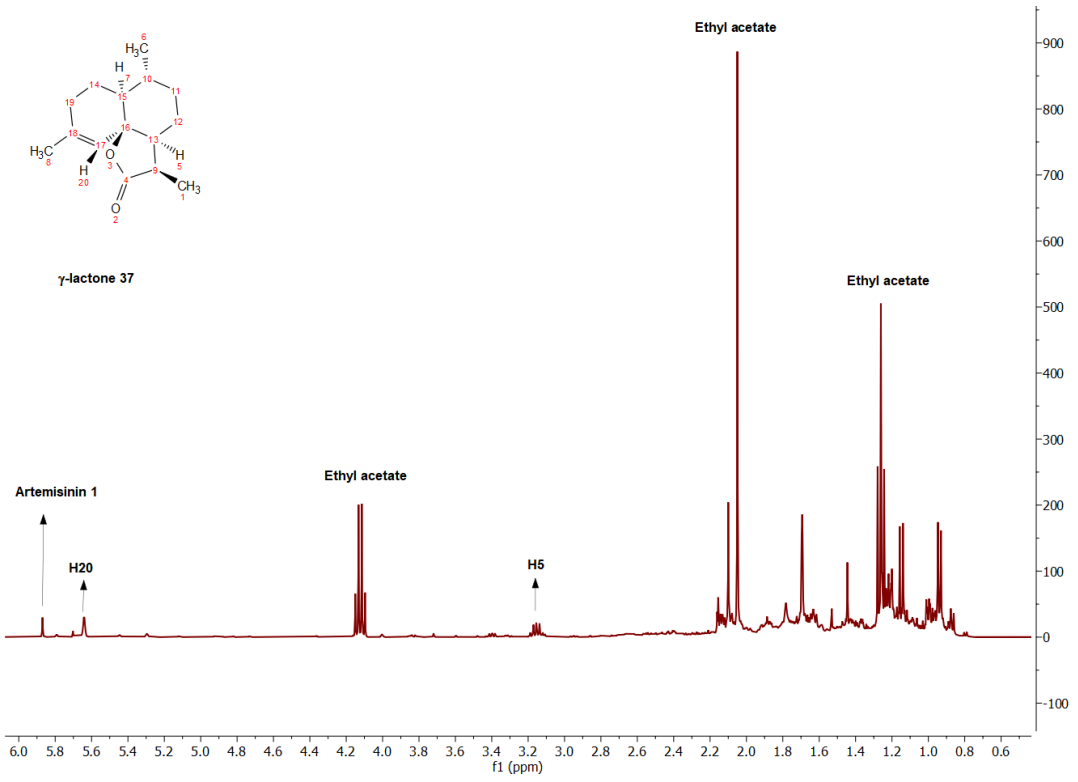


Figure 29: ^{1}H-NMR spectrum showing some peaks due to g-lactone **37** in $CDCl_3$

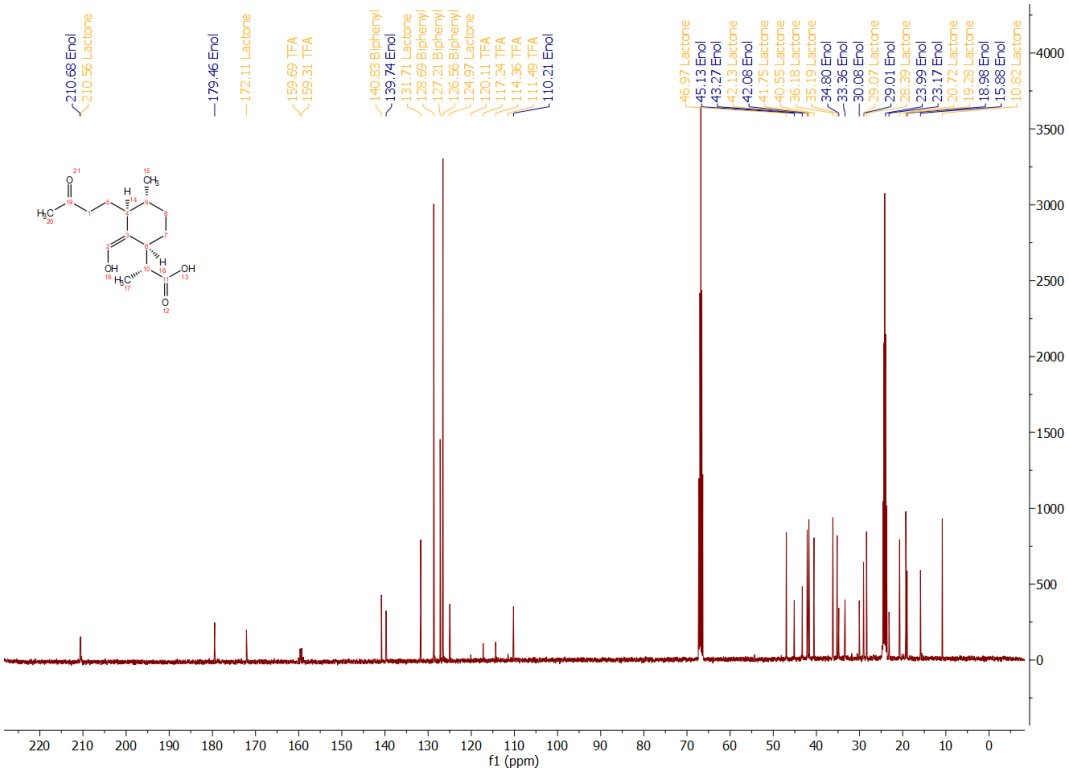


Figure 30: ^{13}C-NMR spectrum for the crude mixture of enol **32** and δ-lactone **33** in THF/D2O solution.

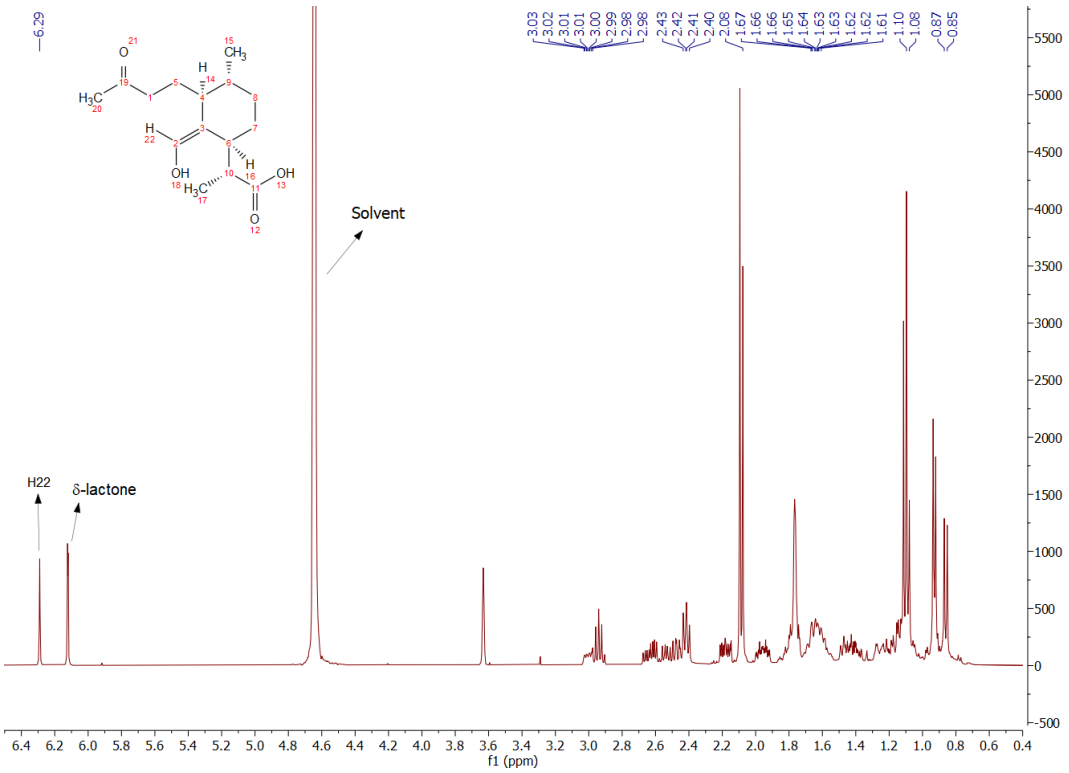


Figure 31: ^{1}H-NMR spectrum for the crude mixture of enol **32** and δ-lactone **33** in THF/D_2O solution.

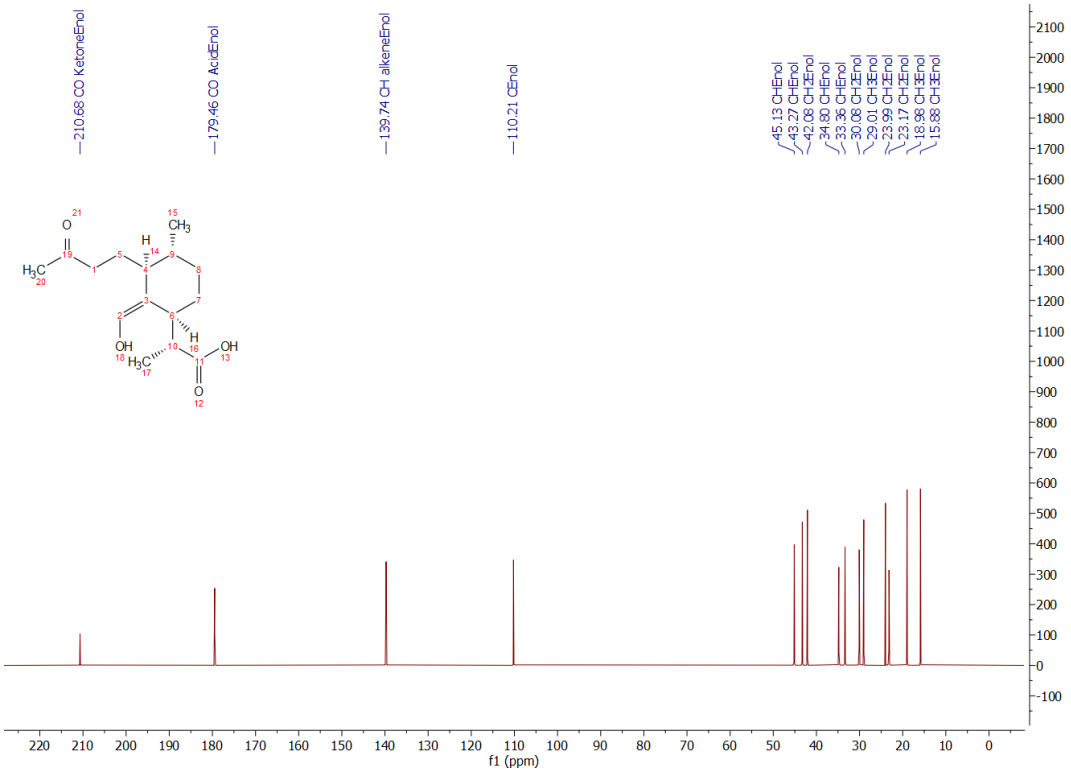


Figure 32: ^{13}C-NMR spectrum for the crude mixture of enol **32** in THF/D_2O solution, after subtracting the δ-lactone **33** peaks using MesteNova software.

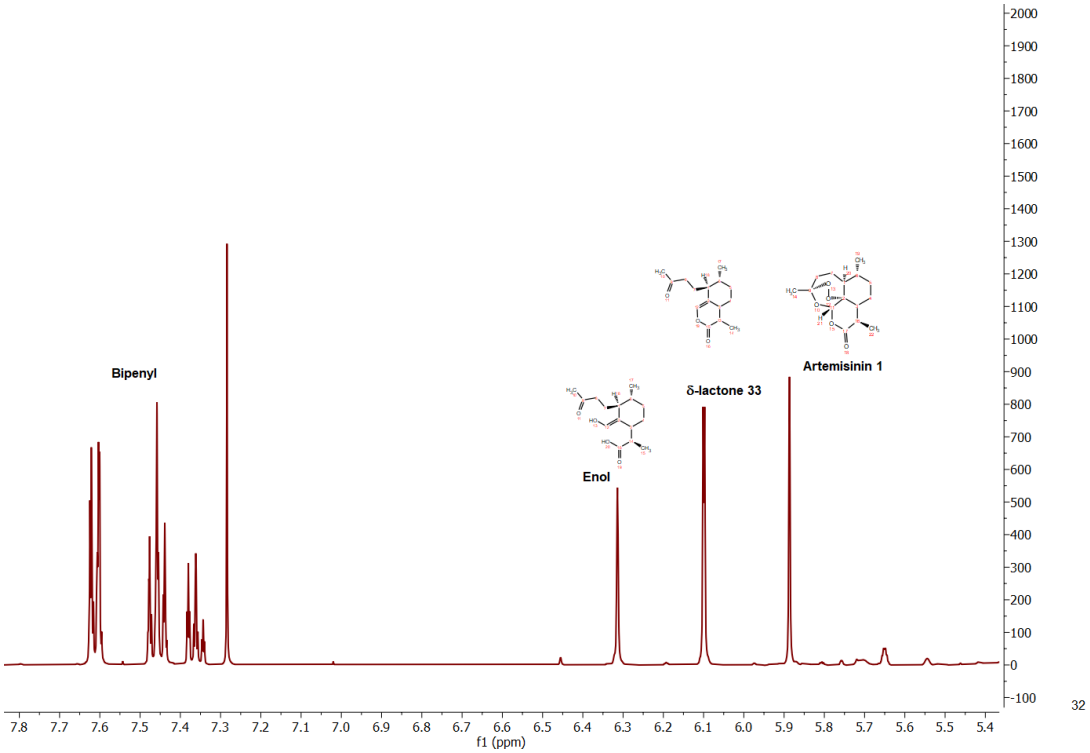


Figure 33: ^{1}H-NMR spectrum for the crude mixture of enol **32,** δ-lactone **33** and artemisinin **1** in ethyl acetate solution.

*Table 1: solubility screening of 0.5 and 0.05 M of DHAA Methyl carbonate **93** and Ethyl carbonates **43** at room temperature*

Entry	Substrate	Solvents	Conc. (M)	Mixture composition of Solvent/Water [v/v]										
				10:0	9:1	8:2	7:3	6:4	5:5	4:6	3:7	2:8	1:9	0:10
1	DHAMC **93**	EtOH	0.05											
2		*n*-PrOH	0.05											
3		*t*-BuOH	0.05											
4	DHAEC **43**	EtOH	0.05											
5		*n*-PrOH	0.05											
6		*t*-BuOH	0.05											
7		EtOH	0.5											
8		*n*-PrOH	0.5											
9		*t*-BuOH	0.5											

In all cases, the substrate was dissolved in the organic component first and then water was added and mixed with a vortex mixer, **Red Color** = Precipitation of substrate upon addition of the water and the Green Color = complete dissolution of the substrate. DHAMC **93**, and DHAEC **43**.